# NUMERICAL SIMULATION AND OPTIMISATION OF IOR AND EOR PROCESSES IN HIGH-RESOLUTION MODELS FOR FRACTURED CARBONATE RESERVOIRS

SIMEON AGADA

Submitted for the degree of Doctor of Philosophy

School of Energy Geoscience Infrastructure and Society

Institute of Petroleum Engineering

Heriot-Watt University

July 2015

To my mother

# ABSTRACT

Carbonate reservoirs contain more than half of the world's conventional hydrocarbon resources. Hydrocarbon recovery in carbonates, however, is typically low, due to multi-scale geological heterogeneities that are a result of complex diagenetic, reactive, depositional and deformational processes. Improved Oil Recovery (IOR) and Enhanced Oil Recovery (EOR) methods are increasingly considered to maximise oil recovery and minimise field development costs. This is particularly important for carbonate reservoirs containing fractures networks, which can act as high permeability fluid flow pathways or impermeable barriers during interaction with the complex host rock matrix.

In this thesis, three important contributions relating to EOR simulation and optimisation in fractured carbonate reservoirs are made using a high-resolution analogue reservoir model for the Arab D formation. First, a systematic approach is employed to investigate, analyse and increase understanding of the fundamental controls on fluid flow in heterogeneous carbonate systems using numerical well testing, secondary and tertiary recovery simulations. Secondly, the interplay between wettability, hysteresis and fracture-matrix exchange during combined $CO_2$ EOR and sequestration is examined. Finally, data-driven surrogates, which construct an approximation of time-consuming numerical simulations, are used for rapid simulation and optimisation of EOR processes in fractured carbonate reservoirs while considering multiple geological uncertainty scenarios.

# PUBLICATIONS

This thesis contains excerpts from the following papers:

- **Agada, S.**, Geiger, S., Optimising Gas Injection in Carbonate Reservoirs Using High-Resolution Outcrop Analogue Models. SPE Paper 166061, 2013.
- **Agada, S.**, Chen, F., Geiger, S. et al., Numerical simulation of fluid-flow processes in a 3D high-resolution carbonate reservoir analogue. Petroleum Geoscience, 20(1), 125-142, 2014.
- **Agada, S.**, Geiger, S., Wettability, Trapping and Fracture-Matrix Interaction during WAG Injection in Fractured Carbonate Reservoirs. SPE Paper 169054, 2014.
- Ahmed Elfeel, M., **Agada, S.**, Maier, C., Geiger, S., Integrating Discrete Fracture Models for Static and Dynamic Calibration of Fractured Reservoirs. EAGE Paper E103-05, 2014.
- **Agada, S.**, Geiger, S., Ahmed, E., Oladyshkin, S., Reduced Order Models for Rapid EOR Simulation in Fractured Carbonate Reservoirs. SPE Paper 173205, 2015.
- **Agada, S.**, Soni, K., Geiger, S., Numerical Simulation of Foam EOR Processes in Fractured Carbonate Reservoirs. EAGE Paper Th-A02, 2015.
- **Agada, S.**, Geiger, S., Doster, F., Wettability, Hysteresis and Fracture-Matrix Interaction during $CO_2$ EOR and Storage in Fractured Carbonate Reservoirs. International Journal of Greenhouse Gas Control, In review.
- **Agada, S.**, Geiger, S., Ahmed, E., Oladyshkin, S., Data-driven Surrogates for Rapid Simulation and Optimisation of WAG Injection in Fractured Carbonate Reservoirs. Journal of Petroleum Science and Engineering, In review.

*If I have seen further,*
*it is by standing on the shoulders of giants.*

— Isaac Newton

## ACKNOWLEDGMENTS

I am indebted to many people who have helped me on this incredible journey. I would like to thank Sebastian Geiger, for being an excellent main supervisor. I have learnt so much from you. Your attention to scientific detail, careful organisation and personal kindness has left a big impression on me. Thanks so much for believing in me and giving countless opportunities for self development. Thanks to Eric Mackay for offering technical and nontechnical guidance throughout the PhD. I would like to thank Vasily Demyanov and Martin Ferno for examining my thesis and providing constructive feedback. I am pleased that you enjoyed reading the thesis.

I would also like to thank individuals and groups that collaborated with me during this project. Thanks to members of the former ExxonMobil $(FC)^2$ research alliance for many insightful discussions and specifically for providing the geological model upon which the simulation studies in this thesis are based. Thanks to Susan Agar, for approving the funding of my PhD project, monitoring my progress and for reviewing my paper on the numerical simulation of fluid flow processes in carbonates. Thanks to Florian Doster for reviewing my paper on wettability, hysteresis and fracture-matrix interaction. I appreciate Sergey Oladyshkin and Ahmed Elsheikh for providing MATLAB codes for generating surrogate models using polynomial chaos expansion and for reviewing my paper on data-driven surrogates.

I have had the most amazing colleagues in the carbonate reservoir group. Thanks Mohamed for your help with Petrel, Fracman and Frontsim. Your support enabled me translate my ideas to research outputs. Thanks Christine and Santhi for being very friendly and organising various social events. I only wish my hat making skills improved during the time we had together. Our 'weekend' trip to Vancouver was filled with the anxiety, stress and hassle, but it was also very memorable because it allowed us to bond, share ideas and aspirations. Thanks Alessandro for many interesting discussions. Buddy, your passion for 'Humus' and 'Beirut' would be unforgettable. Thanks Robert for sharing your ideas on hysteresis and being the guy that's never afraid of controversial topics. Talking to you is always insightful.

Thanks to Yan, Karen and Adnan (I) who finished just as I was beginning my PhD and gave invaluable advice on taking responsibility, planning and complet-

ing a PhD project. To the new guys on the block - Rafael, David, Zhao, Tianshen, Emmanuel and Nathalia - it has been an exciting experience getting to know you and sharing many laughs during coffee breaks. Thanks Adnan (II) for being a pleasant travel companion to Dresden and Delft. The baton for EOR studies in fractured carbonates is now firmly in your hands.
Finally, I would like to thank my family for all their care, love, support and understanding. This achievement would not be possible without you. Thanks to you mum. Thanks to Samson, James, Omeche and Stella for visiting me in Edinburgh. To my cute nieces and nephews - Uncle misses you terribly and can't wait to see you again.

Edinburgh, July 2015

ACADEMIC REGISTRY
# Research Thesis Submission

| | | | |
|---|---|---|---|
| Name*:* | Simeon Agada | | |
| School/PGI: | EGIS/IPE | | |
| Version: *(i.e. First, Resubmission, Final)* | Final | Degree Sought (Award **and** Subject area) | PhD in Petroleum Engineering |

## Declaration

In accordance with the appropriate regulations I hereby submit my thesis and I declare that:

1) the thesis embodies the results of my own work and has been composed by myself
2) where appropriate, I have made acknowledgement of the work of others and have made reference to work carried out in collaboration with other persons
3) the thesis is the correct version of the thesis for submission and is the same version as any electronic versions submitted*.
4) my thesis for the award referred to, deposited in the Heriot-Watt University Library, should be made available for loan or photocopying and be available via the Institutional Repository, subject to such conditions as the Librarian may require
5) I understand that as a student of the University I am required to abide by the Regulations of the University and to conform to its discipline.

* *Please note that it is the responsibility of the candidate to ensure that the correct version of the thesis is submitted.*

| | | | |
|---|---|---|---|
| Signature of Candidate*:* | | Date: | |

## Submission

| | |
|---|---|
| Submitted By *(name in capitals):* | |
| Signature of Individual Submitting: | |
| Date Submitted: | |

## For Completion in the Student Service Centre (SSC)

| | | | |
|---|---|---|---|
| Received in the SSC by *(name in capitals):* | | | |
| *Method of Submission*<br>*(Handed in to SSC; posted through internal/external mail):* | | | |
| *E-thesis Submitted (**mandatory for final theses)*** | | | |
| Signature: | | Date: | |

Please note this form should bound into the submitted thesis.

Updated February 2008, November 2008, February 2009, January 2011

# CONTENTS

# LIST OF FIGURES

## LIST OF TABLES

## ACRONYMS

aPCE Arbitrary Polynomial Chaos Expansion

ASP Alkali-Surfactant-Polymer

CCS Carbon Capture and Storage

DFM Discrete Fracture and Matrix

DFN Discrete Fracture Network

DOE Design of Experiments

DP Dual-Porosity

DPDP Dual-Porosity-Dual-Permeability

EOR Enhanced Oil Recovery

FE Finite Element

FV Finite Volume

GA Genetic Algorithm

GUF Gas Utilisation Factor

IFT Interfacial Tension

IOR Improved Oil Recovery

MMP Minimum Miscibility Pressure

MRF Mobility-Reduction-Factor

NFR Naturally Fractured Reservoirs

PCE Polynomial Chaos Expansion

PR Polynomial Regression

RMSE Root Mean Square Error

ROS Residual Oil Saturation

SAG Surfactant-Alternating-Gas

sPCE Sparse Polynomial Chaos Expansion

WAG Water-Alternating-Gas

# 1

# INTRODUCTION

A significant proportion of the world's conventional and unconventional hydrocarbon resources are located in carbonate reservoirs, commonly estimated at around 60% of global reserves (Beydoun, 1998; Burchette, 2012; Machel et al., 2012). Carbonate reservoirs, however, suffer from poor recovery, estimated to be below 35% on average (Montaron, 2008). Hence, a small increase in recovery (1 to 2%) would have a significant impact on hydrocarbon reserves (Agar and Geiger, 2015). Optimising the development of existing fields and new discoveries in carbonate reservoirs requires a reliable prediction of hydrocarbon recovery. Performance prediction in turn needs a sound understanding of how geological heterogeneities impact the flow behaviour of oil, gas and brine.

Carbonate reservoirs are highly heterogeneous across all length scales (from pore- to field-scale), rendering it difficult to predict flow behaviour in the subsurface (Fig. 1.1). The multi-scale heterogeneities result from complex depositional, reactive and diagenetic processes (e.g., Kenter, 1990; Kerans et al., 1994; Mutti et al., 1996; Cantrell and Hagerty, 1999; Corbett and Jenson, 2000; Jennings et al., 2000; Pomar et al., 2002; Lucia et al., 2003; Hollis et al., 2010; Koehrer et al., 2011; Amour et al., 2012; van der Land et al., 2013; Chandra et al., 2015). In addition, most carbonate reservoirs are naturally fractured, with fractures forming over a wide range of scales, commonly generating complex connected networks, which provide the essential flow paths and/or link different reservoir horizons (e.g., Ericsson et al., 1998; Guerreiro et al., 2000; Azeemuddin et al., 2002; Gale et al., 2004; Toublanc et al., 2005; Belayneh et al., 2006; Agar et al., 2010; Belayneh and Cosgrove, 2010; Bush, 2010; Hollis et al., 2011; Geiger and Matthai, 2012).

An accurate characterisation of reservoir architecture, diagenetic evolution and deformation is, therefore, critical for the successful modelling of carbonate reservoirs, predicting flow behaviour and estimating hydrocarbon recoveries. Carbonate reservoir characterisation, however, is associated with a high degree of uncertainty. Typical characterisation workflows integrate data from multiple sources such as seismic surveys, wireline logs, borehole imaging, petrophysics, well-tests, and core analysis (Garland et al., 2012). These data are usually complemented by outcrop analogue information to bridge the near wellbore and reservoir scale data. Although, there are limitations as to how outcrop analogues reflect the behaviour of subsurface reservoirs and how quantitative outcrop data can be scaled to the subsurface (Bryant et al., 2000; Kuchuk and Biryukov, 2012), it is now common to use observed outcrop geometries as a subsurface modelling template to improve the descriptions of the inter-well space (e.g., Kerans et al., 1994; Aurell et al., 1998; Vennin et al., 2003; Vaughan et al., 2004; Castel et al.,

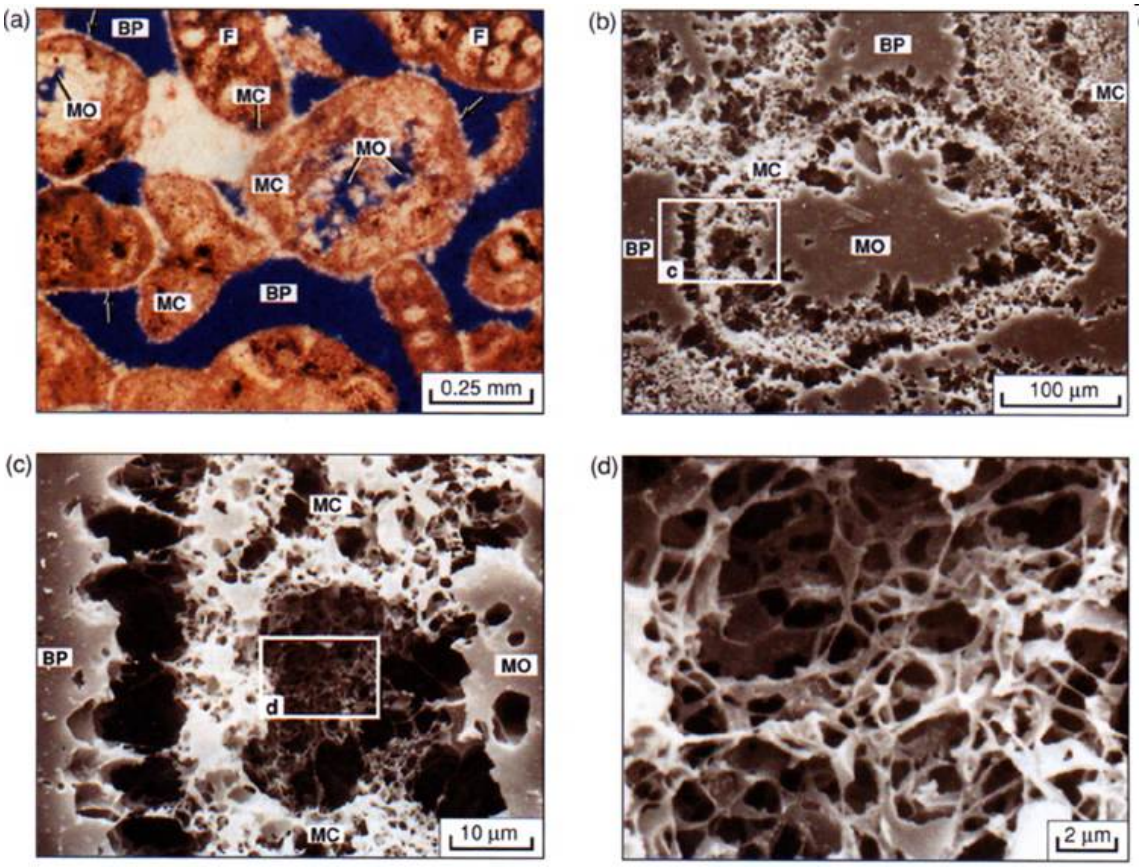


Figure 1.1: Pore-size distribution controlled by depositional and diagenetic fabrics (micro- and macro porosity) in the Arab formation. Pore space is filled with blue resin (a). Pore casts of increasingly higher magnification (b, c, d) indicate carbonate heterogeneity at multiple scales. After Cantrell and Hagerty (1999).

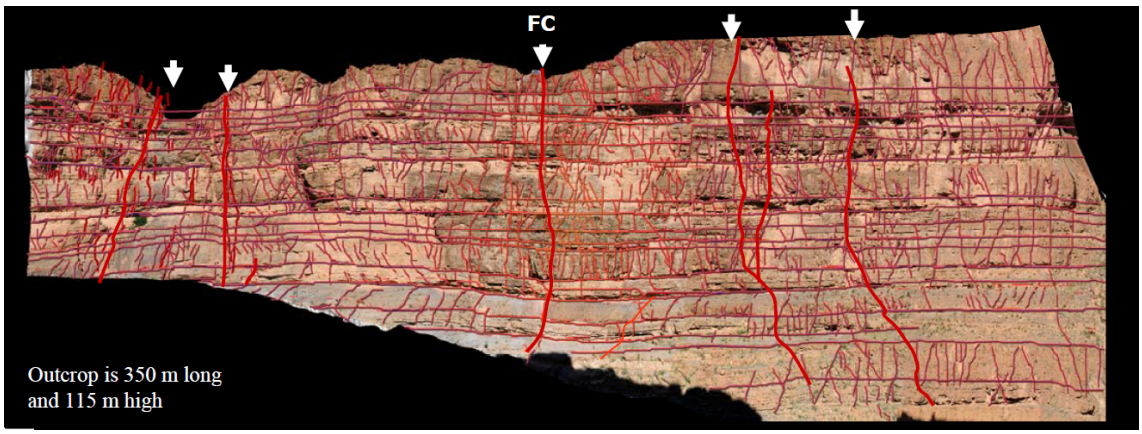


Figure 1.2: Interpretation of fracture traces of a Jurassic Carbonate Ramp outcrop from the High Atlas Mountains, Morroco. Horizontal lines represent bed boundaries. Fractures are represented by vertical lines while thick red lines indicate locations of fracture corridors. After Agar et al. (2010).

2007; Reijnders et al., 2008; Palermo et al., 2010; Koehrer et al., 2011; Lapponi et al., 2011; Garcia-Fresca et al., 2012).

In addition to using outcrop analogues as a means to improve the static modelling of carbonate reservoirs, high-quality digital outcrop models are increasingly employed to investigate the interaction of flow processes with small-scale geological heterogeneities that have been observed in the outcrop. Outcrop-based flow simulation models tend to represent small-scale geological heterogeneities at great detail (Fig. 1.2). This is in stark contrast to typical reservoir simulation models that are used to predict reservoir performance and to guide reservoir development. Such reservoir simulation models require significant upscaling, which lead to the reduction of geological features and heterogeneities that are contained in the original geological model of the reservoir (e.g., Christie, 2001; Gerritsen and Durlofsky, 2005; King et al., 2006).

Hence, high-resolution outcrop-based flow simulations enable us to study systematically how certain geological structures, which are typically not preserved explicitly in reservoir-scale flow simulations, impact fluid flow and hydrocarbon recovery. Ideally, this understanding can then be used to rank the relative importance of geological structures with respect to their impact on fluid flow and hydrocarbon recovery. The ranking then enables geologists to focus on improving the description of these structures and engineers to include them accurately

in field-scale reservoir simulation models. The use of outcrop analogues for detailed geological and fluid flow studies is now well established and increasingly used in the oil and gas industry, both for clastic reservoirs (e.g., Ringrose et al., 1999; White and Barton, 1999; Stephen and Dalrymple, 2002; Pringle et al., 2004; Kirstetter et al., 2006; Enge et al., 2007; Jackson et al., 2009; Rotevatn et al., 2009; Sech et al., 2009; Choi et al., 2011; Deveugle et al., 2011) and carbonate reservoirs (e.g., Vaughan et al., 2004; Belayneh et al., 2006; Agar et al., 2010; Fitch et al., 2014; Shekhar et al., 2014).

Due to the generally low hydrocarbon recovery from carbonate reservoirs (Montaron, 2008), enhanced oil recovery (EOR) techniques can be essential to reduce the residual oil saturation and increase the economic value of carbonate reservoirs. EOR methods encompass gas (miscible/immiscible), chemical and thermal methods that produce previously unrecoverable oil by various mechanisms including oil swelling, viscosity reduction, interfacial tension reduction and mobility control (Lake, 1989; Christensen et al., 2001; Dake, 2001; Manrique et al., 2007; Awan et al., 2008; Bourdarot and Ghedan, 2011; Talebian et al., 2014).

Although, EOR methods have been successfully applied across a wide range of clastic and carbonate reservoirs (Fig. 1.3 and Table 1.1), the interactions be-

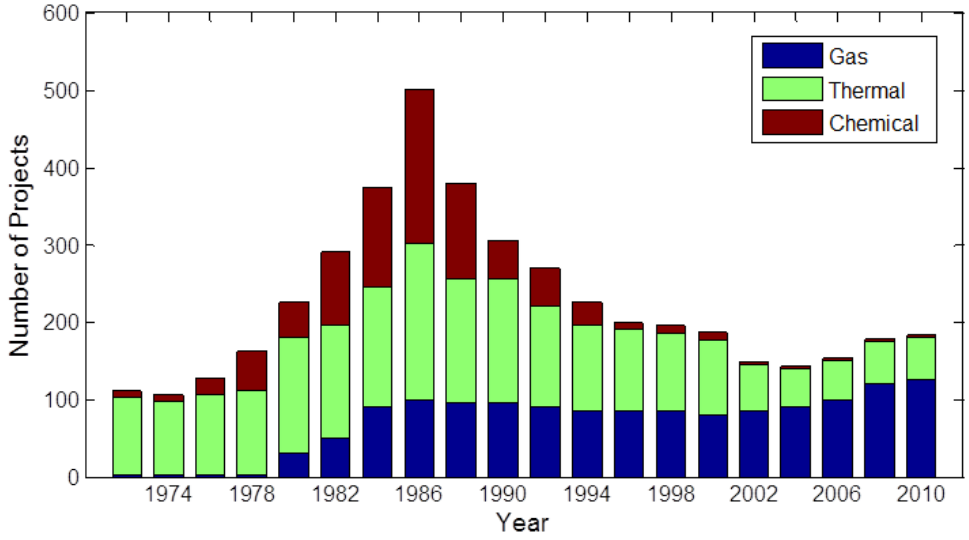


Figure 1.3: EOR project history in the United States. The number of EOR projects peaked in 1986 and then declined (due to the oil price crash) for nearly 20 years. Since 2004 the number of projects has been increasing again. Modified after Manrique et al. (2007, 2010).

| Field | Location | Lithology | EOR technique |
|---|---|---|---|
| Stepanovskoye | Russia | Limestone | Gas |
| San Andres | USA | Dolomite | Gas |
| Ekofisk | Norway | Limestone | Gas |
| Bibi Hakimeh | Iran | Limestone | Gas |
| Harweel | Oman | Dolomite | Gas |
| Bati Raman | Turkey | Limestone | Gas |
| Yates | USA | Dolomite | Thermal |
| Garland | USA | Limestone | Thermal |
| Qarn Alam | Oman | Limestone | Thermal |
| Clearfork | USA | Dolomite | Chemical |
| Cottonwood Creek | USA | Limestone | Chemical |

Table 1.1: Examples of EOR field application in carbonate reservoirs (Christensen et al., 2001; Manrique et al., 2007; Awan et al., 2008)

.

tween complex EOR flow processes and geological heterogeneity, especially in carbonate formations is not yet fully understood. Detailed simulation studies using high-resolution outcrop-based models are an excellent tool to evaluate EOR processes for specific reservoirs and analyse the impact of geological and engineering uncertainties on reservoir performance. Detailed simulation studies can then help to guide decision making and increase the number of carbonate reservoir EOR projects that are sanctioned to progress from evaluation to execution in the light of technical and economic constraints.

Uncertainty in geological parameters occurs because carbonate reservoirs are highly heterogeneous, making it difficult to predict flow behaviour in the subsurface and the accompanying geological flow parameters. Such uncertainties are typically beyond the control of the modeller but must be considered to ensure that model predictions are holistic and cover the range of possible outcomes. Geological parameter uncertainties include but are not limited to the nature and flow significance of the matrix, faults and subseismic fractures and the role of wettability and hysteresis when controlling imbibition and drainage mechanisms (Fig. 1.4). Conversely, engineering uncertainties can be operationally controlled and modified to achieve optimal outcomes. Engineering parameter uncertainties include but are not limited to injection strategy, well locations, injection rates, production rates and reservoir depletion strategy. Robust optimisation which

has now become a common workflow in the industry couples the exploration of both geological and engineering uncertainty to obtain an optimal solution (e.g., Petvipusit et al., 2014).

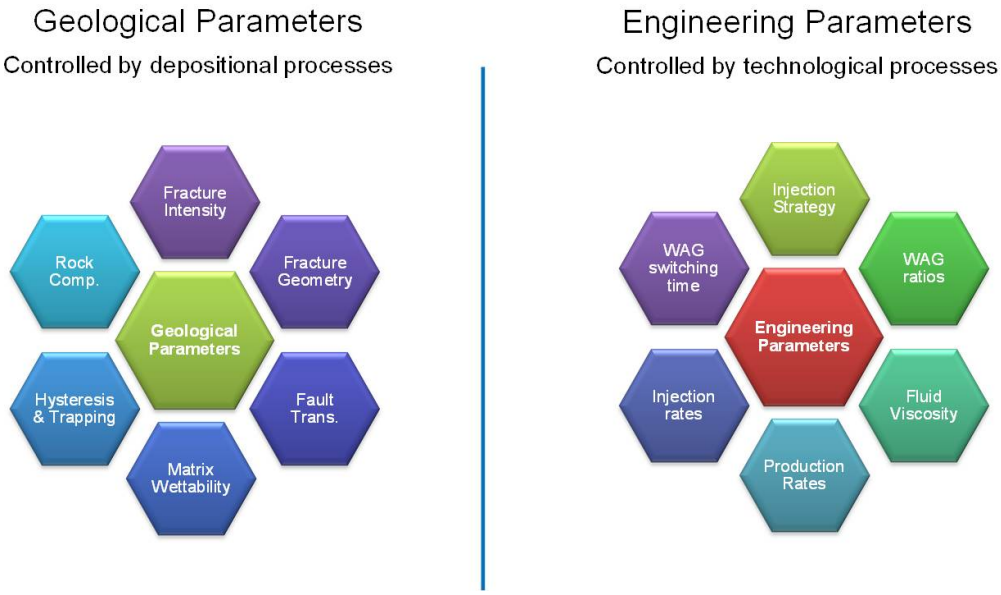


Figure 1.4: Comparison of geological uncertainties (beyond our control but inferable from data) and engineering uncertainties (based on operational choices and under our control.

## 1.1 OBJECTIVES AND STRUCTURE OF THE THESIS

This thesis integrates reservoir characterisation with reservoir simulation to explore fundamental aspects of EOR simulation and optimisation for fractured carbonate reservoirs using a high-resolution fractured carbonate reservoir model. This thesis, therefore, aims to improve the simulation of fractured carbonate reservoirs by analysing the controls on fluid flow in heterogeneous carbonate systems and investigating how different EOR processes can be used to obtain optimum recovery in the presence of multiple uncertainties arising from intrinsic carbonate reservoir heterogeneity. Specifically, the objectives of this thesis are:

- To improve understanding of carbonate reservoir simulation by using a high-resolution analogue reservoir model for the Arab D formation to perform numerical well test analysis and simulations of improved and enhanced oil recovery.

- To identify flow signatures for variations in production behaviour, when different injection fluids and well patterns are employed, and to identify reservoir engineering measures that can be used to improve recovery in the presence of geological heterogeneities.
- To improve understanding of carbonate reservoir simulation by analysing how small-scale heterogeneties typical for this carbonate reservoir setting impact fluid-flow behaviour and hydrocarbon production.
- To investigate and demonstrate how the interplay between hysteresis, wettability and fracture-matrix exchange impacts simultaneous oil recovery and $CO_2$ storage in relation to the multiscale heterogeneities that are pervasive for fractured carbonate reservoirs.
- To generate, analyse and compare data-driven surrogate models for rapid simulation and optimisation of EOR processes in fractured carbonate reservoirs.

In general, this thesis provides three important contributions to EOR simulation and optimisation in fractured carbonate reservoirs using a high-resolution analogue reservoir model for the Arab D formation; (1) The fundamental controls on fluid flow in heterogeneous carbonate systems are investigated using a systematic approach (often called a 'geoengineering workflow') that evaluates simulations of numerical well testing, secondary recovery and tertiary recovery (e.g., Corbett, 2009; Corbett et al., 2012; Chandra et al., 2013), (2) the interplay between wettability, hysteresis and fracture-matrix exchange during concurrent $CO_2$ EOR and sequestration is examined and (3) simulation and optimisation of EOR processes (including application of Monte Carlo analysis and stochastic algorithms) are achieved using reasonably reliable surrogate (proxy) models generated from time-consuming numerical simulations.

This thesis contains 7 chapters in total.

- Chapter 1 is the current chapter. It gives a brief overview of carbonate reservoirs and the applicability of outcrop analogue models for reservoir simulation studies. Chapter 1 also highlights suitable enhanced oil recovery techniques for carbonate reservoirs and states the objectives of the thesis.

- Chapter 2 introduces the main principles governing multiphase fluid flow simulation of naturally fractured reservoirs. This includes the description of fractured reservoir simulation models and the governing equations. Chapter 2 also highlights the main principles governing black oil and compositional reservoir fluid models, relative permeabilities and hysteresis in saturation functions before describing measures for managing the computational cost of the simulations.

- Chapter 3 introduces the high-resolution geological and flow simulation analogue reservoir model used for the IOR and EOR studies in this thesis. Numerical well-test and secondary (black oil) recovery simulations are then used to investigate the main geological and engineering controls on fluid-flow in carbonate reservoirs. This chapter is based on Agada et al. (2014).

- Chapter 4 presents the compositional simulation of miscible and immiscible gas injection in carbonate reservoirs using the model introduced in Chapter 3. The use of foam EOR to control gas mobility and improve reservoir conformance is demonstrated. This chapter is based on Agada and Geiger (2013) and Agada et al. (2015b).

- Chapter 5 extends the work from Chapter 3 by investigating the interplay between wettability, hysteresis and fracture-matrix transfer during $CO_2$ EOR and storage. End-member wettability scenarios and multiple wettability distribution approaches are tested, while effective fracture permeabilities are computed based on geological modelling rules linked to the evolution of the fracture systems. This chapter is based on Agada and Geiger (2014).

- Chapter 6 presents the development of data-driven surrogates for the rapid simulation and optimisation of EOR processes in fractured carbonate reservoirs. Different surrogate modelling techniques coupled with experimental design are used to develop proxy models to represent simulation models inside and outside of the design space. The surrogates are then used for rapid uncertainty quantification using Monte Carlo analysis and rapid op-

timisation using stochastic algorithms. This chapter is based on Agada et al. (2015a).

- Chapter 7 gives a summary of the key outcomes of the thesis and provides the concluding remarks followed by recommendations for future work.

# 2

# MULTISCALE SIMULATION OF FLUID FLOW IN NATURALLY FRACTURED RESERVOIRS

## 2.1 INTRODUCTION

Fractures, which are ubiquitous in subsurface reservoirs throughout the world, are often the principal pathways through otherwise impermeable or low permeability rocks (rock matrix) and are key to quantifying flow processes in hydrogeological, geothermal, $CO_2$ storage and enhanced/improved oil recovery applications (Berkowitz, 2002). Naturally fractured hydrocarbon reservoirs display complex production behaviour since hydrocarbon recovery is influenced, to a greater or lesser extent, by fractures (Nelson, 2001; Makel, 2007). Understanding, managing and predicting production behaviour for fractured reservoirs requires a good understanding of how fluid flow can be impacted by geological heterogeneity, particularly fracture networks but also complex matrix properties.

For example, the influence of natural fractures on subsurface fluid flow can be observed during the migration of the water front in a fractured Middle Eastern carbonate reservoir (Fig. 2.1). The presence of connected fractures in the eastern flank of the field leads to rapid and irregular migration of the water front compared to the western flank, where the fractures are less connected and hence more uniform migration of the water front and better sweep is observed. Such displacement patterns evoke important questions that ought to be answered during fractured reservoir characterisation and modelling: Are fractures present in the subsurface rock? If fractures are present, are they connected? How can fractures be accurately represented in subsurface reservoir models? To

what extent do the fractures affect Improved Oil Recovery (IOR) and Enhanced Oil Recovery (EOR) processes in fractured carbonate reservoirs? What mitigating measures can be employed to accommodate fracture impact on IOR and EOR? The aforementioned questions are non-trivial and require extensive reservoir characterisation, modelling, simulation, sensitivity analysis and uncertainty quantification before they can be answered. The accuracy and applicability of IOR and EOR reservoir simulation, therefore, requires appropriate and robust conceptual models which are discussed in this chapter.

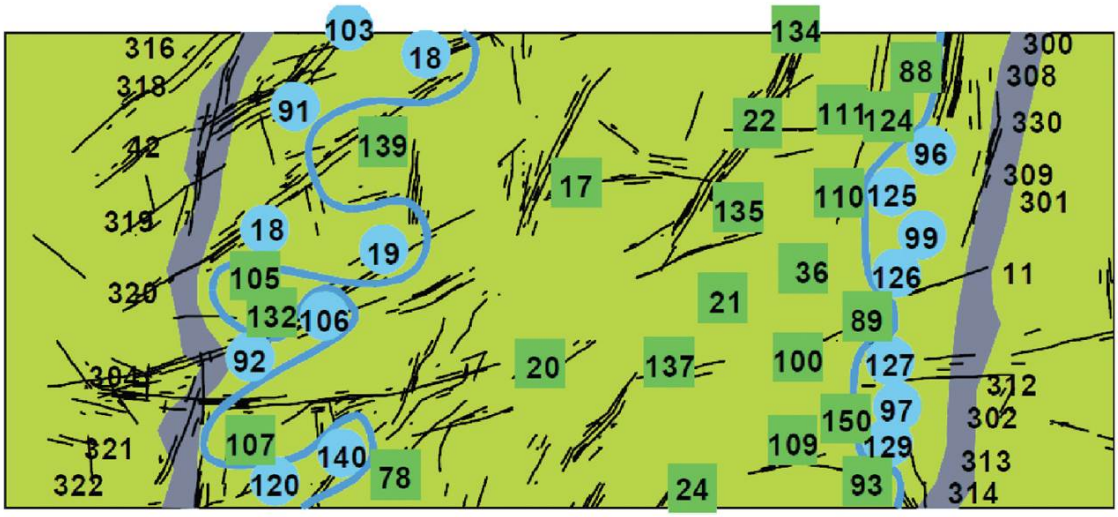


Figure 2.1: Irregular water front progression in a giant Middle Eastern carbonate field crossed by sub-seismic faults and fractures. The original position of the water-oil contact is shown as grey bands and the present position as blue lines. Wet wells are shown as blue circles and dry wells as green squares. After Cosentino et al. (2001).

## 2.2 FRACTURED RESERVOIR SIMULATION MODELS

Several conceptual models exist to represent multiphase fluid flow and multi-component transport processes in fractured porous media and account for heterogeneities arising from the rock matrix, fracture networks and matrix-fracture exchange. In general, these conceptual models assume that fractures exhibit high permeability and low storage capacity, while the rock matrix exhibits low permeability and high storage capacity.

When fractures exist on a sub-grid scale, it is typically sufficient to use a single porosity model to capture the matrix and fracture effects (Fig. 2.2). The fracture-

matrix complexity increases significantly when the fractures are larger than the grid blocks and are often connected. In such cases (models with connected fractures larger than the grid size), dual continuum and discrete fracture models are often used (Bourbiaux et al., 2002; Bourbiaux, 2010).

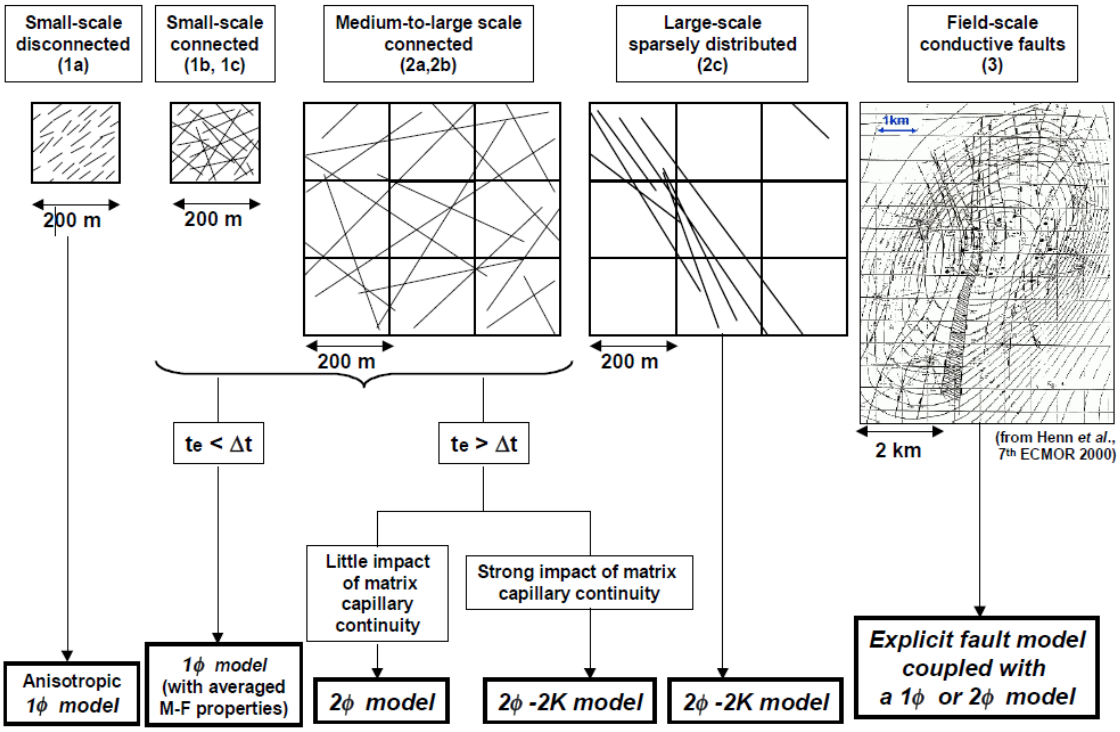


Figure 2.2: Guidelines for selecting flow modelling approach for fractured reservoir simulation. After Bourbiaux et al. (2002).

### 2.2.1 *Dual Continuum Models*

The dual continuum models account for the different time scale of flow in Naturally Fractured Reservoirs (NFR) by treating the fractures and matrix as two separate continua, which are coupled via a transfer function. Fracture-matrix transfer occurs by capillary forces (depending on the wettability of the medium), gravity forces (due to density differences), fluid expansion and diffusion (due to pressure gradient exerting a driving force across the matrix medium) (Fig. 2.3).

Generally, during water flooding oil recovery from a water-wet matrix is dominated by spontaneous imbibition, while recovery from an oil-wet matrix during gas flooding is dominated by gravity drainage. Carbonate rocks are typically

mixed- to oil-wet, hence, oil recovery is influenced to a greater or lesser extent by both spontaneous imbibition and gravity drainage. The transfer function needs to conserve momentum and define the rate of fracture-matrix fluid exchange by taking the aforementioned recovery mechanisms into account (Lu et al., 2008).

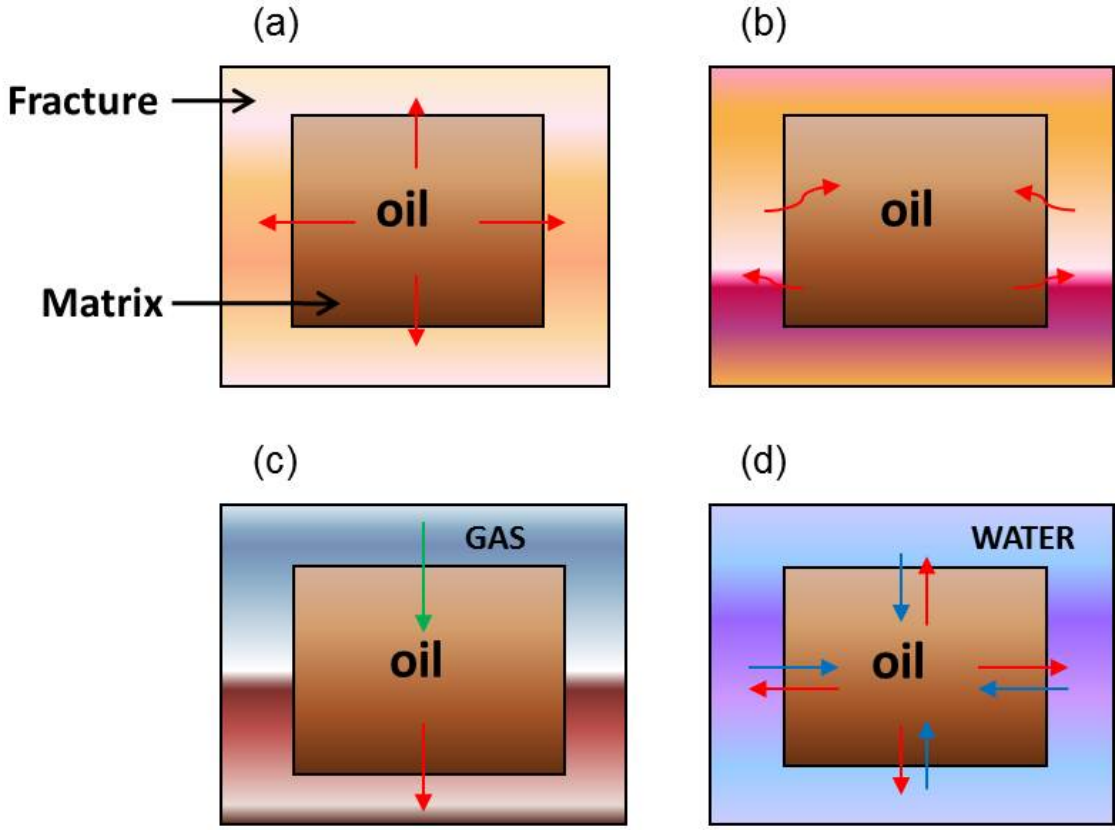


Figure 2.3: Oil recovery from a matrix that is surrounded by fractures. Oil is recovered by fluid expansion (a), diffusion (b), gravity drainage (c), and spontaneous imbibition (d). Modified after Lu et al. (2008).

Traditionally, transfer functions follow the classic Warren and Root (1963) assumption that the flow towards the well bore takes place in the fracture network, while the matrix feeds the system with stored hydrocarbons. The Gilman and Kazemi (1983) transfer function (eqns. 2.1 and 2.2) was employed throughout this thesis to model the fluid exchange between fracture and matrix. The formulation by Quandalle and Sabathier (1989), which is known to capture gravitational effects more accurately (Abushaikha and Gosselin, 2008), was also tested but the results were found to be identical. Testing the similarity of transfer functions was accomplished by comparing water injection, gas injection and water-alternating-gas injection production profiles using the reservoir model and well configura-

tions described in Chapter 3.

$$T_o = \sigma \frac{k_m k_{ro}}{\mu_o} \left( p_o^m - p_o^f + (\rho_w - \rho_o) \left( S_{wD}^f - S_{wD}^m \right) \frac{gh}{2} \right) \tag{2.1}$$

$$T_w = \sigma \frac{k_m k_{rw}}{\mu_w} \left( p_o^m - pc_o^m - p_o^f + pc_o^f + (\rho_w - \rho_o) \left( S_{wD}^f - S_{wD}^m \right) \frac{gh}{2} \right) \tag{2.2}$$

where $T_o$ represents the transfer of oil from the matrix to the fractures and $T_w$ represents the transfer of water from the fractures to the matrix in the case of capillary imbibition. $\sigma$ is the shape factor which describes the area of the fracture-matrix interface in each grid block. $k_{ro}$ and $k_{rw}$ are the oil and water relative permeabilities, respectively. $g$ is the gravity term while $h$ is the height of the matrix blocks. $\rho_o$, $\rho_w$ represent the oil/water density and $S_{wD}$ is the dimensionless water saturation. $m$ and $f$ refer to the matrix and fracture respectively, while, $p$ represents the pressure.

The dual continuum model distinguishes between two different approaches, the Dual-Porosity (DP) and the Dual-Porosity-Dual-Permeability (DPDP) model (Fig. 2.4). The DP model accounts for fluid exchange between the fracture and matrix but does not consider matrix-matrix flow. Conversely, the DPDP model represents both the fracture-matrix flow and the interaction between two matrix blocks, which is essential to capture capillary continuity and reimbibition. The DPDP model is typically preferred in situations where the matrix permeability is relatively high and there is matrix hydraulic continuity such as are encountered in this thesis. The equations for a single-phase DPDP model are presented below. Equation 2.3 represents the flow in the fractures with an additional term for the matrix flow contribution while equation 2.4 represents flow in the matrix.

$$\nabla . \left( \frac{k_f}{\mu} \nabla p_f \right) - \frac{\sigma k_m}{\mu} \left( p_f - p_m \right) + q_f = \phi_f c_{tf} \frac{\partial p_f}{\partial t} \tag{2.3}$$

$$\nabla . \left( \frac{k_m}{\mu} \nabla p_m \right) - \frac{\sigma k_m}{\mu} \left( p_f - p_m \right) + q_m = \phi_m c_{tm} \frac{\partial p_m}{\partial t} \tag{2.4}$$

where $k_f$, $p_f$, $q_f$, $\phi_f$, $c_{tf}$ and $k_m$, $p_m$, $q_m$, $\phi_m$, $c_{tm}$ represent the fracture and matrix permeability, pressure, source/sink, porosity and total compressibility respectively. $\mu$ is the fluid viscosity and $\sigma$ is the shape factor.

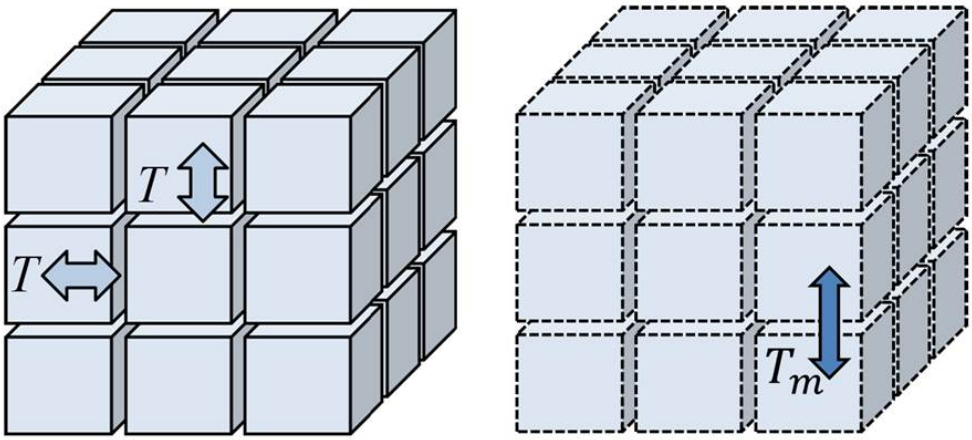


Figure 2.4: Conceptual representation of a dual-porosity (DP) model, left, and a dual-porosity dual-permeability (DPDP) model, right. Dashed lines indicate flow between matrix blocks while solid lines indicate no flow. Fracture-matrix fluid transfer is computed via a transfer function, $T$. Matrix-matrix fluid exchange is computed on a virtual grid via a transfer function $T_m$. After Maier et al. (2013).

### 2.2.2 *Discrete Fracture Network Models*

The Discrete Fracture Network (DFN) approach is commonly used to estimate fracture permeabilities. DFNs are stochastic representations of the fracture network constrained by a wide range of reservoir data. The DFN approach is an efficient, and geologically consistent way, to model multiscale fractures as it can capture the connectivity and scale dependent heterogeneity of the fracture system (Dershowitz et al., 2000; Wei, 2000; Makel, 2007; Spence et al., 2014). In a DFN model, fractures are represented by planar elements.

To build a DFN constrained by deterministic observations of fractures, five geometrical fracture characteristics that control the interconnectedness of the subsurface fracture network are required. These characteristics include the fracture intensity/density, orientation, aperture, length and aspect ratio. Multiple equiprobable realisations of the fracture system can then be generated stochas-

tically with a given set of input parameters to account for uncertainties in the fracture network characterisation.

For example, the fracture intensity in a given reservoir may be generated as a result of faulting and hence cluster around faults (fault related intensity), may be part of a more stratigraphically confined fracture system giving rise to layered high fracture permeability (bedding related intensity) or part of a pervasive background fracture system (regional intensity) (Fig. 2.5). Analysing the influence of fracture intensity scenarios on hydrocarbon production in a given reservoir will enable us to link flow patterns to the fracture network characterisation especially for EOR simulation. Hence, a systematic and integrated analysis of the fracture network geometry, can provide a pathway to better understand the fracture system, fracture contribution to subsurface fluid displacement, the best way to accurately model the fracture flow impact and to develop the reservoir accordingly.

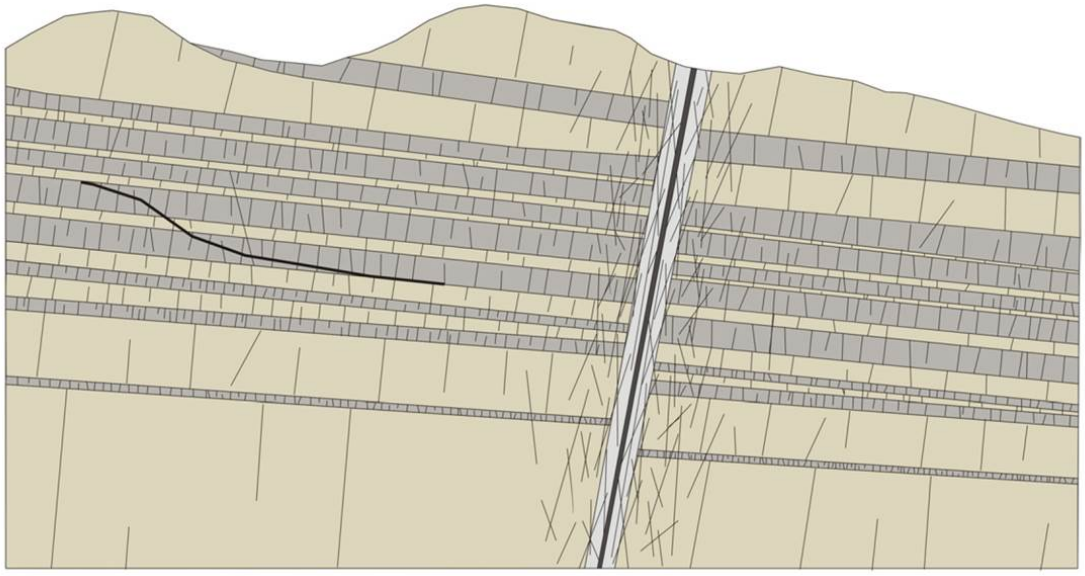

Figure 2.5: Hydrostructural domains of the Galiano Island, Canada showing fault-related, bed-related and regional fracture systems respectively. After Chesnaux et al. (2009).

### 2.2.3 *Connectivity of Fracture Networks*

Fracture network connectivity describes the interaction between fracture sets and reservoir sequences (Makel, 2007). In other words, the fracture connectivity indicates the continuity of flow across a network of fractures bound by a reservoir sequence. In a network with low fracture density, the fractures are few and isolated thereby leading to poor interconnectivity (Fig. 2.6). As the fracture density increases, a percolation threshold is reached where the fracture network is connected across the reservoir sequence leading to a rapid rise in fracture interconnectivity (Stauffer and Aharony, 1994; King et al., 2001). The percolation threshold depends on the aperture, height, length and orientation of individual fractures and the density and clustering of fractures within a fracture network (Bour and Davy, 1998; Odling et al., 1999; Bech et al., 2001; Manzocchi, 2002).

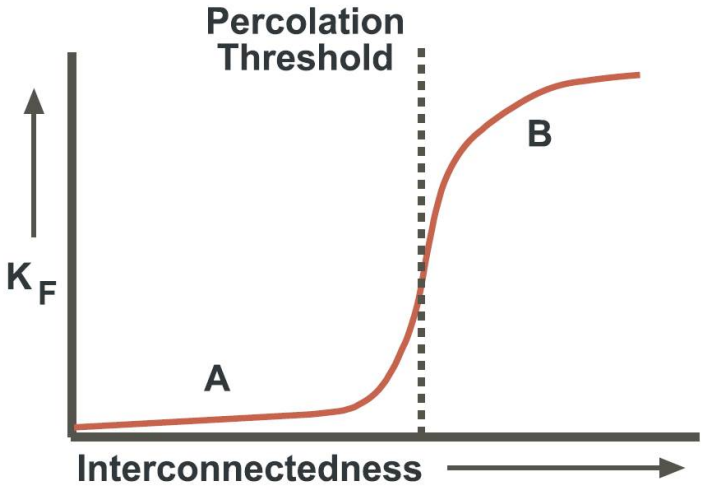


Figure 2.6: The percolation threshold of a fracture network, on the scale of the sampling region, is reached where the fractures interact in such a way that flow from one boundary to another becomes possible. 'A' indicates a macroscopically disconnected sampling region, while, 'B' represents a macroscopically connected sampling region. '$K_F$' denotes increasing fracture permeability. After Makel (2007).

As indicated in the previous subsection an important aspect of connectivity is the interaction of fractures with lithostratigraphy where bedding planes and/or intervening shale layers may inhibit fracture propagation (Makel, 2007). In general, the fracture connectivity is greater for thin beds where higher interaction between fracture sets and reservoir sequences is encountered (Chesnaux et al.,

2009). This may be, in parts, due to higher fracture densities encountered in thin beds where increased brittle deformation occurs compared to relatively thicker beds. See figure 2.5 for example.

### 2.2.4 *Discrete Fracture Network Upscaling*

In standard reservoir simulation applications that use conventional finite difference formulation, the DFN fracture representation is employed in dual continuum models. The effective properties for the fracture medium are obtained via analytical or flow based fracture upscaling methods (Dershowitz et al., 2000). Analytical upscaling methods such as the Oda (1985) method are usually preferred for field-scale applications due to the significant computational efficiency compared to flow-based upscaling, but can be inaccurate for poorly connected fracture networks (Ahmed-Elfeel and Geiger, 2012). Generally, the upscaling of the DFN must be done with utmost care to ensure that geological uncertainties captured in the DFN are not masked by uncertainties in the upscaling step. The effective fracture porosity, $\phi_f$, is calculated as:

$$\phi_f = P32 \times a_f \tag{2.5}$$

where, P32 represents the volumetric fracture intensity (total fracture area per unit volume) and $a_f$ denotes the fracture aperture.

### 2.2.5 *Oda Fracture Permeability Upscaling*

To compute the effective fracture permeability for a specific simulation grid cell from a DFN model, a permeability tensor, $F_{ij}$, which denotes flow along the fractures' unit normal, $n$, needs to be estimated. The tensor is calculated by summing over the individual fractures, $f$, in the grid cell provided the fracture area, $A_f$, and transmissibility, $T_f$, are known.

$$F_{ij} = \frac{1}{V} \sum_{f=1}^{N} A_f T_f n_{if} n_{jf}, \tag{2.6}$$

where the number of fractures is denoted by $N$, the fracture unit normal representing its direction and orientation is represented by $n$, and the total fracture pore volume is represented by $V$. If $F_{ij}$ is rotated into the planes of the permeability tensor by multiplication with $\delta_{ij}$, the fracture permeability can be approximated as (Dershowitz et al., 2000):

$$k_{ij} = \frac{1}{12}\left(F_{ff}\delta_{ij} - F_{ij}\right), \tag{2.7}$$

where $F_{ff}$ defines the principal directions of the permeability. The application of Oda's method is based on equation 2.7. A limitation of equation 2.7, however, is the assumption that fractures of any length will contribute to the upscaled permeability even if fractures do not form a percolating network in the grid block. Therefore a modified version of Oda's method was introduced for situations where fractures are not connected in a grid block (Golder-Associates, 2010):

$$k_{ij} = M\left(F_{ff}\delta_{ij} - F_{ij}\right) - MC\left(F_{ff}\delta_{ij} - F_{ij}\right), \qquad C \geq C_o, \tag{2.8}$$

where $M$ is a multiplier for scenarios where fractures are not connected and $C_o$ determines the threshold fracture connectivity.

### 2.2.6 *Flow-based Fracture Permeability Upscaling*

Flow-based upscaling is considered to be a more accurate, but more time consuming, fracture upscaling technique that can be used to evaluate DFN models and generate reference solutions (Ahmed-Elfeel and Geiger, 2012; Ahmed-Elfeel et al., 2013). During flow-based upscaling, fixed pressure or no flow boundary conditions are assigned to grid cells in the DFN model. The pressure field, $\nabla p$, and the total throughput, $q_t$, through the fractures in the reference grid cell is then obtained by single-phase flow simulation directly on the DFN. The pressures are computed at fracture intersections represented by nodes. Under incompressible flow, the mass balance at a given node implies that:

$$\sum_{i=1}^{I} q_{ij} = 0, \tag{2.9}$$

where $q_{ij}$ represents flow from node $i$ to node $j$. $I$ denotes the total number of nodes connected to $j$. Flow through the fractures is related to the pressure differential by:

$$q_{ij} = \frac{a_{f_{ij}}^2}{12\mu L_{ij}} \left(p_i - p_j\right), \tag{2.10}$$

where $a_{f_{ij}}^2$ represents the effective aperture of the link between $i$ and $j$, while, $L_{ij}$ and $p$ represent the corresponding length and nodal pressure, respectively. Subsequently, the upscaled effective permeability for porous media can be obtained by using Darcy's law and solving for the permeability:

$$K_{eff} = \frac{q_t \mu L}{\Delta p}, \tag{2.11}$$

where $\Delta p$ and $L$ denote the pressure difference and length, respectively, between the sides of the grid cells in the DFN model.

Various challenges affect flow-based upscaling and limit its application to field-scale reservoir studies. The challenges include sensitivity to the type of boundary conditions and significantly high computation cost during numerical simulation (Dershowitz et al., 2000; Ahmed-Elfeel and Geiger, 2012).

### 2.2.7 *Calibration of Discrete Fracture Network Models*

Stochastic representations of the fracture system using the DFN workflow often require calibration to static and dynamic field data. Static calibration to image log observations and well-fracture intersections is well established (Bourbiaux et al., 2002; Bush, 2010; Chandra et al., 2013; Ahmed-Elfeel et al., 2014). Static calibration can, therefore, indicate the validity of the static fracture model depending on the agreement between fracture observations in the field and fracture representation in the DFN model (Fig. 2.7).

Similarly, dynamic calibration requires a comparison of dynamic data (e.g., pressure transient or production data) in the field to dynamic data generated using the simulation model to ascertain and update the validity of the simula-

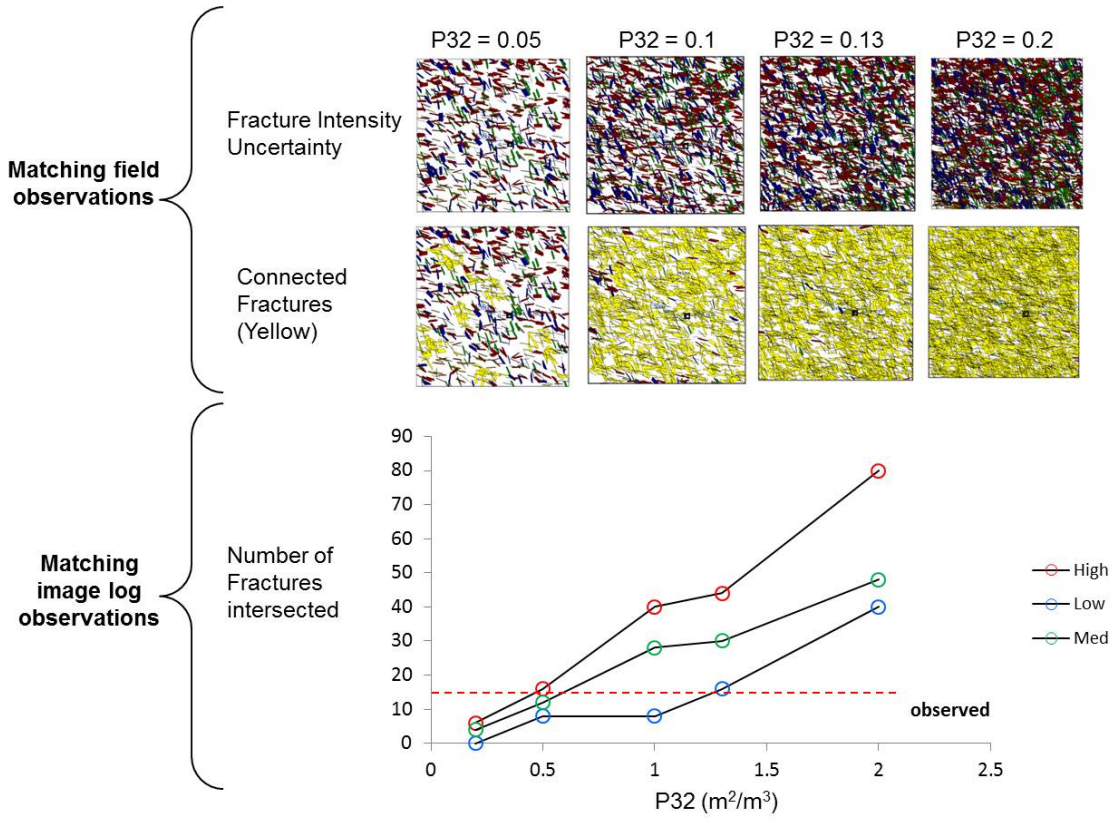


Figure 2.7: Static calibration of DFN models using image log observations and well-fracture intersections. Fracture intensity uncertainty is represented with multiple volumetric intensity, P32, scenarios. Low, medium and high DFN scenarios for each P32 are compared to observed well-fracture intersections. After Ahmed-Elfeel et al. (2014).

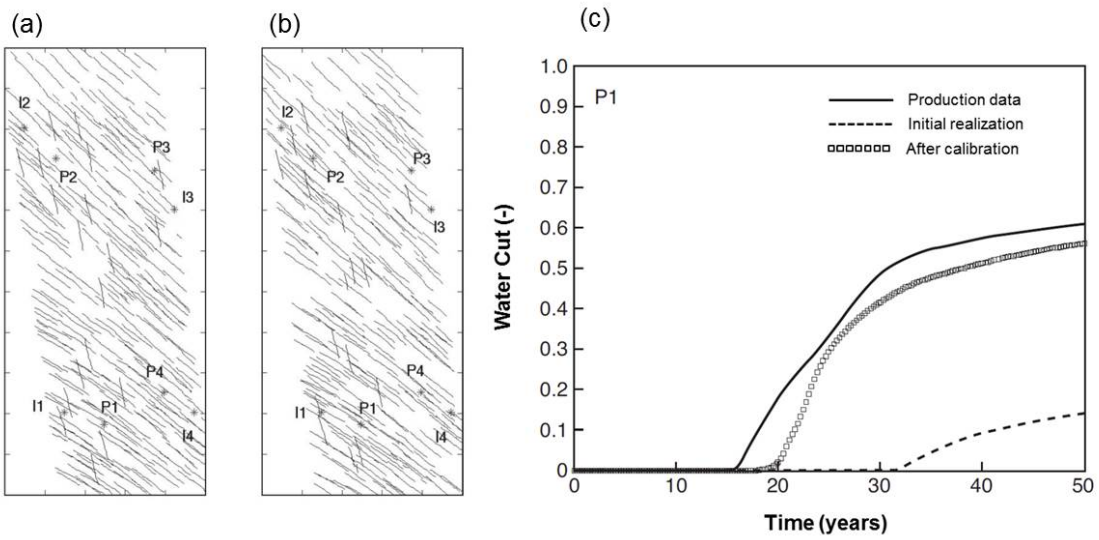


Figure 2.8: Initial fracture model (a) and fracture model after calibration with fracture attributes, geostatistical data and production data (b). Water cut profile indicates that the fracture calibration to static and dynamic data improves the predictability of the fracture model. Modified after Jenni et al. (2007).

tion model. Jenni et al. (2007) demonstrated the updating of a fracture model for a North African field initially developed stochastically from fracture/fault-related seismic attributes, fault-related strain field, structural information (e.g., curvature, fault proximity) and geostatistical data (e.g., fracture density, fracture orientation). By constraining the fracture network to production data, a more reliable description of the fracture network was obtained as indicated by improved water cut profiles (Fig. 2.8).

### 2.2.8 *Discrete Fracture Network Limitations*

DFNs are based on stochastic methods and lack dependence on geomechanical constraints, hence, they are limited in the extent to which they can represent fractures in the subsurface. As an alternative, Discrete Fracture and Matrix (DFM) models have received increasing attention as a means of accurately representing fracture networks (e.g., Matthäi et al., 2007; Geiger et al., 2009; Maier et al., 2013). DFM models generate deterministic representation of fractures and account for flow in both, the interconnected fractures and the rock matrix, using a combination of Finite Element (FE) and Finite Volume (FV) numerical approaches (e.g., Matthäi et al., 2007; Geiger et al., 2009; Geiger and Matthai, 2012). Fluid flow is computed directly and simultaneously in fractures, faults and rock matrix when using the DFM approach. The development and application of DFMs, however, still encounters several challenges, including extensive high computational cost and the need for complex time-consuming field application workflows.

### 2.2.9 *Wettability Considerations*

Flow in fractures and transport between the fracture and matrix is to a large degree influenced by the wettability. Knowledge of the wetting preference in a fractured carbonate reservoir is fundamental to understanding the flow behaviour during EOR. This is because the main recovery mechanisms in fractured formations (i.e. spontaneous imbibition and gravity drainage) are heavily influenced

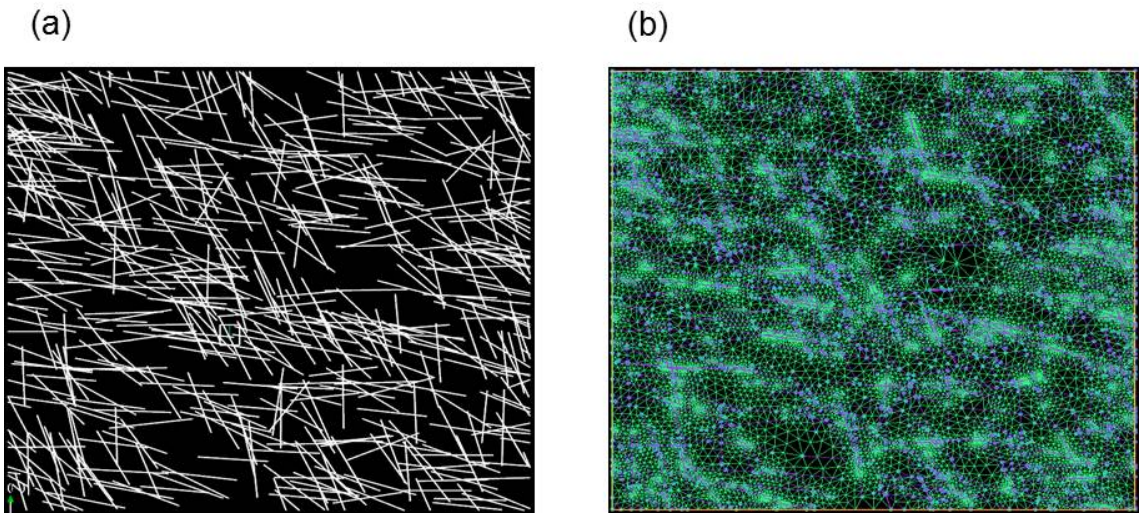


Figure 2.9: Discrete fracture network (DFN) model (a) and discrete fracture and matrix (DFM) model (b) for a simple 2D model. Note that DFM accounts for both fracture and matrix flow, while DFN only accounts for fracture flow. Courtesy, M. Ahmed.

by the wettability. A more water-wet rock will support efficient imbibition of water from the fractures to displace oil from the matrix through a counter-current or co-current mechanism. Hence, the oil recovery efficiency during water injection is highest for strongly water wet formations and decreases as the wettability changes to oil wet. Conversely, gas injection efficiency is limited by strongly water-wet conditions and enhanced by more oil-wet conditions. This is because strong water-wetness indicates high capillary entry pressures that oppose entry of gas into the matrix.

In addition to the aforementioned recovery mechanisms, several authors (e.g., Thomas et al., 1987; Hermansen et al., 1997; Agarwal et al., 2000; Aspenes et al., 2008) have suggested that a significant amount of capillary continuity between matrix blocks would allow viscous displacement of oil to provide an alternate path for oil recovery through the matrix pore network. Hence, fractured systems exhibiting high levels of capillary continuity that allows significant matrix-matrix viscous displacement may be treated as non-fractured systems during reservoir modelling and simulation. Capillary continuity preserves the hydraulic continuum in the water phase over the fractures and transfers the injection pressure needed for viscous oil recovery. Such viscous displacement due to capillary continuity has the best potential in more water-wet formations (Hermansen et al., 2000; Aspenes et al., 2008).

## 2.3 FLUID MODELS FOR NFR SIMULATION

### 2.3.1 *Black Oil Fluid Model*

The black oil model is a conventional thermodynamic model for compressible three-phase flow in a gas/oil/water system where the phase properties of the gaseous and oleic phases are known functions of pressure (Dake, 1998). The black oil mass conservation equation for each component (oil/water/gas) is defined such that the total mass of each component is conserved (Chen et al., 2006b). Lowercase and uppercase subscripts are used to denote phases and components, respectively. The water phase consists only of the water component, while the oil phase consists of both the oil and gas components.
The mass conservation equations for the phases can be described as:

$$\frac{\partial \left(\phi \rho_w S_w\right)}{\partial t} = -\nabla . \left(\rho_w v_w\right) + q_w \tag{2.12}$$

$$\frac{\partial \left(\phi \rho_{o_o} S_o\right)}{\partial t} = -\nabla . \left(\rho_{o_o} v_o\right) + q_o \tag{2.13}$$

$$\frac{\partial}{\partial t}\left(\phi \left(\rho_{G_o} S_o + \rho_g S_g\right)\right) = -\nabla . \left(\rho_{G_o} v_o + \rho_g v_g\right) + q_g \tag{2.14}$$

for the water, oil and gas components, where, $\rho_{G_o}$ and $\rho_{O_o}$ denote the partial densities of the gas and oil components in the oil phase, respectively. $\phi$, $\rho$, $S$, $v$, and $q$ represent the porosity, density, saturation, velocity and source/sink term respectively. Equation 2.14 indicates that the gas component exists in both the oil and gas phases.
Therefore, Darcy's law for each phase can be written as:

$$v_\alpha = -\frac{k_{r\alpha}}{\mu_\alpha} K \left(\nabla P_\alpha - \rho_\alpha \gamma \nabla z\right), \qquad \alpha = w, o, g, \tag{2.15}$$

where, $K$, $\gamma$ and $\nabla z$ denote the total permeability, gravity term and depth respectively. Similarly, $k_r$, $\mu$ and $\nabla P$ denote the phase relative permeability, phase

viscosity and phase pressure change respectively. The phase pressures are related by capillary pressures, $P_c$, where,

$$P_{cow} = P_o - P_w, \qquad P_{cgo} = P_g - P_o \tag{2.16}$$

The contribution of each phase is given by equation:

$$S_w + S_o + S_g = 1 \tag{2.17}$$

### 2.3.2 *Compositional Fluid Model*

Compositional simulations can capture complex interactions of flow with phase behaviour but are also computationally expensive for large fractured reservoirs because equation of state calculations, multi-component interactions and fracture-matrix exchange must be represented. A finite number of hydrocarbon components, $N_c$, are used to represent reservoir fluid composition during compositional modelling (Chen et al., 2006b). If $\xi_{io}$ and $\xi_{ig}$ are the molar densities of component $i$ in the liquid and gaseous phases and $W_i$ is the molar mass of component $i$, then $\xi_i$ and $W_i$ for all phases can be related:

$$\xi_{i\alpha} = \frac{\rho_{i\alpha}}{W_i}, \qquad i = 1, 2, 3, ..., N_c, \tag{2.18}$$

where $\rho_{i\alpha}$ is the mass density of each phase. Hence, the molar density of phase $\alpha$ is:

$$\xi_\alpha = \sum_{i=1}^{N_c} \xi_{i\alpha}, \qquad \alpha = o, g. \tag{2.19}$$

The mole fraction of component $i$ in phase $\alpha$ can then be written as:

$$x_{i\alpha} = \frac{\xi_{i\alpha}}{\xi_\alpha}, \qquad i = 1, 2, 3, ..., N_c, \qquad \alpha = o, g. \tag{2.20}$$

Due to the mass interchange between phases, mass is not conserved within each phase, rather the total mass is conserved for each component (Chen et al., 2006b) and written as:

$$\frac{\partial\left(\phi\xi_w S_w\right)}{\partial t} + \nabla.\left(\xi_w v_w\right) = q_w, \tag{2.21}$$

$$\frac{\partial\left(\phi\left[x_{io}\xi_o S_o + x_{ig}\xi_g S_g\right]\right)}{\partial t} + \nabla.\left(x_{io}\xi_o v_o + x_{ig}\xi_g v_g\right) + \nabla.\left(d_{io} + d_{ig}\right) = q_i, \tag{2.22}$$

$$\sum_{i=1}^{N_c} x_{io} = 1, \qquad \sum_{i=1}^{N_c} x_{ig} = 1. \tag{2.23}$$

where $q_w$ and $q_i$ are the molar flow rates of water and the $i$th component, respectively, while $d_{i\alpha}$ defines the diffusive flux of the $i$th component in the $\alpha$-phase, where $\alpha = o, g$. In addition to the partial differential equations 2.21 and 2.22, equations 2.23, 2.16 and 2.17 indicate algebraic constraints that must be adhered to for the mole fraction, phase pressures and saturation balance respectively (Chen et al., 2006b).

### 2.3.3 *Miscibility Considerations*

Miscible displacement processes have been shown to improve microscopic sweep efficiency in subsurface reservoirs (Healy et al., 1994; Taber et al., 1997; Bon et al., 2005; Bourdarot and Ghedan, 2011). In a miscible displacement process, two fluids form a single homogeneous phase when mixed in all proportions (Holm, 1986; Bourdarot and Ghedan, 2011). Miscible processes occur when the reservoir pressure is above the minimum miscibility pressure (MMP) for a given injection gas and in-situ oil composition (Taber et al., 1997). When the fluids are fully miscible, the interfacial tension between them reduces to zero, capillary forces are eliminated and under idealized conditions, the residual oil saturation is reduced to zero in the swept region, leading to significantly higher oil recoveries.

Miscible displacement in oil reservoirs results in complex interactions of flow with phase behaviour that are best modelled with compositional simulation (Zick, 1986; Johns et al., 2002; Christensen et al., 2001; Egwuenu et al., 2008). Pseudo-miscible models have also been developed that capture miscibility during black oil simulation, but such models are lacking in their capacity to represent laboratory experiments of miscibility (CMG, 2014). Further detail on miscibility and its impact on reservoir simulation and prediction is presented in Chapter 4.

## 2.4 DESCRIPTION OF ROCK WETTABILITY

### 2.4.1 *Corey Formulation*

The oil-water and gas-oil two-phase relative permeability and capillary pressure curves for the matrix can be generated using Corey (1954) relationships. The parameters of the Corey formulation can be adjusted to match field data or extended to evaluate the effects of end-member wettability scenarios. The Corey formulation for oil-water and gas-oil relative permeability and capillary pressures are described as:

$$k_{rw} = k_{rw,max} \left( \frac{S_w - S_{wi}}{1 - S_{wi} - S_{orw}} \right)^m , \tag{2.24}$$

$$k_{ro} = \left( \frac{1 - S_w - S_{orw}}{1 - S_{wi} - S_{orw}} \right)^n , \tag{2.25}$$

$$P_c = P_e \left( S_{wn} \right)^{-\frac{1}{\lambda}} , \tag{2.26}$$

where, $m$ and $n$ are the Corey exponents for oil-water relative permeability (eqn. 2.24) and gas-oil relative permeability (eqn. 2.25) respectively. $P_c$ and $P_e$ denote the capillary pressure and the threshold capillary entry pressure, respectively. $\lambda$

represents the pore size distribution index, while $S_{wn}$ denotes the normalized water saturation described by:

$$S_{wn} = \left( \frac{S_w - S_{wir}}{1 - S_{wir}} \right), \tag{2.27}$$

where, $S_w$ is the water saturation and $S_{wir}$ is the irreducible water saturation.

The choice of the Corey formulation followed the work of Clerke (2009) who used the Corey equations to match a large body of relative permeability data for carbonate rocks in the Middle East analogous to the confidential subsurface data that formed the basis of the models in this thesis. It was also found that the Corey formulation matched the relative permeability data employed in this thesis.

Straight line (i.e. linear) two-phase relative permeabilities first introduced by Romm (1966) are traditionally used for multiphase flow in the fractures. More recently, several authors (e.g., Murphy and Thomson, 1993; Speyer et al., 2007; Chima and Geiger, 2012; Li et al., 2014) have suggested from experimental and numerical observations that two-phase fracture relative permeabilities may be non-linear. Both representations of fracture relative permeability were tested in this thesis, but the results were identical. Hence, straight line two-phase fracture relative permeability curves were used throughout this thesis.

### 2.4.2 *Three Phase Relative Permeability*

To compute three-phase relative permeabilities that account for multiphase flow interactions in the three-phase flow regions generated during enhanced oil recovery, traditional interpolation models (e.g., Stone, 1970, 1973; Baker, 1988) are frequently used. The Stone II interpolation model (Stone, 1973), which computes three-phase relative permeabilities while offering a relatively more predictive de-

scription of residual oil saturation, was used throughout this thesis. In normalized form, the Stone II model is given by:

$$k_{ro} = k_{ro(cw)} \left( \left( \frac{k^i_{ro(w)}}{k_{ro(cw)}} + k^d_{rw(o)} \right) \left( \frac{k^d_{ro(g)}}{k_{ro(cw)}} + k^d_{rg(o)} \right) \right), \tag{2.28}$$

where the superscripts $i$ and $d$ refer to imbibition and drainage respectively. Similarly, the subscripts $o$, $w$, $g$ and $cw$ refer to oil, water, gas and connate-water respectively. $k_r$ represents the relative permeability.

#### 2.4.2.1 *Pore Network Models*

More recently, pore-network models have been used to provide a physically consistent description of three phase relative permeabilities (Blunt, 2000; Piri and Blunt, 2005; Al-Dhahli et al., 2013, 2014). Such pore network models encapsulate microscopic displacement processes that have been observed in laboratory experiments of three phase flow. They also use realistic 3D pore structures (Fig. 2.10) to account for the complexity of real reservoir rocks. Pore-network models have been benchmarked successfully against three-phase flow experiments, showing good agreement between numerical and experimental data.

Recent simulations of EOR at the intermediate grid-block scale (Ahmed-Elfeel et al., 2013), sector scale (Jiang et al., 2013), and reservoir scale (Al-Dhahli, 2013) show that the traditional interpolation models over-predict oil recovery when compared to the 3D pore network models. This is because the interpolation models do not adequately capture the intrinsic pore scale physics during three-phase flow and tend to over-predict oil relative permeabilities at low oil saturation. However, generating workflows to adequately integrate pore network models with conventional simulation approaches especially for fractured carbonates, remains an active area of research (Blunt, 2001; Holm et al., 2010; Al-Dhahli et al., 2013; Blunt et al., 2013; Ryazanov et al., 2014). Specifically, limitations exist in the network extraction step because current workflows fail to capture network heterogeneity at the appropriate scale for carbonates and may be inadequate to represent micro-scale heterogeneities. Furthermore, traditional interpolation

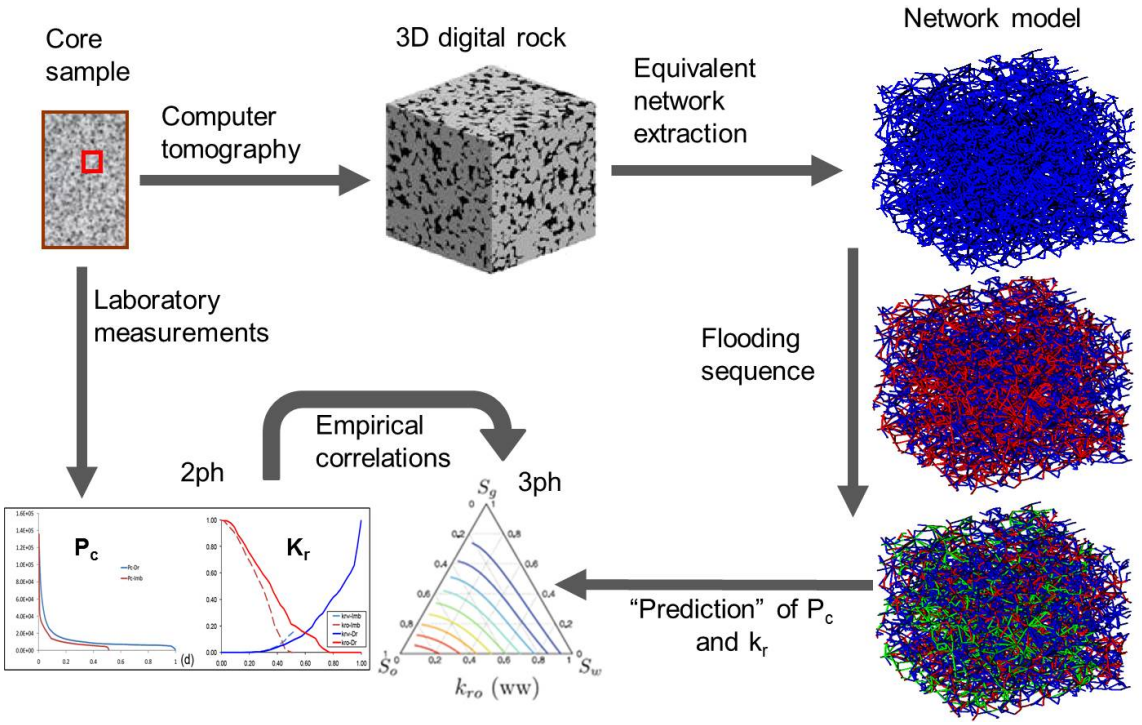


Figure 2.10: Three-phase pore network modelling workflow to obtain relative permeability and capillary pressures as an alternative to traditional interpolation models. After Al-Dhahli (2013).

models, such as the Stone II model, are more practical for the time-consuming continuum-scale models encountered in this thesis.

### 2.4.3 *Relative Permeability Hysteresis*

During cyclic EOR processes such as water-alternating-gas injection (WAG), relative permeabilities typically show dependence on the saturation path. This dependence (or hysteresis) occurs due to residual trapping of gas during repeat drainage and imbibition cycles (Fig. 2.11) and needs to be captured in reservoir simulation models. Hysteresis is discussed extensively in Chapter 5. Here, the Killough (1976) hysteresis model which is used throughout this thesis is presented. The Killough hysteresis formulation given by:

$$k^i_{rg}\left(S_g\right) = k^i_{rg}\left(S^*_g\right)\frac{k^d_{rg}\left(S_{gi}\right)}{k^d_{rg}\left(S_{gi,max}\right)}, \tag{2.29}$$

where,

$$S_g^* = S_{gt,max} + \frac{\left(S_g - S_{gt}\right)\left(S_{gi,max} - S_{gt,max}\right)}{S_{gi} - S_{gt}}, \tag{2.30}$$

where the superscripts $i$ and $d$ refer to imbibition and drainage respectively. Similarly, subscripts $i$ and $t$ refer to the initial and total gas saturation ($S_g$) respectively. $k_{rg}$ represents the gas relative permeability.

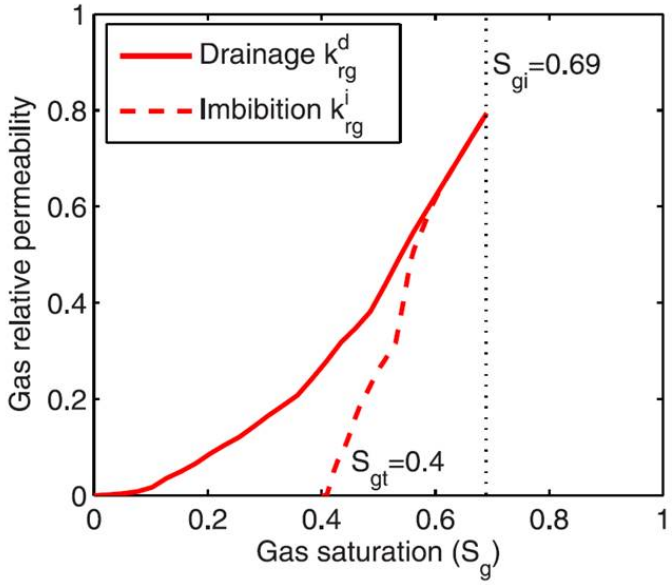


Figure 2.11: Gas relative permeability curves indicating hysteresis during drainage and imbibition cycles. $S_{gi}$ represents the initial gas saturation while $S_{gt}$ denotes the trapped gas saturation. After Juanes et al. (2006).

## 2.5 MANAGING COMPUTATIONAL TIME

Fractured reservoir simulation is typically time-consuming because of the various complexities (e.g. geological heterogeneity, fluid models, fracture-matrix exchange) that must be taken into account. Table 2.1 shows the computational time for various levels of complexity that are considered in fractured reservoir simulation and indicates that up to 40 days simulation time can be encountered to incorporate high levels of computational complexity in a single simulation evaluation. Hence, it was necessary at various points during this thesis to reduce the total level of complexity in order to understand critical subsurface flow mechanisms and guiding principles. Some of the measures employed include

the use of matrix upscaling, sector models, simplified fluid models, surrogate (proxy) models and parallel computing using high performance clusters.

| Simulation model | Model type | Fluid description | Run time (days) |
|---|---|---|---|
| Matrix | Sector | Black Oil | 0.04 |
| Matrix | Sector | Compositional | 0.13 |
| Matrix | Full-field | Black Oil | 0.10 |
| Matrix | Full-field | Compositional | 0.40 |
| Matrix w/Fractures | Sector | Black Oil | 0.90 |
| Matrix w/Fractures | Sector | Compositional | 13.30 |
| Matrix w/Fractures | Full-field | Black Oil | 2.80 |
| Matrix w/Fractures | Full-field | Compositional | 39.80 |

Table 2.1: Computational time for EOR simulations. Sector model consists of 42,840 grid cells while full-field model consists of 199,800 grid cells. When fractures are considered, the number of grid cells for each scenario is doubled. Computer Modelling Group's IMEX and GEM are used for black oil and compositional simulations respectively. Each simulation is run in parallel with four processors.

### 2.5.1 *Matrix Upscaling*

To subject a static geological model to dynamic modelling of relevant fluid flow processes, a coarser grid is typically required to reduce computational costs. The process of coarsening the grid, while simultaneously averaging the grid flow properties (i.e. porosity and directional permeability), is referred to as matrix upscaling. The averaging may be uniform across the grid cells or non-uniform to account for local heterogeneities (e.g. due to layering).

#### 2.5.1.1 *Matrix upscaling validation with streamline simulation*

Upscaling techniques (i.e. analytical and numerical) have been applied and tested successfully in heterogeneous (carbonate) reservoirs (e.g., Li and Beckner, 2000; Christie and Blunt, 2001; King et al., 2006; Zhang et al., 2008). The accuracy of the upscaled models must then be confirmed with validation techniques such as streamline simulation (e.g., Samier et al., 2002; Ates et al., 2005; Datta-Gupta and King, 2007; Thiele et al., 2011).

Figure 2.12 illustrates the use of streamline simulation to validate the accuracy of upscaled representations of a fine grid geological model. Using a quarter 5-spot well pattern, water is injected from the bottom left of the model which then displaces oil to the producer at the top right. Streamline simulation using FRONTSIM$^{TM}$ indicates that the displacement streamline flow pattern is preserved in both the fine grid model and the upscaled models thereby validating the upscaling accuracy.

As the fine grid model is upscaled by a factor of 20 and 30 respectively (Fig. 2.12c, d), some degree of numerical dispersion can be observed in the bottom right of the streamline profiles. Numerical dispersion is due to discontinuities in the saturation front due to changes in the numerical discretization (Li and Beckner, 2000; King et al., 2006; Thiele et al., 2011). Dynamic (adaptive) grid refinement has been identified as a means of refining the flow simulation grid at the saturation front to reduce the effect of numerical dispersion, while reducing the computational time. The application of advanced algorithms for dynamic grid refinement during EOR is, however, not within the scope of this thesis.

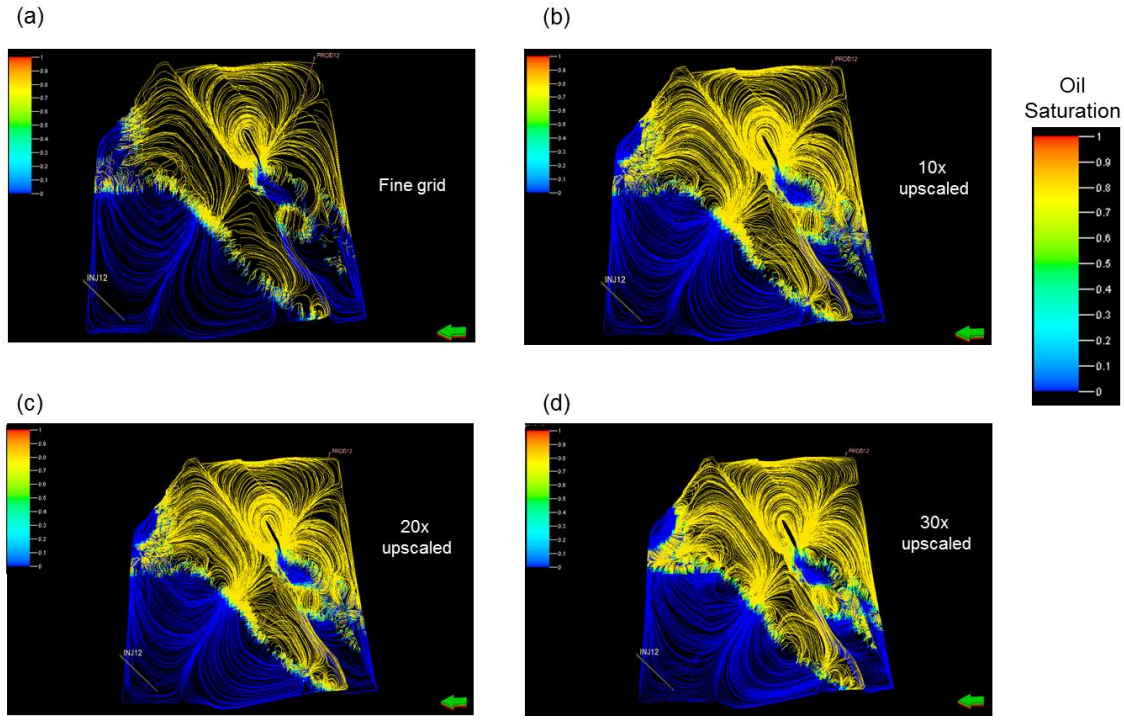


Figure 2.12: Streamline validation to ensure that upscaled model captures the flow pattern in the fine model. Oil saturation streamlines indicate that the displacement flow pattern is preserved after upscaling.

#### 2.5.1.2 *Matrix upscaling validation with finite difference simulation*

The validity of matrix upscaling can also be evaluated by comparing finite different simulations using the fine and upscaled models. Subsequently, the oil recovery and oil production rate of the fine and upscaled models can be compared for a given recovery mechanism (e.g., secondary water injection) to give an indication of the upscaling accuracy for the matrix (Fig. 2.13).

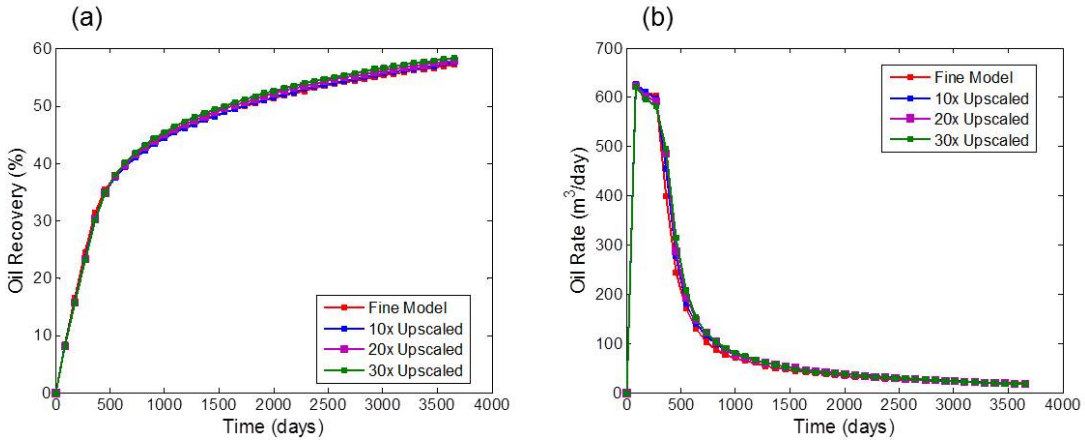


Figure 2.13: Validation with finite difference simulation to ensure that upscaled model represents fine scale model when oil recovery (a) and oil rate (b) profiles are compared. Simulation results indicate that the flow response is preserved after upscaling.

The geological model employed in this thesis was upscaled vertically by a factor of 10 for numerical well-testing and secondary recovery simulations (chapter 3), and by a factor of 30 (chapters 4, 5 and 6) to simulate more complicated EOR processes such as miscible gas injection, water-alternating-gas (WAG) injection and foam displacement. In all cases the flow response of the models was preserved after upscaling (Fig. 2.12 and 2.13).

### 2.5.2 *Sector Models*

Another means of managing the computational time to ensure that investigators evaluate key recovery mechanisms is to use a sector delineated from the dynamic simulation model. Multiple simulations can then be carried out on the sector

model to test important enhanced oil recovery processes. Sector models were employed in chapters 4 and 6 of this thesis.

### 2.5.3 *Simplified Fluid Models*

Compositional fluid models require the flow equations to be evaluated for a given number of components. Hence, reducing the number of components in the reservoir fluid model (i.e. component lumping) decreases the computational cost. Furthermore, black oil models that represent the reservoir fluid with dead oil and solution gas reduce the computational cost significantly and may be sufficient for many applications. Component lumping was employed to set-up the compositional simulations in chapter 4, while, black oil fluid models were used in chapters 3, 5 and 6.

### 2.5.4 *Surrogate (Proxy) Models*

Finally, surrogate (proxy) models (Fig. 2.14) that generate an approximation of the full-physics simulation model by using a limited number of experimentally designed simulations can be used for rapid simulation, evaluation and optimisation under uncertainty and significantly reduce the overall computational cost of fractured reservoir simulation. Surrogate modelling and optimisation is discussed in chapter 6.

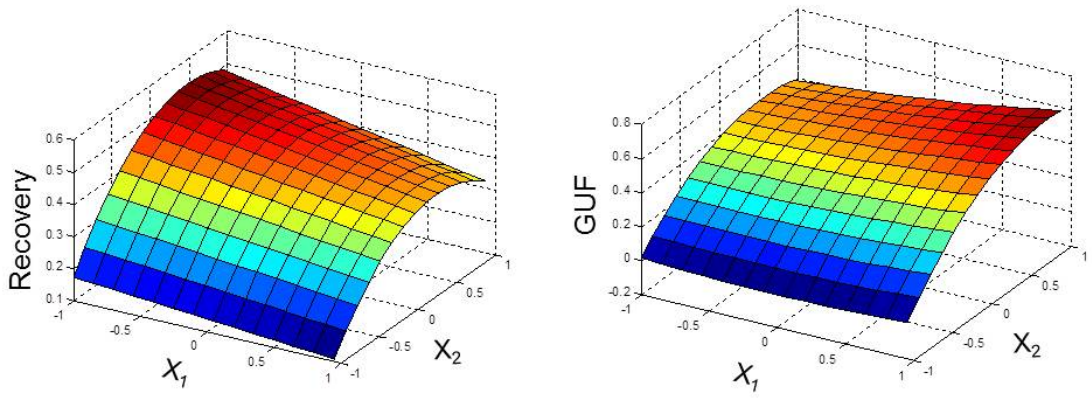


Figure 2.14: Surrogate model response surface approximation of full-physics simulations to evaluate the oil recovery and gas utilisation (GUF) based on uncertain parameters $X_1$ and $X_2$.

# 3

# DECIPHERING THE FUNDAMENTAL CONTROLS OF FLOW IN CARBONATES USING NUMERICAL WELL TESTING AND PRODUCTION OPTIMISATION

## 3.1 INTRODUCTION

Digital outcrop models have been used for numerical well test analysis, an approach that is also commonly referred to as geological well testing (Massonat and Bandizol, 1991). During numerical well test analysis, the propagation of a pressure front due to changes in flow rate at a producing or injecting well in a reservoir or outcrop model is simulated. Simulation results yield a numerically generated pressure response at the well, commonly referred to as a 'pressure transient'. Pressure transients can be evaluated by standard well-test analysis procedure in reservoir engineering. The analysis enables us to extract key reservoir performance indicators such as the drainage area of the well, permeability and skin factor (Bourdet, 2002). During numerical well-testing, systematic responses in the pressure transients are generated for different geological realisations. Performing pressure transient analysis numerically, using digital outcrop models, enables us to link known geological structures directly to the transient pressure response and therefore investigate how different geological structures that have been observed in the outcrop may impact reservoir performance (Corbett et al., 2012).

Numerical well-testing has three key benefits that are closely related: First, by systematically including or excluding certain geological features observed in the outcrop, it is possible to generate 'type curves' for the pressure response

and to analyse how readily the geological structures can be distinguished using well-test analysis in real fields and how they could affect reservoir performance. Secondly, the theoretical pressure responses (e.g. linear flow and recharge in a high-permeability fracture), which are derived for idealised geological structures, can be validated by comparing them to the pressure responses obtained for realistic geological structures. Third, knowledge obtained from numerical well-test analysis can be employed to improve the calibration of static and dynamic reservoir models with production data (Rawnsley and Wei, 2001; Corbett, 2009; Chandra et al., 2013).

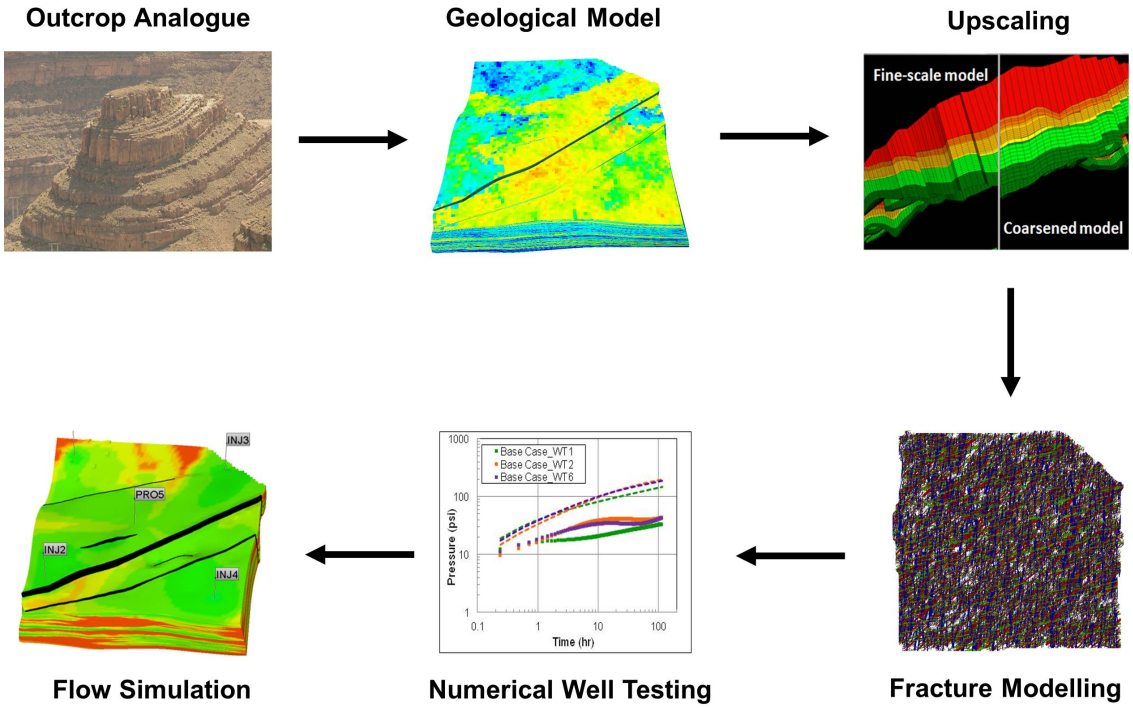


Figure 3.1: Geoengineering workflow utilised in this chapter, linking field data from 3D outcrop models to well test analysis and flow simulation. Simulation results can be interpreted in the context of the sedimentological, diagenetic, and structural features that have been observed in the outcrop.

In the context of outcrop-based flow modelling, the contribution of this chapter is two-fold. Firstly, an outcrop-based 3D high-resolution analogue model of unprecedented quality for a Jurassic carbonate ramp (Shekhar et al., 2010; Christ et al., 2012; Amour et al., 2013) is used to perform numerical well test analysis and black oil simulations of secondary hydrocarbon recovery. As discussed above, by using numerical well testing for this outcrop analogue the aim is to link the observed geological structures directly to the transient pressure

response and investigate how these structures could impact the reservoir performance. Secondly, the chapter focuses on analysing how recovery changes when different injection fluids and well patterns are used to simulate secondary recovery. The aim is to highlight how certain reservoir engineering measures can be used to increase recovery in the presence of geological heterogeneities that commonly occur in a carbonate reservoir. This geoengineering workflow (Corbett et al., 2012; Chandra et al., 2013) is employed to study how small-scale heterogeneities typical for this carbonate reservoir setting impact fluid flow behaviour and hydrocarbon production (Fig. 3.1).

## 3.2 OVERVIEW OF THE OUTCROP GEOLOGY

The Amellago Canyon outcrop (Fig. 3.2a) of a Middle Jurassic carbonate ramp in the High Atlas Mountains of Morocco, is used as an analogue reservoir for the flow simulations in this thesis. The outcrops can be considered as a reservoir analogue for tidal- and wave-dominated, peloidal oolitic shoal bodies deposited in a low-angle carbonate ramp setting, similar to the deposits of the Jurassic Arab Formation in Qatar (Al-Saad and Ibrahim, 2005). Such carbonate reservoirs display a layer-cake stratigraphic architecture with sheet-like grainstone geobodies few meters thick and from few to tens of kilometres long.

Carbonate strata in the Amellago canyon are exposed continuously over many kilometres. Stratigraphic features characteristic of the depositional environment are evident at sub-metre to kilometre scales. Most of the outcrops are weakly deformed. Deformation intensifies close to low-offset, oblique reverse and normal faults, both within fault damage zones (most are less than 1 meter wide) and localized, fault-related flexures (Agar et al., 2010; Pierre et al., 2010; Amour et al., 2013). The outcrop that forms the basis of these models is referred to here as the Island outcrop. This is an elliptical outcrop isolated by fluvial erosion in the Amellago Canyon. The Island exposes the Middle to Upper Bajocian Assoul Formation (Fig. 3.2b), a shallow-water carbonate ramp, which provides the analogue for stratigraphy and diagenesis in this study.

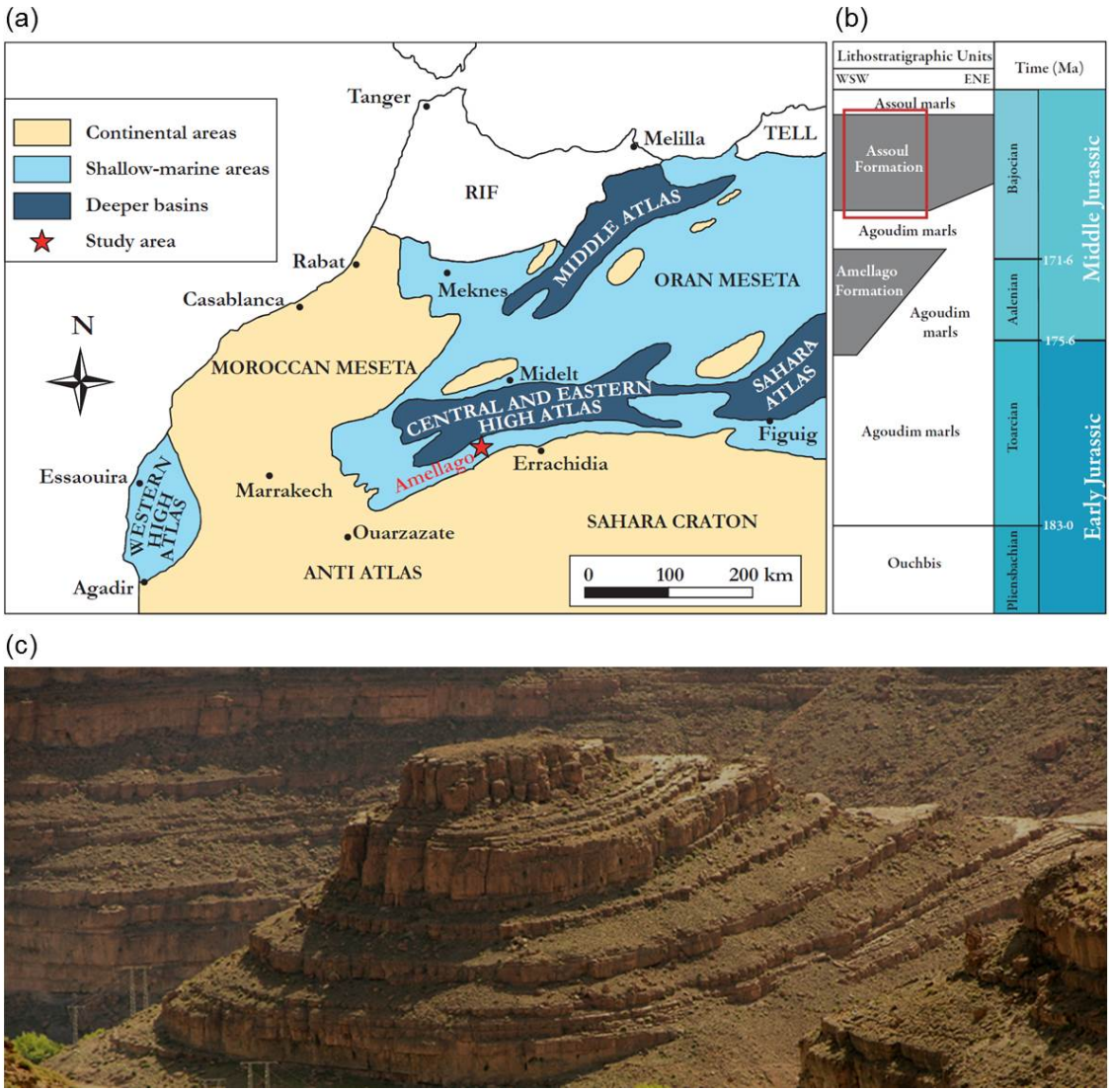


Figure 3.2: (a) Location of study area (red star). (b) Simplified stratigraphic setting. The outcrops of the Amellago Canyon are part of the Middle Jurassic Assoul Formation (red box), a stratigraphic interval dominated by shallow-water carbonate deposits such as ooid and peloidal grainstone. (c) Aerial view of the Island window of the Amellago Canyon outcrop. Note the power-lines in the lower left for scale. Modified after Christ et al. (2012).

The Assoul Formation reaches a stratigraphic thickness of 300m and represents a grainy carbonate ramp system that prograded north-east ward into the subsiding basin (Poisson et al., 1998; Pierre et al., 2010; Christ et al., 2012; Amour et al., 2013). The dominant facies include ooidal and peloidal grainstones, bioclastic wackstones and packstones, and bioclastic floatstones and rudstones. The depositional profile of the ramp consists of oolitic and peloidal shoals in the inner ramp, which grade basinward to mud-dominated facies with debris of gastropods, bivalves, and corals in the middle ramp and to alternating mudstone and marl in the outer ramp (Christ et al., 2012; Amour et al., 2012). Tidally influ-

enced shoal, wave influenced shoal and coarse-grained shoal comprise the main facies types in the inner ramp deposits. They exhibit decimetre-sized asymmetrical, symmetrical and bi-directional ripples as well as metre-scale cross bedding. The carbonate ramp is characterised by lithological heterogeneity exemplified by coral patch reefs, mud mounds (Tomás et al., 2013), regionally significant discontinuity surfaces in the form of early marine hardgrounds, bedding-related layering, penetrative fracture networks and vertical variations in grain size and texture (Fig. 3.2c).

In addition to the sedimentological heterogeneity, the Island outcrop also exposes two main structural systems: a network of faults that has been mapped using high-resolution photopanels and LiDAR data and fractures (bed-bound and inter-bedded) whose characteristics (orientations, spacings, apertures and fill) have been analysed with detailed photomapping and scanlines in a series of seven outcrop windows. These windows (approx. 5 m high by 30 m long) were selected to represent fracture populations in distinct facies. Several low-offset (on the order of 1 m or less) oblique-normal and oblique-reverse faults dissect the Island.

One of the most pronounced faults is located at the south end of the Island. On the Island, this fault has an apparent normal displacement of approximately 10 metres with the downthrown side to the south. In the subsurface, such faults can impact fluid flow by the extent to which the fault zone materials affect cross-fault flow (e.g., the properties of fault gouge, cementation within the fault and/or fault damage zones). There may be minimal impact or the fault-zone properties may act as seals or baffles that compartmentalize the reservoir on production timescales. If the fault has little or no gouge or cement, then it may act as a large open fracture, providing a preferential flow pathway during production. This study examines variations in fault transmissibility, but does not attempt to simulate the case of the fault acting as a large open fracture (e.g., Agar et al., 2010).

Over 1200 fractures were measured on the outcrop, some of which are cemented by calcite and/or dolomite (Shekhar et al., 2010). Although, the highest

measured fracture intensities occur close to low-offset faults, there is no clear gradient or logarithmic variation of intensity away from the fault. Instead, in the few instances where increases in deformation do occur, there is an abrupt transition from a thin (less than 1m) zone of higher intensity fracturing to the 'background' fracture intensity that is representative of most of the Island outcrop. The fractures formed over multiple scales ranging from fine scale fractures restricted to individual beds (approx. 0.5m - 2m) to fracture corridors that extend across the entire vertical extent of the outcrop (approx. 100m). In addition to fractures, stylolites have also been observed in the outcrops. In a few instances on the Island outcrop, fractures were seen to terminate against moderately dipping stylolites. This relationship has also been observed in other outcrops in the Amellago Canyon and suggests that at least some of the fractures pre-date stylolites that probably formed during contraction of the Atlas Mountains.

## 3.3 GEOLOGICAL MODEL

### 3.3.1 *Matrix Modelling*

This study uses a 3D high-resolution geological model developed for the Assoul Formation ramp by Shekhar et al. (2010) and Amour et al. (2013). The outcrop topography was determined from GPS and Laser Range Finder data. Major bedding surfaces were identified in the field and mapped using GPS. The model contains twelve lithofacies based on the Dunham (1962) classification. Each lithofacies can be grouped into three depositional environments: inner ramp, proximal middle ramp, and distal middle to outer ramp.

The lithofacies distribution was simulated in PETREL$^{TM}$ using a scale-dependent modelling approach developed by Amour et al. (2013). Porosity was assigned stochastically to the lithofacies. Permeability-porosity transforms, based on the Dunham (1962) classification and statistical analysis of subsurface reservoirs, were used to model the permeability field. This porosity-permeability modelling approach was needed because the outcrop rocks have undergone significant post-depositional diagenetic alteration, which occludes most of the original poros-

ity. Therefore, porosities and permeabilities measured for the outcrop rocks are likely not representative of a subsurface reservoir.

Subsurface data were selected based on information from the Arab D formation in Qatar. The chosen data were relevant because, as discussed above, the sedimentological and diagenetic features closely matched the Amellago platform. A standardized method for estimating porosity and permeability properties was required to produce geomodels for flow simulation for several very different settings, and produce flow simulation results to test differences in facies architecture, fracturing, and early diagenetic overprinting. Therefore, a proprietary Standard Property Calculator (SPC) was used to assign standardised values to similar rocks from separate locations. The SPC ensured that reservoir quality was held constant so that architectural elements of the study areas could be investigated.

The SPC is a spreadsheet application calibrated to Mesozoic rocks from the Middle East. The calibration process involved multivariate linear regression using as independent variables various indices of abundance for sedimentary fabric elements like grain size, sorting, cementation, and vuggy porosity. To estimate the reservoir properties of an analogue rock type, the observed abundances of these fabric elements are needed. The application produces five summary statistics for them that provide the input for geostatistical algorithms that enable us to populate the model with porosity and permeability. These summary statistics are (1) average porosity, (2) standard deviation of porosity, (3) log-log porosity-permeability transform slope, (4) log-log porosity-permeability transform intercept, and (5) the standard deviation of the log permeability with respect to the transform. After generating a facies model, each facies was transformed into petrophysical properties according to its specific permeability and porosity values, which were applied to the grid blocks of the geo-cellular model (Amour et al., 2013). Scatter was added to the porosity and permeability values, which is considered typical of such data in subsurface reservoirs, when each facies was transformed into petrophysical properties.

The hardground surfaces are 10 to 30 cm thick and laterally continuous across the entire study area, such that they were deterministically included as a layer or layers of cells in the model. Christ et al. (2012) described three types of condensed surfaces, which differ in their degree of synsedimentary lithification of the seafloor. The increase of the degree of lithification leads to a decrease of the porosity and permeability values caused by cementation processes at the seafloor during periods of sediment starvation. Hence, different porosity and permeability values were assigned to layers of cells along each type of surface (Amour et al., 2013).

This workflow resulted in a geo-cellular geological model with dimensions of 1.15 km x 1.17 km x 0.11 km, containing 74 x 75 x 1099 grid cells (6,099,450 cells in total) (Fig. 3.3). Individual cells have dimensions of 15m x 15m x 0.1m. Eight stratigraphic zones were delineated in the model. Each consists of grid cells with a similar range of properties. Several high-angle normal faults, which offset low- and high-permeability layers, were also represented in the model. A coefficient of variation ($C_v$) of 2.048 for the model permeability illustrates the high degree of heterogeneity in the model (Jensen et al., 1997).

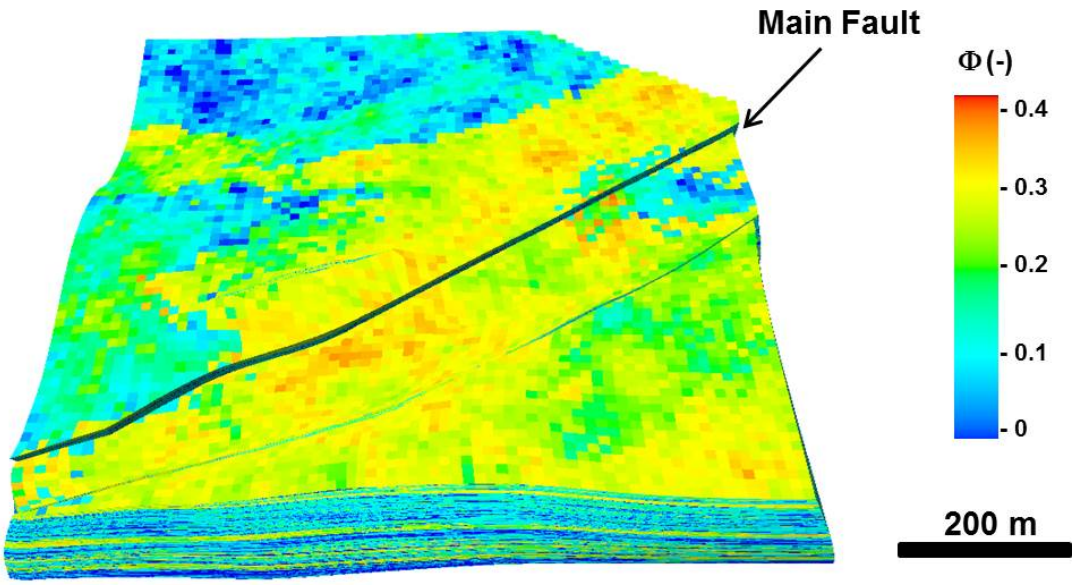


Figure 3.3: High-resolution 3D geo-cellular model of the Assoul Formation ramp exposed in the Amellago canyon outcrops (Fig. 2), showing the simulated porosity distribution. The model dimensions are 1.15 x 1.17 x 0.11 km. Individual cells have dimensions of 15 x 15 x 0.1 m. After Amour et al. (2013).

The geological model was upscaled vertically for flow simulations by a factor 10 using non-uniform upgridding and flow-based upscaling, resulting in a flow simulation model containing 74 x 75 x 110 grid cells (610,500 grid cells in total). The upscaled flow simulation model was validated against the fine-scale geological model using streamline simulations for the full model and finite difference simulations for representative model sub-regions. The validation ensured that the same flow response was obtained for the flow simulation and geological model, therefore, no significant loss in heterogeneity occurred, while computational costs for the flow simulations became tractable (Toigulova, 2012).

| Realisation | Base | Diagenesis | Mud Mound | Oyster Bioherms |
|---|---|---|---|---|
| 1 | Amellago Model | N | N | N |
| 2 | Amellago Model | Y | N | N |
| 3 | Amellago Model | N | Y | N |
| 4 | Amellago Model | Y | Y | N |
| 5 | Amellago Model | N | N | Y |
| 6 | Amellago Model | Y | N | Y |
| 7 | Amellago Model | N | Y | Y |
| 8 | Amellago Model | Y | Y | Y |

Table 3.1: Summary of geological realisations. Diagenesis refers to layer boundary discontinuity surfaces. Mud mounds are build-ups with depositional relief composed dominantly of carbonate mud, peloidal mud, and micrite. Oyster bioherms are high permeability features incorporated in molluscan banks.

Eight different realisations of the geological model were available (Table 3.1), which were used to systematically test the impact of geological features on flow. The base case included the key sedimentological and diagenetic features constrained by field data. The other realisations successively included additional diagenetic, sedimentary, and structural features that were also observed in the outcrop, such as subaqueously lithified marine hardgrounds, mud mounds and oyster bioherms (Fig. 3.4). Fractures were included separately as discuessed in the next section. Mud mounds, oyster bioherms, and hardgrounds comprised small volume fractions of 0.0004%, 0.34%, and 0.02% of the model, respectively. Different geological realisations were only considered in the well-test simulations because of the high computational run time and additional sensitivities considered for the secondary recovery simulations.

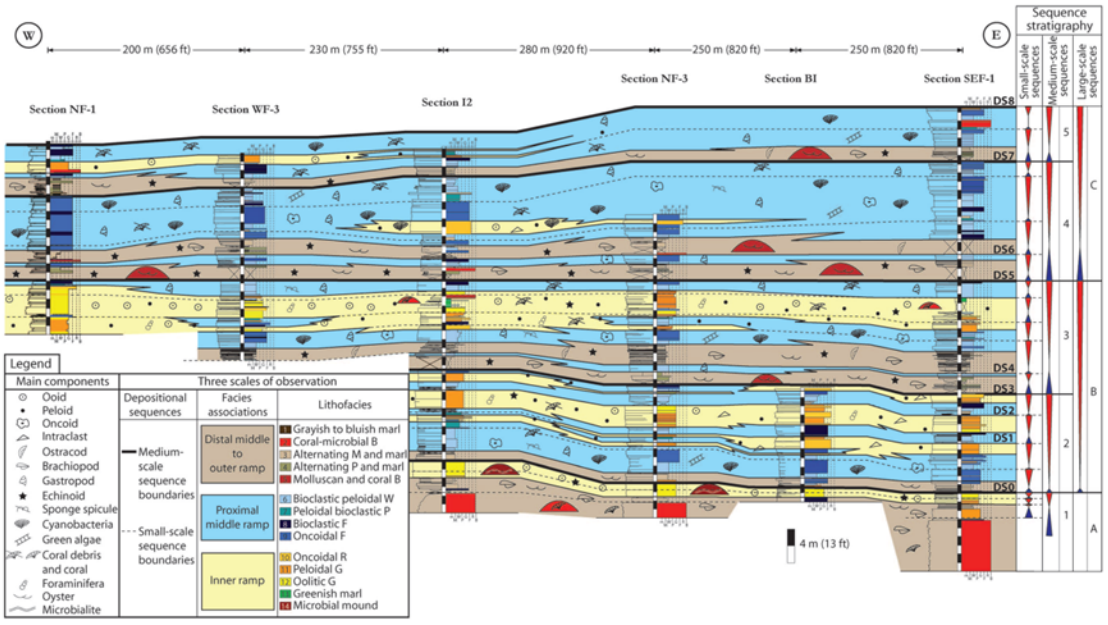


Figure 3.4: Summary of features captured in the geological model. Oyster bioherms are indicated as red domes with oyster symbols. Discontinuity surfaces due to diagenesis marks multiple layers and are indicated with DS. In addition, diverse lithofacies are indicated throughout the model. The entire west-east cross section shows the facies distribution and sequence stratigraphy of the Amellago outcrop study area. DS = discontinuity surface or hardground; M = mudstone; W = wackestone; P = packstone; G = grainstone; F = floatstone; R = rudstones; B = boundstone. After Amour et al. (2013).

Dunham class assignments were used to stochastically populate heterogeneous porosity and permeability in the grid cells of the geological model, while, diagenesis was captured with layer bound discontinuity surfaces (Fig. 3.5). Oyster bioherms were introduced as high permeability features that vary in aerial extent from 15 x 15 m to 300 x 130 m. Permeability of oyster bioherms varies between 1000 and 10,000 mD higher than the permeability of the remaining model.

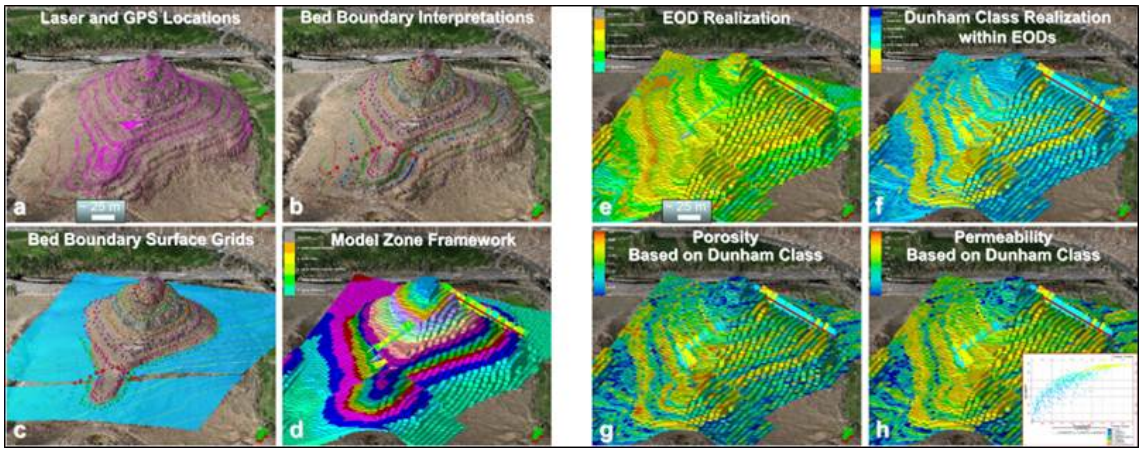


Figure 3.5: Amellago outcrop characterisation and modelling. After Shekhar et al. (2010).

### 3.3.2 *Fracture Modelling*

Fracture data acquired from the Island outcrops were included in the geological model using a discrete fracture network (DFN) approach (Dershowitz et al., 2000). The DFN method generates fracture networks stochastically based on the available fracture data (e.g., fracture orientation, length distribution, and density). The fracture modelling presented in this study follows and extends the work of Shekhar et al. (2010), who focused on generating DFNs for a smaller geological model of the same outcrop. Shekhar et al. (2010) generated DFN models that honoured static observations of the background fracture orientation. The uncertainty in fracture connectivity was addressed by varying the fracture intensity.

For this study, DFNs were generated in FRACMAN$^{TM}$ with varying fracture volumetric intensity (P32) (Fig. 3.6). An average fracture length of 20 m and an aspect ratio (height to length) of 1:5 was employed based on field data for the Island outcrop (Table 3.2). All fractures were assumed to be open, therefore, partially or fully closed fractures acting as barriers were not investigated. Fracture corridors and small background fractures, partly because data of appropriate detail were not available for the entire modelled area. In addition, representation of all the fine-scale background fractures was not viable from a computational standpoint, and so localized increases in fracture intensity close to the fault were represented by the aggregate fault zone properties.

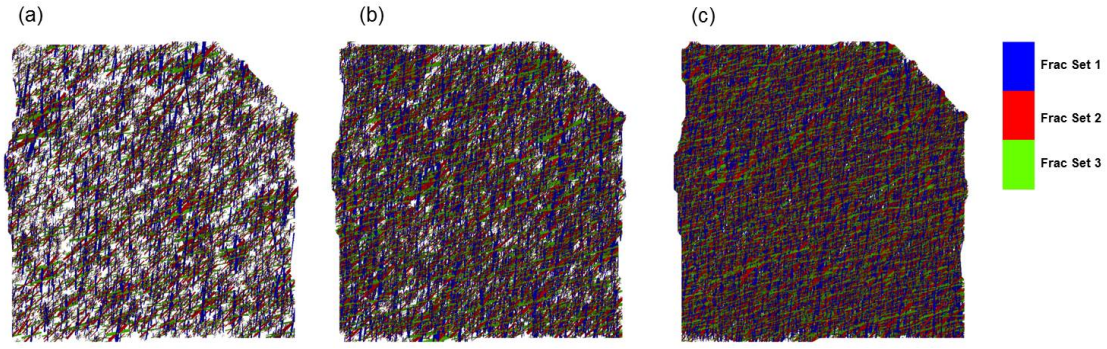


Figure 3.6: Stochastically generated discrete fracture networks (DFNs) for the Amellogo outcrop, which honour the observed fracture orientation, mean fracture length, and aspect ratio. (a) DFN for low fracture intensity of P32 = 0.05 (b) DFN for medium fracture intensity of P32 = 0.1 (c) DFN for high fracture intensity of P32 = 0.2

| | Distribution | Dip direction average | Dip average | Fracture length average | Fracture aperture average |
|---|---|---|---|---|---|
| Set 1 | Fisher | 275 | 74 | 20 m | 0.5 mm |
| Set 2 | Fisher | 315 | 75 | 20 m | 0.5 mm |
| Set 3 | Fisher | 345 | 76 | 20 m | 0.5 mm |

Table 3.2: Fracture sets used for stochastic fracture generation in all DFN models.

The DFN models were upscaled to obtain the equivalent permeability tensor, porosity and shape factor for the fractures at the same resolution as the flow simulation model discussed above. A modified Oda method was used for the permeability upscaling (Golder-Associates, 2010). In contrast to the classical Oda method (Oda, 1985) it ensures that the local fracture connectivity is captured. The modified Oda method is significantly more computationally efficient than flow-based upscaling of DFNs, whose results also depend strongly on the chosen boundary conditions (Ahmed-Elfeel and Geiger, 2012).

A dual-porosity dual-permeability (DPDP) model was employed to couple fluid flow in the fractures with fluid flow in the matrix, considering the high permeability and heterogeneity of the matrix. The average fracture permeability is 867 mD, in contrast to an average matrix permeability of 84 mD. The Gilman and Kazemi (1983) transfer function was used to define the rate of fracture and matrix exchange. Simulations were also run for the transfer function of Quandalle and Sabathier (1989), which is known to capture gravitational flow more adequately (Abushaikha and Gosselin, 2008), but results were virtually identical. Flow simulations considering the presence of fractures were only carried out for the numerical well test analysis and not for the secondary recovery simulations in this chapter. Detailed secondary and tertiary recovery simulations considering fractures are presented in chapters 4, 5 and 6.

## 3.4 FLOW-SIMULATION MODEL

The final flow simulation model, containing 74 x 75 x 110 cells, was assumed to have a large oil column (100 m). The reservoir was also assumed to have an initial pressure of 20.6 x $10^3$ kPa and a bubble point of 15.2 x $10^3$ kPa. A two-phase

oil-water model was used, which does not allow for the formation of solution gas and requires the reservoir pressure to be above the bubble point pressure at all times. Oil viscosities were either 0.52 x $10^{-3}$ Pa sec or 4 x $10^{-3}$ Pa sec, leading to a favourable and unfavourable oil-water mobility ratio (i.e. ratio of the displacing fluid mobility to displaced fluid mobility), respectively, if water is injected during secondary recovery.

Since most real carbonate reservoirs are mixed-wet, relative permeability and capillary pressure curves were chosen to represent an intermediate oil-wet rock. The relative permeability curves were generated using Corey (1954) relations and were intended to mimic the average behaviour of intermediate oil-wet carbonates such as those discussed in Clerke (2009) but also extended to oil-wet and water-wet end-member scenarios (Fig. 3.7 and Table 3.3). The curves were then re-calibrated based on a large body of real but confidential data on carbonate reservoirs of similar permeability. Drainage and imbibition capillary pressures vary for carbonate reservoirs, hence Killough (1976) formulation was used to model capillary pressure hysteresis. Relative permeability hysteresis is investigated in Chapter 5.

| Parameters | Symbol | Water-wet | Mixed-wet | Oil-wet |
|---|---|---|---|---|
| Max. Water Relative Permeability | $K_{rw,max}$ | 0.20 | 0.65 | 0.90 |
| Initial Water Saturation | $S_{wi}$ | 0.22 | 0.10 | 0.05 |
| Residual Oil Saturation | $S_{orw}$ | 0.26 | 0.15 | 0.08 |
| Oil Corey Exponent | $m$ | 2.50 | 3.50 | 4.50 |
| Water Corey Exponent | $n$ | 4.50 | 3.50 | 2.50 |
| Maximum Capillary Pressure (kPa) | $P_{max}$ | 483 | 379 | 276 |

Table 3.3: Main parameters used to generate wettability functions with Corey (1954) equations.

The distribution of relative permeability and capillary pressure curves in the model was approached in two stages. In the first stage, a single pair of relative permeability and single drainage and imbibition capillary pressure curves was used across the entire model. The relative permeability and capillary pressure curves for this case correspond to the mixed-wet curve (Fig. 3.7). In the second stage, three different relative permeability and capillary pressure curves were applied using a facies based approach that tied relative permeability to horizon-

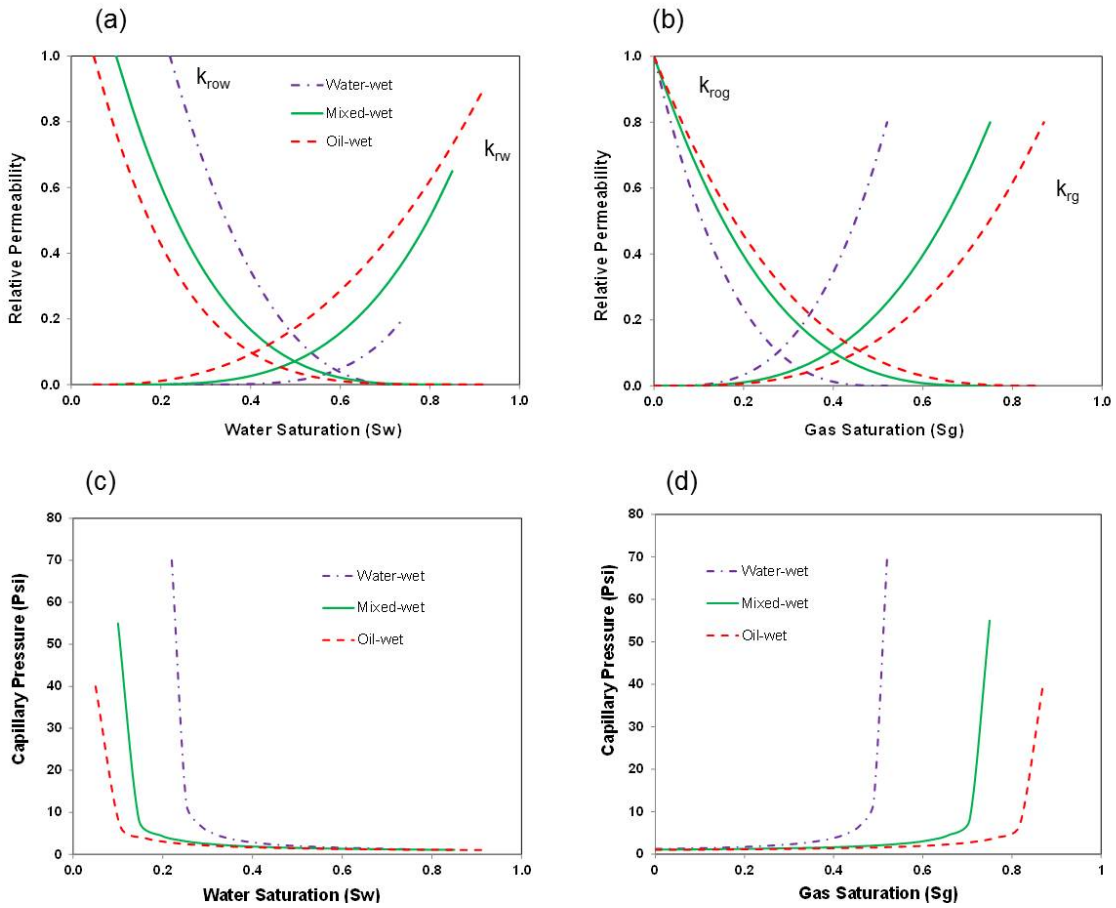


Figure 3.7: Relative permeability curves (a) and drainage capillary pressure curves (b) used in the flow simulations. For numerical well testing and the base-case secondary recovery simulations, the single relative permeability and capillary pressure curve is used, corresponding to the mixed-wet case. When permeability cut-offs linked to facies types are considered, permeability cut-offs of less than 10 md ('water-wet'), between 10 md and 100 mD ('mixed-wet') and above 100 mD ('oil-wet') were used to distribute the relative permeability and capillary pressure curves in the model.

tal permeabilities in grid cells. The assumption was that permeability thresholds could be used as a proxy to represent three groups of facies. Hence, permeability thresholds of 'less than 10mD', '10mD to 100 mD' and 'above 100 mD' were used to assign three different wettability functions to the facies in the reservoir (Fig. 3.7). Because the relative permeability and capillary pressure curves are only intended to mimic the average two-phase flow behaviour of an intermediate oil-wet carbonate reservoir based on real but confidential relative permeability data, assigning the relative permeability based on model permeability seemed to be the most feasible option at this stage, although this may be too simplistic for real carbonate reservoirs (e.g., Hollis et al., 2010; Gomes et al., 2008). Numerical well testing only used a model with a single relative permeability curve because fluid flow during well testing is dominated by the movement of the oil phase.

For the secondary recovery simulations, the well controls were set to honour the constraint that the reservoir pressure must remain above the bubble point pressure at all times. Hence, the minimum producer bottom-hole pressure (BHP) was set at $15.2 \times 10^3$ kPa. The injector well control was set at a maximum injection pressure of $32.0 \times 10^3$ kPa. This maintains a prescribed reservoir pressure gradient between injection and production wells of 10 to 45 kPa $m^{-1}$ and leads to viscous dominated flow. The base case for secondary recovery simulation was water injection at a favourable mobility ratio, i.e. oil viscosity of $0.52 \times 10^{-3}$ Pa sec. Water injection was also considered at an unfavourable mobility ratio, i.e. at an oil viscosity of $4 \times 10^{-3}$ Pa sec. In addition, simulations where gas was injected to displace oil at a low viscosity of $0.52 \times 10^{-3}$ Pa sec and where polymers were injected to displace oil at both, high and low oil viscosity were investigated.

Gas injection has been successfully applied to carbonate reservoirs, especially when the oil is light (e.g., Sajjadian et al., 2005; Kalam et al., 2011; Kallehbasti et al., 2012). It is well known that polymer injection reduces the oil-water mobility ratio, causing a more effective sweep of the reservoir (Sorbie, 1991). This could be beneficial for a highly heterogeneous reservoir corresponding to the Island model, where water is expected to channel preferentially through the high-permeability layers, leaving much of the oil behind in the low-permeability layers, especially if the oil-water mobility ratio is high. Although, polymer in-

jection has mainly been applied to sandstone reservoirs (Hirasaki et al., 2011), recent studies show that Alkali-Surfactant-Polymer (ASP) flooding has the potential to increase ultimate recovery in carbonate reservoirs as well (e.g., Bortolotti et al., 2009; SayedAkram and Mamora, 2011; Levitt et al., 2012).

The secondary recovery simulation used a variety of well patterns including 5-spot patterns, direct line drive well patterns and staggered line drive well patterns where the main flow direction was sub-parallel to and across the faults present in the geological model (Fig. 3.2). All these patterns employed vertical wells. A 5-spot pattern was also tested where the central production well was horizontal. Vertical wells were completed over the entire reservoir, while horizontal wells were completed over a 300 metre lateral interval. All secondary recovery simulations were run for 20 years.

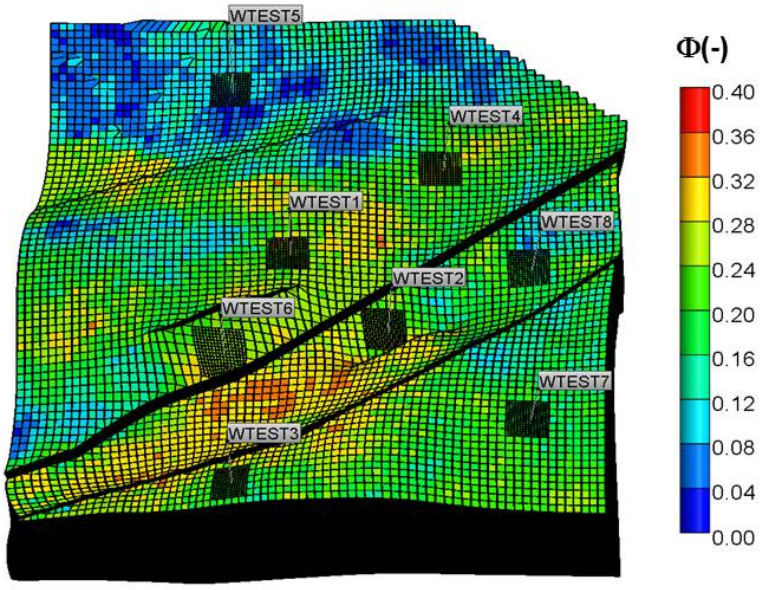


Figure 3.8: Reservoir simulation model showing the porosity distribution and the eight different well locations for the numerical well test simulation. Note the local grid refinement around the well, which was included to minimise numerical artefacts.

Numerical well tests were simulated for an individual well operating at a fixed oil production rate of 500 $m^3$ $day^{-1}$. The well was also vertical and completed over the entire reservoir height. Wellbore storage effects were assumed to be negligible in the early time region of the well tests and the skin factor was set to zero. The well was placed at eight different locations in the model such that it is

| Parameter | Value | Unit |
|---|---|---|
| Reservoir Pressure | $20.7 \times 10^3$ | $kPa$ |
| Bubble point pressure | $15.2 \times 10^3$ | $kPa$ |
| Rock compressibility | $7.25 \times 10^{-7}$ | $kPa^{-1}$ |
| Oil compressibility | $1.0 \times 10^{-6}$ | $kPa^{-1}$ |
| Water compressibility | $5.0 \times 10^{-7}$ | $kPa^{-1}$ |
| Favourable oil viscosity | $0.52 \times 10^{-3}$ | $Pas^{-1}$ |
| Unfavourable oil viscosity | $4.0 \times 10^{-3}$ | $Pas^{-1}$ |
| Water viscosity | $0.36 \times 10^{-3}$ | $Pas^{-1}$ |
| Reservoir pressure gradient | $10 - 45$ | $kPam^{-1}$ |
| Oil density | 850.0 | $kgm^{-3}$ |
| Water density | 950.0 | $kgm^{-3}$ |
| Reservoir Temperature | 121 | $^0C$ |

Table 3.4: Rock and fluid properties used in the numerical simulations

at different distances to one or more faults and model boundaries. The grid was locally refined around the well to minimise numerical errors. Sensitivity studies were run to determine the local grid refinement at which the resulting pressure transient no longer changed (Fig. 3.8). Well test simulations were run for 120 hours, allowing the pressure transients to encounter the boundaries. Time steps were kept small at 0.24 hours to ensure that data points properly represent flow periods, especially in the late time region of the pressure transient. Sensitivity studies were carried out to ensure that the pressure transients did not change as the time step was reduced. In all cases, the middle-time region (MTR) of the pressure transient response was used to estimate permeability.

The fluid properties and well controls for the different simulations are summarised in Table 3.4. In all cases, Computer Modelling Group IMEX$^{TM}$ simulator was used (CMG, 2014). The resulting pressure transients for the numerical well testing were further analysed using SAPHIR$^{TM}$.

## 3.5 NUMERICAL WELL TEST ANALYSIS

Numerical well-test simulations were approached in a systematic way, starting with the base case where the well position was changed (Fig. 3.8). Next the influ-

ence of fault transmissibility was studied for selected wells. The fault transmissibility was varied between two end-members. In the first one, a transmissibility of zero was applied to model an impermeable fault rock that causes all faults to become barriers. In the other end-member, a transmissibility multiplier of 5 was applied to model a permeable fault rock.

It should be noted that, regardless of the chosen transmissibility multiplier, flow across the faults can be reduced due to the juxtaposition of high- and low-permeability layers. More detailed fault models were beyond the scope of this study. We then used different geological models where the level of diagenetic and sedimentological complexity was increased by including marine hardgrounds and coral patch reefs, followed by the inclusion of mud mounds and oyster bioherms. Finally, fractures were added to the base case model.

A comprehensive list of simulation results is provided in Table 3.5. Note that the skin factor is always zero and hence not listed in Table 3.5. In general, the average formation permeability that was recorded from well-test analysis is closest to the geometric mean of the horizontal permeability of the entire geological model, which indicates that the permeability distribution of the geological model is random. The radius of investigation, which represents the area over which the fluid pressure changes around a well before reaching the nearest boundary or low-transmissibility fault, varies from less than 300 m to more than 500 m as wells are located at different distances from the faults and/or reservoir boundaries.

The permeability variation near a fault or reservoir boundary is also reflected in the permeability-thickness product, which indicates the ease with which the reservoir can deliver fluids to the well. The closer the well is placed to a fault or boundary, the lower the permeability-thickness product becomes. This is because the well is placed at a different location within the permeability distribution. Furthermore, the derivative slope and the radius of investigation change with varying proximity to the fault, which indicates a decrease in the ability of the well to produce hydrocarbons. These behaviours yield a good indication of those wells that may be most profitable, particularly during primary recovery

| Geological realisation | Variable | $K_{avg}(mD)$ | Kh(mDm) | $P_i(kPa)$ | $R_{inv}(m)$ |
|---|---|---|---|---|---|
| Base case | WT1 | 24.6 | 2709.7 | 20156.0 | 497 |
| | WT2 | 10.5 | 1152.1 | 20154.2 | 323 |
| | WT3 | 13.6 | 1502.7 | 20119.5 | 369 |
| | WT4 | 15.1 | 1658.1 | 20034.4 | 393 |
| | WT5 | 28.3 | 3109.0 | 20314.1 | 533 |
| | WT6 | 12.6 | 1383.8 | 20037.3 | 354 |
| | WT7 | 8.0 | 877.80 | 19812.4 | 286 |
| | WT8 | 33.0 | 3627.1 | 19906.3 | 573 |
| Base case+diagenesis | WT1 | 24.4 | 2688.3 | 20153.7 | 494 |
| | WT2 | 10.4 | 1140.0 | 20152.4 | 326 |
| | WT3 | 13.5 | 1481.3 | 20116.4 | 366 |
| | WT4 | 14.9 | 1642.9 | 20030.6 | 390 |
| | WT5 | 38.5 | 4236.7 | 20310.2 | 628 |
| | WT6 | 12.5 | 1371.6 | 20034.9 | 354 |
| | WT7 | 28.5 | 3139.4 | 19809.5 | 533 |
| | WT8 | 32.6 | 3596.6 | 19901.6 | 579 |
| Base case+mud mounds | WT1 | 24.6 | 2709.7 | 20156.0 | 503 |
| | WT2 | 10.5 | 1152.1 | 20154.2 | 154 |
| | WT3 | 13.6 | 1502.7 | 20119.5 | 375 |
| | WT4 | 12.5 | 1658.1 | 20034.4 | 393 |
| | WT5 | 38.9 | 4267.2 | 20314.1 | 631 |
| | WT6 | 12.6 | 1383.8 | 30037.3 | 360 |
| | WT7 | 28.7 | 3169.9 | 19812.4 | 543 |
| | WT8 | 33.0 | 3627.1 | 19906.3 | 582 |
| Base case+oyster bioherms | WT1 | 12.3 | 1359.4 | 20149.3 | 357 |
| | WT2 | 10.5 | 1158.2 | 20156.8 | 329 |
| | WT3 | 13.6 | 1502.7 | 20121.0 | 375 |
| | WT4 | 11.6 | 1271.0 | 20028.6 | 344 |
| | WT5 | 38.9 | 4267.2 | 20317.9 | 631 |
| | WT6 | 12.6 | 1386.8 | 20038.1 | 360 |
| | WT7 | 28.7 | 3169.9 | 19813.1 | 543 |
| | WT8 | 7.4 | 816.9 | 19907.9 | 276 |
| Base case+diagenesis+mud mounds+oyster bioherms | WT1 | 11.7 | 1289.3 | 20143.2 | 347 |
| | WT2 | 10.4 | 1149.1 | 20154.8 | 326 |
| | WT3 | 13.5 | 1481.3 | 20117.8 | 372 |
| | WT4 | 10.5 | 1158.2 | 20022.9 | 329 |
| | WT5 | 38.5 | 4236.7 | 20313.1 | 628 |
| | WT6 | 12.5 | 1374.6 | 20035.5 | 357 |
| | WT7 | 28.5 | 3139.4 | 19810.3 | 533 |
| | WT8 | 32.6 | 3596.6 | 19903.1 | 570 |
| Base case+fractures | WT1 | 63.8 | 7010.4 | 20440.7 | 997 |
| | WT2 | 41.6 | 4572.0 | 20489.3 | 805 |
| | WT3 | 45.6 | 5029.2 | 20514.0 | 323 |
| | WT4 | 45.2 | 4968.2 | 20437.0 | 323 |
| | WT5 | 65.1 | 7162.8 | 20646.1 | 323 |
| | WT6 | 45.4 | 4998.7 | 20438.5 | 323 |
| | WT7 | 72.5 | 7985.5 | 20419.7 | 323 |
| Base Case (WT6): Vary fault transmissibility | 0.00 Trans | 5.6 | 618.7 | 19797.2 | 240 |
| | 0.25 Trans | 10.5 | 1152.1 | 20011.7 | 326 |
| | 0.50 Trans | 11.6 | 1280.2 | 20027.5 | 344 |
| | 1.00 Trans | 12.6 | 1383.8 | 20037.3 | 354 |
| | 5.00 Trans | 14.0 | 1542.3 | 20049.1 | 378 |

Table 3.5: Summary of all well-test simulations. *WT1* to *WT8* stand for well-test 1 to 8, corresponding to the well location shown in Figure 3.8. *Trans* refers to the transmissibility multiplier which either enhanced or lowered the transmissibility of all faults uniformly in the model. Diagenesis incorporates the effect of marine hardgrounds and coral patch reefs.

when no fluids are injected into the reservoir to enhance oil production and extend field life.

The pressure transients that are recorded at the well, i.e. the pressure drop and rate of pressure change (pressure derivative) against time can be modelled by solving the partial differential equation describing the spatio-temporal evolution of the fluid pressure $p$ during single-phase flow for the entire reservoir model

$$c_t \frac{\partial p}{\partial t} = \nabla \frac{k(x)}{\mu} \nabla p, \tag{3.1}$$

where $c_t$ is the total fluid and rock compressibility, $\mu$ is the fluid viscosity (under single-phase flow conditions), and $k(x)$ is the spatially varying permeability tensor.

### 3.5.1 *Influence of Faults*

By subjecting these curves to standard techniques for advanced well-test analysis, geological features can be identified from subtle variations in the pressure derivative (Bourdet, 2002). It should be noted that only selected results are shown because several geological models yield pressure transients that are very similar, as will be discussed below. Figures 3.9 and 3.10 reinforce that the pressure transients are dominated by faults at wells 1, 2, 5, 6 and 7. The fault impact is indicated by the positive slope of all pressure derivatives at late time, which shows that the pressure front has reached a flow boundary.

Since the faults juxtapose low- and high-permeability layers in the geological model, flow across the faults is reduced, thereby altering the propagation of the pressure front and hence the shape of the drainage area around each well. These effects combine to result in measurable change in the rate at which the pressure in the well decreases. While an increase in the pressure derivative with a constant slope may be due to mobility reduction or permeability variation away from the well, changes in the pressure derivative also give an indication of the configuration of the faults and other boundaries in the reservoir (Bourdet, 2002). However, as discussed above, the fluid pressure changes are simulated under

single-phase flow conditions, hence the mobility does not change as a function of saturation and cannot impact the pressure derivative.

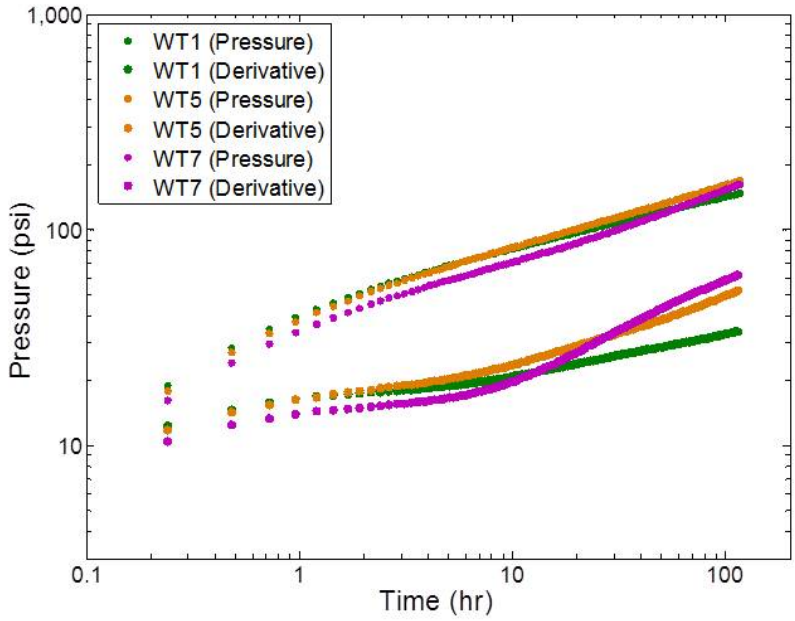


Figure 3.9: Selected pressure transients from Table 3.5 showing the impact of well location near a single fault. See figure 3.8 for well locations. Curves at the top represent numerical pressure data at the wells. Curves at the bottom indicate the pressure derivative, i.e. the rate at which the pressure changes in the wells.

The constant slope of the pressure derivative of well 1, which implies that the pressure changes at a constant rate at the well (Fig. 3.9), indicates that the drainage area of well 1 is influenced by a single boundary. Figure 3.8 shows that this well is located close to the central fault in the geological model. The steep upward pressure derivative trend of well 5 (Fig. 3.9) is consistent with a well that is located in a region where the flow boundaries are U-shaped (Stewart, 2005). Pressure derivatives for wells 2 and 6 (Fig. 3.10) indicate an asymmetrical drainage area between two faults, identified by multiple slopes of the derivative curve in the middle time that stabilise to an upward slope in late time (Bourdet, 2002).

Additional simulations for well 6 showed that if the fault transmissibility decreases, for example because of a low permeability or impermeable fault gouge, the radius of investigation and permeability-thickness product decrease. Hence the positive slope of the pressure derivative increases because the pressure in

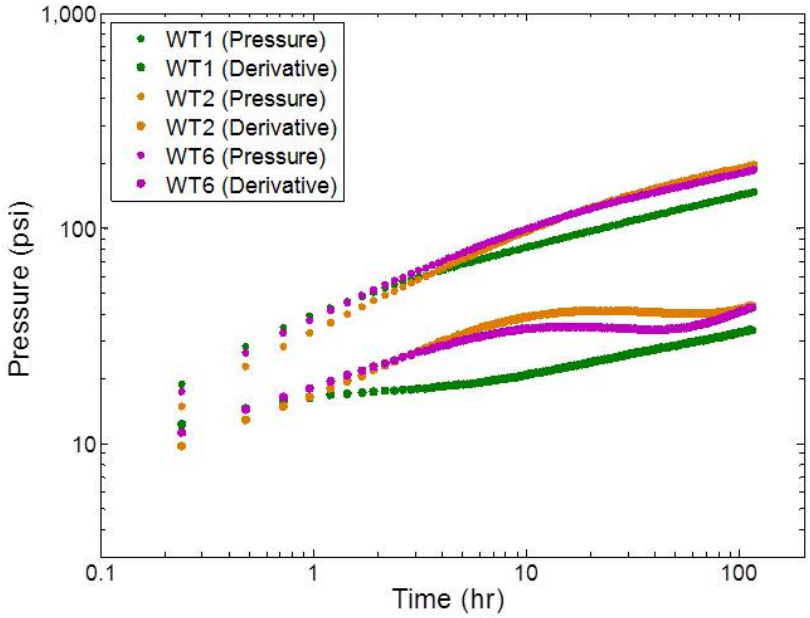


Figure 3.10: Selected pressure transients from Table 3.5 showing the impact of U-shaped boundaries. See figure 3.8 for well locations. Curves at the top of each represent numerical pressure data at the wells. Curves at the bottom indicate the pressure derivatives.

the well changes more rapidly. This indicates that the ability of the well to deliver hydrocarbons is reduced. On the other hand, if the fault transmissibility is increased, for example because of a fractured fault core, the drainage area and permeability-thickness value increase and the slope of the pressure derivative decreases at late time because the pressure in the well changes less rapidly (Table 3.5 and Figure 3.11).

It is not surprising that the faults are a first order control on reservoir connectivity and hence impact large-scale fluid flow as well as reservoir performance during primary and secondary recovery. Since the offset of sedimentary layers at the faults is small, most faults would probably be below seismic resolution if this was a real reservoir. Yet, this offset juxtaposes high- and low-permeability layers and hence flow across the faults is reduced. Numerical well-testing on outcrop reservoir analogues is therefore an efficient tool to detect first-order fluid flow controls and guide reservoir engineering solutions that may aid well placement in a real reservoir. Generating a transient pressure response numerically is relatively fast computationally, therefore, a large number of well-test simulations can be run quickly to test the performance for different geological scenarios in

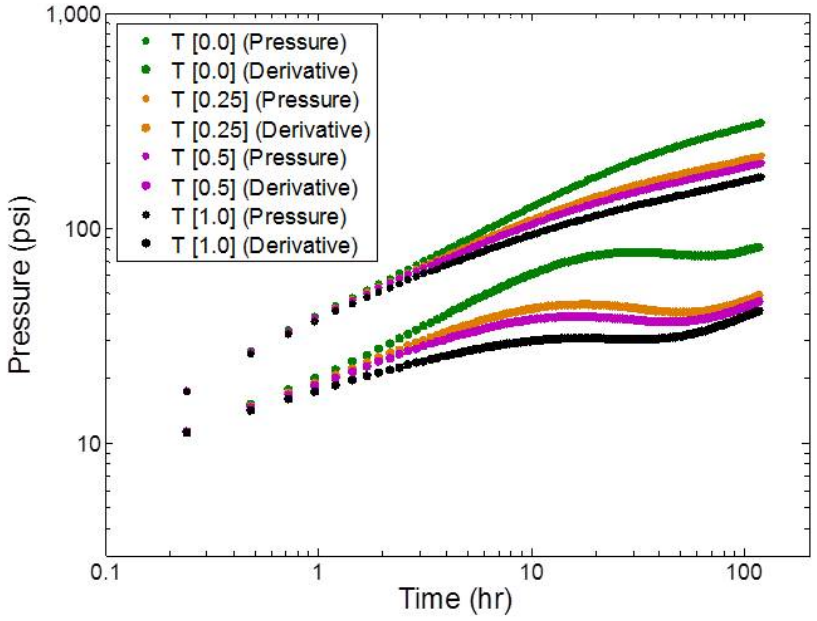


Figure 3.11: Selected pressure transients from Table 3.5 showing the impact of fault transmissibility at well WT6. See figure 3.8 for well locations. Curves at the top represent numerical pressure data at the wells. Curves at the bottom indicate the pressure derivative.

selected sub-regions of a real reservoir model. However, it is important that geological structures are captured at detail in these model sub-regions to obtain reliable well-testing results. This requires information from an outcrop analogue model. Especially in the vicinity of the well it is important to resolve the geology at great detail in order to model the inflow into the well accurately. Workflows for this particular purpose are available that resolve geological structures even beyond what is achieved in this chapter (Chandra et al., 2013).

### 3.5.2 *Influence of Sedimentological and Diageneitic Heterogeneities*

Since faults have such a first-order effect on the pressure transients, an important question is whether other geological features will change the pressure transients and could be identified in a well test. In other words, could other geological features affect the recovery behaviour or do the faults dominate? Surprisingly, none of the diagenetic (e.g. marine hardgrounds) or depositional features (e.g. mud mounds) display a visible impact on the pressure transients (Table 3.5), probably because their volume fractions are negligibly small. The hypothesis is

that the high degree of heterogeneity that is already present in the reservoir homogenises the flow behaviour and hence renders the pressure derivatives indistinguishable. Only the geological model with oyster bioherms included shows a definite variation in pressure transients for those wells that penetrate oyster bioherms, because these features act as high permeability thief zones.

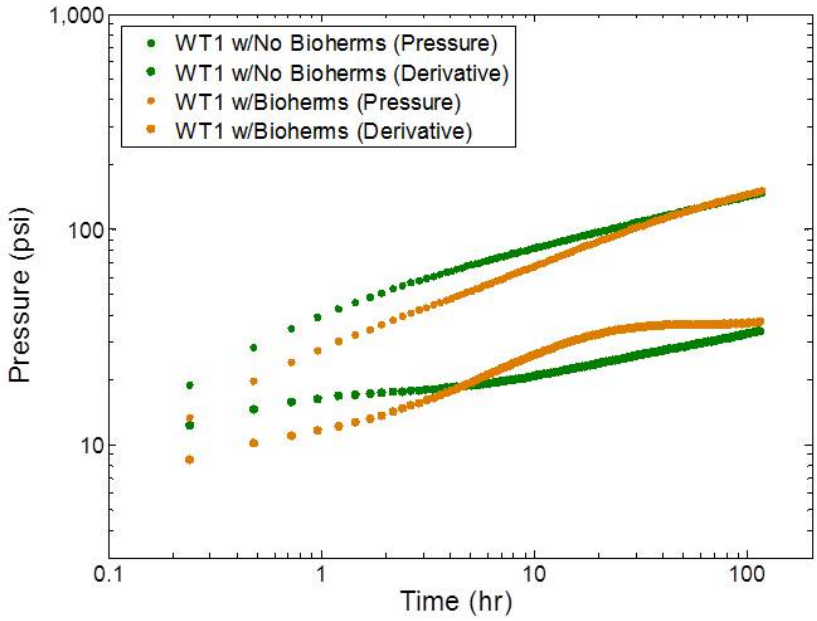


Figure 3.12: Selected pressure transients from Table 3.5 showing the impact of highly permeable oyster bioherms at well WT1. Curves at the top represent numerical pressure data at the wells. Curves at the bottom indicate the pressure derivative.

The oyster bioherms vary in aerial extent from 15 x 15 m to 300 x 130 m, but still only comprise 0.34% of the total reservoir volume. Their permeability is between 1000 and 10,000 mD higher than the permeability of the remaining model. Figures 3.12 and 3.13 show that the permeability contrast between oyster bioherms and other reservoir facies causes an upward movement in the pressure transient compared to the base case. This movement is due to the fact that the pressure front propagates from the high permeability oyster bioherms to the lower permeability matrix. The upward movement in the pressure transient stabilises just before the pressure front is influenced by boundaries.

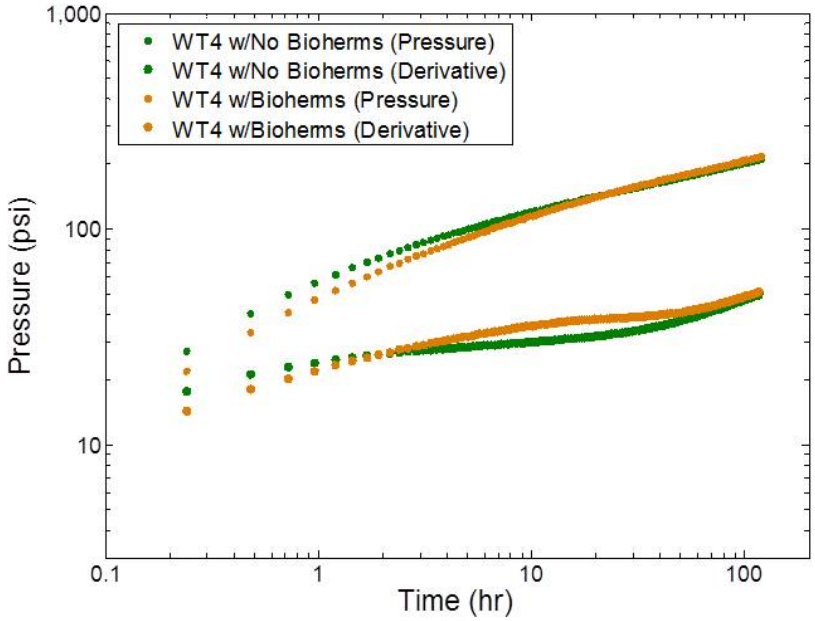


Figure 3.13: Selected pressure transients from Table 3.5 showing the impact of highly permeable oyster bioherms at well WT4. See figure 3.8 for well locations. Curves at the top represent numerical pressure data at the wells. Curves at the bottom indicate the pressure derivative.

### 3.5.3 *Influence of Fracture Networks*

Considering how critical fractures are in many cases for controlling recovery in carbonate reservoirs, an important question is whether the fractures that are observed in the Island outcrop can be detected in a numerically generated well-test profile once they have been included in the geological model. The classical pressure transient analysis for fractured reservoirs is based on the dual porosity model (Warren and Root, 1963), which causes a distinct V-shape in the middle time region of the pressure derivative (Cinco-Ley, 1996; Bourdet, 2002; Kuchuk and Biryukov, 2012). This is due to a flow process commonly known as recharge. Recharge occurs because the fluids in the fractures are produced at a faster rate than they are replaced from the matrix, causing significant changes in the rate at which the pressure in the well declines. Classical theory predicts that this recharge effect increases with increasing fracture-matrix porosity contrast (dual-porosity model) and/or permeability contrast (dual-permeability model) and that the width and depth of the V in the pressure transient allows us to back-calculate the fracture-matrix permeability contrast and the difference in flow rates of fluids stored in the fractures and the matrix (Cinco-Ley, 1996; Bourdet,

2002). However, this behaviour is not observed in the pressure transient in the current modelling effort, regardless of the chosen fracture intensity (Fig. 3.14).

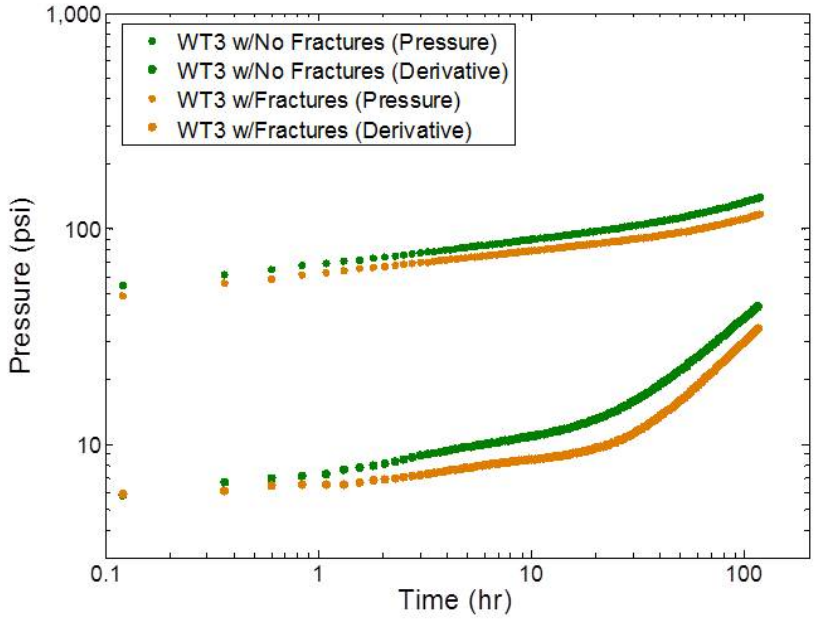


Figure 3.14: Selected pressure transients from Table 3.5 showing the impact of fractures at well WT3. See figure 3.8 for well locations. Curves at the top represent numerical pressure data at the wells. Curves at the bottom indicate the pressure derivative.

It is concluded that the absence of a V-shape in the pressure transient might be due to the high matrix permeability, which can flatten the pressure derivative and reduce the influence of fractures on the pressure decline in a well (Wei, 2000). In the model the average fracture permeability is less than 10 times higher than the average matrix permeability (84 mD vs. 867 mD). It has been observed previously that pressure transient data for fractured reservoirs does not always reflect theoretical models (Wei et al., 1998; Corbett et al., 2012) and the model results confirm that fractures may not be distinguishable in classical well-test analysis if the matrix is highly heterogeneous. However, Kuchuk and Biryukov (2012) discuss that dual-continuum models are sometimes too simplistic and cannot produce the theoretical pressure transients for fractured reservoirs, a fact that is generally known but not always accounted for in fractured reservoir simulation (Bourbiaux et al., 2002; Ahmed-Elfeel and Geiger, 2012; Geiger and Matthai, 2012).

In other words, the numerical simulation approach that has been followed here, in which fracture permeability is estimated from a DFN and fractures are coupled to the rock matrix using a dual-porosity dual-permeability model, may be too simplistic for reproducing the actual flow behaviour in a real fractured reservoir with the same fracture and matrix properties. However, the observation that the fractures present in the numerical model appear not to influence the simulated well-test response is still an important outcome of this study. This result reinforces that classical reservoir simulation approaches for fractured carbonate reservoirs, which are based on dual continuum models, may lead to inadequate predictions, especially if the rock matrix is highly heterogeneous. Since numerical well-testing using outcrop-based reservoir analogues is computationally efficient, this approach could be used to gain confidence in the chosen simulation approach: if there is good (qualitative) agreement between a real well-test that indicates presence of fractures and the numerical results that are based on a dual continuum approach, then the simulation model is more likely to capture the essential flow behaviours in future reservoir simulation approaches.

A detailed representation of the rock matrix, informed from outcrop analogue studies, however, is important such that fluid flow and pressure changes in the rock matrix are not oversimplified in the numerical simulation. If there is poor agreement between the observed and simulated well-test behaviour, other simulation approaches should be used to complement the dual-porosity and/or dual-permeability method, most notably Discrete Fracture and Matrix (DFM) modelling where the fractures and the matrix are represented explicitly (e.g., Karimi-Fard et al., 2004; Matthäi et al., 2007; Haegland et al., 2009; Geiger et al., 2009; Geiger and Matthai, 2012).

## 3.6 INSIGHTS FROM SECONDARY RECOVERY SIMULATIONS

The well-test simulations discussed above provide key indications as to how a reservoir may perform during primary recovery. Since recovery factors are low for this type of production, most reservoirs are subjected to water and/or gas

injection, which drives fluids from the injection wells to the production wells, thereby displacing additional oil while maintaining the reservoir pressure. The sweep efficiency of hydrocarbons from a reservoir depends on the degree of geological heterogeneity, the fluids present in and injected into the reservoir, and the placement and configuration of the wells. The sweep efficiency is investigated next and it should be reiterated that the impact of fractures on oil recovery simulations are not considered here but in chapters 4, 5 and 6.

### 3.6.1 *Influence of Fluid Properties*

Figure 3.15 shows the impact of the injection fluid on sweep efficiency after 20 years production. Gas, water and polymers were injected at favourable oil-water mobility ratio (an oil viscosity of $0.52x10^{-3}$ Pa sec). Water was also injected at an unfavourable oil-water mobility ratio where the oil viscosity is $4x10^{-3}$ Pa sec. A regular 5-spot pattern with a central production well and four injection wells located in the model corners was used. An unfavourable mobility ratio between the injection fluid and oil, i.e. for gas injection at oil viscosity of $0.52x10^{-3}$ Pa sec (Fig. 3.15a, b) or water injection at oil viscosity of $4x10^{-3}$ Pa sec (Fig. 3.15c, d), caused the injected fluid to channel through the high permeability layers, leaving much of the oil in the low-permeability layers behind. Only at favourable mobility ratio, i.e. when water (Fig. 3.15e, f) or polymers (Fig. 8g, h) were injected at an oil viscosity of $0.52x10^{-3}$ Pa sec, was channelling reduced and sweep efficiency increased. A favourable mobility resulted in significantly higher oil recoveries for water injection (43% recovery) and polymer injection (49% recovery) compared to gas injection (22% recovery) or water injection (27% recovery) at unfavourable mobility ratio (Fig. 3.16). Polymer flooding also reduced the water cut greatly, from 87% and 93% for water injection to 75% (Fig. 3.17).

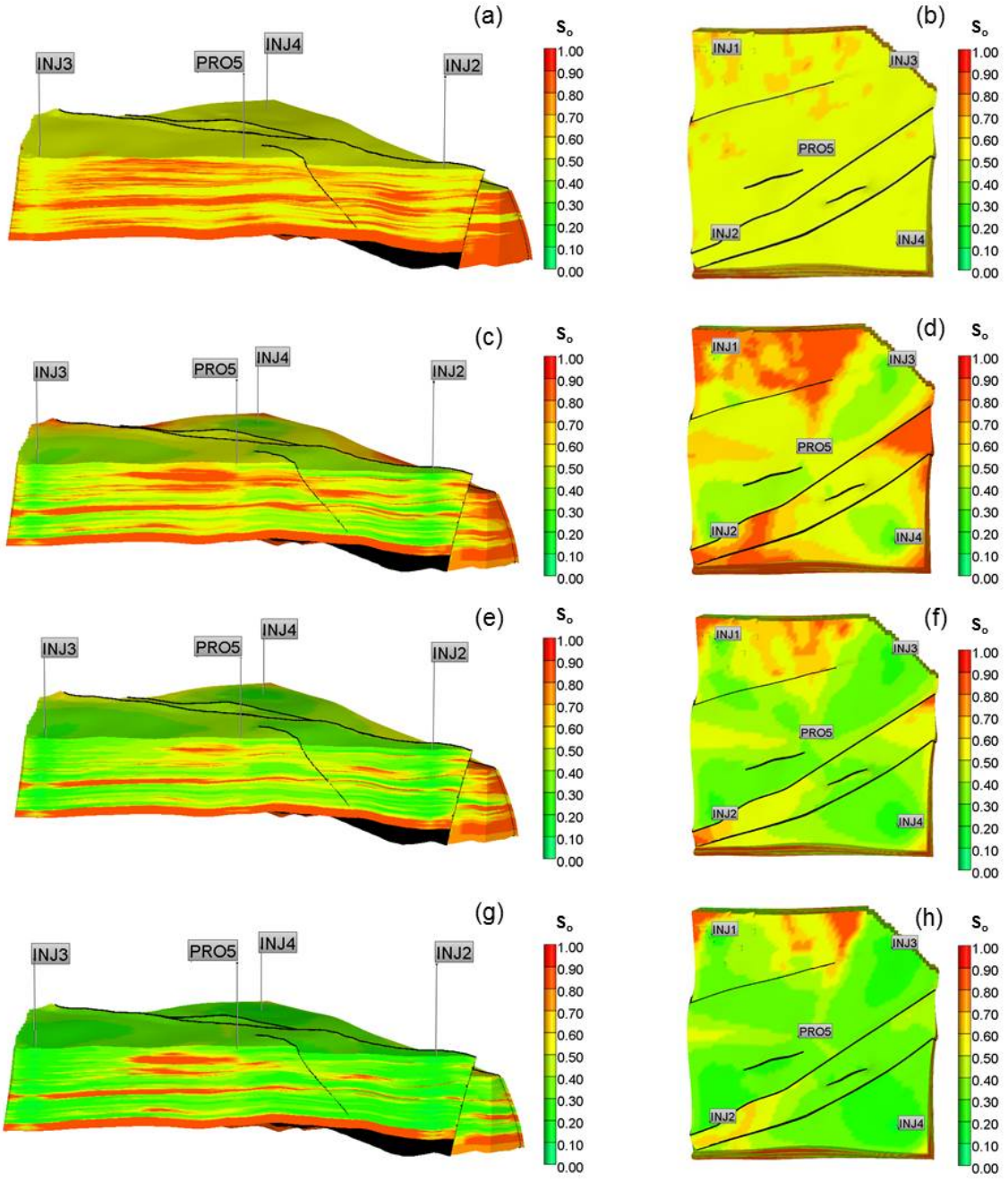


Figure 3.15: Cross sectional and aerial view of oil saturation after 20 years production for a regular 5-spot well pattern where the injected fluid is gas at an oil viscosity of $0.52 \times 10^{-3}$ Pa sec (a, b), water at an unfavourable oil-water mobility ratio with an oil viscosity of $4 \times 10^{-3}$ Pa sec (c, d), water at a favourable oil-water mobility ratio with an oil viscosity of $0.52 \times 10^{-3}$ Pa sec (e, f), and polymers at an oil viscosity of $0.52 \times 10^{-3}$ Pa sec (g, h).

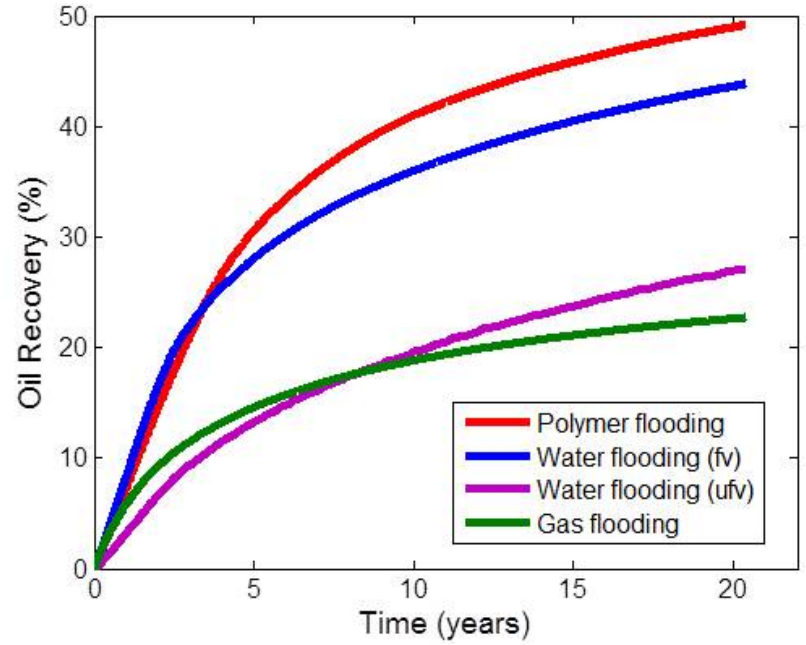


Figure 3.16: Oil recovery for the injection of gas, polymers and water at favourable (fv) and unfavourable (ufv) oil-water mobility ratios. See Figure 3.15 for corresponding saturation distributions after 20 years production. Note that there is no water produced during gas flooding and hence the water cut is not shown.

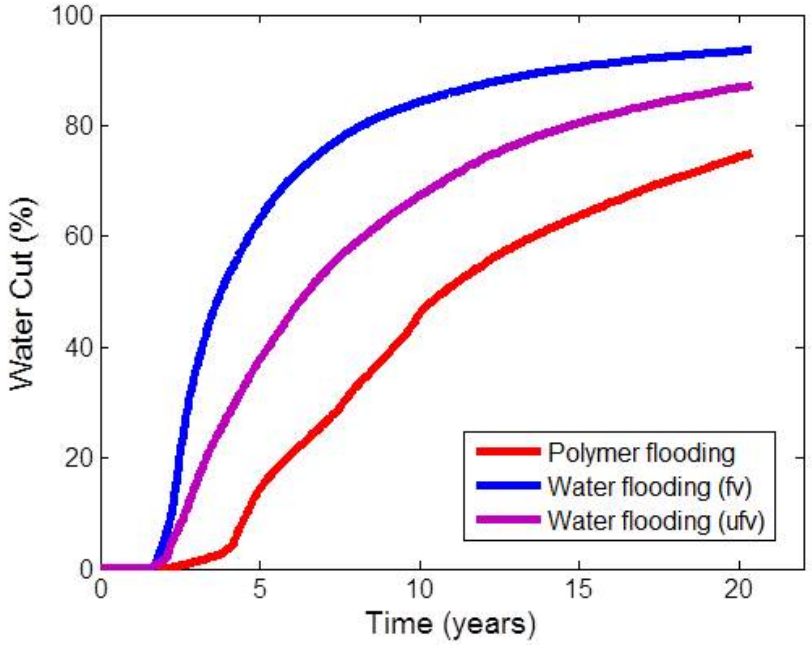


Figure 3.17: Water cut for the injection of gas, polymers and water at favourable (fv) and unfavourable (ufv) oil-water mobility ratios. See Figure 3.15 for corresponding saturation distributions after 20 years production. Note that there is no water produced during gas flooding and hence the water cut is not shown.

### 3.6.2 *Influence of Influence of Well Placement*

It is interesting and important to note that the recovery for this particular well pattern is not final. It can be further improved by finding the optimum placement for the central production well such that the recovery factor is maximised without changing any other well controls. Well pattern optimisation is now a standard technique in reservoir simulation (e.g., Bangerth et al., 2006; Onwunalu and Durlofsky, 2011). CMOST$^{TM}$, an optimisation and history matching engine, was used to drive IMEX$^{TM}$ and search for the worst and optimum well position for the central producer in an area of 300 x 300 m around the base case position of the production well.

Waterflooding was only considered for a favourable oil-water mobility ratio. The difference between the best (45% recovery) and worst position (38% recovery) of the central production well is 7% for this particular geological model if no other well properties are changed. However, optimisation simulations are costly to run because a large parameter space needs to be explored, particularly if there are many uncertain parameters such as different geological model realisations. One possible application of optimisation in outcrop based flow simulations is to find the geological heterogeneities that dominate flow behaviour: if geological heterogeneities are simplified, for example during upscaling, the optimisation algorithm still must find the same worst and best location for the production wells as in a high-resolution model that captures more geological heterogeneities.

When well patterns are varied, the 5-spot pattern yields the best recovery compared to all other investigated well-patterns (Fig. 3.18). Only a direct line drive where the main flow directions are along the East-West trending faults of the geological model yields a comparable recovery. If the main flow direction is across the faults in the direct or staggered line drives, sweep efficiency is reduced because, as indicated by the well-testing results, faults form less permeable boundaries to flow. Staggered line drives perform generally poorer for this heterogeneous reservoir, yielding recoveries of 43% compared to 45% recovery

for a direct line drive across the fault. This result again emphasises the need for carefully testing well placements in optimisation runs once the general well pattern has been decided.

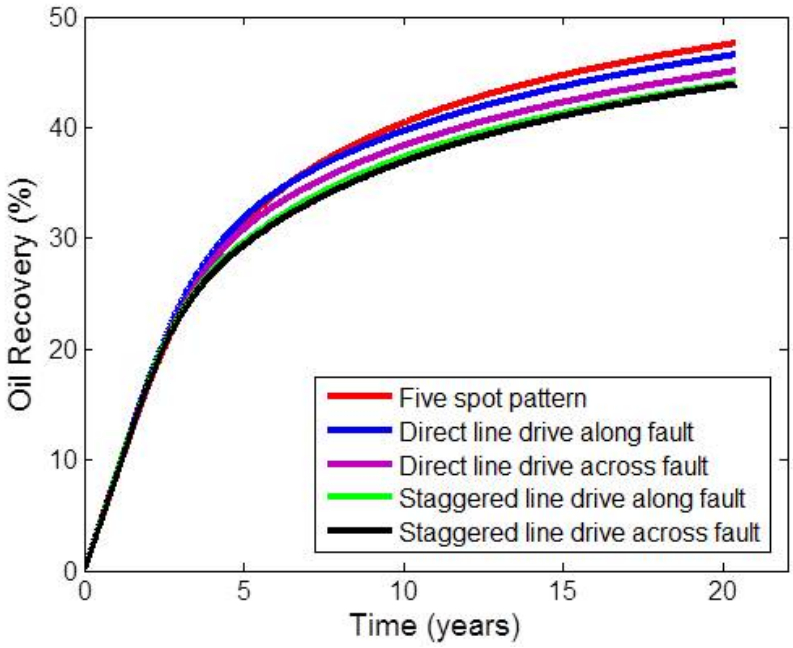


Figure 3.18: Comparison of oil recovery for different well patterns using vertical wells. All simulation cases assume waterflooding for the favourable oil-water mobility ratio with an oil viscosity of $0.52 \times 10^{-3}$ Pa sec.

### 3.6.3 *Influence of Well Design*

All of the studies above considered vertical wells. Today, deviated and horizontal wells are frequently used in carbonate reservoir development because they can drain a larger reservoir volume. However, it has been observed that horizontal wells are less efficient if carbonate reservoirs exhibit strong vertical heterogeneity, as is the case for the Island model (e.g., AlHanai et al., 1995; Farran et al., 2005; Leung et al., 2010). The model simulations confirm this: placing a central horizontal producer of 300 m length parallel to the main fault in the reservoir yields significantly lower recoveries (10% to 20% recovery), irrespective of the depth of the producer (Fig. 3.19). This is because structurally lower and higher reservoir units are more difficult to drain by a horizontal producer if heterogeneities decrease flow in the vertical direction. Upscaling a static geological model to a

reservoir simulation model involves, first and foremost, loss of vertical heterogeneity. Hence outcrop-based flow simulations could be an important tool to investigate the performance of horizontal wells more accurately if a reservoir appears to have strong vertical heterogeneity.

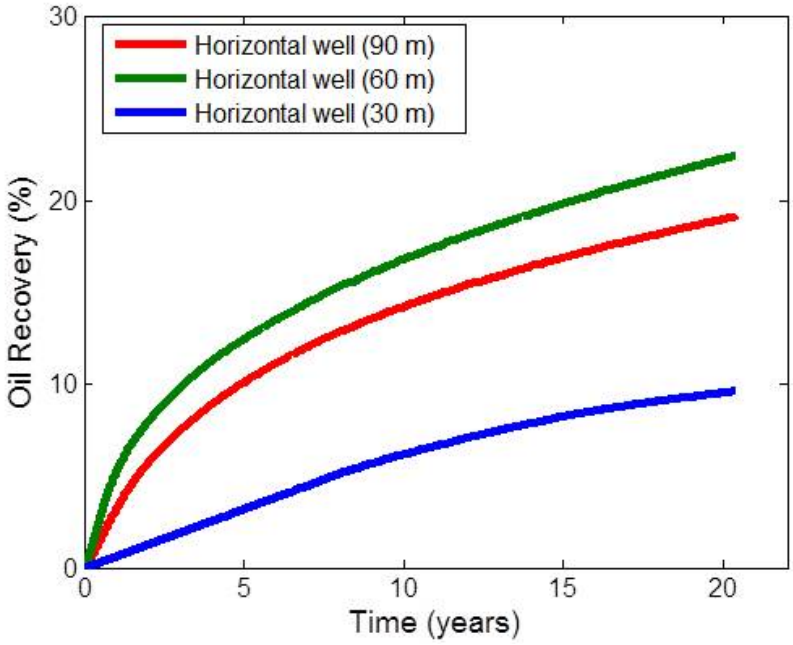


Figure 3.19: Comparison of oil recovery for a regular 5-spot well pattern with a central horizontal producer located at different depths from the top of the reservoir. Simulations assume waterflooding for the favourable oil-water mobility ratio with an oil viscosity of $0.52 \times 10^{-3}$ Pa sec.

### 3.6.4 *Influence of Capillary Pressure Hysteresis*

Accounting for capillary pressure hysteresis in the simulations for waterflooding at favourable oil-water mobility had a negligible impact on recovery and water-cut. It is well known rock typing which accounts for capillary and relative permeability hysteresis in carbonate reservoirs, is notoriously challenging (e.g., Hollis et al., 2010; Gomes et al., 2008) and generating saturation functions from special core analysis is time consuming and expensive. Nevertheless, it is possible to estimate saturation functions quickly and reliably from pore-scale modelling, even for three-phase flow (Blunt, 2001; Al-Dhahli et al., 2013; Blunt et al., 2013). These can be included straightforwardly in outcrop-based analogue flow simulations to investigate how production behaviour changes if the number

of saturation functions is increased or decreased. Relative permeability hysteresis is discussed in chapter 5.

## 3.7 DISCUSSION

### 3.7.1 *Numerical Well-test Simulation*

Numerical well-test simulation and analysis are known to be powerful and computationally efficient tools that help to calibrate reservoir models and simulation approaches (Rawnsley and Wei, 2001; Corbett, 2009; Corbett et al., 2012; Chandra et al., 2013). They allow us to test, quickly and systematically, how different geological realisations can affect the ability of new wells to deliver hydrocarbons. In addition, if well-test data are available, they enable a qualitative and fast comparison between numerically generated type curves for the different geological models and observed well-test data. Therefore it becomes possible to rank different geological scenarios and improve engineering judgement as to which geological structures can be expected to impact flow the most and which are of lesser importance.

The use of a high-resolution flow simulation model that incorporates small-scale structures from outcrop analogues is crucial because certain geological features will always be excluded a priori if upscaled reservoir simulation models are used instead. Hence flow behaviour, especially in the near-wellbore region, can be misrepresented and results from such simulations may be biased (Chandra et al., 2013). As discussed above, numerical well-test simulations may also help to build confidence in configuring reservoir simulation models for fractured reservoirs: if there is good qualitative agreement between observed well-test data showing a clear fracture signal and the outcrop-based simulation result, then this indicates that the chosen model (e.g. dual-porosity dual-permeability model) is likely to capture the flow behaviour in the real reservoir sufficiently, at least for primary production.

During the pressure transient analysis in this chapter, the transmissibility of all the faults has been varied simultaneously. This was in order to investigate and analyse the end member transmissibility impacts of faults that are fully sealing, partially sealing and fully open. It was observed that an increasing the sealing capacity of the faults led to an increase the slope of the pressure transients irrespective of the nature or symmetry of the drainage area. It has been established that if the well is placed asymmetrically between two faults that are fully sealing, a derivative hump is observed. If one of the faults is non sealing, the derivative hump can still be expected if the pressure transient reaches the sealing fault first. Subsequently, the transient would flatten out as it reaches the second fault that is partially sealing or fully open. Hence, the end-member fault transmissibility scenarios considered here provide a framework for understanding the pressure response if the fault configuration or sealing capacity were to be different from the scenarios considered in this thesis.

### 3.7.2 *Secondary Recovery Simulation*

The secondary recovery simulations in this chapter show that channelling of fluid flow into the high-permeability layers is the primary control on oil recovery because it generates a positive feedback loop where the channelling effect increases as more fluid is channelled into the high-permeability layers. Channelling may not be predicted accurately if the reservoir is overly upscaled using conventional methods that group too many of the small-scale layers together (Pavlas, 2001). The secondary recovery simulations also demonstrate that the oil recovery is strongly affected by well type (horizontal vs. vertical well and well pattern), gas injection and mobility ratio. The first two are engineering measures which can be mitigated through appropriate reservoir development. Likewise, optimising the placement of injection and production wells once the basic well pattern has been selected is now possible by combining reservoir simulation and experimental design techniques (e.g., Bangerth et al., 2006; Onwunalu and Durlofsky, 2011).

Even an unfavourable mobility ratio, which decreases oil recovery significantly (Fig. 3.16), can be mitigated at least in part by the appropriate choice of injection fluid. Indeed, adding polymers to the injection fluid has a significant impact on both oil recovery and water cut, and polymer injection appears to emerge as viable recovery mechanism for carbonate reservoirs (e.g., Bortolotti et al., 2009; Hirasaki et al., 2011; SayedAkram and Mamora, 2011; Levitt et al., 2012). Furthermore, Alkali-Surfactant-Polymer (ASP) flooding can use Alkali and Surfactant to improve microscopic sweep efficiency so that in combination with polymer the ASP treatment can achieve improved microscopic and macroscopic sweep efficiency. Alkali can reduce the in-situ interfacial tension while surfactant can potentially alter the wettability favourably towards water-wetness which improves hydrocarbon recovery.

### 3.7.3 *Small-scale Heterogeneities*

For all the sensitivities described in this chapter, it was essential to consider the impact of small-scale heterogeneities. Traditional reservoir simulation workflows, which do not typically account for small-scale geological features, should therefore be complemented with simulations performed on digital outcrop models, as discussed here. The choice of well pattern and well placement may be affected if small-scale heterogeneities are neglected in upscaled simulation models, particularly when considering vertical wells or attempting to optimise the well spacing for a given well pattern. In turn, reservoir simulation models using outcrop analogues can help to ensure that the geological features that are primary controls on recovery are included properly in the reservoir simulation model. They enable us to test systematically how recovery behaviour changes if known geological features that have been observed in the outcrop are added to the model or removed from it. In particular, use of costly injection strategies such as polymer flooding requires a sound understanding of how polymers will interact with heterogeneities that are representative of the real reservoir, in addition to simplified representations in an upscaled flow simulation model.

### 3.7.4 *Relative Permeability and Capillary Pressure Curves*

Measuring additional relative permeability and capillary pressure curves in the laboratory is time consuming and costly. It is hence critical to have good a-priori knowledge when the addition of further saturation functions will no longer affect the predicted reservoir performance. Since saturation functions can be estimated reliably and efficiently from pore-network modelling (Blunt, 2001; Al-Dhahli et al., 2013; Blunt et al., 2013), outcrop-based flow simulations are an excellent experimental tool to test how recovery may change if different geological structures and saturation functions are included. It is of particular importance if enhanced oil recovery techniques are considered, such as injecting wettability altering fluids or tertiary gas injection (e.g., Christensen et al., 2001; Gupta and Mohanty, 2011; Kalam et al., 2011; Al-Dhahli et al., 2013).

### 3.7.5 *Fracture Network Concepts*

The fracture network flow concepts were generated and developed to honour fracture data from the outcrop. In a real scenario, this would be equivalent to honouring the data that has been obtained from core analysis, borehole imaging, surface and subsurface analogues. For example, three fracture sets were identifiable from the outcrop, while, fault-related, bedding-related and regional fracture geometries can also be identified from the outcrop data. However, due to uncertainties in the data, fracture concepts could vary from our initial hypothesis. In a situation where a single fracture set is encountered, it is expected that the connectivity of the fracture system could be much less, which would decrease the predicted impact of rapid water and gas breakthrough. This is because multiple fracture sets with varying orientations would have an increased possibility of fracture sets crossing each other and reaching the percolation threshold much faster. In general, the impact of the nature or number of fracture sets would depend on how these concepts affect the fracture network properties. Higher connectivity across the fracture network would lead to rapid breakthrough of injected fluids and poor hydrocarbon recovery. Similarly, poor connectivity across

the fracture network would increase the residence time of injected fluids and support more efficient displacement of oil and storage of gas in the matrix.

## 3.8 SUMMARY

In this chapter, a series of numerical well-testing and secondary oil recovery simulations have been performed on a high-resolution analogue model for the Arab D formation. The geological model was derived from a series of well-exposed outcrops in the Island area of Amellago Canyon in Morocco and is a representative analogue for reservoir case studies situated in Jurassic carbonate ramp settings. Systematic numerical simulations of well-testing and subsequent well-test analysis on synthetically generated pressure transients revealed that faults dominate the large-scale flow behaviour in the model. Hardly any other diagenetic or sedimentary features can be distinguished from pressure transients when they are included into the geological model. Even including fractures by upscaling them from a DFN model does not change the pressure transients significantly. The hypothesis is that this is because the heterogeneity of the high-permeability rock matrix is resolved at the appropriate scale in the numerical simulation, which suppresses the signal from the fractures.

Similar observations were made in earlier studies of numerical well-testing in fractured reservoirs although the current simulation study employs a realistic matrix model for the first time. It could also be possible that the dual-porosity dual-permeability model, which was used to couple flow in the fractures and matrix, may not be able to resolve the flow physics in a real fractured reservoir appropriately. This remains to be investigated using more advanced numerical techniques such as Discrete Fracture and Matrix methods, which incorporate fractures explicitly in the reservoir simulation model.

Secondary recovery simulations demonstrate that channelling of flow into high-permeability layers is a primary control on oil recovery. This channelling effect increases with increasing viscosity contrast between injection fluid and oil. The conductivity between low- and high-permeability layers increases once the

high-permeability layers are saturated with a low-viscosity fluid while the low-permeability layers still contain high-viscosity oil, resulting in even more, flow channelling into the high-permeability layers. Selecting the appropriate injection fluid and well configuration is hence crucial as it can mitigate this effect by reducing the viscosity contrast and increasing sweep efficiency. High-resolution geological models that capture small-scale permeability variations are needed to study these effects accurately.

Generating the 3D model for the Island outcrop was a time consuming process, and this time investment may be perceived as a major obstacle in performing outcrop-based reservoir simulations that complement traditional reservoir modelling and simulation workflows on a regular basis. There is already a wealth of excellent outcrop analogue data available to perform similar simulations more routinely. Results from these simulations allow for systematic and consistent testing of how different depositional environments and different structural overprints can affect certain recovery mechanisms and hence the overall reservoir performance. Outcrop-analogue based high-resolution simulations can provide important guidelines as to which geological heterogeneities need to be captured in the real reservoir model (and which only have secondary effects on recovery) such that the model can be history-matched more reliably and the optimal field development plan can be selected. This would not only add further value to the outcrop analogue datasets, but in time would also yield a valuable library of models that allow for quick comparison and ranking of the performance of certain recovery mechanisms for a specific carbonate reservoir type, hence guiding reservoir modelling and simulation workflows.

# 4

# COMPOSITIONAL SIMULATION, OPTIMISATION AND MOBILITY CONTROL OF GAS INJECTION PROCESSES

## 4.1 INTRODUCTION

Gas injection has been widely applied in the oil and gas industry for subsurface hydrocarbon displacement and pressure maintenance. The displacement of oil by gas injection can be classified as miscible or immiscible based on the reservoir fluid properties at reservoir conditions. Miscible processes occur when the reservoir pressure is above the Minimum Miscibility Pressure (MMP) for a given injection gas and in-situ oil composition (Taber et al., 1997). In a miscible displacement process, two fluids form a single homogeneous phase when mixed in all proportions (Holm, 1986; Bourdarot and Ghedan, 2011).

When the fluids are fully miscible, the Interfacial Tension (IFT) between them reduces to zero, capillary forces are eliminated and under idealized conditions, the Residual Oil Saturation (ROS) is reduced to zero in the swept region, leading to significantly higher oil recoveries. In miscible flooding, the gas is generally injected at super-critical conditions and mixes with the oil mainly by solubility, diffusion and dispersion. The key oil recovery mechanisms include oil swelling, viscosity reduction, low IFT displacement and subsequent reduction of ROS (Holm, 1986; Stern, 1991; Healy et al., 1994; Taber et al., 1997; Lange, 1998; Bon et al., 2005; Bourdarot and Ghedan, 2011).

Miscible displacements can occur at the first contact of the injected gas with the reservoir oil in which case any amount of solvent injected will exist as

a single phase with the oil. More frequently, gases are not directly miscible with the reservoir oils, but under appropriate conditions of pressure and fluid composition achieve miscibility in-situ by mass transfer of mostly intermediate-molecular-weight oil and solvent components through repeated contact, in a process known as multiple-contact or 'dynamic' miscibility. Conversely, immiscible displacements occur at pressures below the MMP for a given solvent and oil composition. Due to the existence of a substantial IFT between the phases, capillary forces prevent the complete displacement of one phase by the other, leading to a high ROS post displacement. The presence of oil- to mixed-wettability in carbonates also leads to sub-optimal displacement by immiscible floods due to the development of preferred gas travel pathways through small oil-wet pores as a result of capillarity-induced bypassing (Stern, 1991; Christensen et al., 2001; Vatanparast et al., 2011; Mohan et al., 2011; Martavaltzi et al., 2012). Miscible flooding displacements are therefore preferable if reservoir conditions (heterogeneity, pressure, temperature and fluid composition) and economic factors, favour their deployment.

Gas injection into oil reservoirs results in complex interactions of flow with phase behaviour that are best modelled by compositional simulation. Compositional simulation in turn requires a good understanding of the phase behaviour of in-situ oil and injected gas under reservoir conditions and how their components interact (Zick, 1986; Stalkup, 1987; Johns et al., 2002; Christensen et al., 2001; Egwuenu et al., 2008). This is achieved by accurate characterization of the reservoir fluids based on equation of state (EOS) models that are calibrated to pressure-volume-temperature (PVT) laboratory experiments.

Most EOR projects are capital intensive with high risk of undesirable consequences in case of failure, and therefore have to go through a screening study to evaluate available options (Taber et al., 1997; Alvarado et al., 2002; Manrique et al., 2007; Teletzke et al., 2010; Bourdarot and Ghedan, 2011). In the context of gas injection, screening usually involves the choice of injected gas, miscibility conditions and slug sizes. The reservoir type (heterogeneous or homogeneous), field location as it relates to gas availability (offshore or onshore), and optimum hydrocarbon recovery will usually guide this choice. A detailed understanding

of the reservoir type is discernible from high resolution outcrop analogue studies as such studies attempt to correlate reservoir flow patterns to geological features that have been observed in the outcrop. Miscibility is achieved at a lower MMP with $CO_2$ than with hydrocarbon gas, nitrogen or flue gas, and therefore $CO_2$ is miscible with reservoir oil at conditions (pressure and composition) where other gases remain immiscible. Hence, $CO_2$ injection is employed in this chapter.

## 4.2 GAS MOBILITY CONTROL STRATEGIES

A major problem with gas flooding is the unfavourable mobility ratio caused by low viscosity of the injection gas compared to the oil. An unstable mobility front is formed between gas and oil that enables viscous fingers to develop and propagate through the displaced fluid, leaving much of the reservoir oil uncontacted (Fig. 4.1). Gas flood efficiency is also adversely affected by injectant channelling through high permeability layers (in a stratified reservoir), and/or gravity override (in a vertically communicating reservoir) due to lower density of displacing gas relative to the displaced oil (Healy et al., 1994).

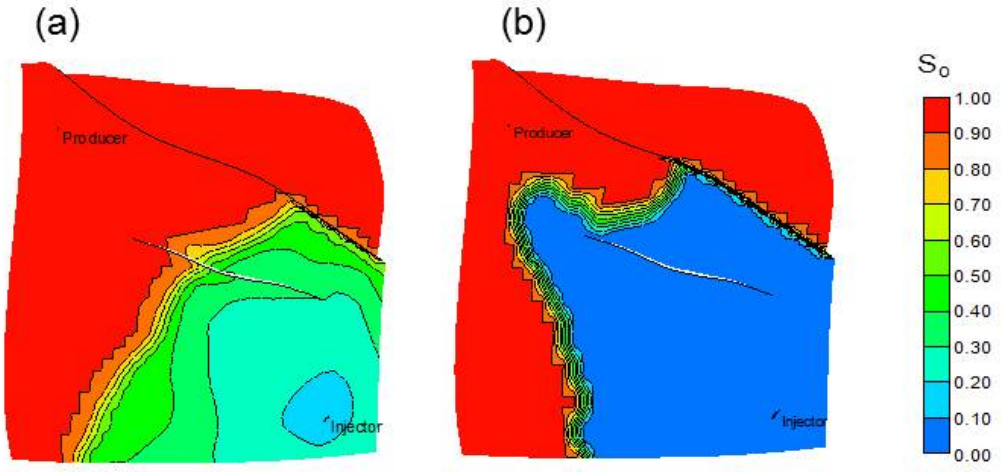


Figure 4.1: Oil saturation distribution in a high permeability top layer of the Amellago sector model during water injection (a) and miscible gas injection (b). Miscible gas injection reduces the residual oil saturation but is limited by an unfavourable mobility ratio and poor frontal stability. Figure shows simulation results after 0.2 PVI.

In the case of fractured carbonate reservoirs, injected gas may flow through connected fracture networks and bypass oil in the rock matrix, leading to early breakthrough of injected fluids and consequently, lower hydrocarbon recoveries. Mobility control is therefore essential to increase sweep efficiency and hydrocarbon recovery.

### 4.2.1 *Improve Frontal Stability with WAG Injection*

To minimize displacement problems, Water-Alternating-Gas (WAG) injection mechanisms have been applied that employ a planned alternate injection of water and gas in ratios varying from 0.5 to 4. The fundamental benefit of the WAG process is to ensure better mobility control and frontal stability, thereby enhancing the contact of un-swept zones (e.g. attic and cellar oil) and improving overall recovery (Fig. 4.2).

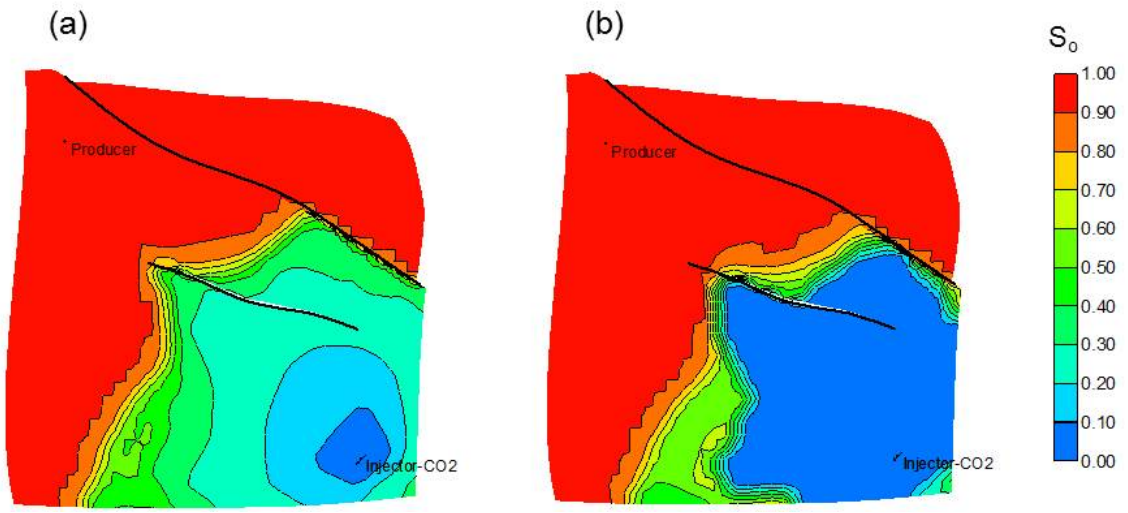


Figure 4.2: Oil saturation distribution in a high-permeability top layer of the Amellago sector model during immiscible WAG injection (a) and miscible WAG injection (b). Miscible WAG injection stabilises the displacement front while reducing the residual oil saturation and improving overall hydrocarbon recovery. Figure shows simulation results after 0.2 PVI.

WAG flooding is also cheaper than continuous gas flooding as it involves the replacement of some of the 'expensive' gas with relatively 'inexpensive' water (Lake et al., 1992; Christensen et al., 2001). Hence, WAG injection is now considered for many carbonate reservoirs in the Middle East as well as the pre-salt

carbonate reservoirs offshore Brazil (Kalam et al., 2011; Pizarro and Branco, 2012; Rawahi et al., 2012). When combined with miscible flooding, miscible WAG can lead to an enhanced microscopic oil displacement and macroscopic sweep efficiency that improves hydrocarbon recovery from the reservoir.

### 4.2.2 *Improve Mobility Control with Foam EOR*

Foam mobility control techniques can also be employed to mitigate gas displacement problems by capturing gas in foam bubbles, which reduces the gas mobility and improves the overall microscopic and macroscopic sweep efficiency in the reservoir (e.g., Patzek, 1996; Ma et al., 2014). The improvement in mobility control and reservoir conformance is achieved by increasing the flow resistance and viscous pressure drop during foam EOR, which diverts injected fluids from high permeability zones and fractures to the lower permeability regions of the reservoir.

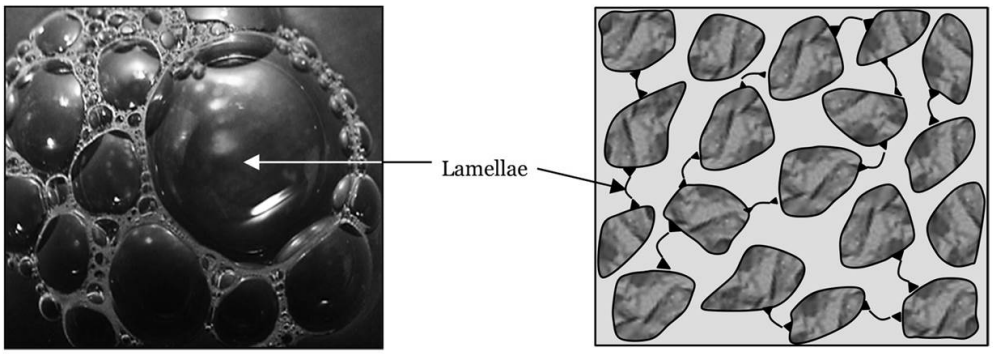


Figure 4.3: Bulk foam that is experienced in everyday life (a) and foam in porous media (b). Lamellae are thin liquid films with a thickness of the order of 10-100 nm. Foam lamellae reduces the gas mobility by trapping a large fraction of gas in place and increasing the effective gas viscosity. After Namdar Zanganeh (2011)

Foam in porous media is defined as a dispersion of gas in a liquid (Fig. 4.3) such that the liquid phase is continuous, and at least some part of the gas is rendered discontinuous by thin liquid films called lamellae (Hirasaki, 1989; Kovscek and Radke, 1994; Namdar Zanganeh, 2011). Foams for mobility control in oil reservoirs are formed when gas contacts surfactant in the presence of mechani-

cal agitation. Pre-generated foam injection, coinjection of gas and surfactant solution, and Surfactant-Alternating-Gas (SAG) injection processes have been commonly used as injection strategies to achieve the generation and transport of foam in porous media (Skauge et al., 2002; Shan and Rossen, 2004; Haugen et al., 2012). The choice of injection method is typically based on the ability of a given strategy to propagate foams deeply into a porous media for mobility control.

During the numerical simulation of foam migration, local-steady-state (e.g. semi-empirical) models (Surguchev et al., 1995; Skauge et al., 2002; Namdar Zanganeh and Rossen, 2013) or fully mechanistic (e.g. dynamic population balance) models (Falls et al., 1988; Kovscek et al., 1995) are used to describe foam generation and transport in porous media. Local steady state models implicitly account for the role of foam texture on gas mobility using an algebraic relation between gas mobility and the factors that determine foam texture. Fully mechanistic models take the rate of change of foam texture into account, introduce additional complexity to foam modelling, and are thought to include the essential flow physics during foam displacement. However, the results from fully mechanistic models in several studies converge to the results of semi-empirical foam models (i.e. standard models) at distances comparable to pattern or reservoir scale (Renkema and Rossen, 2007; Chen et al., 2010). Standard models are employed in this thesis to limit the overall level of complexity when capturing foam flow physics, fracture-matrix interaction and wettability effects.

Foam EOR has been employed in several field pilots which report significant improvement in sweep efficiency (e.g., Enick et al., 2012; Talebian et al., 2014), delayed gas breakthrough (e.g., Blaker et al., 1999) and consequently incremental oil recovery. Despite various field trials, foam behaviour in porous media in general and fractured reservoirs in particular is not well understood (e.g., Yan et al., 2006; Haugen et al., 2012; Pancharoen et al., 2012). Extensive field application of foam EOR that is technically and economically successful would, therefore, require detailed reservoir evaluation and process optimization which can be achieved using a predictive numerical model such as the high-resolution analogue reservoir model used in this study.

## 4.3 COMPOSITIONAL FLUID AND RESERVOIR MODEL

The simulation model and wettability data are similar to those used in chapter 3. Compositional phase behaviour was modelled with the Peng and Robinson (1976) equation of state. The fluid properties are similar to those used by Egwuenu et al. (2008), consisting of a six component fluid model that was lumped and tuned to match constant volume depletion, differential liberation and constant composition expansion PVT experiments (Table 4.1). The bubble-point pressure of the fluid is 1,650 psi. The multi-contact minimum miscibility pressure (MMP) is 2325 psi for $CO_2$ injection estimated at the given reservoir conditions using numerical slim tube simulations.

| Initial Compositions | | | | | |
|---|---|---|---|---|---|
| $CO_2$ | $C_1$ | $C_2$ | $C_3$ | $C_{4-6}$ | $C_{7+}$ |
| 0.001 | 0.3467 | 0.0313 | 0.0396 | 0.1307 | 0.4507 |

Table 4.1: Properties for compositional fluid model

The flow simulations were constrained to a sector scale model containing 34 x 35 x 36 cells (Fig. 4.1 and Fig. 4.2). The sector scale simulation model was used in order to reduce the large computational costs required to account for fracture-matrix interaction with dual-porosity dual-permeability compositional models. The reservoir is simulated using a quarter 5-spot well pattern. As in chapter 3, fractures are included stochastically in the geological model using the discrete fracture network (DFN) approach (Dershowitz et al., 2000). Subsequently, equivalent permeability tensor, porosity and shape factors are obtained by DFN upscaling using the modified Oda method. A summary of some important reservoir properties is given in Table 4.2.

To model foam EOR, the semi-empirical foam model available in STARS$^{TM}$ was employed (Surguchev et al., 1995; CMG, 2014). In this formulation, the effects of foam on gas mobility and flow pathways are modelled by modifying gas relative permeability curves (Fig. 4.4). The relative gas mobility in the absence of foam is rescaled to the relative gas mobility in the presence of foam by multiplying it with a dimensionless reduction factor (Renkema and Rossen,

| Parameter | Value |
|---|---|
| Grid dimension | 34 x 35 x 36 |
| Grid block size (m) | 15 x 15 x 3 |
| Initial reservoir pressure (kPa) | 20,684 |
| Maximum BHP (kPa) | 41,300 |
| Minimum BHP (kPa) | 16,500 |
| Average matrix permeability (mD) | 84 |
| Average fracture permeability (mD) | 867 |

Table 4.2: Reservoir Properties

2007; Namdar Zanganeh and Rossen, 2013). Subsequently, the gas mobility used in each computation is obtained by interpolating between relative permeability curves that account for the presence or absence of foam, depending on the coexistence (or lack thereof) of surfactant and gas in the reservoir.
The semi-emperical foam model is defined by:

$$\lambda_{rg}^{f} = \frac{\lambda_{rg}^{nf}}{MRF}, \qquad where \qquad MRF = 1 + fmmob \times F_w \times F_o \times F_s \tag{4.1}$$

where the gas relative mobility in the absence of foam ($\lambda_{rg}^{nf}$) is rescaled to the gas relative mobility in the presence of foam ($\lambda_{rg}^{nf}$) by dividing $\lambda_{rg}^{nf}$ by the gas Mobility-Reduction-Factor (MRF). $fmmob$ represents the maximum resistance to flow. $F_w$, $F_o$, and $F_s$ are functions that describe the stability of foam in the presence of water, oil, and surfactant, respectively (Surguchev et al., 1995; Namdar Zanganeh and Rossen, 2013; Namdar Zanganeh et al., 2014). In general, foam is weakened at low water saturations ($S_w \leq S_w^*$), foam is killed at high oil saturations ($S_o \geq S_o^*$) and foam is active above the critical surfactant concentration, ($C_s \geq C_s^*$) (Fig. 4.5).

Coinjection and SAG foam injection strategies which have been used in several field applications (e.g., Skauge et al., 2002; Talebian et al., 2014) were tested. The injected surfactant concentration was 0.3 $wt\%$ which is consistent with experimental surfactant concentrations required for the generation, coalescence and transport of foam in porous media (e.g., Apaydin and Kovscek, 2001). A summary of some important foam parameters is presented in Table 4.3.

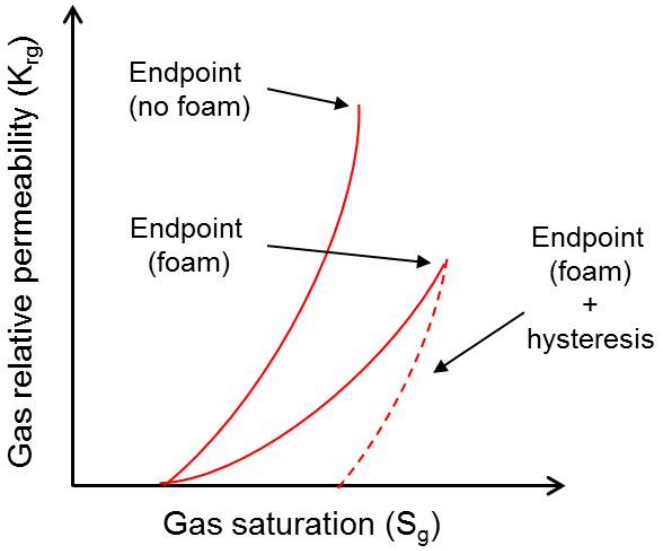


Figure 4.4: Relative permeability interpolation implemented in foam reservoir simulation models. Value of gas mobility during simulation is obtained by interpolating between the gas relative permeability curves in the presence and absence of foam. Modified after CMG (2014).

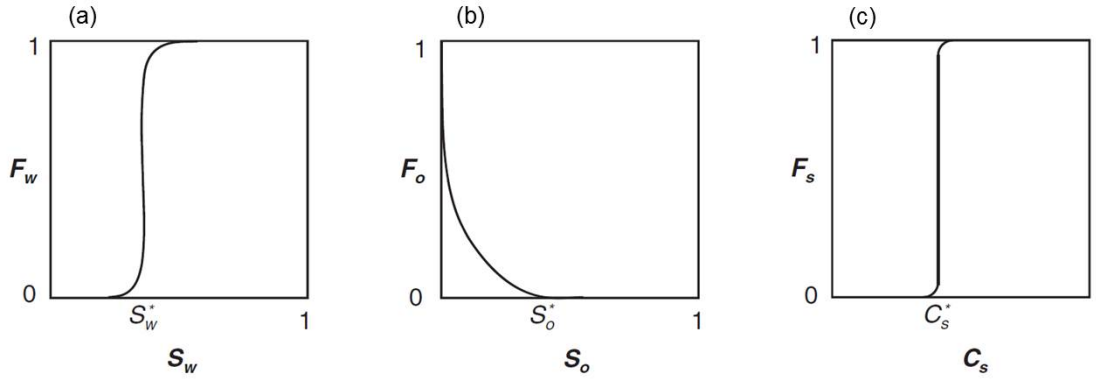


Figure 4.5: Foam model indicating foam sensitivity to water saturation (a), oil saturation (b) and surfactant concentration (c). From Namdar Zanganeh et al. (2014).

| Foam Parameter | Symbol | Value |
|---|---|---|
| Reference Mobility Reduction Factor | fmmob | 100 |
| Reference Capillary Number | fmcap | $2.0^{-4}$ |
| Critical Oil Saturation | fmoil ($S_o^*$) | 1.0 |
| Critical Surfactant Concentration | fmsurf ($C_s^*$) | $5.0^{-5}$ |
| Injected Surfactant Concentration | fmsurf ($C_s$) | $3.0^{-3}$ |
| Exponent for Surfactant Contribution | epsurf | 1.0 |
| Exponent for Oil Saturation Contribution | epoil | 0.0 |

Table 4.3: Semi-empirical foam model parameters.

## 4.4 GAS INJECTION STRATEGIES

### 4.4.1 *Continuous Gas Injection and WAG*

When continuous injection strategies were compared (Fig. 4.6a), water injection, immiscible continuous gas injection, miscible immiscible continuous gas injection, immiscible WAG and miscible WAG achieved recovery estimates of 66%, 48%, 55%, 61% and 73% respectively. It is evident from the above results that unfavourable mobility due to channelling (see Fig. 3.2 and 3.3) and gravity override negatively impact the efficiency of gas injection and that the application of WAG injection combined with miscible displacement significantly improves hydrocarbon recovery.

### 4.4.2 *Hybrid Gas Injection and WAG*

When a three year water injection period preceded continuous gas injection or WAG (Fig. 4.6b), recoveries were consistently higher compared to the cases where gas injection or WAG was implemented from the outset (Table 4.4). Hence, WAG could have significant potential for incremental recovery in carbonate reservoirs, which have been experiencing waterflooding previously (e.g.,

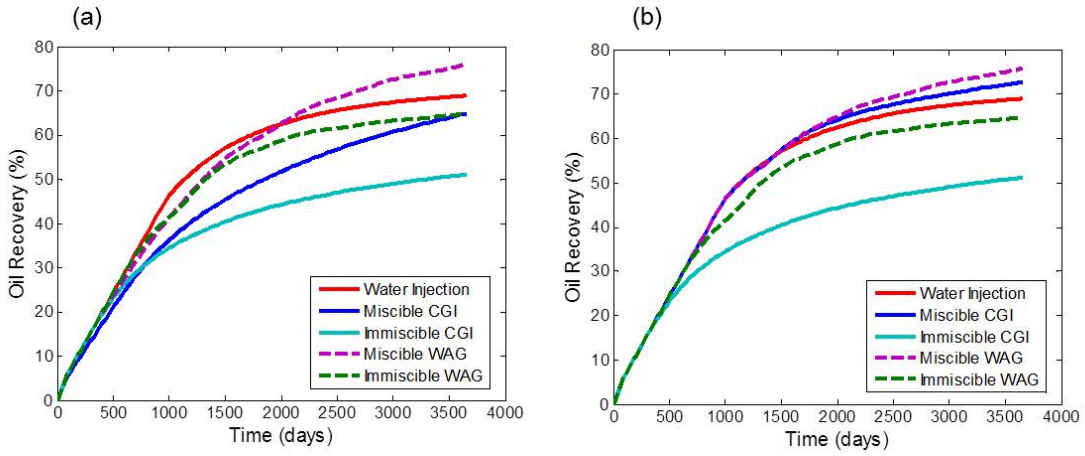


Figure 4.6: Oil recovery profiles for regular (a) and hybrid (b) gas injection. The combination of WAG injection and miscible displacement to improve overall sweep efficiency yields relatively higher oil recovery. Slightly better results are obtained for all scenarios when water injection precedes CGI or WAG. CGI refers to continuous gas injection. WAG refers to water alternating gas injection.

Rawahi et al., 2012). Conversely, initiating WAG from day one, such as currently considered for the Brazilian pre-salt reservoirs (e.g., Pizarro and Branco, 2012), may be detrimental to oil recovery. The improved results can be attributed to the tendency of the initially injected water to minimise gas channelling, reduce the rate of encroachment of the gas front and decrease viscous fingering effects.

| Simulation Model | Recovery (%) | Inc. Rec. (%) |
|---|---|---|
| Water Injection | 66.31 | – |
| CGI (Immiscible) | 48.25 | −18.06 |
| CGI (Miscible) | 55.20 | −11.11 |
| WAG (Immiscible) | 60.91 | −5.40 |
| WAG (Miscible) | 73.17 | 6.86 |
| Hybrid WI/CGI (Immiscible) | 57.51 | −8.80 |
| Hybrid WI/CGI (Miscible) | 64.23 | −2.08 |
| Hybrid WI/WAG (Immiscible) | 63.34 | −2.97 |
| Hybrid WI/WAG (Miscible) | 73.61 | 7.30 |
| Foam (SAG) | 76.23 | 9.92 |

Table 4.4: Summary of gas injection simulation results. CGI refers to continuous gas injection. WAG refers to water alternating gas injection. WI refers to water injection.

## 4.5 FOAM MOBILITY CONTROL

Foam generated in the reservoir captures gas in foam bubbles, creates a viscous pressure drop and diverts injected fluids from the high permeability fractures to the low permeability matrix. Foam EOR, therefore, reduces the gas mobility and improves the overall sweep efficiency (Table 4.4). Foam also delays gas breakthrough.

### 4.5.1 *Foam Injection Strategy*

When different injection strategies are compared, it can be observed that surfactant-alternating-gas (SAG) consistently outperforms coinjection for all the wettability scenarios in terms of oil recovered (Fig. 4.7a). The semi-empirical foam model used in this study assumes that foam is generated in-situ wherever surfactant

and gas coexist. As a result, the coinjection strategy generates foam in the near wellbore region, limits fluid injectivity and consequently reduces the oil recovered. Limited injectivity also makes it difficult to perform coinjection below the formation fracturing pressure (Awan et al., 2008).

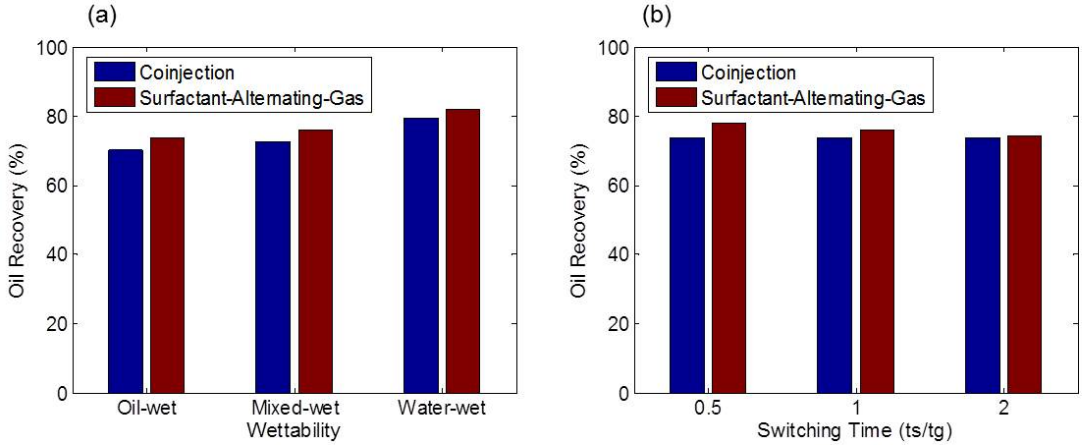


Figure 4.7: Impact of injection strategy on oil recovery during numerical simulation with multiple wettability (a) and switching time (b) scenarios. The switching time ratio ($t_s/t_g$) is the ratio of the time of surfactant injection ($t_s$) to the time of gas injection ($t_g$) within SAG cycles.

On the other hand, SAG injection allows surfactants to be displaced some distance into the reservoir prior to gas injection and subsequent foam generation, thereby, leading to relatively better injectivity. However, it is important to identify the optimum period of surfactant injection (switching time) during SAG cycles to maximize oil recovery. The simulation results show that due to the high permeability fluid transport through the connected fracture networks, shorter switching times improve oil recovery by limiting surfactant breakthrough and generating adequate pressure drop for improved recovery from the matrix (Fig. 4.7b). The higher oil recovery in the water-wet scenario (Fig. 4.7a) can be attributed to the foam strength which is typically higher in water-wet rocks and can divert more of the injected fluids to the unswept regions of the reservoir. Furthermore, the potential for oil recovery by spontaneous imbibition into the matrix increases with increasing water-wetness of the matrix (Morrow, 1990; Tavassoli et al., 2005; Schmid and Geiger, 2013).

It can be observed that the gas-oil-ratio (GOR) is generally low when foam is injected, irrespective of the wettability scenario due to the trapping of gas in

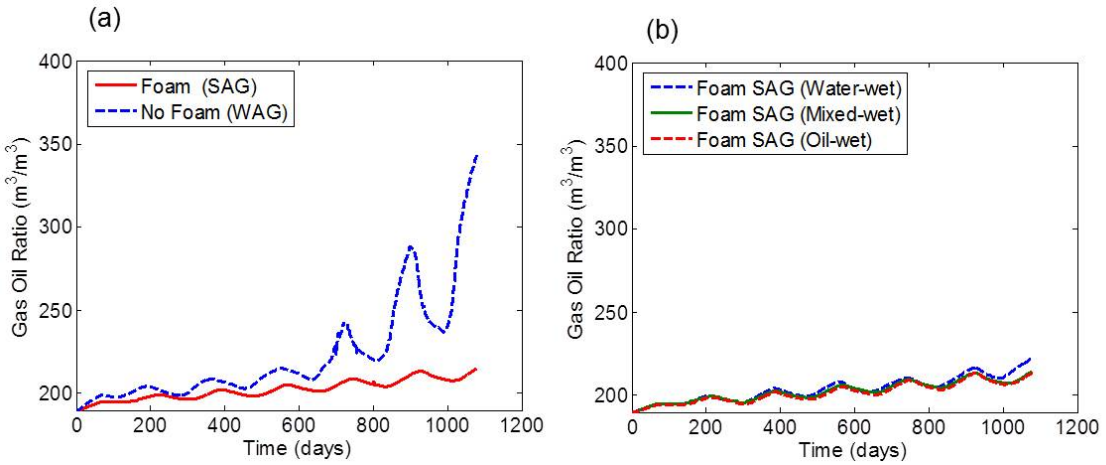


Figure 4.8: Gas-Oil-Ratio (GOR) for numerical simulations with and without foam EOR (a) and simulations varying matrix wettability (b). Foam captures gas in foam bubbles and reduces the gas mobility.

foam bubbles (Fig. 4.8). Again, the water-wet scenario shows a slight increase in GOR compared to the mixed-wet and oil-wet scenarios. This is because water-wet rocks have high capillary entry pressures that relatively limit gas entry to the matrix. More detailed analysis of wettability effects on subsurface flow modelling for fractured carbonate reservoirs is presented in chapter 5.

### 4.5.2 *Viscous Pressure Drop*

In the presence of foam, relatively large pressure drops are generated in the reservoir especially in the near wellbore region (Fig. 4.9a). Such large viscous pressure drop due to foam generation is typically responsible for diverting surfactant solution and injected gas from high permeability to lower permeability regions in the reservoir, thereby improving the sweep efficiency. Figure 4.9b shows that compared to the case without fractures, the viscous pressure drop when fracture networks are present is low. This is to be expected since connected fractures act as paths for rapid transport of injected fluids thereby causing lower near wellbore pressures. Similarly, when wettability scenarios are varied (Fig. 4.9c), higher viscous pressure drop is encountered in the water-wet scenario compared to the mixed-wet and oil-wet scenarios. As discussed previously, stronger foam is generated in more water-wet formations while the presence of oil weakens foam.

One way of modifying the influence of the viscous pressure drop during SAG foam injection is by varying the switching time ratio (i.e. ratio of the time of surfactant injection ($t_s$) to the time of gas injection ($t_g$) within SAG cycles). When the switching time ratio is varied from 0.1 to 2, the pressure drop decreases from 23,000 kPa to 20,000 kPa (Fig. 4.9d), which indicates that shorter switching times are required to optimise the viscous pressure drop and improve sweep efficiency in fractured carbonate reservoirs. Longer switching times perform poorly because of the tendency for early surfactant breakthrough due to the high permeability fracture network.

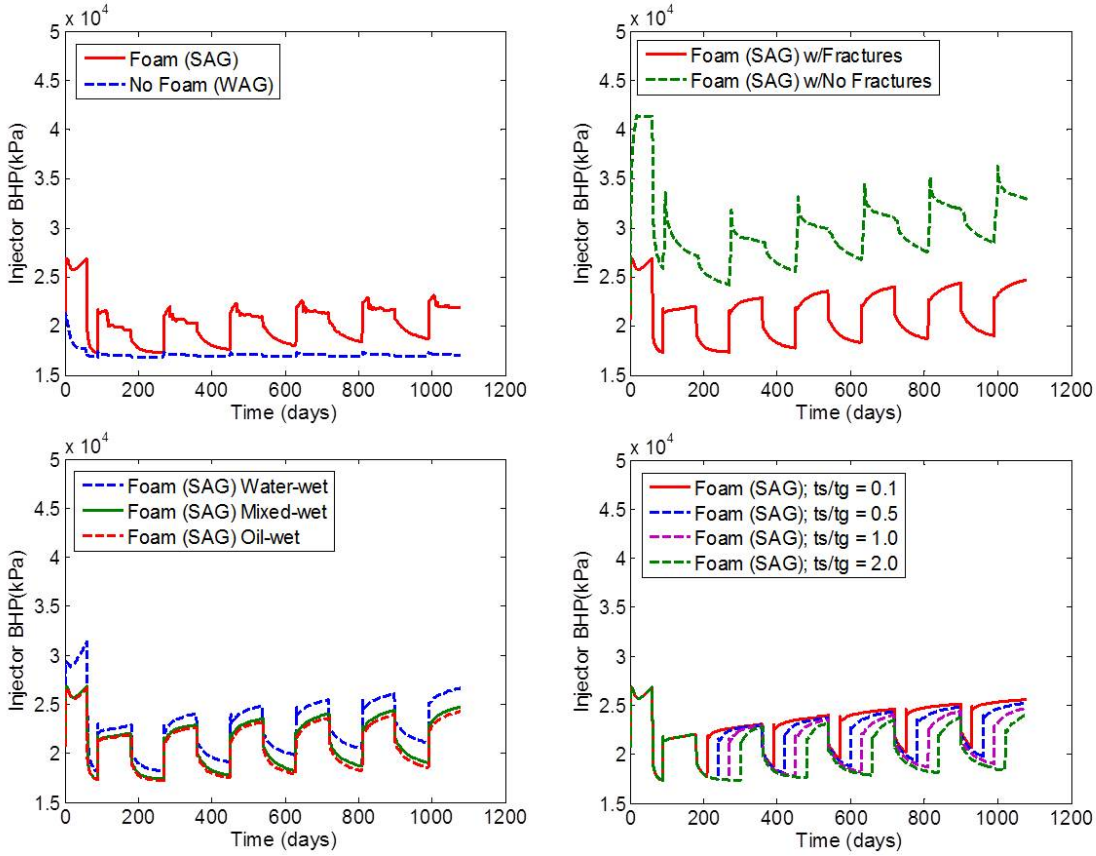


Figure 4.9: Effect of foam (a), fractures (b), wettability (c) and and switching time (d) on the injector bottom-hole-pressure (BHP) and overall viscous pressure drop during foam EOR. The switching time ratio ($t_s/t_g$) is the ratio of the time of surfactant injection ($t_s$) to the time of gas injection ($t_g$) within SAG cycles.

## 4.6 SUMMARY

This chapter shows that reservoir specific (i.e. tailored) EOR methods are essential for recovery optimisation in carbonates and the use of high-resolution outcrop models to account for geological heterogeneities in detail can improve the selection of the best displacement technology for a given reservoir. Suitable outcrop exist for a wide range of carbonate reservoirs and value can be added by subjecting such analogues more frequently to flow simulations to study specific IOR and EOR techniques rather than only using them to constrain the geology of the inter-well space.

Compositional simulations of gas injection using a sector of the Amellago model demonstrate the impact of heterogeneity on fluid flow. The results are directly correlated to the heterogenous nature of the analogue reservoir, highlighting the importance of adequate reservoir characterisation for accurate prediction of subsurface behaviour. For the investigated gas injection processes, channelling and structurally induced bypassing lead to generally lower hydrocarbon recoveries. The results show that WAG can improve the stability of the displacement front. Miscibility also improves the microscopic sweep efficiency and improves the overall recovery. When waterflooding precedes gas injection or WAG (i.e. hybrid scenario), improved recovery estimates are obtained. Prior waterflooding is desirable for operational efficiency as it enables more extensive data gathering before EOR implementation. Such extensive data gathering can reduce uncertainties during EOR deployment. In general, combining static and dynamic reservoir modelling with the knowledge of observed geological structures in the outcrop enables the calibration of reservoir simulation models for accurate full-field predictions. The calibrated simulation models can then be used to identify an optimised displacement strategy for a given reservoir.

Finally, this chapter shows that foam EOR can further mitigate the adverse unfavourable mobility of gas and improve sweep efficiency in carbonate formations. Viscous pressure drop due to foam generation in the fractures complements drainage and imbibition oil recovery mechanisms by diverting surfactant

and gas from the high permeability fractures to the low permeability matrix. Gas breakthrough is delayed when foam EOR is employed, resulting in improved recoveries of up to 9%. Also, SAG injection outperforms coinjection when in-situ foam generation strategies are compared for this reservoir because SAG injection encounters less flow restriction in the near wellbore zone.

# 5

# WETTABILITY, HYSTERESIS AND FRACTURE-MATRIX INTERACTION DURING $CO_2$ EOR AND STORAGE

## 5.1 INTRODUCTION

Carbon Capture and Storage (CCS) in subsurface reservoirs can potentially contribute to reducing $CO_2$ emissions and mitigating global climate change (e.g., Qi et al., 2009; Liu et al., 2012; Szulczewski et al., 2012; Petvipusit et al., 2014; Wriedt et al., 2014). CCS can be implemented simultaneously with $CO_2$ enhanced oil recovery (EOR) to achieve mutual benefits of subsurface CO2 storage and increased oil production in mature hydrocarbon fields. Oil reservoirs are particularly attractive for $CO_2$ storage because the geology is relatively well known thereby reducing geological uncertainties associated with $CO_2$ migration and geological storage (Kovscek, 2002; Kovscek and Cakici, 2005; Iding and Ringrose, 2010; Leach et al., 2011; Liu et al., 2012; Ettehadtavakkol et al., 2014).

Carbonate reservoirs which are estimated to contain about 60 % of global conventional and unconventional hydrocarbon resources (Beydoun, 1998; Burchette, 2012; Agar and Geiger, 2015) form suitable candidates for $CO_2$ EOR and storage because of the potentially large amounts of CO2 that can be sequestered in carbonate formations while improving hydrocarbon recovery (Liu et al., 2012). Carbonate reservoirs, however, are often difficult to exploit due to multiscale heterogeneities that arise from complex diagenetic, reactive, depositional and deformational processes, resulting in complicated subsurface flow behaviours. Carbonate reservoirs may also contain multiscale natural fracture networks that comprise complex high permeability flow paths in the reservoir (e.g., Guerreiro

et al., 2000; Gale et al., 2004; Toublanc et al., 2005; Spence et al., 2014). The variability in matrix structure and fracture network connectivity is the main reason why fractured carbonate reservoirs show a large variety of flow behaviours, leading to significant uncertainties in predicting $CO_2$ plume distributions and hydrocarbon recovery (Cosentino et al., 2001; Bourbiaux et al., 2002; Makel, 2007).

The reliability of underground $CO_2$ storage during EOR in fractured carbonate reservoirs depends on a number of interrelated trapping mechanisms. Structural trapping defines the geometry within which more permanent storage can occur. Solubility trapping occurs when $CO_2$ dissolves into the formation brine. Mineral trapping which entails geochemical binding of $CO_2$ to the rock due to mineral precipitation, guarantees permanent $CO_2$ immobilisation but on a scale of hundreds to thousands of years, too long to have a bearing on storage security over an operational period. Residual trapping is due to snap-off (or disconnection) of the $CO_2$ phase such that it becomes an immobile (trapped) phase when droplets of $CO_2$ become isolated from the $CO_2$ plume by encroaching brine (Juanes et al., 2006). Residual trapping occurs due to differences in the advancing and receding contact angles during repeat imbibition and drainage cycles. It is this sequestration mechanism, residual trapping, which occurs over years to decades (short-term storage), that is investigated in this study. Understanding the underlying physicochemical processes responsible for residual trapping can therefore provide a conservative estimate of $CO_2$ storage security over timescales in line with EOR projects (Bachu et al., 1994; Pruess et al., 2003; Juanes et al., 2006; Qi et al., 2008, 2009; Wilkinson et al., 2009; Burnside and Naylor, 2014).

This chapter considers the relationship between residual trapping of $CO_2$ and WAG injection which has been found to be a successful EOR mechanism for carbonate reservoirs (Christensen et al., 2001; Manrique et al., 2007; Awan et al., 2008; Kalam et al., 2011; Pizarro and Branco, 2012; Rawahi et al., 2012). $CO_2$ WAG injection combines the benefits of gas injection to reduce the residual oil saturation and water injection to improve mobility control and frontal stability (Fig. 5.1). Due to the cyclic nature of $CO_2$ WAG injection, hysteresis is common and leads to the residual trapping of $CO_2$. Hysteresis occurs as a result of the dependence of relative permeability and capillary pressure curves on the satu-

ration path (Fig. 5.2). Only hysteresis models are able to capture the overall benefit of residual trapping, which lies in the fact that it can safely trap $CO_2$ in the subsurface while reducing the overall $CO_2$ phase mobility and improving oil recovery (Spiteri and Juanes, 2006; Spiteri et al., 2008; Burnside and Naylor, 2014).

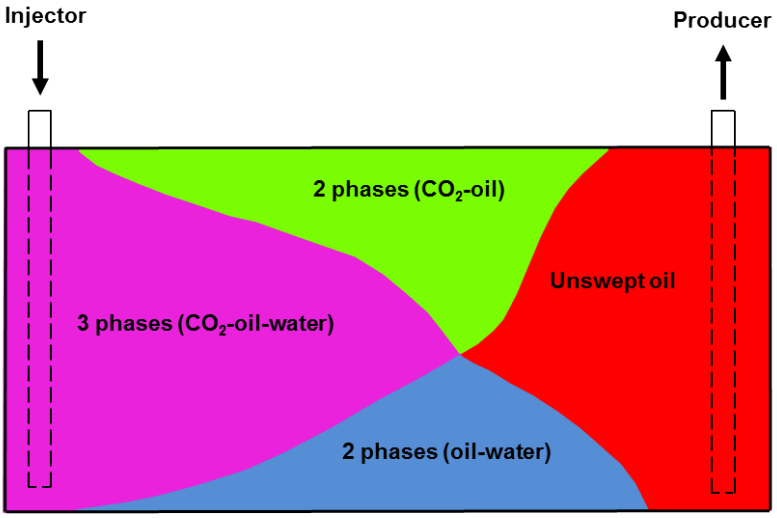


Figure 5.1: Conceptual model of immiscible $CO_2$ WAG injection. Water and $CO_2$ are injected through same well, generating two- and three-phase regions. $CO_2$ WAG injection combines the benefits of gas injection to reduce the residual oil saturation and water injection to improve mobility control and frontal stability.

Several models have been developed to account for hysteresis during multiphase flow in subsurface reservoirs. They are based on the use of scanning curves in which the direction of saturation change is reversed at a number of intermediate saturations. Killough (1976) two-phase hysteresis model accounts for hysteresis as a function of the Land trapping parameter (Land, 1968). This model allows for reversibility of drainage and imbibition cycles along the same scanning curve. The Carlson (1981) model accounts for hysteresis by predicting the trapped non-wetting phase saturation via shifting of the bounding imbibition curve. The Carlson (1981) model, which also employs reversible scanning curves, is only adequate if the intermediate scanning curves are almost parallel and the imbibition curve has minimal curvature. Three-phase hysteresis models have been developed that represent non reversibility (or cycle dependence) of scanning curves during hysteresis (e.g., Lenhard and Parker, 1987; Lenhard and Oostroom, 1998; Larsen and Skauge, 1998; Egermann et al., 2000) and are

thought to include the essential flow physics during cyclic flooding. Furthermore, detailed numerical models which represent hysteresis mechanisms at the pore scale (e.g., Blunt et al., 2002; Jackson et al., 2003; Joekar-Niasar et al., 2008, 2013) can increase investigators understanding of the pore scale physics of hysteresis and residual trapping during cyclic displacement processes.

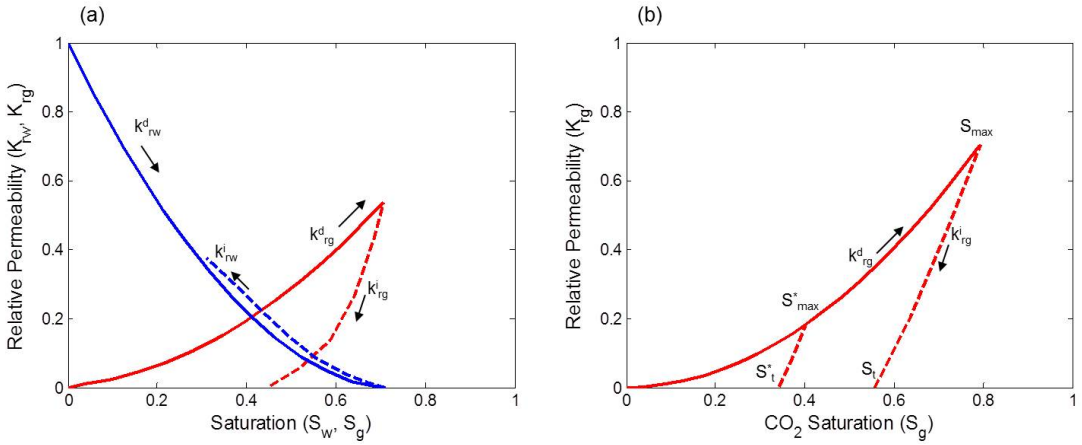


Figure 5.2: Relative permeability curves (a, b) illustrating hysteresis and residual $CO_2$ trapping during WAG injection. Hysteresis effect is more significant for the non-wetting $CO_2$ phase (a). Scanning curves illustrate the maximum trapped fraction ($S^*_t$, $S_t$) corresponding to the maximum $CO_2$ saturation ($S^*_{max}$, $S_{max}$) at flow reversal (b). Superscripts $d$ and $i$ refer to drainage and imbibition respectively.

Hysteresis is also influenced by wettability. Knowledge of the wetting preference and its variation in a carbonate reservoir rock is fundamental to understanding flow behaviour during $CO_2$ EOR and storage but is difficult to quantify due to the intrinsic heterogeneity of carbonates (Okasha et al., 2007; Ferno et al., 2011; Dernaika et al., 2013). Several authors (e.g., Kovscek et al., 1993; Jadhunandan and Morrow, 1995; Blunt, 1997; Hui and Blunt, 2000; Van Dijke et al., 2001; Al-Futaisi and Patzek, 2003; Valvatne and Blunt, 2004; Ryazanov et al., 2009, 2014) have demonstrated how wettability changes alter relative permeability functions, using a number of drainage and imbibition simulations and experiments where the range of advancing and receding contact angles was modified. They found that during imbibition, the transport properties of permeable porous media are sensitive to the hysteresis between receding and advancing contact angles. This difference ultimately controls the amount of trapped fluids due to hysteresis and needs to be captured in reservoir simulation models.

This chapter investigates the effect of residual trapping on $CO_2$ EOR and storage in relation to the multi-scale heterogeneities that are pervasive in fractured carbonate reservoirs. Residual trapping is demonstrated using hysteresis models with reversible scanning curves during WAG imbibition and drainage cycles. The fracture system is represented with discrete fracture network (DFN) models generated using detailed geological observations. The DFN is then upscaled to obtain effective permeability tensors for the fracture grid that is coupled to the matrix using a dual-porosity dual-permeability model. Because the specific geometry of the DFN is difficult to constrain, three distinct hypotheses for the evolution of the fracture system were investigated; (1) Regional fracture geometry which represents a pervasive background fracture system (2) Fault related fracture geometry where fractures cluster around faults and decrease in intensity as the distance to faults increase (3) Bedding related fracture geometry where the fractures are stratigraphically confined to the bedding and give rise to high fracture permeability layers. Such fracture systems have been previously observed in other fractured carbonate formations (e.g., Chesnaux et al., 2009; Agar et al., 2010; Shekhar et al., 2014).

Since the structural, multiphase flow and transport properties encountered in the reservoir exhibit such significant uncertainties, multiple numerical simulations were used to analyse the following questions: How can the understanding and prediction of subsurface flow behaviour during $CO_2$ EOR and storage under geological uncertainty be improved? By investigating the range of uncertainties in wettability, residual trapping and the fracture network, can their impact on the efficiency of $CO_2$ EOR and storage in fractured carbonate formations be ranked? What engineering measures can be used to mitigate the effect of geological uncertainties? Can this workflow be used to screen different $CO_2$ EOR and storage projects, determine the best solutions for specific reservoirs and identify optimum $CO_2$ EOR and sequestration strategies? Is there a competition between maximising $CO_2$ EOR and maximising $CO_2$ storage?

## 5.2 SETUP OF NUMERICAL SIMULATION MODELS

### 5.2.1 *Matrix Simulation Model*

A flow simulation model (Fig. 5.3) upscaled from the detailed geological model described in chapter 3 is discretized into 74 x 75 x 36 grid cells (199,800 cells in total). The simulation model captures key structural and sedimentological heterogeneities observed in the Amellago Island outcrop as indicated by the distribution of porosity and permeability in the model (Fig. 5.4). $CO_2$ EOR and storage was simulated using WAG injection with 20 alternating cycles in which 0.075 PV of water or gas was injected per cycle. The WAG ratio was set to 1:1 and the cycle length to 1 year to ensure proper gravity segregation of injected fluids. A regular five-spot well pattern was used with a vertical producer at the centre of the model and four vertical injectors situated at the corners of the model. The reference densities of water, oil and $CO_2$ were set to 1000 kg/m$^3$, 800 kg/m$^3$ and 1.35 kg/m$^3$) respectively.

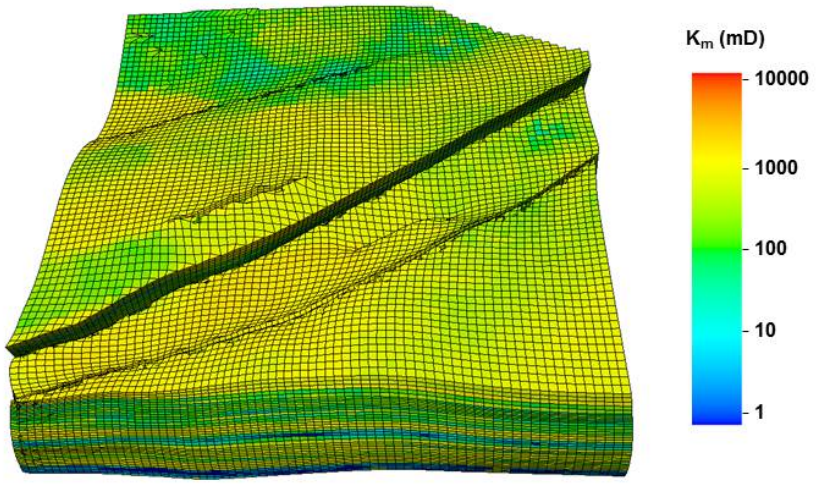


Figure 5.3: Matrix simulation model of the Amellago Island Outcrop, showing the permeability distribution. Individual grid blocks have dimensions of 15x15x3m.

Compositional simulations can capture complex interactions of flow with phase behaviour (e.g. solubility and geochemical effects) especially during long-term $CO_2$ EOR and storage. Compositional simulations for large fractured reservoirs, however, are computationally very expensive because equation of state calcula-

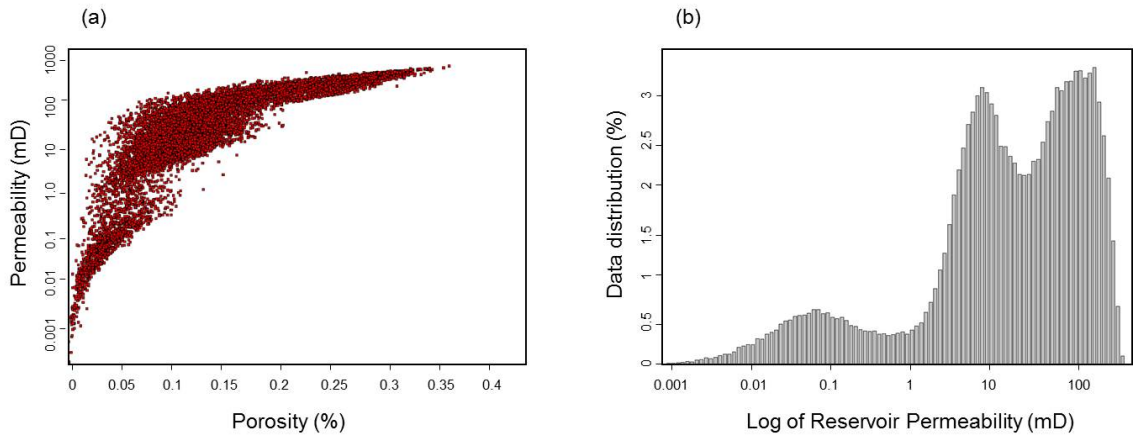


Figure 5.4: Porosity-Permeability distribution (a) and permeability histogram (b) for the matrix used in the reservoir simulation model.

tions, multi-component interactions and fracture-matrix exchange must be taken into account. Hence, this chapter employs full physics black oil simulation of immiscible $CO_2$ WAG injection which can be run much faster than compositional simulations for large fractured carbonate reservoirs to study $CO_2$ EOR and storage. Black oil simulation models can capture the flow physics of the short term $CO_2$ EOR and storage aspects that have been considered in this chapter. This approach is consistent with previous studies which have used black oil models to investigate $CO_2$ EOR and/or $CO_2$ storage in geological reservoirs (e.g., Egermann et al., 2000; Jessen et al., 2005; Juanes et al., 2006; Spiteri and Juanes, 2006; Benisch and Bauer, 2013; Petvipusit et al., 2014).

### 5.2.2 *Distribution of Wettability Functions*

Since wettability functions typically vary both laterally and vertically in subsurface reservoirs, a depth based distribution approach and a facies based distribution approach were compared to the more common approach of using single wettability functions for the whole reservoir. Distributing the wettability functions on the basis of variation with depth (Fig. 5.5a) is consistent with the method employed in previous field studies for clastic and carbonate reservoirs (e.g., Jerauld, 1997; Jackson et al., 2005; Okasha et al., 2007). An alternative method involves distributing the wettability functions by using a facies based approach that correlates wettability to the horizontal permeability of individual grid blocks (Fig.

5.5b) based on the facies types (Clerke, 2009; Agada et al., 2014). Multiple wettability distribution approaches were considered because the wettability functions are only meant to mimic the behaviour of real carbonate reservoirs and the approaches considered seemed to be the most feasible, although, they may be too simplistic for real carbonate reservoirs (e.g., Gomes et al., 2008; Hollis et al., 2010; Chandra et al., 2015).

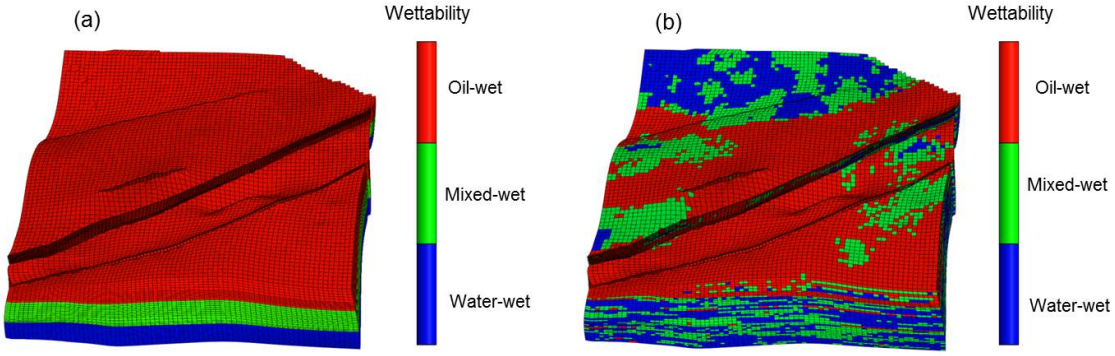


Figure 5.5: Distribution of wettability functions in the simulation model (a) using a depth based approach 'DBA' and (b) using a facies based approach 'FBA'. DBA distributes wettability functions based on variation with depth while FBA correlates wettability functions to the horizontal permeability of individual grid blocks based on the facies type.

### 5.2.3 *Fracture-Matrix Interaction*

The special nature of fractured reservoirs lies in the interaction between the low permeability matrix which provides the main storage in the reservoir and the high permeability fracture system which has low storage. This combination of low-permeability matrix and high-permeability fractures leads to variety of flow behaviours in fractured carbonate reservoirs, including permeability enhancement, flow anisotropy, structurally induced bypassing of oil and rapid water/$CO_2$ breakthrough. These behaviours must be understood to adequately predict long-term reservoir behaviour. Therefore, special care is required to capture the geological complexity of fracture systems in a form that can be represented in reservoir models. Discrete fracture network (DFN) models are commonly used to generate static fracture models (Dershowitz et al., 2000). The models are then calibrated to dynamic data from well tests or production logging

tests (e.g., Wei et al., 1998; Hoffman and Narr, 2012) before they are upscaled to provide permeability distributions for the fracture network. In commercial reservoir simulators, the fracture system, modelled and upscaled using the DFN approach, is coupled to the matrix system using dual continuum models (e.g., Bourbiaux et al., 2002; Casabianca et al., 2007; Al-Kobaisi et al., 2009).

The interaction between fracture and matrix depends on the matrix properties (e.g. porosity, permeability and wettability) and fracture network geometry. The interaction also depends on the displacement mechanisms and physical processes. Fracture-matrix fluid transfer during water injection in a naturally fractured reservoir is controlled by viscous forces and spontaneous imbibition (Schmid and Geiger, 2012, 2013). During spontaneous imbibition, water in the fracture displaces oil from the matrix due to counter-current or co-current flow. The rate of displacement can be modelled using a transfer function that depends on the matrix wettability, matrix permeability and fracture intensity (e.g., Abushaikha and Gosselin, 2008; Ramirez et al., 2009). During $CO_2$ injection, gravity drainage controls the transfer of $CO_2$ into the matrix and concurrently the transfer of oil from the matrix into the fracture due to fluid density differences. This transfer mechanism is particularly important for mixed- to oil-wet reservoirs such as carbonates because the gravitational head can overcome the capillary entry pressure for the displacing gas phase (Di Donato et al., 2007; Lu et al., 2008).

### 5.2.4 *Fracture Network Modelling and Upscaling*

The fracture system was modelled using the DFN approach (Dershowitz et al., 2000) and honours fracture observations in the outcrop. Shekhar et al. (2010) identified three major fracture sets (Fig. 5.6). The mean fracture length was 20 m, while the aspect ratio (length to height) was 4:1. Variation of the fracture length with respect to the mean was defined using an exponential distribution. Fracture apertures with a mean of 0.5 mm were used to estimate fracture permeabilities with the cubic law. Although, the models honour static observations of

the fracture orientation, it is difficult to adequately capture the connectivity of the fracture network.

Hence, the uncertainty in fracture connectivity is investigated by varying the fracture network volumetric intensity (P32). As previously noted, three distinct fracture geometry scenarios are investigated. First, we investigate a pervasive regional fracture scenario where the stochastic fracture intensity is constant across the whole model and defined by intensity values which vary from a poorly-connected system to a well-connected system (Fig. 5.7). A bedding related fracture scenario defined in relation to bed-bound (stratigraphically confined) and interbedded fractures (Fig. 5.8) is also investigated. Finally, a fracture scenario where the fracture intensity is related to the fault zone is investigated. In this case high fracture intensity close to the faults decreases away from the faults (Fig. 5.9). The fracture models focus on open fractures and do not consider closed fractures that might have formed as a result of secondary mineralization. Vertical wells intersect fractures in all cases.

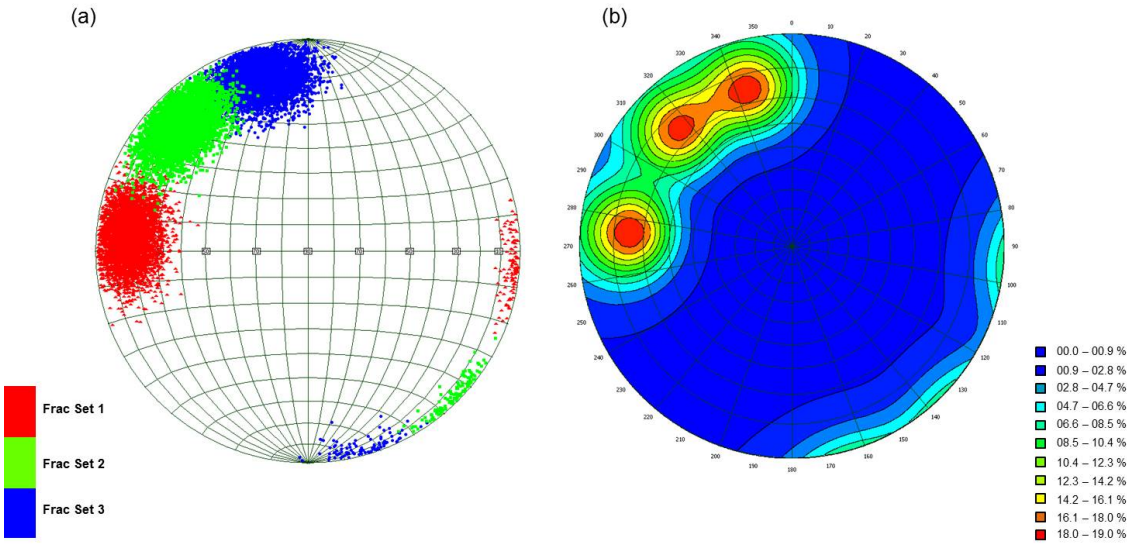


Figure 5.6: Schmidt diagram showing the orientation distribution of three fracture-sets (red, green, blue) with equal projection of the poles in the upper hemisphere (a) and contoured density of fracture poles (b) based on fractures generated for the 3D reservoir model.

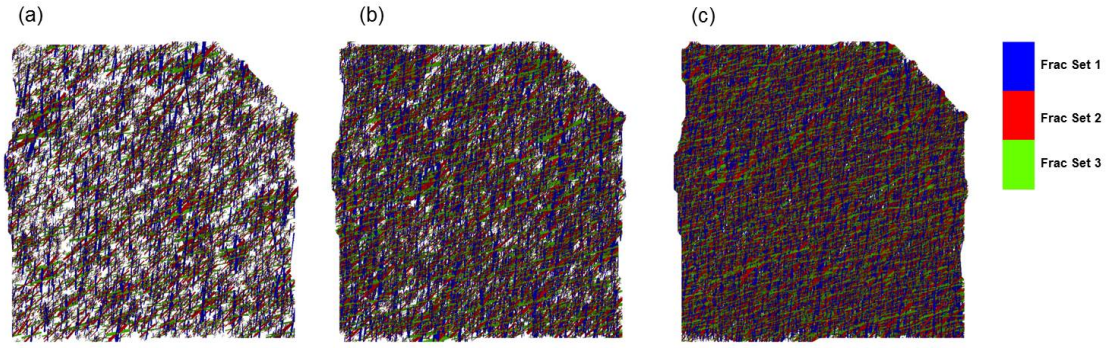


Figure 5.7: Discrete fracture network for regional fracture scenario with fracture intensity of 0.05 $m^2/m^3$ (a), 0.1 $m^2/m^3$ (b) and 0.2 $m^2/m^3$ (c).

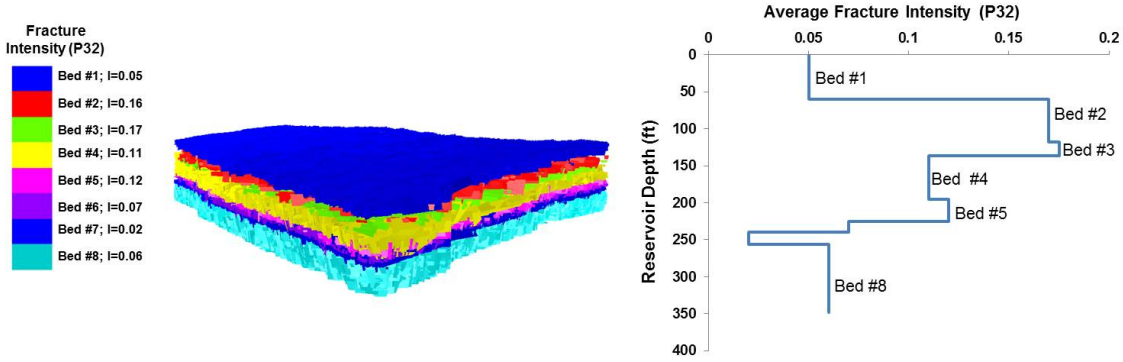


Figure 5.8: Discrete fracture network for bedding related fracture scenario. 70% of the fractures terminate within a single bed, while 30% of the fractures penetrate multiple beds. The average fracture intensity for the entire model is 0.1 $m^2/m^3$.

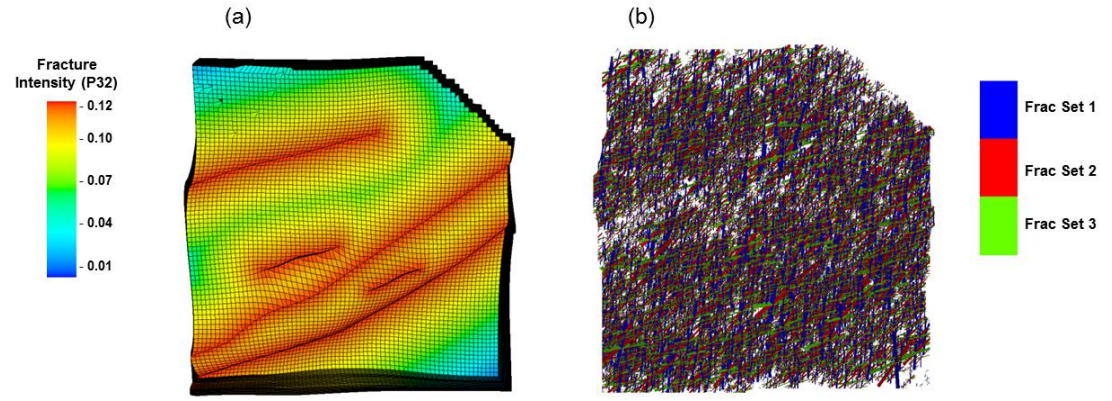


Figure 5.9: Fracture intensity property (a) and discrete fracture network (b) for fault-related fracture scenario. The average fracture intensity for the entire model is 0.1 $m^2/m^3$.

Fracture network flow parameters for each DFN were obtained by upscaling the fracture networks to the grid cells of the simulation model (Fig. 5.10 and 5.11). The modified Oda (1985) DFN upscaling method that is more computationally efficient than flow-based DFN upscaling and accurate for fracture systems with good connectivity was employed. DFN upscaling, results in diagonal fracture permeability tensors that are anisotropic and heterogeneous and honour outcrop observations reasonably well.

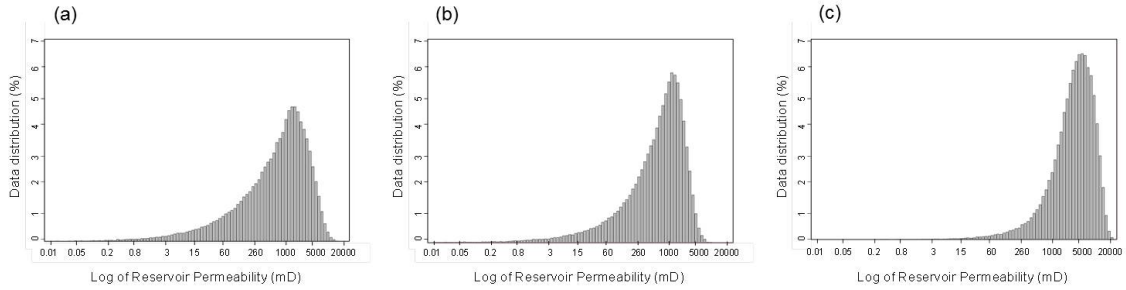


Figure 5.10: Fracture permeability histogram for (a) regional, (b) fault related and (c) bedding related fracture scenarios. Note that fracture permeability is on average about ten times higher than matrix permeability (see figure 5.4).

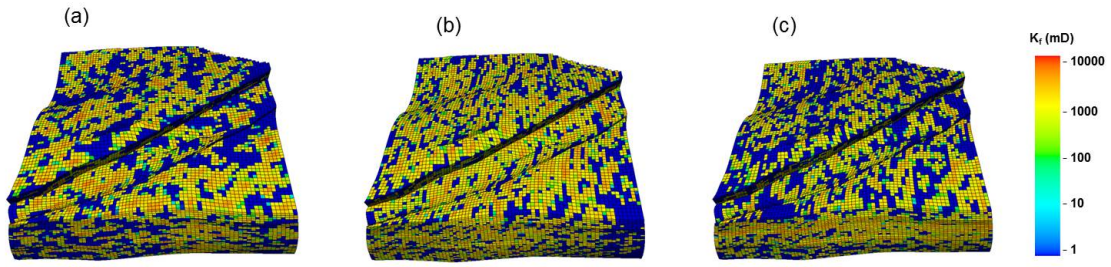


Figure 5.11: Upscaled fracture permeability distribution for (a) regional, (b) fault related and (c) bedding related fracture scenarios. Average fracture intensity is 0.1 $m^2/m^3$ for all cases. Note high fracture permeability around faults in (b) and high fracture permeability layers due to stratigraphically confined fractures in (c).

Due to the, relatively high permeability in the matrix, a dual-porosity dual-permeability model was used to couple fluid flow in the matrix with fluid flow in the fractures and simulate multiphase flow for the range of plausible geological scenarios. It is well known that the dual-permeability formulation is preferable in situations where there is hydraulic continuity in the matrix and high variability in the connectivity of the fracture network (Kazemi et al., 1992; Bourbiaux et al., 2002). The resulting reservoir models, containing fractures and matrix,

are populated with the same fault network, mapped using high-resolution photopanels and LiDAR (Light Detection And Ranging). The faults are represented as discrete non-volumetric features in the geological model. In general, the faults are considered to be fully conductive, with flow reduction across faults occurring only due to the juxtaposition of high and low permeability layers. Fault transmissibility multipliers are used to investigate the impact of fault sealing on multiphase flow in the reservoir. Here, fault transmissibility multipliers of zero correspond to fully sealing faults, while fault transmissibility multipliers of 1 and above correspond to fully conductive faults. More detailed fault models are not within the scope of this study.

## 5.3 WETTABILITY, HYSTERESIS AND FRACTURE-MATRIX INTERACTION

### 5.3.1 *Effect of fracture network intensity*

Figure 5.12 shows upscaled fracture permeabilities and the corresponding matrix saturation distributions for the DFN models assuming P32 of 0.05 $m^2/m^3$, 0.1 $m^2/m^3$, 0.2 $m^2/m^3$ and 0.4 $m^2/m^3$ (a, b, c and d). The oil saturation distributions (e, f, g and h) and $CO_2$ saturation distributions (i, j, k and l), show a clear link between the fracture intensity and the predicted oil and $CO_2$ distributions. As the fracture intensity increases, there is more rapid transport of injected water and CO2 leading to significant bypassing of oil in the matrix. Similarly, as the fracture intensity increases, rapid transport of $CO_2$ leads to high $CO_2$ concentration at the top of the reservoir. Such rapid gas transport will lead to less efficient $CO_2$ sequestration in the matrix. As noted previously, capillary imbibition and gravity drainage are important oil recovery and $CO_2$ storage mechanisms for fractured reservoirs. These mechanisms depend on exchange of fluids between the fracture and the matrix. However, if the flow in the fractures is rapid due to a well-connected fracture network, the residence time of injected fluids in the fracture becomes insufficient to adequately recover oil or store $CO_2$ in the matrix via spontaneous imbibition and gravity drainage, thereby leading to poor hydrocarbon recovery and $CO_2$ sequestration.

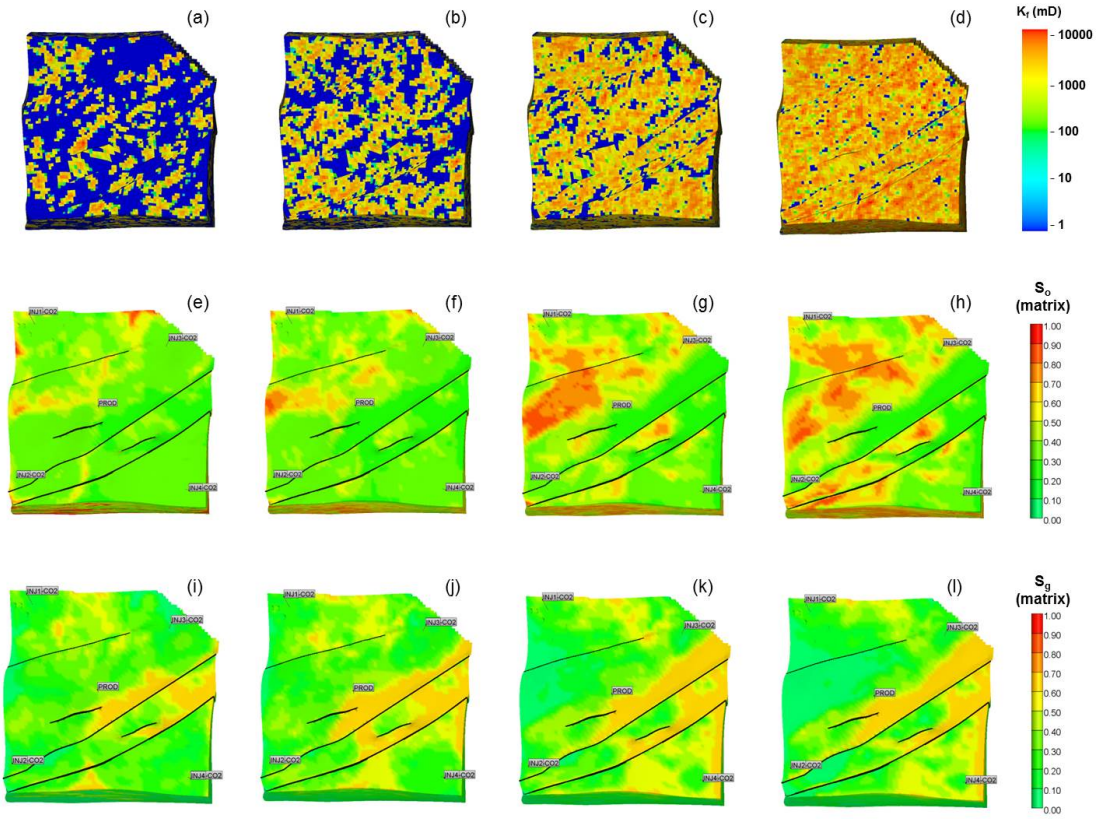


Figure 5.12: Upscaled fracture permeability distribution with increasing regional fracture intensity of 0.05 (a) 0.1 (b) 0.2 (c) 0.4 (d) and corresponding matrix oil saturation (e, f, g, h) and $CO_2$ saturation (i, j, k, l) distributions after immiscible WAG injection. Notice the bypassed oil and high $CO_2$ concentration at the top of the model due to rapid flow of reservoir fluids.

The influence of the fracture network can also be observed in the oil recovery, water cut and $CO_2$ storage profiles (Fig. 5.13). Notice that the presence of open and connected fractures in the reservoir results in lower oil recoveries (Fig. 5.13). Similarly the presence of open and connected fractures results in early water breakthrough (Fig. 5.14a), and lower fractions of $CO_2$ stored (Fig. 5.14b). The bypassing effect that leads to lower oil recovery increases as fracture intensity increases but becomes less significant at higher fracture intensities (P32 greater than 0.4). This behaviour may suggest that in systems where the fracture network is very dense, above a certain threshold, variations in model output due to changes to the fracture network could be negligible thereby potentially reducing the impact of the fracture uncertainty on the model outcomes.

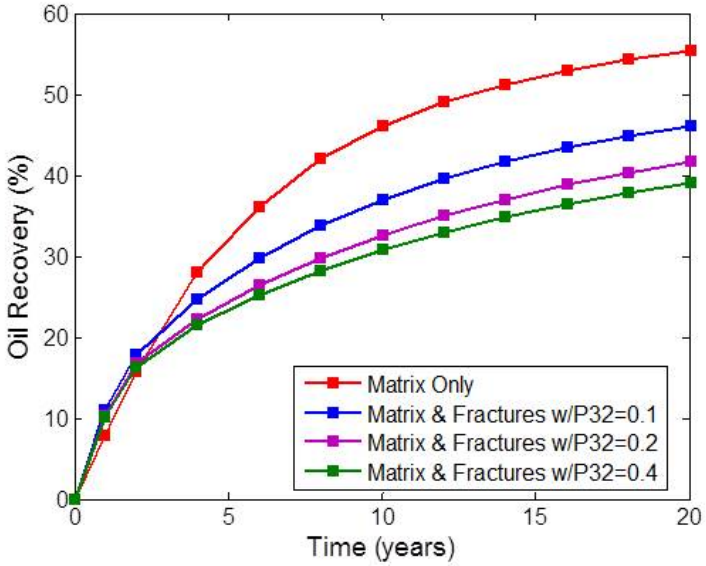


Figure 5.13: Oil recovery during immiscible WAG injection. Fractures are incorporated with dual-porosity dual-permeability models of increasing fracture intensity (P32). Fracture networks cause bypassing and act as fluid flow high ways leading to rapid transport of injected fluids and lower oil recovery.

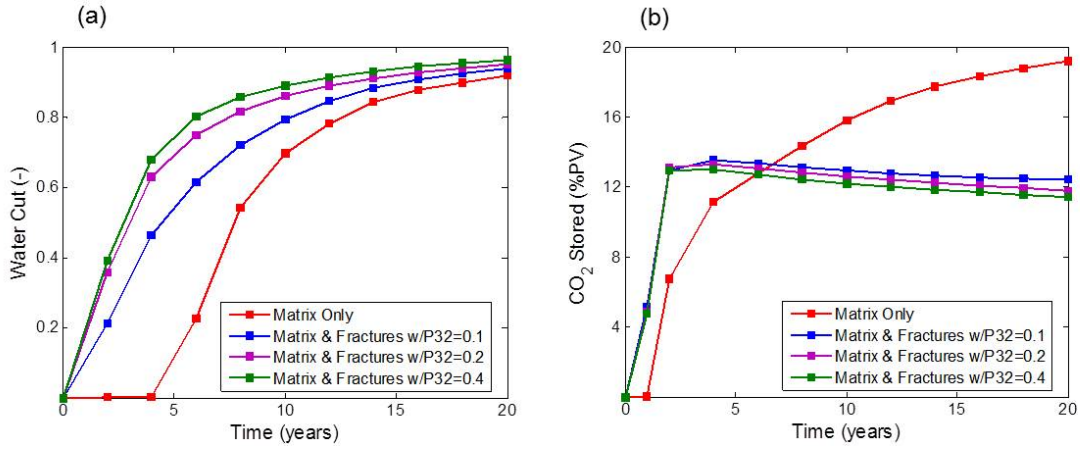


Figure 5.14: Water cut (a) and $CO_2$ stored (b) during immiscible WAG injection. Fractures are incorporated with dual-porosity dual-permeability models of increasing fracture intensity (P32).

### 5.3.2 *Effect of fracture network geometry*

At low fracture network intensity, subtle changes impact the fracture geometry more significantly. Three fracture scenarios were considered; (1) Regional fracture geometry (2) Fault related fracture geometry and (3) Bedding related fracture geometry. For an average fracture intensity of 0.1, the oil recovery varies between 47%, 43% and 40%, assuming regional, fault related or bedding related fracture geometry respectively (Fig. 5.15a, b, c and Fig. 5.16a).

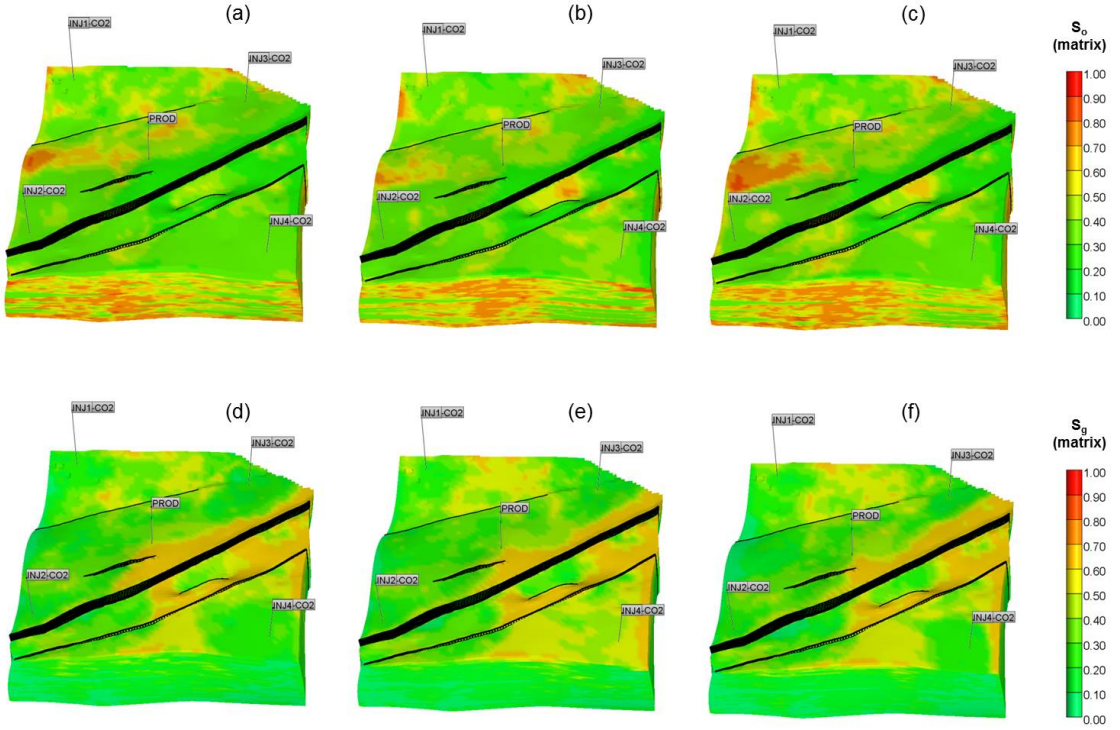


Figure 5.15: Oil saturation (a, b, c) and $CO_2$ saturation (d, e, f) distribution during immiscible WAG injection in the fractured carbonate reservoir with regional (a, d), fault related (b, e), and bedding related (c, f) fracture geometries. The average fracture intensity is 0.1 $^2/m^3$ in all cases.

Similarly, the water cut varies between 97%, 94% and 91% (Fig. 5.16b), while the $CO_2$ stored varies between 11%, 14% and 16% of the pore volume assuming bedding related, fault related or regional fracture geometry respectively (Fig. 5.15d, e, f and Fig. 5.16c). The bedding related fracture system contains layer-oriented fracture permeabilities that may lead to the prevalence of high permeability layers and exacerbate flow channelling, thereby yielding the lowest estimated oil recovery and $CO_2$ stored. At high fracture intensity, the influence of the specific fracture geometry is less distinguishable because the fracture den-

sity is so high that fractures are highly connected and form long-range high-permeability flow paths irrespective of the specific geometry (Fig. 5.16d, e, f).

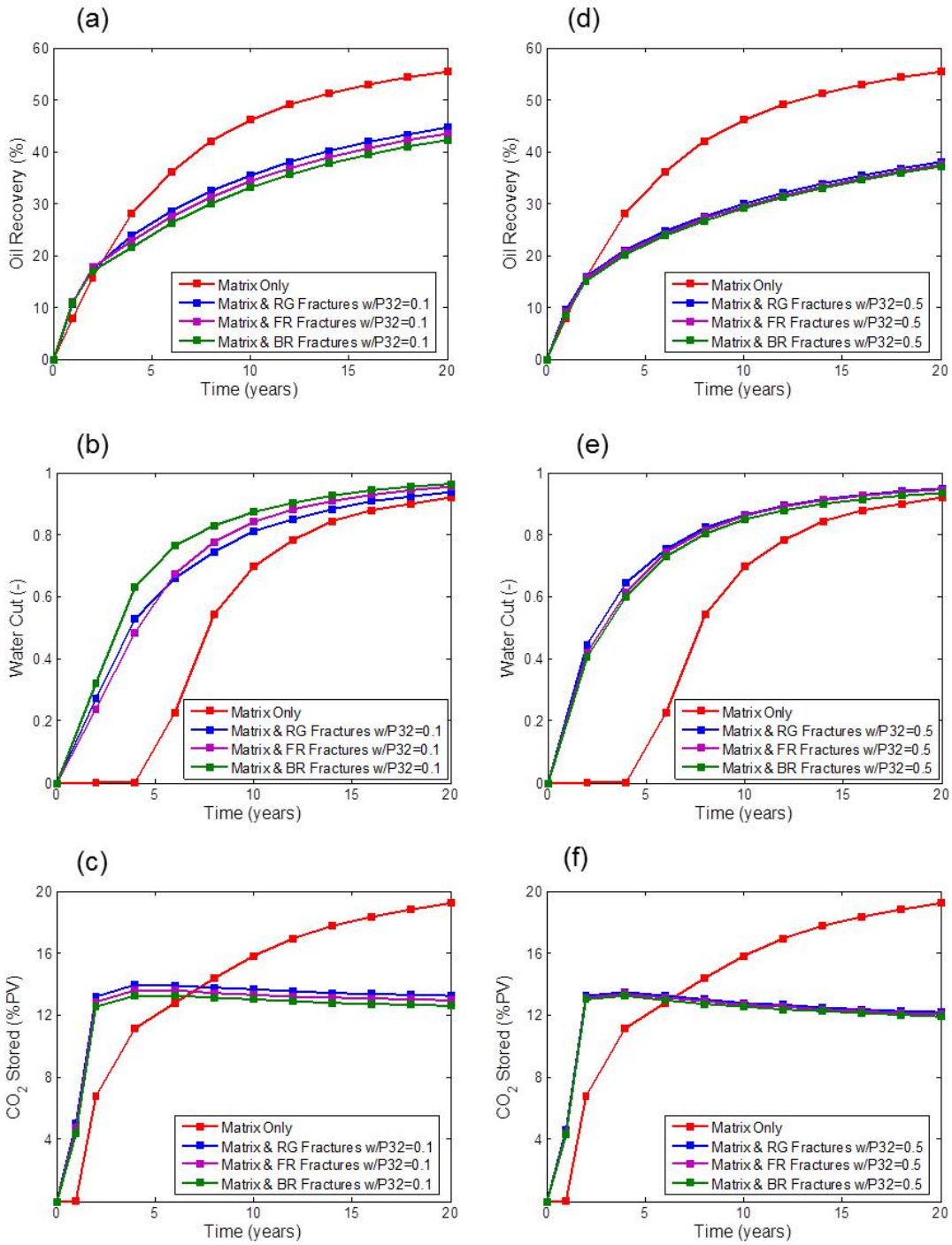


Figure 5.16: Oil recovery (a, d), water cut (b, e) and $CO_2$ stored (c, f) when regional (RG), fault-related (FR) and bedding-related (BR) fracture geometry scenarios are considered. P32 refers to the 'average fracture intensity'. It is assumed that P32 = 0.1 $m^2/m^3$ indicates low fracture intensity while P32 = 0.5 $m^2/m^3$ indicates high fracture intensity. Oil recovery and $CO_2$ storage profiles are less distinguishable at high fracture intensities.

### 5.3.3 *Effect of matrix wettability*

To ensure a tractable number of simulations while investigating important fluid flow effects, the regional fracture scenario with average fracture intensity of 0.1 was used for all subsequent simulations. Unless otherwise stated, the base case for wettability in all simulations is the single mixed-wet wettability function. In general, higher oil recovery factors are encountered in all wettability scenarios when hysteresis is employed due to reduced mobility of the $CO_2$ phase and better oil displacement (Fig. 5.17a). When matrix wettability is varied in the flow simulations, it is observed that WAG injection in a more water-wet formation gives higher oil recovery, which decreases under mixed-wet conditions and further decreases in oil-wet conditions (Fig. 5.17a). This is due to the high imbibition potential of water-wet formations (Morrow, 1990; Morrow and Mason, 2001; Tavassoli et al., 2005; Schmid and Geiger, 2012, 2013).

As previously noted, spontaneous imbibition is a major recovery mechanism in fractured reservoirs and a more water-wet rock will support efficient imbibition of water from the fractures to displace oil from the matrix through a counter-current or co-current mechanism. The imbibition efficiency can also be compared using the water cut profiles (Fig. 5.17b). It is observed that the water cut increases more rapidly in the mixed-wet and oil-wet cases compared to the water-wet case due to the more efficient imbibition in the water-wet scenario. Conversely, the fraction of $CO_2$ stored is significantly lower in the water-wet case compared to the mixed-wet and oil-wet cases (Fig. 5.17c). The low $CO_2$ storage fraction in the water-wet case is due to high capillary entry pressure of water-wet rocks that makes it difficult for $CO_2$ to be displaced into the matrix.

Furthermore, impact of multiple approaches for distributing wettability functions in the model was tested (see fig. 5.5). Three scenarios were included; (1) Single mixed-wet wettability function for the whole reservoir, (2) Multiple wettability functions distributed using a depth based approach where the wettability varies from oil-wet at the top to water-wet at the bottom of the reservoir and (3) Multiple wettability functions distributed using a facies based approach where

the wettability is assigned based on correlation to the horizontal permeabilities of the grid cells (Fig. 5.17 d, e, f).

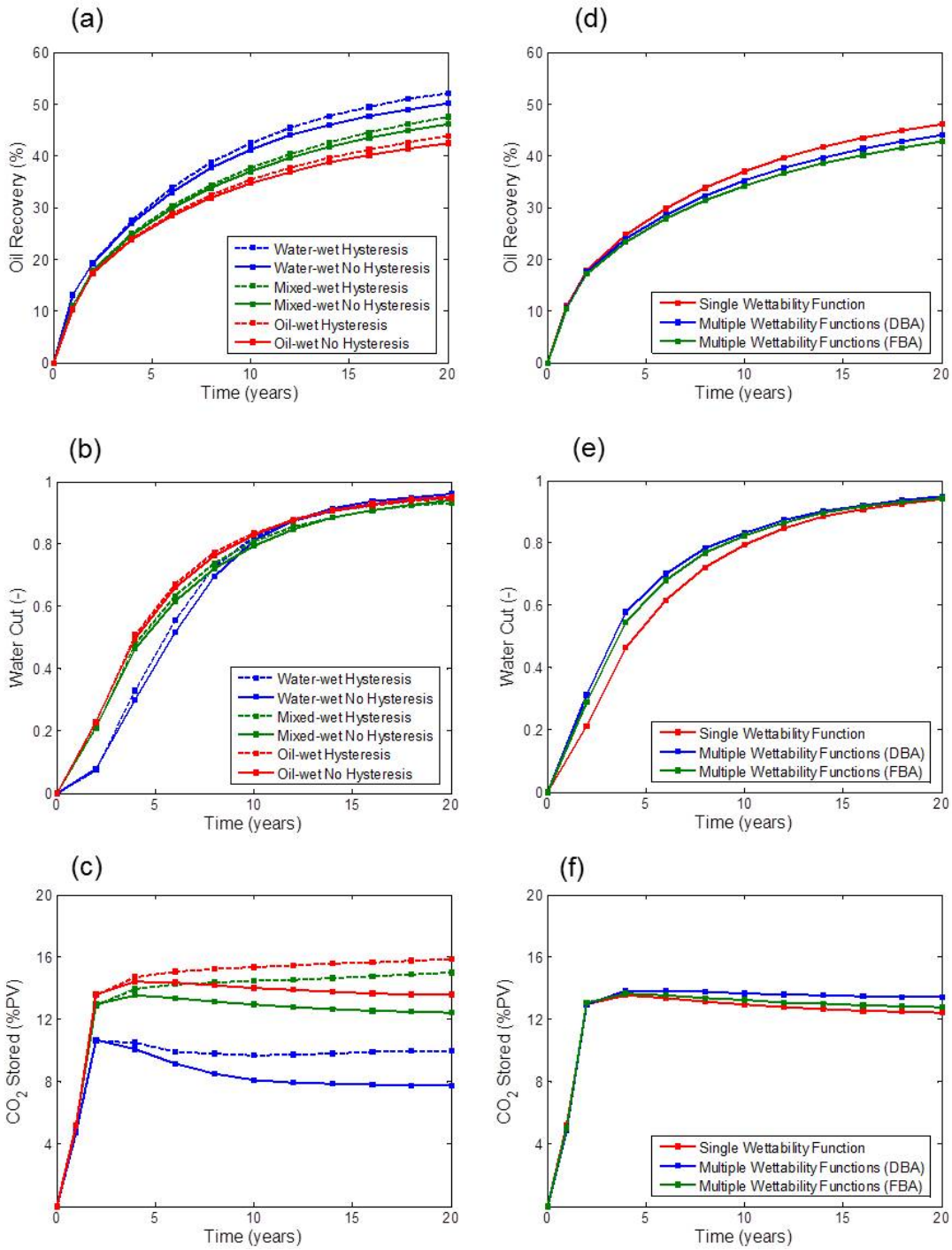


Figure 5.17: Oil recovery (a, d), water cut (b, e) and $CO_2$ storage (c, f) profiles during immiscible WAG injection. Water-wetness improves imbibition, gives highest recovery fractions and results in slower water transport, however, lower volumes of $CO_2$ are stored under water-wet conditions due to high capillary entry pressure.

When multiple wettability functions are employed, lower oil recovery but higher $CO_2$ storage fractions are observed. Since wettability functions control imbibition and drainage mechanisms which in turn control oil recovery and $CO_2$ storage, such lower oil recoveries and higher $CO_2$ storage fractions are not surprising. In other words, the combined effect of the multiple wettability functions depend on how the end-members (oil-wet to water-wet) have been allocated to the grid cells based on the distribution approach. In this case the combined effect of the multiple wettability functions indicates that the oil recovery efficiency is less than for the scenario with a mixed-wet single wettability function. The results demonstrate the uncertainties inherent to the wettability distribution method chosen and the importance of rigorous approaches for defining and distributing the wettability functions in simulation models for evaluating $CO_2$ EOR and storage (e.g., Gomes et al., 2008; Hollis et al., 2010).

### 5.3.4 *Effect of Relative Permeability Hysteresis*

To gain insight into the dynamic behaviour of the reservoir in cases with and without hysteresis, three observation points were identified in the simulation model and monitored to observe the evolution of $CO_2$ saturation over 20 years (Fig. 19). Observation point 1 (grid cell 64, 67, 1) and observation point 2 (grid cell 57, 16, 1) are close to injection wells in the simulation model, while observation point 3 (grid cell 71, 30, 1) is located between two faults. Choosing the observation points in this way allowed for not only the observation of $CO_2$ saturation path evolution, but also to show the influence of geological features such as faults on trapping. It can be observed that the $CO_2$ saturation distribution at the top of the reservoir when hysteresis is not considered (Fig. 5.18a) is higher than the $CO_2$ saturation at the top of the reservoir when hysteresis is considered (Fig. 5.18b), indicating that the $CO_2$ plume migration to the top of the reservoir is much slower when hysteresis is considered and residual trapping is accounted for.

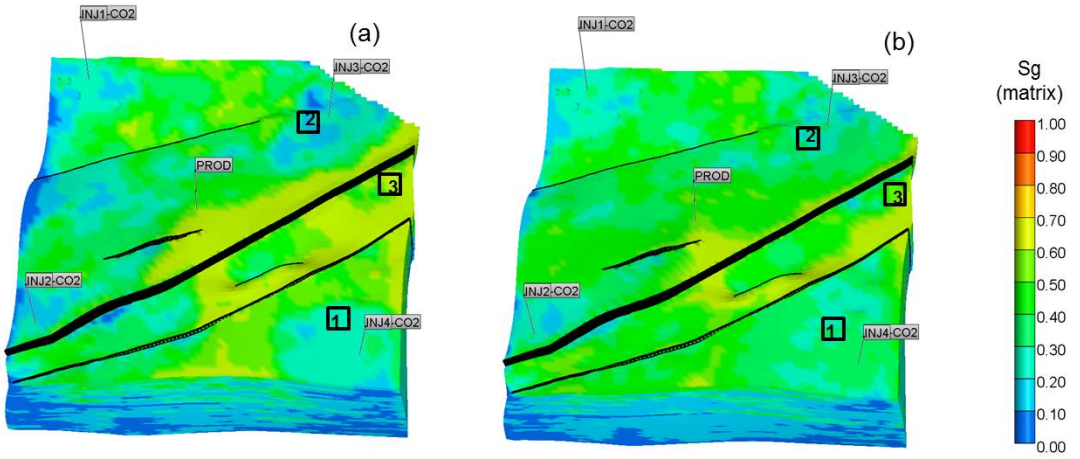


Figure 5.18: Matrix gas saturation distribution during WAG injection without hysteresis (a) and with hysteresis (b). Three observation points (1, 2, 3) are shown on the simulation model where $CO_2$ saturation is monitored over 20 years.

When hysteresis is considered, the model predicts a trail of residual, immobile $CO_2$ during the migration of the plume that reduces the overall mobility of $CO_2$ and leads to a more conservative estimate of the $CO_2$ distribution at the top of the reservoir (e.g., Juanes et al., 2006; Spiteri and Juanes, 2006; Qi et al., 2008, 2009; MacMinn et al., 2011). Lower $CO_2$ distribution at the reservoir top is favourable for $CO_2$ sequestration because it reduces the potential of the gas to damage the cap rock and generate fissures in the cap rock which may then be conduits for $CO_2$ leakage to upper formations and ultimately to the atmosphere.

Figure 5.19 shows $CO_2$ saturation evolution at the three observation points during WAG injection under water-wet, mixed-wet and oil-wet conditions. All the observation points indicate that the difference in $CO_2$ saturation profiles between the models with and without hysteresis begins in the third injection cycle. In the third injection cycle (W-G-W-G), water is injected into the reservoir after a flow reversal. If hysteresis is considered, water injection after flow reversal instigates residual $CO_2$ immobilisation and trapping, hence, the decrease in gas saturation follows a different evolution path compared to the model where hysteresis is not considered. Hence, residual trapping due to hysteresis reduces the overall gas mobility and increases the stored gasas illustrated in figure 5.18.

On average, the $CO_2$ saturation in the matrix of the water-wet models (Fig. 5.19a, d, g) is approximately 39% less than the $CO_2$ saturation in the matrix of

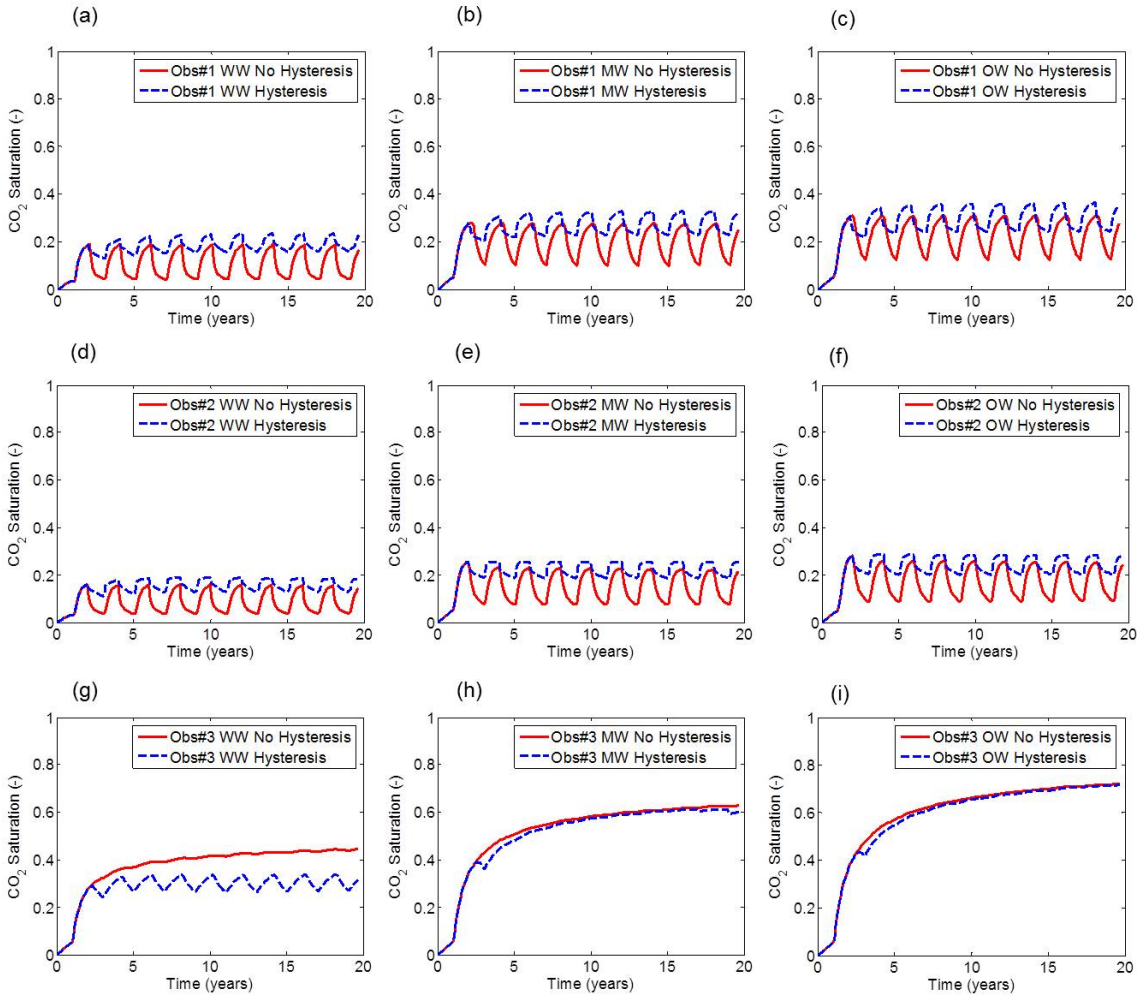


Figure 5.19: Gas saturation profiles at observation points 1, 2, 3 (Fig. 5.18) under water-wet (a, d, g), mixed-wet (b, e, h) and oil-wet (c, f, i) conditions respectively. Water and $CO_2$ are injected during alternate cycles at equivalent rates of 1589 $m^3$/day.

the mixed-wet models (Fig. 5.19b, e, h) and 56% less than the $CO_2$ saturation in the matrix of the oil-wet models (Fig. 5.19c, f, i). The difference in matrix $CO_2$ saturation can be attributed to the high capillary entry pressure in water-wet rocks which supports spontaneous imbibition but opposes gas-oil gravity drainage. Hence, water-wet rocks exhibit high oil recovery during imbibition but low oil recovery and $CO_2$ storage during gas-oil gravity drainage. Conversely, oil-wet rocks exhibit low oil recovery during spontaneous imbibition but higher oil recovery and $CO_2$ storage during gas-oil gravity drainage.

At observation point 3, the behaviour of the gas saturation profiles differs from the other two observation points for all the wettability scenarios (Fig. 5.19g, h, i). This is due its location between two faults. The faults are considered to be fully

conductive, with flow reduction across faults occurring only due to the juxtaposition of high and low permeability layers. Hence, only a small fraction of injected fluids reach observation point 3 due to viscous displacement. Consequently, hysteresis and residual $CO_2$ trapping due to repeat imbibition and drainage cycles is limited and only observed in the water-wet scenario (due to the relatively stronger imbibition). The mixed-wet and oil-wet cases do not show hysteresis effects. The evolution of $CO_2$ saturation at the observation points therefore highlights the interaction and competition between recovery/sequestration mechanisms (e.g. gravity, capillary, viscous forces) and geological heterogeneity during $CO_2$ EOR and storage which needs to be captured in simulation models as has been done in this study.

### 5.3.5 *Effect of WAG ratio and maximum trapped $CO_2$ saturation*

Furthermore, the effect of the WAG ratio and maximum trapped $CO_2$ saturation on the performance of $CO_2$ EOR and storage is investigated. The motivation is to consider what other factors influence the optimization of $CO_2$ sequestration during EOR. Specifically, to determine what factors can mitigate the influence of geological uncertainties and enable us to obtain the optimum displacement strategy for a specific reservoir (e.g., Wildenschild et al., 2011; Doster et al., 2013). It is observed that when the WAG ratio varies between 1:2, 1:1, 2:1 and 4:1, the total $CO_2$ stored (as a percentage of the reservoir pore volume) varies between 15%, 14%, 12% and 11% respectively (Fig. 5.20a). This is to be expected because as the WAG ratio increases a smaller fraction of $CO_2$ is injected into and subsequently stored in the reservoir.

More importantly, figure 5.20a indicates that the WAG ratio can be varied to maximize $CO_2$ sequestration while producing oil within economic limits. The challenge, however, is that maximizing $CO_2$ sequestration simultaneously competes with maximizing the oil production (Fig. 5.20c). Obtaining an optimal economic solution for $CO_2$ EOR and storage is therefore nontrivial and may require the use of advanced optimization workflows to obtain the best solution while

varying the model input parameters (e.g., Queipo et al., 2005; Oladyshkin et al., 2011; Koziel and Yang, 2011; Petvipusit et al., 2014). Similarly, it can be observed that when the maximum trapped $CO_2$ saturation varies between 0, 0.2 and 0.4, the total $CO_2$ pore volume stored varies between 13%, 15% and 16% respectively (Fig. 5.20b) indicating a direct link between the maximum trapped saturation

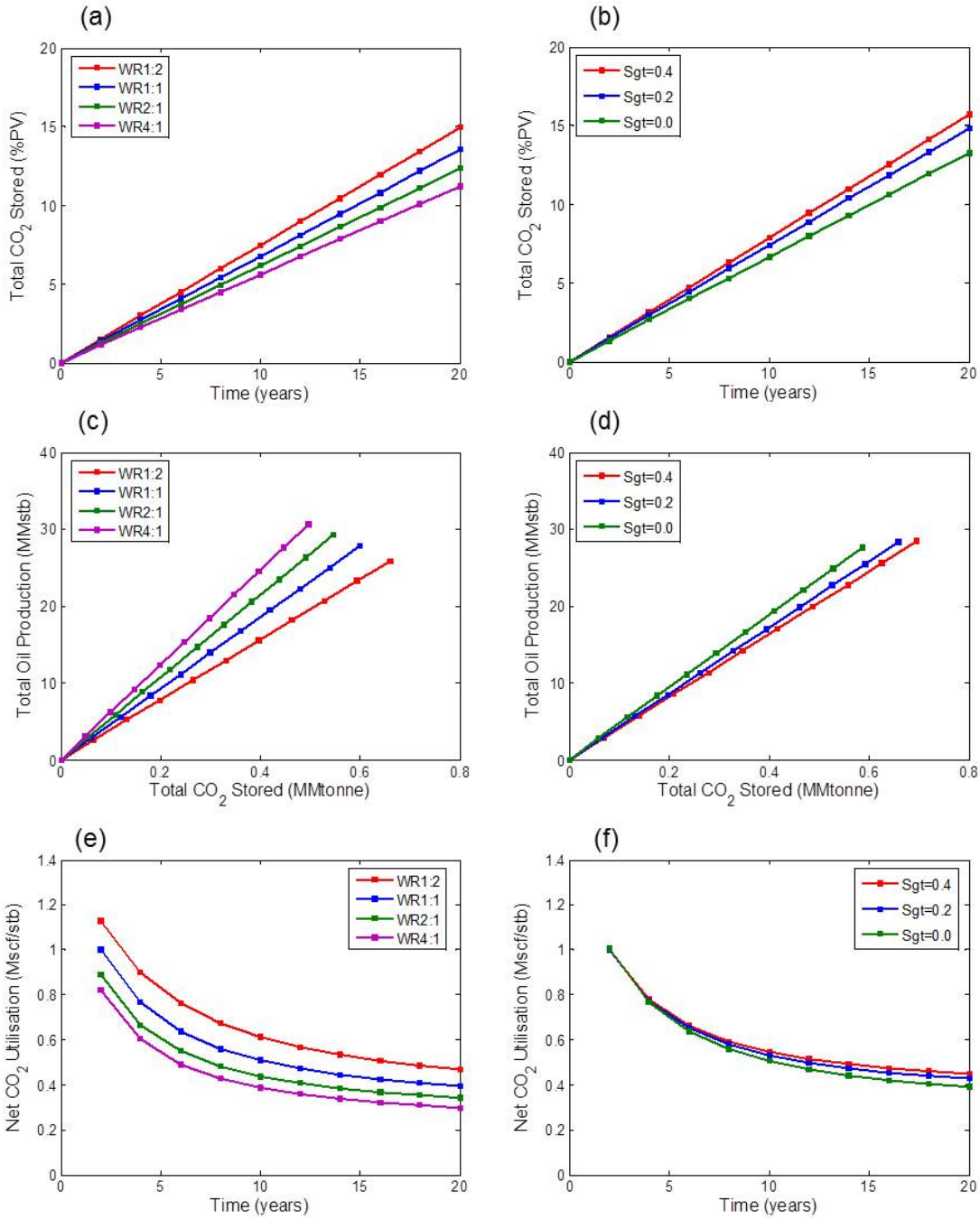


Figure 5.20: Total $CO_2$ stored in the reservoir when WAG ratio (a, c) and maximum trapped gas saturation (b, d) are varied. As expected, larger volume of $CO_2$ is stored with low WAG ratios or high trapped saturations. The net $CO_2$ utilisation is higher at low WAG ratios (e) and increasing maximum trapped $CO_2$ saturation (f).

and the amount of $CO_2$ stored in the reservoir. Figure 5.20d demonstrates that improving the maximum trapped $CO_2$ saturation can increase the total amount of $CO_2$ stored in the reservoir with the total oil production remaining relatively constant.

The effect of the WAG ratio and maximum trapped $CO_2$ saturation on the net gas utilization factor (GUF) is evaluated. The GUF (estimated in Mscf/stb) indicates the amount of $CO_2$ that is stored in the reservoir for every barrel of oil produced (eqn. 5.1). The GUF is an important sequestration and economic parameter that quantifies the amount of $CO_2$ that can be safely stored in the reservoir during EOR.

$$GUF = \frac{CO_2 \quad Injected - CO_2 \quad Produced}{Oil \quad Produced} \tag{5.1}$$

In general, a higher volume of $CO_2$ is stored initially per barrel of oil produced (Fig. 5.20e, f). As the reservoir becomes gas saturated, the GUF reduces and becomes nearly constant. Figure 5.20e indicates that as the WAG ratio increases the GUF decreases. This is because higher WAG ratios produce larger quantities of oil at the expense of lower $CO_2$ storage (Fig. 5.20c). Finally, figure 5.20f illustrates the impact of residual trapping on the net GUF. It can be seen that as the trapped gas fraction increases, the net GUF increases indicating that a higher fraction of $CO_2$ is stored in the reservoir. This direct correlation between the trapped gas fraction and the net GUF, further reaffirms the fact that a better understanding of the mechanism of trapping can be used to optimize $CO_2$ sequestration (during EOR) within economic limits.

## 5.4 DISCUSSION

### 5.4.1 *Reservoir Simulation Results*

Reservoir simulation is an important tool for investigating the fundamental controls on fluid flow in fractured carbonate reservoirs during $CO_2$ EOR and storage. Results from reservoir simulation can be used to evaluate the reservoir's

suitability for $CO_2$ EOR and storage based on the influence of uncertain physical and geological parameters. The simulation study in this chapter shows that the fracture properties are a first order control on oil recovery and $CO_2$ storage efficiency in fractured carbonate reservoirs. Significant variations in subsurface flow behaviour was observed when low intensity fractures were encountered compared to high intensity fractures, thereby, emphasising geological tipping points that influence simulation predictions and decision making. Hence, accurate characterization and calibration of the hydrodynamic properties of the fracture network is essential. Calibrating simulation results based on static data with dynamic information from pressure transient, tracer and field tests can increase our understanding of a dynamically coupled fracture-matrix system. However, it should be noted that the complex interaction of fracture-matrix flow in fractured carbonate reservoirs can render the calibration of fractured carbonate reservoir models with pressure transient data difficult (e.g., Wei et al., 1998; Corbett et al., 2012; Agada et al., 2014).

### 5.4.2 *Wettability Functions*

This chapter has demonstrated that the choice and number of wettability functions can influence oil recovery and $CO_2$ storage predictions in fractured carbonates. It has been shown previously that an accurate distribution of wettability functions for carbonates is a crucial aspect of carbonate reservoir characterization (e.g., Lichaa et al., 1993; Jerauld, 1997; Jackson et al., 2005; Hollis et al., 2010). In particular, using single wettability functions based on the assumption of uniform reservoir wettability is insufficient and the distribution of multiple functions to reflect heterogeneous wettability may offer more robust results. Relative permeability hysteresis also has a significant impact on subsurface $CO_2$ EOR and storage, as has been demonstrated. Modelling hysteresis in detail will account for the residually trapped (immobilised) $CO_2$ fraction and lead to reduction of the overall $CO_2$ phase mobility. Hence, understanding the mechanism of residual trapping means that trapping may be optimized to obtain significant economic and environmental benefit (e.g., Wildenschild et al., 2011; Doster et al., 2013).

### 5.4.3 *Fracture-matrix Interaction*

The fracture network was coupled with the rock matrix using traditional DFN modelling approaches and dual continuum formulations. Employing discrete fracture and matrix models (DFM) where the fractures are explicitly represented may provide additional insights into fracture-matrix transfer processes, especially in reservoirs where flow in the matrix is significant (e.g., Matthäi et al., 2007; Haegland et al., 2009; Geiger et al., 2009). Another source of uncertainty in the dual continuum simulations is the shape factor (embedded in the transfer function) which for classical models (Warren and Root, 1963; Gilman and Kazemi, 1983) determines the speed of recovery from the matrix, but does not adequately capture the changes in recovery speed over time. This variability in recovery speed is due to sub-grid heterogeneities that are typical for fractured carbonate reservoirs and have been shown to significantly influence multiphase flow predictions. Hence, current research efforts are tailored towards generating novel multi-rate transfer functions that account for variable recovery speeds as a result of sub-grid heterogeneities (Di Donato et al., 2007; Geiger et al., 2013; Maier et al., 2013).

### 5.4.4 *Well Pattern Optimisation*

A regular five-spot well pattern was chosen as the standard well placement option for all the simulations in this chapter. It is important to note that the chosen well placement was not final and the oil recovery and $CO_2$ sequestration estimates may be improved by exploring different well placement approaches. More common well placement options that may have an impact on the simulation results include inverted five-spot, direct line drive and staggered line drive well patterns. Alternatively, robust well-pattern optimization which is now a standard technique in reservoir simulation may be employed to maximize $CO_2$ EOR and storage for a given well placement option while accounting for geological uncertainty with multiple model realisations (Bangerth et al., 2006; Onwunalu and Durlofsky, 2011; Petvipusit et al., 2014).

### 5.4.5 *Benefit of Experimental Design*

For all the sensitivities described above, a traditional sensitivity analysis carried out by varying 'one parameter at a time' was used to show that the fracture intensity, matrix wettability, fracture geometry and residual trapping are key uncertainties for $CO_2$ EOR and storage prediction. This kind of sensitivity analysis, though very useful, could be biased because it may not fully explore the parameter space. Traditional sensitivity analysis assumes that the varied parameters are independent of one another, although in reality the parameters are often correlated. For example, matrix wettability and fracture intensity may have an interrelated rather than independent impact when controlling imbibition, drainage and residual trapping mechanisms.

Recently, design of experiments (DoE) has been increasingly used as a means to set up multiple numerical simulations that maximize the amount of information acquired from a limited number of simulation runs. DoE provides a structured way to change multiple settings in order to understand the impact of the most influential and interrelated factors on $CO_2$ EOR and storage. Furthermore, DoE can be coupled with advanced optimization workflows to optimise and improve the economics of oil recovery and $CO_2$ sequestration in fractured carbonate reservoirs (Friedmann et al., 2003; Koziel and Yang, 2011; Li and Zhang, 2014).

### 5.4.6 *Limitation of Black Oil Simulation*

Since this study focused on short term $CO_2$ EOR and storage (only 20 years), it was assumed that black oil simulation was sufficient to capture the short term effects of hysteresis, wettability and fracture-matrix interaction. Longer term $CO_2$ EOR and storage studies (up to 1000 years) that need to capture complex flow physics including $CO_2$ solubility and geochemical $CO_2$-rock interactions would benefit greatly from applying compositional simulations. The challenge remains that field-scale simulation of fractured carbonate reservoirs is very time consuming. Hence, it is worthwhile to investigate non-reactive $CO_2$ behaviour using

black oil simulations prior to investigating reactive and multicomponent $CO_2$ behaviour using compositional simulation (e.g., Jessen et al., 2005).

Another drawback of black oil simulation is that it does not adequately capture miscibility between $CO_2$ and the hydrocarbon phase. Miscible displacement during $CO_2$ EOR and storage occurs when $CO_2$ and the hydrocarbon components form a single homogeneous phase when mixed in all proportions typically above the minimum miscibility pressure. Miscible displacement would, therefore, increase the microscopic sweep efficiency and the overall fraction of oil recovered. Furthermore, it has been observed that miscibility increases $CO_2$ injectivity and the amount of $CO_2$ that can be hydrodynamically trapped in the reservoir structure (Agada and Geiger, 2014). The impact of miscibility on residual trapping, however, is less distinguishable since supercritical $CO_2$ is also trapped in the pore network as imbibition follows drainage in a cyclic water-alternating-gas displacement process (Agada and Geiger, 2014).

## 5.5 SUMMARY

The main objective of this chapter was to investigate how the interplay between hysteresis, wettability and fracture-matrix exchange impacts oil recovery and $CO_2$ sequestration in relation to the multi-scale heterogeneities that are pervasive for fractured carbonate reservoirs. It has been shown that the specific fracture network geometry has a direct effect on oil recovery and $CO_2$ storage, especially when the fracture intensity is low. When the fracture intensity is high, the impact of varying fracture network geometry on oil recovery and $CO_2$ storage becomes less distinguishable. This is because the fracture density is so high that fractures are highly connected and form long-range high-permeability flow paths irrespective of the specific geometry. Thus, the fracture network properties, specifically the fracture intensity, exhibit 'tipping point' behaviour that significantly influence the simulation output depending on whether the fracture intensity is low or high. This chapter demonstrates that for a given fracture geometry, the presence of connected fractures leads to increased bypassing of the oil in the matrix by the injected fluids as the fracture intensity increases. The presence of connected

fractures also leads to rapid $CO_2$ transport, relatively poor $CO_2$ sequestration and early water breakthrough.

It was found that although the fracture network properties have the greatest impact on the simulations, yet the effect of wettability on $CO_2$ EOR and storage cannot be neglected. Water-wet reservoir conditions lead to reduced gas saturation in the matrix due to high capillary entry pressures that oppose gas oil gravity drainage. Increased imbibition in the water-wet medium also leads to higher oil recovery during water injection cycles. Conversely, the imbibition potential is very poor in the oil-wet medium leading to much lower recovery from water injection cycles. Residual trapping of the $CO_2$ is more significant in water-wet rocks because snap-off occurs and gas becomes increasingly disconnected in the pore throats from the continuous $CO_2$ phase. Because residual trapping entails a reduction of the $CO_2$ mobility, it ultimately leads to higher oil recovery. Reducing the $CO_2$ mobility further delays $CO_2$ breakthrough, increases the stability of gas-water mobility front and improves contact of $CO_2$ with residual oil, thereby ensuring better macroscopic and microscopic sweep of the reservoir while increasing the residually trapped fraction.

Simulation of fractured carbonate reservoirs can provide valuable insights on the suitability of a given reservoir for $CO_2$ EOR and storage. Simulation studies can also highlight the principal physical and structural uncertainties that control oil recovery and $CO_2$ sequestration with a view to mitigating these uncertainties. Bypassing of oil in the matrix, rapid $CO_2$ migration and early water breakthrough, for example, which are due to high fracture matrix connectivity can be reduced by increasing the viscosity of the injected fluid using polymer injection and foam flooding applications. The wetting preference of the reservoir rock may also be altered by the injection of chemicals (e.g. surfactants) to achieve maximum $CO_2$ EOR and storage. Hysteresis in cyclic floods must be accounted for to ensure that simulations provide robust results that can guide decision making and subsurface reservoir management. The trade-off between the volumes of $CO_2$ trapped and the amount of oil recovered must also be optimised in the light of economic constraints including the source and cost of $CO_2$ delivered to the operational site.

# 6

# DATA-DRIVEN SURROGATES FOR RAPID SIMULATION AND OPTIMISATION OF EOR PROCESSES

## 6.1 INTRODUCTION

Hydrocarbon recovery in carbonates is typically low due to multi-scale heterogeneities and oil- to mixed-wet rock properties (Manrique et al., 2007; Montaron, 2008; Mohan et al., 2011). Low recovery factors are further influenced by complex connected high permeability fracture networks which establish preferential flow paths in the reservoir (e.g., Bourbiaux et al., 2002; Gale et al., 2004; Makel, 2007; Spence et al., 2014). The variability in matrix architecture and fracture network connectivity is the main reason why fractured carbonate reservoirs show a large variety of flow behaviours, leading to significant uncertainties in their evaluation, performance prediction and management (e.g., Cosentino et al., 2001; Makel, 2007; Agada et al., 2014).

To account for multiple geological and engineering uncertainties, a large number of numerical simulations are typically required to adequately explore the parameter space, investigate parameter relationships and optimise hydrocarbon recovery. Sensitivity analysis, uncertainty quantification and recovery optimisation for fractured carbonate reservoirs, however, are computationally expensive because of the multiscale heterogeneities and fracture-matrix transfer mechanisms that must be taken into account using numerical transfer functions and a large number of simulation grid cells. This is particularly important for $CO_2$ WAG injection, a successful EOR method for carbonate reservoirs which combines the benefits of gas injection to reduce the residual oil saturation and water

injection to improve mobility control and frontal stability (Lake et al., 1992; Christensen et al., 2001; Manrique et al., 2007; Taber et al., 1997; Teletzke et al., 2010; Kalam et al., 2011; Pizarro and Branco, 2012; Azzolina et al., 2015).

One efficient way of reducing the computational cost is by using data-driven surrogate modelling techniques that construct an approximation (or proxy) of the simulation response based on a limited number of simulation runs (Queipo et al., 2005; Forrester and Keane, 2009; Gogu et al., 2009; Simpson et al., 2008; Oladyshkin et al., 2011; Gogu and Passieux, 2013; Petvipusit et al., 2014). The modelling process typically involves generating an initial surrogate model with a set of full-physics training simulations. Subsequently, an approximate solution to the objective function is obtained by evaluating the data-driven surrogate. For validation purposes, approximate solutions from the data-driven surrogate are compared to model predictions using high-fidelity simulation (e.g. black oil or compositional simulation). If the comparison shows a mismatch, the data-driven surrogate is iteratively updated with more training runs and testing points added until the mismatch is eliminated (Koziel and Yang, 2011). The data-driven surrogate can then be used to routinely identify flow signatures for variations in production behaviour when reservoir engineering measures are applied in the presence of geological heterogeneities. In this way the surrogates will be representative of flow signatures, rather than a fit to a given number of input data points.

### 6.1.1 *Design of Experiments*

To ensure that the data-driven surrogate fully explores the parameter space and provides a robust representation of the numerical simulation model, Design of Experiments (DOE) is commonly employed. DOE aims to maximize the amount of information acquired from a minimum number of simulation runs by optimally allocating samples in the design space (Chen et al., 2006a; Montgomery, 2008; Simpson et al., 2008; Myers et al., 2009; Koziel and Yang, 2011). DOE employs different sampling methods to identify a subset of experiments from a larger set, according to the number of experimental parameters under investigation. De-

terministic experimental designs such as Box-Behnken, fractional factorial and central composite designs are perfectly orthogonal, explore a large region of the search space and are able to capture model non-linearities (Box et al., 1978; Chen et al., 2006a). To select input parameters from random distributions, random samplers such as Latin Hypercube or nearly orthogonal array are frequently used. Random samplers are also called space filling designs because they are not restricted to sample sizes that are specific multiples of design parameters (Stein, 1987; Giunta et al., 2003; Helton and Davis, 2003).

### 6.1.2 *Polynomial Chaos Expansion*

Experimental design techniques coupled with data-driven surrogates has been widely used in hydrocarbon recovery (Friedmann et al., 2003; Panjalizadeh et al., 2014) and $CO_2$ storage (Ashraf et al., 2013; Li and Zhang, 2014; Wriedt et al., 2014) applications for uncertainty quantification, risk assessment, optimisation and history matching. One group of data-driven surrogate modelling techniques that has received increasing attention is Polynomial Chaos Expansion (PCE) (Eldred and Burkardt, 2009; Oladyshkin et al., 2011; Buzzard, 2012; Ashraf et al., 2013; Elsheikh et al., 2014). PCE methods build a polynomial approximation of the model response by expanding it in an orthogonal polynomial basis. PCE techniques, therefore, provide an efficient high-order accurate way of including non-linear effects in stochastic analysis (Oladyshkin et al., 2012).

PCE techniques are mainly classified into intrusive and non-intrusive approaches. Intrusive approaches such as the stochastic Galerkin methods (Villadsen and Michelson, 1978; Ghanem and Spanos, 1993; Xiu and Karniadakis, 2003; Matthies and Keese, 2005) require manipulation of the governing equations or underlying partial differential equations that are solved within a reservoir simulator. Non-intrusive approaches do not require manipulation of the governing equations and use the reservoir simulator as a black box. They are hence more straightforward to apply and involve the evaluation of the coefficients in the chaos expansion using a given number of model simulations (Isukapalli et al., 1998; Li and Zhang, 2007; Blatman and Sudret, 2010; Oladyshkin et al., 2011, 2012;

Zhang and Sahinidis, 2012; Petvipusit et al., 2014). This chapter focuses on non-intrusive Polynomial Regression (PR), Sparse Polynomial Chaos Expansion (sPCE) and Arbitrary Polynomial Chaos Expansion (aPCE). PR estimates the coefficients for a second-order polynomial by least squares fitting of the data-driven surrogate model to the training data (Myers et al., 2009). sPCE is an extension of the generalised polynomial chaos which is based on the Askey Scheme (Askey and Wilson, 1985) of orthogonal polynomials (Xiu and Karniadakis, 2002, 2003; Blatman and Sudret, 2010; Elsheikh et al., 2014). aPCE techniques have been shown to minimise the subjectivity of input data distributions by directly using the available information in a data-driven formulation of PCE and employing a global polynomial basis for arbitrary distributions of data (Witteveen et al., 2007; Oladyshkin et al., 2011, 2012; Ashraf et al., 2013).

Other surrogate modelling approaches which have been applied to hydrocarbon recovery and CO2 storage applications include Kernel methods (Sarma et al., 2009), Kriging techniques (Yang et al., 2011) and artificial neural networks (Costa et al., 2014) which use complex mathematical relationships between simulator input and output to emulate physical systems and reproduce the output patterns rapidly.

### 6.1.3 *Uncertainties Encountered during $CO_2$ WAG Injection*

In the context of EOR in fractured carbonate reservoirs, data-driven surrogates may be able to provide relevant approximations of time consuming numerical simulations. The surrogate models can then help to understand the respective dependencies and correlations of uncertain input parameters and contribute to rapid simulation, optimisation and decision making under uncertainty. Geological parameter uncertainties that affect immiscible $CO_2$ WAG injection include the nature and flow significance of faults and subseismic fractures (Bourbiaux et al., 2002; Casabianca et al., 2007; Ramirez et al., 2009) and the role of wettability and hysteresis when controlling imbibition and drainage in the rock matrix (Blunt, 1997; Larsen and Skauge, 1998; Hui and Blunt, 2000; Spiteri and Juanes, 2006; Spiteri et al., 2008; Ryazanov et al., 2009; Ferno et al., 2011; Dernaika et al.,

2013; Schmid and Geiger, 2013). Conversely, the engineering parameter uncertainties include WAG design parameters such as the flow rate and location of wells, WAG slug sizes and WAG injectant ratios.

### 6.1.4 *Optimisation*

In the presence of multiple uncertainties, finding the most favourable combination of uncertain input parameters to obtain an optimum value of the objective function (e.g. oil recovery, gas utilisation factor) is very challenging and commonly requires the application of stochastic optimisation algorithms. Stochastic algorithms including simulated annealing (Dowsland and Thompson, 2012), particle-swarm optimization (Mohamed et al., 2010), neighbourhood algorithm (Subbey et al., 2003), differential evolution (Hajizadeh et al., 2011) and genetic algorithm (Sen et al., 1995; McCall, 2005) have been applied to many reservoir engineering problems. Stochastic algorithms incorporate a random component that allows the search during optimisation to move toward worse solutions occasionally, thereby gaining the ability to seek out the global optimum objective function while escaping from local minima efficiently (Abdollahzadeh et al., 2013).

This study uses the genetic algorithm, a heuristic search and optimisation technique based on natural evolution through selection (Bäck and Schwefel, 1993; Gen and Cheng, 2000; Eiben and Smith, 2003; McCall, 2005). The algorithm uses selection, crossover, mutation and recombination of individual reservoir models to obtain a new generation of potentially superior individuals based on ranking with a fitness function (i.e. objective function). The procedure is repeated to obtain multiple generations until an optimum value of the objective function is reached. The genetic algorithm is robust, flexible and easy to adapt to different engineering problems because it uses the objective function value to determine new search steps and does not require gradient information from the optimisation problem. Hence, the genetic algorithm can be applied to optimisation problems for which traditional algorithms fail because of significant non-linearities or discontinuities in the search space. The main limitation of GA compared to

more modern stochastic optimisation methods is the long computer bit strings required to represent the chromosomes of individuals during GA. The long bit strings make GA rigid and less robust when compared to modern algorithms such as neighbourhood algorithm (Subbey et al., 2003) and particle swarm optimization (Mohamed et al., 2010). Several studies provide further details on GA (e.g., Michalewicz, 1996; Mitchell, 1999; Gen and Cheng, 2000) and its application (e.g., Bäck et al., 2000; McCall, 2005; Costa et al., 2014).

### 6.1.5 *Workflow*

In this chapter, Box-Behnken experimental design is used to set up a wide range of full-physics simulations of a high-resolution carbonate reservoir model in order to generate, analyse and compare non-intrusive data-driven surrogate models for rapid simulation and optimisation of $CO_2$ WAG injection. The full-physics simulations are then used to build data-driven surrogates. For validation, additional full-physics simulations with random design parameters are set up using the Latin Hypercube experimental design and compared to the response of the data-driven surrogates for the same input parameters. The most accurate surrogate model after validation is then coupled with Monte Carlo methods to generate cumulative distribution functions of oil recovery and gas utilisation factor. Subsequently, the selected surrogate model is employed for optimisation of the objective function using genetic algorithm. A summary of the workflow employed to construct data-driven surrogates for fractured carbonate reservoirs is shown in figure 6.1.

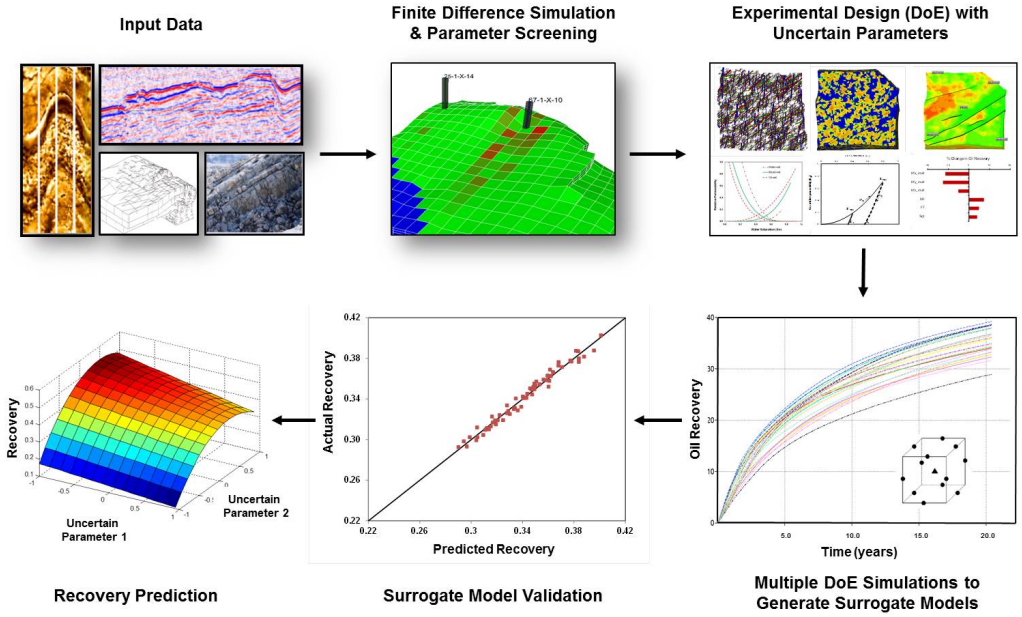


Figure 6.1: Workflow for constructing data-driven surrogates for fractured carbonate reservoirs using multiple experimentally designed full-physics simulations.

## 6.2 SECTOR MODEL DESCRIPTION

### 6.2.1 *Fracture-Matrix Characterisation and Fluid properties*

The simulation model, fluid properties and wettability data are the same as in Chapter 3. Due to the large number of simulations required to generate different surrogates, a sector of the Amellago outcrop model consisting of 34 x 35 x 36 grid cells (42,480 grid cells in total) was employed. Each grid cell has dimensions of 15m x 15m x 3m. An inverted 5-spot well pattern was used with a vertical injection well at the centre of the model and four vertical production wells at the corners. $CO_2$ WAG injection was simulated using a WAG ratio of 1:1 and eight alternate six-month cycles.

This chapter employs full-physics simulation of immiscible $CO_2$ WAG injection which can be run significantly faster in black oil mode compared to compositional simulations that require significantly longer run times for fractured carbonate reservoirs. Data-driven surrogates are generated for two objective functions: the oil recovery factor and the net Gas Utilisation Factor (GUF). The oil recovery factor indicates the fraction of oil that is recovered from the reservoir while the GUF indicates the net amount of gas that is lost in the reservoir for

every barrel of oil produced. In general, it is economically desirable to maximise oil recovery and minimise GUF.

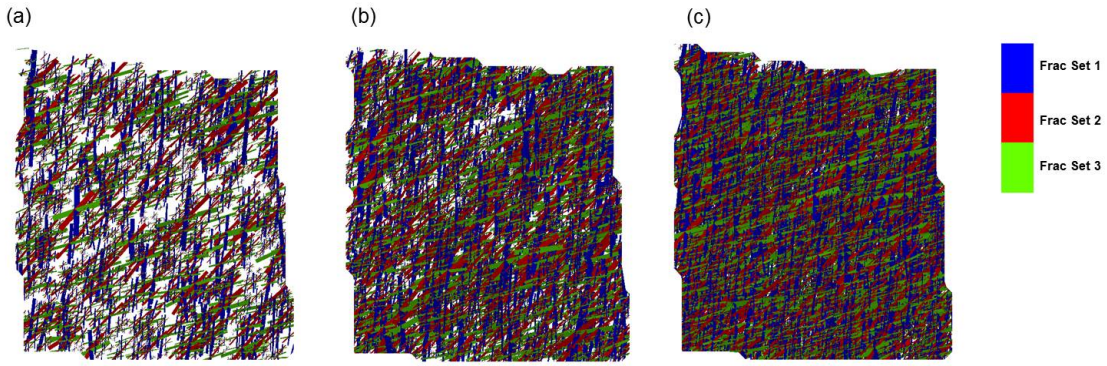


Figure 6.2: Discrete fracture network models for regional fracture system with average fracture intensity of 0.05 (a), 0.1 (b) and 0.2 (c).

Fracture data such as in Chapter 5 were used to construct DFN models for the sector model. The fractures are considered to be part of a regional fracture system with volumetric fracture intensities (P32) that vary from 0.05 to 0.2 $m^2/m^3$ (Fig. 6.2). Fracture network flow parameters including equivalent permeability tensors and shape factors were obtained by upscaling the fracture networks to the grid cells of the simulation model using the modified Oda (1985) DFN upscaling method. The dual-porosity dual-permeability (DPDP) formulation was used to couple matrix and fracture fluid flow (Fig. 6.3).

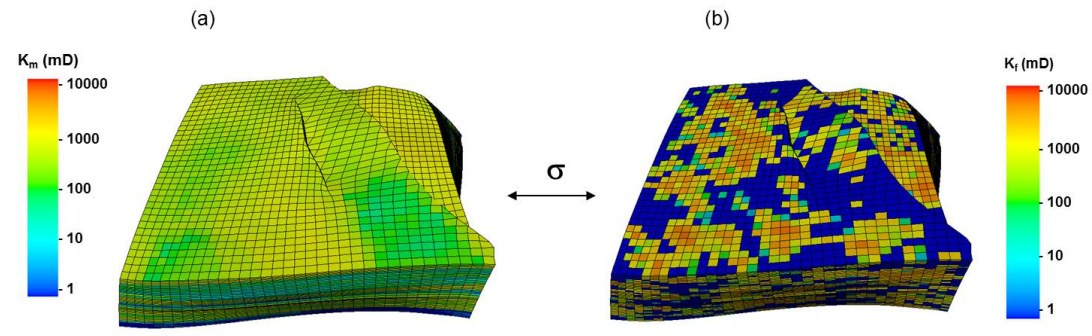


Figure 6.3: Matrix permeability (a) and fracture permeability (b) for the heterogeneous carbonate reservoir. DPDP formulation was used to couple matrix and fracture fluid flow.

## 6.3 SETUP OF DATA-DRIVEN SURROGATE MODELS

### 6.3.1 *Parameter Screening*

A sensitivity analysis carried out by varying one parameter at a time was used to identify, rank and screen input variables with significant impact on the objective function(s). The screening results indicate that the most important uncertainties affecting $CO_2$ WAG injection in this reservoir include the fracture permeability (which is a function of the DFN model, $K_{DFN}$, and the fracture permeability multipliers, $Kf_{mult}$), WAG injection rate ($Inj_{Rate}$), matrix wettability ($KR$), fault transmissibility ($FT$) and the maximum trapped gas saturation ($S_{gt}$) (Fig. 6.4). The screening study shows that as uncertain parameters vary between their minimum and maximum values, increasing the fracture permeability typically results in up to a 16% decrease in the oil recovered and the GUF. Conversely, an increase in trapped gas saturation, wettability or fault transmissibility results in increased oil recovery and GUF of up to 15%. The WAG injection rate can influence the output by 18% while the WAG injection location ($IL_x$, $IL_y$) only has up to 3% influence on the results for this model. Subsequently, only uncertainties that show significant impact on the simulation model response as indicated in figure 6.4 are considered in the subsequent analysis and surrogate model set-up.

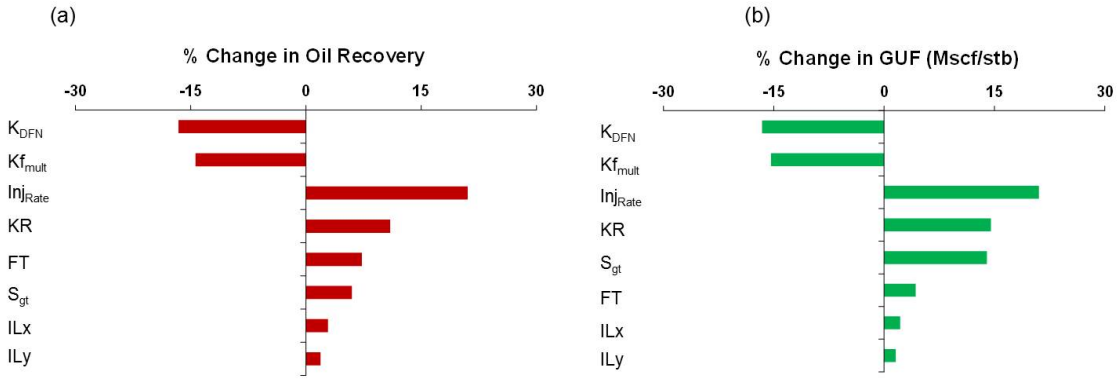


Figure 6.4: Summary of parameter sensitivities affecting oil recovery and gas utilisation factor (GUF) during $CO_2$ WAG. Tornado chart shows the difference in the model response when individual parameters are varied between their minimum and maximum values indicated in Table 6.1.

### 6.3.2 *Experimental Design*

A Box-Behnken design (Box et al., 1978) was used to vary the uncertain parameters. Identical well configurations, flow rates and pressure constraints were maintained to ensure that the variability in simulation outcomes was due to the main uncertain parameters, except in the cases where the WAG injector location or flow rate were varied. A normal prior probability distribution was used to allocate uncertain parameter samples in the design space. Three regional fracture permeability models were included in the design ranging from DFN models with fracture intensity of 0.05 to 0.2. Fracture permeability multipliers were varied between 0.1 and 10 to account for end-member fracture permeability scenarios (Table 6.1). The fault transmissibility was varied between low transmissibility scenarios where the faults were completely sealing ($FT$ = 0) and high transmissibility scenarios where the faults were fully conductive ($FT$ = 1). Relative permeability and capillary pressure curves varied from oil-wet to water-wet corresponding to the low and high end-members respectively. The trapped gas saturation varied from zero (no hysteresis) to a maximum trapped gas saturation of 0.4.

| Parameter | Symbol | Low | Intermediate | High |
|---|---|---|---|---|
| Fracture (DFN) Permeability Model | $Kf_{DFN}$ | -1.0 | 0.0 | 1.0 |
| Fracture Permeability Multiplier X | $Kfx_{mult}$ | 0.1 | 5.0 | 10.0 |
| Fracture Permeability Multiplier Y | $Kfy_{mult}$ | 0.1 | 5.0 | 10.0 |
| Fracture Permeability Multiplier Z | $Kfz_{mult}$ | 0.1 | 5.0 | 10.0 |
| Fault Transmissibility | $FT$ | 0.0 | 0.5 | 1.0 |
| Matrix Wettability | $KR$ | -1.0 | 0.0 | 1.0 |
| Maximum Trapped Gas Saturation | $S_{gt}$ | 0.0 | 0.2 | 0.4 |
| WAG Injector Location X | $IL_x$ | 13 | 17 | 21 |
| WAG Injector Location Y | $IL_y$ | 13 | 17 | 21 |
| WAG Injection Rate | $Inj_{rate}$ | 7,500 | 10,000 | 12,500 |

Table 6.1: Parameters, symbols and ranges of the uncertain parameters varied in the experimental design. Fracture (DFN) permeability models are varied with discrete variables. '-1', '0' and '1' correspond to DFNs with fracture intensity of 0.05, 0.1 and 0.2 respectively. Matrix relative permeability and capillary pressure curves that indicate the wettability (KR) are also represented with discrete variables. '-1' corresponds to oil-wet, '0' corresponds to mixed-wet and '1' corresponds to water-wet.

### 6.3.3 *Simulation, Validation and Optimisation*

Full-physics reservoir simulations were carried out employing the Box-Behnken experimental design using a training data set of 312 samples. The simulation input variables and the corresponding outputs were used to train polynomial regression, sparse polynomial chaos and arbitrary polynomial chaos algorithms to generate approximations of the simulator output. To test the prediction accuracy of the surrogate models, validation simulations using 105 Latin Hypercube samples were evaluated. The response of the data-driven surrogates at both the training and testing data points was then compared to the full-physics numerical simulation output.

The coefficient of determination ($R^2$) and Root Mean Square Error (RMSE) were used as goodness of fit measures. Finally, Monte Carlo simulations using the surrogate models were employed to generate cumulative distribution functions of the oil recovery and GUF. The equations used to generate data-driven surrogates from polynomial regression and polynomial chaos expansions are shown below.

#### 6.3.3.1 *Mathematical Formulation of Surrogate Models*

The general equation for a second-order polynomial regression can be described as:

$$f(x) = c_o + \sum_{i_1=1}^{N} c_{i_1} x_{i_1} + \sum_{i_1=1}^{N} c_{i_1 i_1} x_{i_1}^2 + \sum_{i_1=1}^{N} \sum_{i_2=2}^{N} c_{i_1 i_2} x_{i_1} x_{i_2}, \tag{6.1}$$

where $f(x)$ is the objective function, $x_i$ are the uncertain parameters, $c_0$ is the intercept, $c_{i_1}$are the coefficients of the linear terms, $c_{i_1 i_1}$ are the coefficients of the quadratic terms and $c_{i_1 i_2}$ are the coefficients of interaction terms.

The polynomial chaos expansion for a model output $\Omega$ is given by:

$$\Omega(x) = \sum_{i_1=1}^{M} c_i \Psi_i(\omega), \tag{6.2}$$

where the coefficients $c_i$ represent the dependence of the model output $\Omega$ on the input parameters $\omega$. The function $\Psi_i$ is a simplified form of the multivariate orthogonal polynomial basis for $\Omega$. The number of $M$ terms in the expansion depends on the total of input parameters $N$ and the order $d$ of the expansion, according to equation 6.3 (Oladyshkin et al., 2011; Hosder, 2012):

$$M = \frac{(N+d)!}{N!\,d!}, \tag{6.3}$$

Subsequently, the unknown coefficients in the expansion (eqn. 6.2) are evaluated using a non-intrusive least-square collocation method (Moritz, 1978; Chen et al., 2009). For arbitrary polynomial chaos expansion, the data-driven polynomial basis for one random variable ($\omega_j$) of degree $k$ is defined as:

$$P_j^{(k)}\left(\omega_j\right) = \sum_{i=0}^{k} p_{i,j}^{(k)} \omega_j^i, \qquad k = \overline{0,d}, \qquad j = \overline{0,N}, \tag{6.4}$$

Here $p_{i,j}^{(k)}$ are the coefficients in $P_j^{(k)}(\omega_j)$. The coefficients $p_{i,j}^{(k)}$ are constructed in such a way that the polynomials in equation 6.4 form a basis that is orthogonal in arbitrarily given distributions of data (Oladyshkin et al., 2011). A detailed description of the polynomial basis functions used in sparse polynomial chaos expansion is presented in Elsheikh et al. (2014).

#### 6.3.3.2 *Genetic Algorithm for Optimisation*

Subsequently, the surrogate models were coupled with the genetic algorithm to obtain an optimum value of the oil recovery and GUF based on the combination of input parameters. The genetic algorithm optimises an objective function by a process of selection, mutation and recombination as indicated by Algorithm 1 (Koziel and Yang, 2011). A population size of 50, a crossover probability of 0.8, and a mutation probability of 0.02, was used to ensure that the algorithm captures a large search space and to avoid being trapped in local minima. Larger population sizes had no effect on the optimisation results. The algorithm was evaluated for 50 generations (i.e. iterations) to obtain optimum results based on a function tolerance of $10^{-6}$. The function tolerance defines the minimum difference between new and existing optimal values, hence, the optimisation

iteration is terminated when a predefined function tolerance is reached.

| Algorithm 1: | Genetic algorithm for optimisation |
|---|---|
| 1 | **Start** |
| 2 | Intialise solutions $\mathbf{x}_i$ of population $\Psi$ |
| 3 | Evaluate objective function for the solutions of $\mathbf{x}_i$ in $\Psi$ |
| 4 | **Repeat** |
| 5 | **For** $i = 0$ to $\beta$ |
| 6 | Select $\rho$ parents from $\Psi$ |
| 7 | Create new $\mathbf{x}_i$ by recombination |
| 8 | Mutate $\mathbf{x}_i$ |
| 9 | Evaluate objective function for $\mathbf{x}_i$ |
| 10 | Add $\mathbf{x}_i$ to $\Psi^{'}$ |
| 11 | **Next** |
| 12 | Select $\mu$ parents from $\Psi^{'}$ and form new $\Psi$ |
| 13 | **Until** termination condition |
| 14 | **End** |

## 6.4 PROXY ANALYSIS

### 6.4.1 *Surrogate Training with Full-Physics Simulations*

Black oil flow simulations were used as a basis for generating data-driven surrogates. The full-physics flow simulations indicate channelling during hydrocarbon displacement in the reservoir which makes $CO_2$ WAG injection a desirable recovery option because WAG injection can ensure better mobility control and frontal stability to improve contact of injected fluids with unswept zones (Fig. 6.5a). $CO_2$ migration to the top of the reservoir due to gas-oil density difference is also apparent (Fig. 6.5b). Furthermore, the full-physics simulations provide the relevant training and testing data sets for generating the proxy models. On average, the computational cost for each black oil simulation run was 8.2 hrs.

The oil recovery and GUF profiles for the training simulations (Fig. 6.6) show a range of simulation responses based on various combinations of uncertain input parameters. As expected, the oil recovery increases as alternate cycles of water and gas are injected into the reservoir. The GUF, however, increases ini-

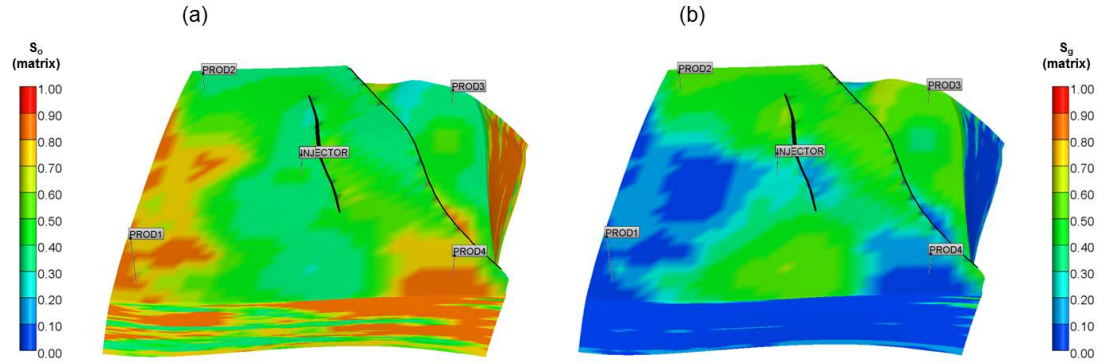


Figure 6.5: Matrix oil saturation (a) and gas saturation (b) distribution after 8 cycles of immiscible $CO_2$ WAG injection using an inverted 5-spot well pattern. Geological layer channelling influences recovery efficiency in (a) while gas migrates to top of the reservoir in (b).

tially but begins to decrease as the reservoir becomes gas saturated.

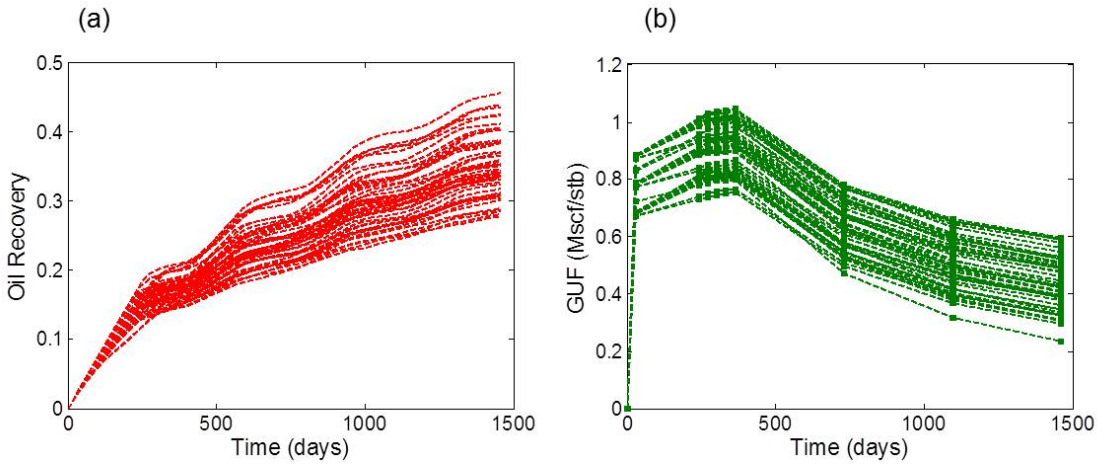


Figure 6.6: Oil recovery (a) and gas utilisation factor (GUF) (b) profiles for the experimentally designed full-physics simulations used to train and test the surrogate models. Only 50 simulation results are shown to avoid overlaps.

### 6.4.2 *Oil Recovery Surrogate Prediction*

The response surfaces that can be generated from training simulations using the three data-driven surrogate models (PR, sPCE and aPCE) are very similar and the relative error between response surfaces is approximately 0.002. For analysis, this section focuses on the aPCE response surfaces (Fig. 6.7). It can be observed from the four response surfaces that the horizontal fracture permeability always has the highest impact on the simulated oil recovery. This clear link between an increase in the fracture connectivity and a decrease in the oil recovery is ex-

pected because increased connectivity across the fracture network results in a reduction in the residence time of injected fluids and subsequently a reduction in the effectiveness of oil recovery from the matrix due to gravity drainage and capillary imbibition.

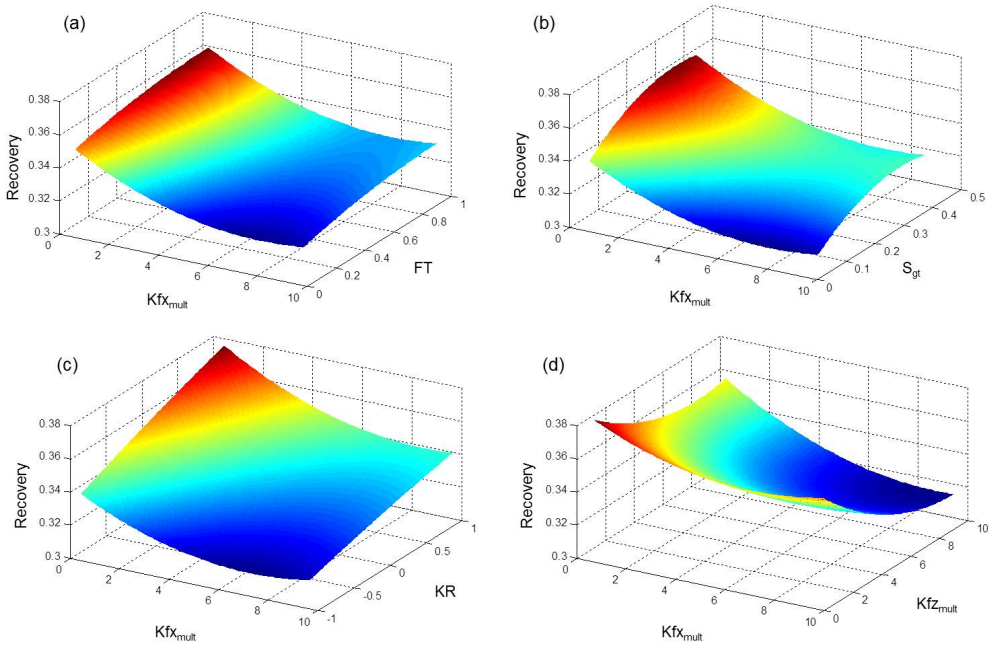


Figure 6.7: Oil recovery factor aPCE response from Box-Behnken design experiments when fault transmissibility (a), maximum trapped gas saturation (b), wettability (c), and vertical fracture permeability multiplier (d) are varied along with the horizontal fracture permeability multiplier.

Consequently, the highest overall oil recovery is observed when the fracture permeability is low and the matrix is water-wet and hence imbibition most effective (Fig. 6.7c). The lowest overall recovery is observed when both the vertical and horizontal fracture permeabilities are at their highest values (Fig. 6.7d) indicating that when the fractures are well connected, fracture networks form fluid flow highways that lead to rapid transport of injected fluids thereby resulting in low oil recovery. Increased fault transmissibility (Fig. 6.7a) allows the injected fluids to access all parts of the reservoir more readily which improves recovery. Similarly, an increase in the maximum trapped gas saturation reduces the overall gas mobility and leads to improved recovery predictions (Fig. 6.7b). This is because a reduction in the gas mobility increases the stability of the gas-water mobility front, delays gas breakthrough and improves the contact of gas with residual oil, thereby ensuring better microscopic and macroscopic sweep

of the reservoir. On average, the computational cost for each surrogate model evaluation was 13.2 seconds indicating significant reduction in CPU time when compared to the 8.2 hrs CPU time required for a single full-physics simulation run.

### 6.4.3 *Gas Utilisation Factor Surrogate Prediction*

The net gas utilisation factor generally increases with increasing horizontal fracture permeability (Fig. 6.8). This increase is caused by high-permeability fracture networks that allow more gas flow per barrel of oil recovered from the matrix due to the rapid fluid transport in the fractures. The results show that the fault transmissibility has a limited effect on the GUF (Fig. 6.8a). This is because the fault transmissibility impacts oil and gas migration in the reservoir in the same way: when the fault transmissibility is low, flow of gas and oil across the faults is limited; when the fault transmissibility is high, flow of gas and oil across the faults is enhanced.

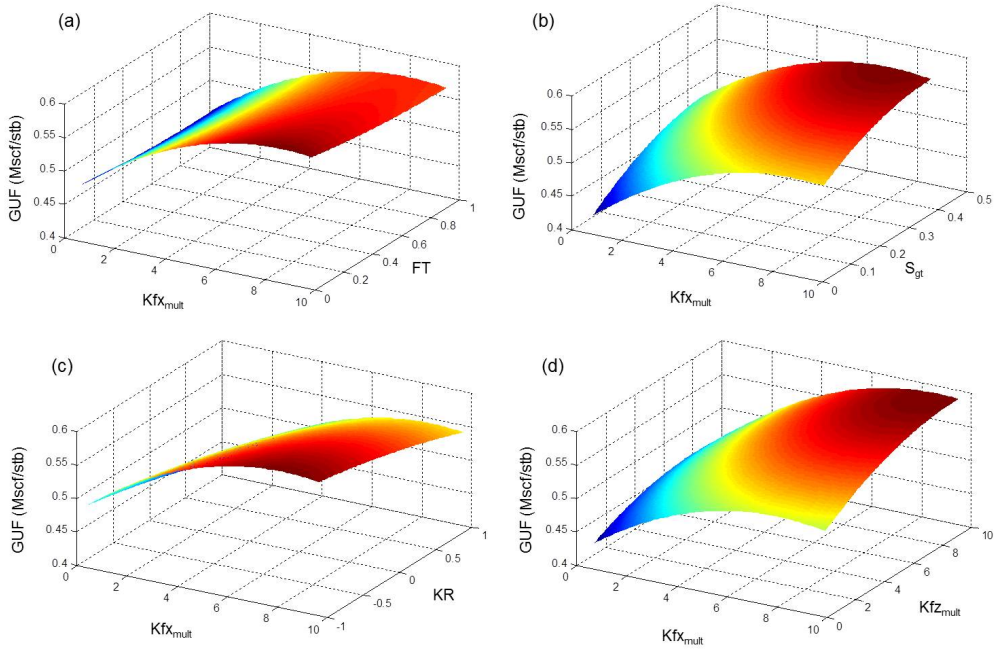


Figure 6.8: Net gas utilisation factor (GUF) aPCE response from Box-Behnken design experiments when fault transmissibility (a), maximum trapped gas saturation (b), wettability (c), and vertical fracture permeability multiplier (d) are varied along with the horizontal fracture permeability multiplier.

The GUF increases with higher values of residual gas trapping due to relative permeability hysteresis (Fig. 6.8b). It is well known that relative permeabilities depend on the saturation path during hydrocarbon displacement cycles (Larsen and Skauge, 1998; Juanes et al., 2006). The cycle dependence influences the amount of gas trapped in the subsurface, thereby resulting in higher values of the GUF as the trapped gas fraction increases. Conversely, the GUF decreases with increasing water-wetness (Fig. 6.8c). Although, the amount of trapped non-wetting gas is higher in a water-wet scenario (Piri and Blunt, 2005; Al-Dhahli et al., 2013), the oil recovery is also very high (Fig. 6.7c). Hence, the GUF which is a ratio of net gas utilised to oil produced decreases with increasing water-wetness. The GUF is highest (Fig. 6.8d) when the vertical and horizontal fracture permeabilities are high, which indicates rapid gas transport and accumulation at the top of the reservoir when the fracture permeability is very high.

The indicated response surfaces are smooth and have a single minimum because this thesis hypothesised that $2^{nd}$ degree polynomials are sufficient to capture the nonlinear interaction of the uncertain parameters considered. Tests with higher degree polynomials (e.g., $4^{th}$ and $5^{th}$ order) show multiple minima but are not focus of this study. The response surfaces have been shown to be convex or concave depending on whether the objective function is oil recovery or GUF respectively and the relationship of given input parameters with the fracture network properties which show the greatest impact on the simulation results.

### 6.4.4 *Goodness of Fit Measures*

To validate the surrogate models that were obtained from the training and testing simulation, the predictions of the surrogates were compared with results from full-physics simulations and relevant cross-plots were generated to estimate goodness of fit measures. The coefficient of determination ($R^2$) for oil recovery obtained for the PR, sPCE and aPCE surrogates was 0.9635, 0.9768 and 0.9770, respectively (Table 6.2 and Fig. 6.9).

The $R^2$ value indicates that all the data-driven surrogates are valid and that the PCE models yield a slightly better approximation of the actual simulation model. The goodness of fit measures for the GUF also show that the PCE models give consistently better predictions of the actual simulation results (Table 6.2 and Fig. 6.9).

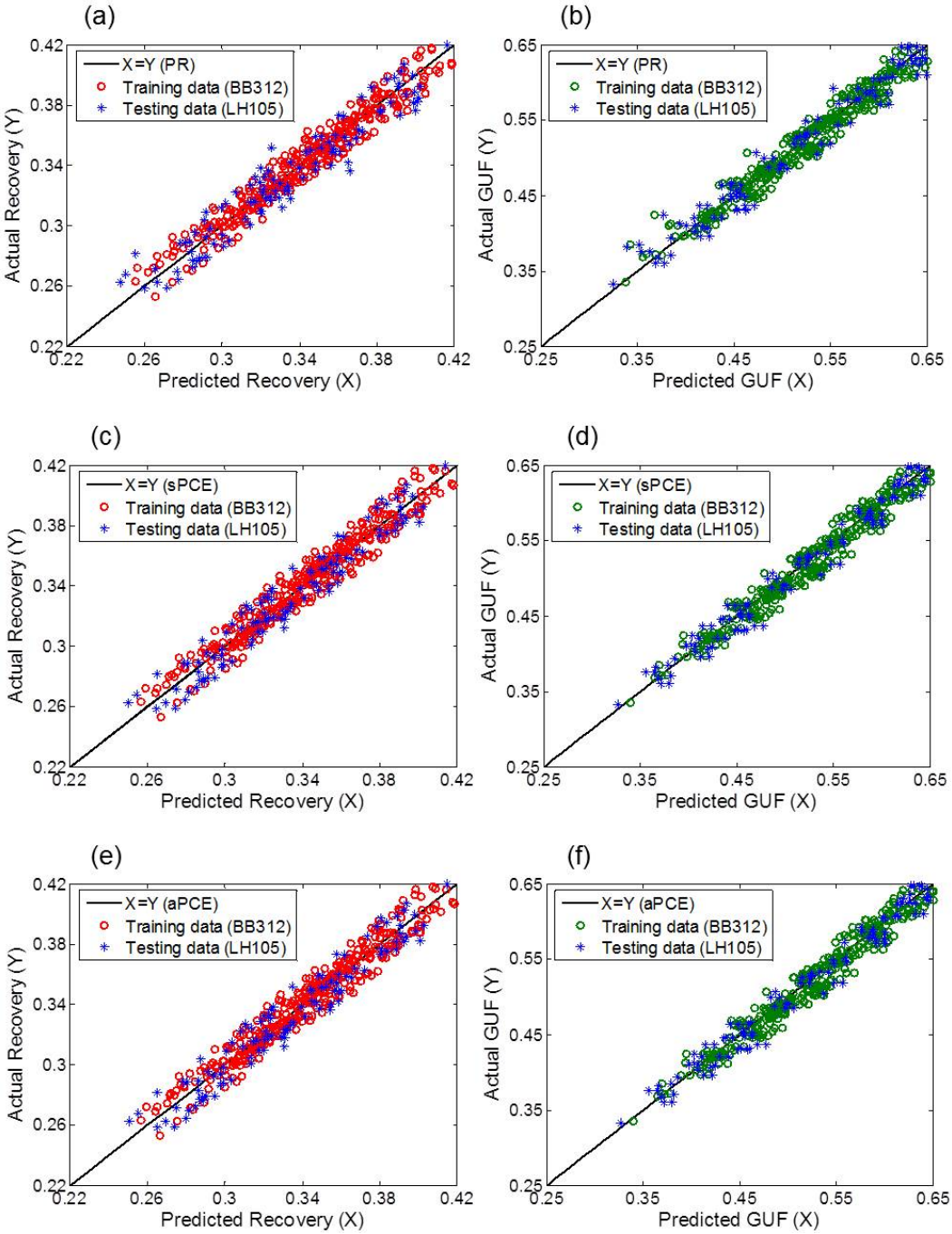


Figure 6.9: Model comparison of oil recovery and gas utilisation factor (GUF) between full-physics simulations and surrogate models from polynomial regression (a, b), sparse polynomial chaos expansion (c, d) and arbitrary polynomial chaos expansion (e, f). Result comparison is for final recovery and GUF.

| Goodness of Fit Measure | Polynomial Regression | | Sparse Polynomial Chaos | | Arbitrary Polynomial Chaos | |
|---|---|---|---|---|---|---|
| | Recovery | GUF | Recovery | GUF | Recovery | GUF |
| $R^2$ | 0.9635 | 0.9823 | 0.9768 | 0.9903 | 0.9770 | 0.9903 |
| $R^2$ Adjusted | 0.9361 | 0.9690 | 0.9594 | 0.9830 | 0.9597 | 0.9830 |
| RMSE | 0.0052 | 0.0098 | 0.0042 | 0.0073 | 0.0042 | 0.0073 |

Table 6.2: Goodness of fit measures for combined training and testing data. $R^2$ is the coefficient of determination which indicates how well the data-driven surrogates predict actual simulation results. '$R^2$ Adjusted' accounts for the number of terms in the polynomial model approximation. RMSE is the root mean square error of the data-driven surrogate compared to the actual simulation.

A comparison of the PCE models for both oil recovery and GUF indicates that the aPCE models give slightly better results compared to the sPCE models. However, it is expected that further tuning of the sPCE model may allow us to eradicate the difference between the aPCE and sPCE model. Subsequent relative error analysis, Monte Carlo simulations and model optimisation focus on proxy models from aPCE.

Furthermore, a comparison of oil recovery flow profiles generated using the aPCE surrogate model and full-physics simulation indicates that the aPCE surrogates slightly under predicts the results especially at late time (Fig. 6.10). Hence, it can be deduced that although it considerably faster to evaluate a data driven

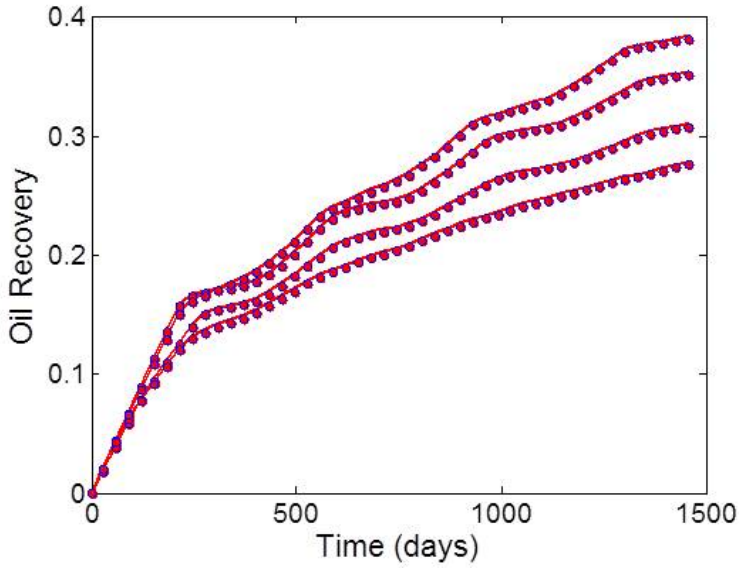


Figure 6.10: Comparison of oil recovery flow profiles for simulations using full-physics and aPCE surrogate model. Solid lines represent flow profiles computed with full-physics simulation, while, dots represent flow profiles computed with aPCE surrogate model. Surrogate model slightly under-predict results from full-physics simulation.

surrogate than to run a full simulation case, it is evident that such a simple model must be constructed and used with care. Increasing the number of testing and training simulations may improve the predictability of the surrogate but care must be taken to ensure that the surrogate prediction is not 'over' specific to the dataset but applicable to data that is outside the design space.

### 6.4.5 *Relative Error*

Relative error response surfaces (Fig. 6.11 and Fig. 6.12) show the discrepancy between the response surfaces from PR and aPCE. In comparison to aPCE, PR always over predicts the oil recovery (Fig. 6.11) and under predicts the GUF (Fig. 6.12). Analysis of the relative error between the aPCE and PR response surfaces shows that although the overall error is minimal, the difference in the prediction is most evident in the middle of the design space. This is because the deterministic Box-Behnken experimental design employed to set up the training simulations in this study generates samples that more adequately capture the actual model behaviour at the boundaries of the design space but have greater uncertainty at the middle of the design space.

To further investigate the deterministic sampling bias, test simulations were generated using the more random Latin Hypercube experimental design (Fig. 6.13). It was observed that when random samples are added to the design, the mismatch between PR and aPCE prediction has a wider spread in the design space. However, the absolute error from such a random design is greater than the error from the deterministic design. The final choice of what design method to employ should be a function of how well the surrogate predicts the behaviour of the actual simulation in any given scenario. Furthermore, combining different experimental design techniques, as shown in this chapter, could also be a reliable way to account for uncertainties that may propagate from the experimental design techniques used to generate the data-driven surrogates.

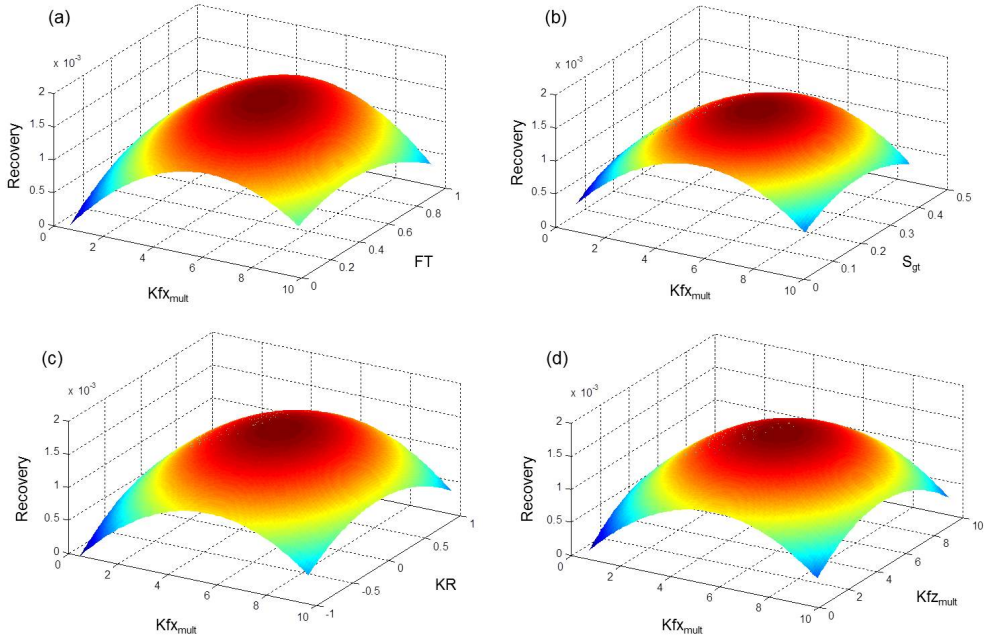


Figure 6.11: Oil recovery relative error response surface when PR is compared to aPCE. PR always under predicts recovery. Overall error is minimal but notice for all surfaces that the error is lowest at the corners and highest in the centre of the design space because of the experimental design method employed.

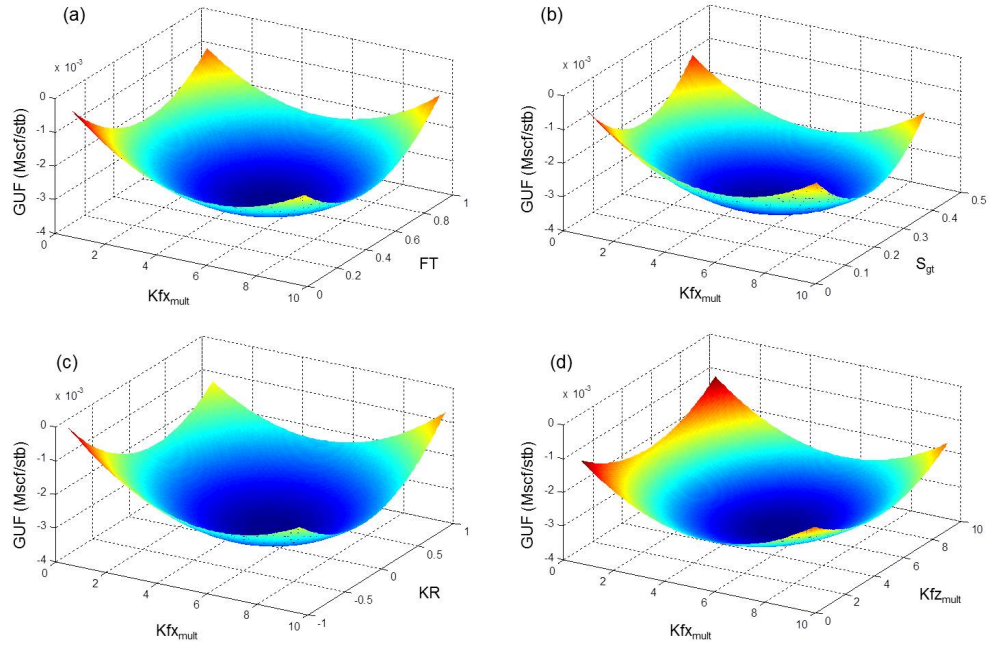


Figure 6.12: Gas utilisation factor relative error response surface when PR is compared to aPCE. PR always over predicts GUF. Overall error is minimal but notice for all surfaces that the error is lowest at the corners and highest in the centre of the design space because of the deterministic experimental design method employed.

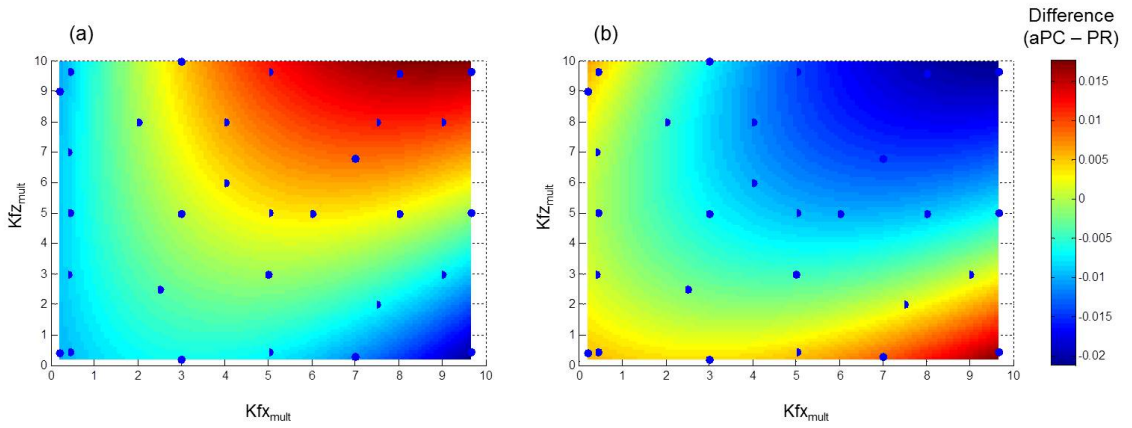


Figure 6.13: The relative difference in the response surface when PR is compared to aPCE for oil recovery (a) and gas utilisation factor (b). Further validation sample points have been added using Latin Hypercube sampling to reduce the deterministic sampling bias. Blue dots refer to actual simulation runs for training (dots at the corners) and validation (random dots within the design).

### 6.4.6 *Surrogate Based Uncertainty Quantification and Probabilistic Assessment*

Monte Carlo simulations carried out using the aPCE model and evaluated 65000 times were used to determine the cumulative distribution functions (cdfs) for oil recovery and GUF over the range of uncertainty for the input parameters (Fig. 6.14).

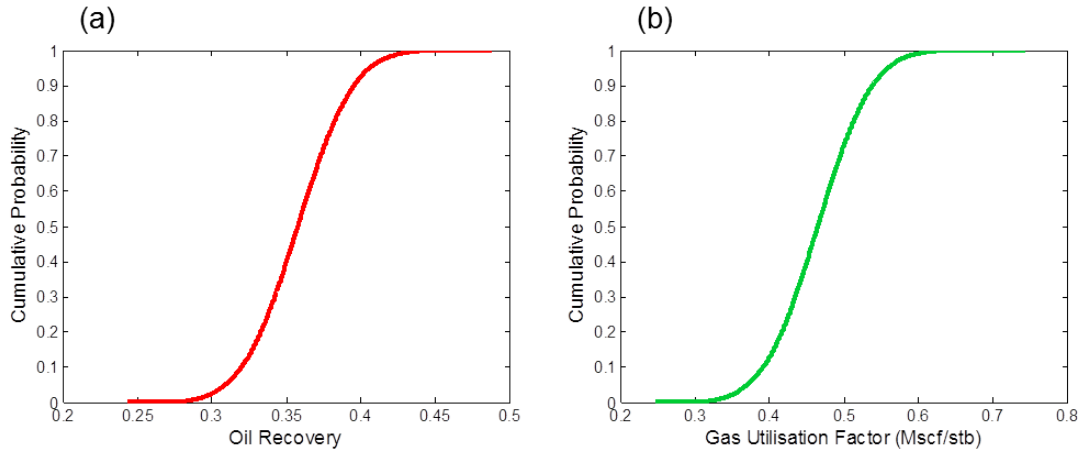


Figure 6.14: Cumulative probability distributions of oil recovery (a) and net gas utilization factor (GUF) (b) generated from 65000 Monte Carlo simulations using the aPC model. Oil recovery P10, P50 and P90 is 0.31, 0.34 and 0.37 respectively. GUF P10, P50 and P90 is 0.45, 0.53 and 0.60 Mscf/stb respectively.

The $10^{th}$, $50^{th}$ and $90^{th}$ (P10, P50 and P90) percentile probabilistic estimate for oil recovery is 0.31, 0.34 and 0.37 respectively for simulation of immiscible $CO_2$

WAG injection over a period of 1400 days. Also, the P10, P50 and P90 probabilistic estimate is 0.45 Mscf/stb, 0.53 Mscf/stb and 0.60 Mscf/stb for GUF.

A normal distribution most closely matches the output data and leads to a symmetric distribution. This is confirmed by the similarity of the illustrated cdfs using aPCE to the cdfs generated in CMOST simulator using polynomial regression surrogates. Such a unimodal symmetric distribution cannot always be expected as the nature of the cdf depends on the distribution of input parameters and the distributions that are used to match the surrogate model outputs.

### 6.4.7 *Surrogate Based Optimisation*

The aPCE surrogate model coupled with the Genetic Algorithm (GA) was applied to optimise the objective functions (i.e. oil recovery and GUF). Optimisation using GA progresses as a minimisation of the fitness value (i.e. -1 x objective function) with the mean fitness value improving during each generation (Fig. 6.15) until the optimum is reached after 50 generations. The optimum oil recovery estimate obtained using the aPCE model for the reservoir is 0.50 while the optimum GUF obtained is 0.36 Mscf/stb. The corresponding values of the modelling parameters are presented in Table 6.3. Figure 6.16 illustrates convergence of the oil recovery to the optimum after over 2000 progressive evaluations of the surrogate model based on the genetic algorithm.

When the proxy optimisation results were compared to evaluations of the full-physics model using the optimum input parameters, an absolute error of 0.0048 and 0.0043 was obtained for the oil recovery and GUF respectively. A few sub-optimal solutions are observed as the algorithm evolves and converges to the optimum due to the random component in the genetic algorithm that allows the search during optimisation to move toward sub-optimal solutions occasionally in order to seek out the global optimum objective function (Fig. 6.16). These random solutions increase confidence that the algorithm adequately explores the parameters space and obtains a global optimum.

In this chapter, it was sufficient to optimise a single objective function (i.e. oil recovery) at a time. Since the oil recovered (or produced) is inversely proportional to the GUF, maximising the oil recovery concurrently minimises the GUF which could both be desirable outcomes from an economic perspective. To study the possibility of optimising two competing objectives, multi-objective optimisation is required. Multi-objective optimisation finds a set of optimal solutions in the range between two optimums. The set of optimal solutions, known as the pareto front, should ideally have a good spread (Mitchell, 1999; Hajizadeh et al., 2011).

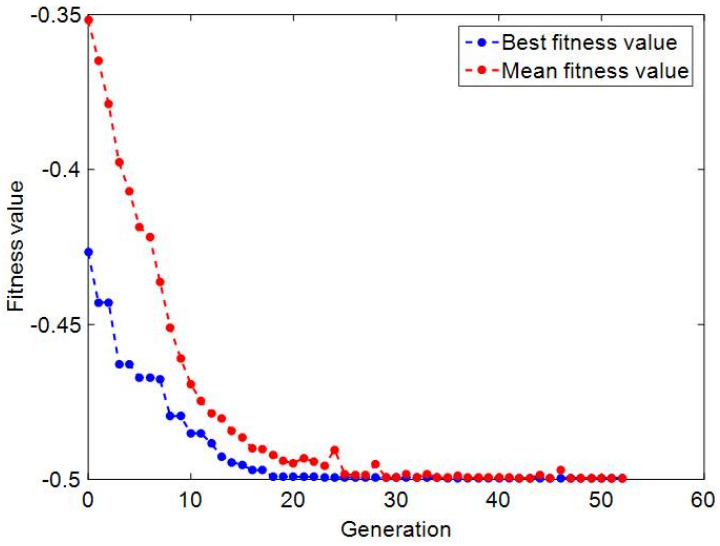


Figure 6.15: Genetic algorithm (GA) optimisation process for the fractured carbonate reservoir model. Note the occasional sub-optimal solutions during optimisation to ensure that the GA obtains the optimal global solution. The algorithm is set to maximise the oil recovery, thereby concurrently minimising the GUF.

| $Gen$ | $Kf_{DFN}$ | $Kf_{mult}$ | $FT$ | $KR$ | $S_{gt}$ | $IL_x$ | $IL_y$ | $Inj_{Rate}$ | $RF$ | $GUF$ |
|---|---|---|---|---|---|---|---|---|---|---|
| 1 | 0 | 1.4057 | 0.3059 | -1 | 0.1844 | 18 | 17 | 10918 | 0.3661 | 0.4292 |
| 2 | 1 | 5.5560 | 0.4917 | 0 | 0.1373 | 16 | 18 | 11455 | 0.3867 | 0.3899 |
| 3 | 1 | 1.8103 | 0.6586 | 1 | 0.1986 | 17 | 18 | 11924 | 0.4444 | 0.3593 |
| 4 | 1 | 1.6540 | 0.5768 | 1 | 0.3155 | 18 | 20 | 11414 | 0.4464 | 0.3838 |
| 5 | 1 | 3.7237 | 0.6547 | 1 | 0.2877 | 17 | 18 | 11970 | 0.4467 | 0.3654 |
| 6 | 1 | 1.1319 | 0.6648 | 1 | 0.1995 | 17 | 19 | 12292 | 0.4575 | 0.3537 |
| 7 | 1 | 1.0484 | 0.7328 | 1 | 0.2018 | 17 | 18 | 12310 | 0.4602 | 0.3530 |
| 8 | 1 | 1.2237 | 0.6542 | 1 | 0.3243 | 17 | 21 | 12285 | 0.4723 | 0.3648 |
| 9 | 1 | 1.9328 | 0.6916 | 1 | 0.3688 | 15 | 21 | 12272 | 0.4732 | 0.3620 |
| 10 | 1 | 1.2223 | 0.8040 | 1 | 0.3243 | 13 | 21 | 12302 | 0.4808 | 0.3557 |
| 11 | 1 | 0.6790 | 0.8777 | 1 | 0.3348 | 13 | 18 | 12351 | 0.4797 | 0.3605 |
| 12 | 1 | 0.8006 | 0.8771 | 1 | 0.3566 | 14 | 21 | 12193 | 0.4829 | 0.3603 |
| 13 | 1 | 0.6183 | 0.8671 | 1 | 0.3882 | 16 | 21 | 12440 | 0.4881 | 0.3641 |
| 14 | 1 | 0.9967 | 0.8762 | 1 | 0.3892 | 13 | 21 | 12429 | 0.4899 | 0.3566 |
| 15 | 1 | 0.2848 | 0.9702 | 1 | 0.4117 | 14 | 21 | 12467 | 0.4961 | 0.3599 |
| 16 | 1 | 0.2863 | 0.9758 | 1 | 0.4122 | 13 | 21 | 12471 | 0.4971 | 0.3579 |
| 17 | 1 | 0.2474 | 0.9694 | 1 | 0.4125 | 14 | 21 | 12469 | 0.4969 | 0.3589 |
| 18 | 1 | 0.1059 | 0.9992 | 1 | 0.4184 | 13 | 21 | 12497 | 0.4993 | 0.3581 |
| 19 | 1 | 0.1132 | 0.9916 | 1 | 0.4182 | 13 | 21 | 12493 | 0.4991 | 0.3580 |
| 20 | 1 | 0.1975 | 0.9504 | 1 | 0.4117 | 13 | 21 | 12474 | 0.4978 | 0.3578 |
| 21 | 1 | 0.1047 | 0.9979 | 1 | 0.4185 | 13 | 21 | 12498 | 0.4993 | 0.3581 |
| 22 | 1 | 0.1547 | 0.9985 | 1 | 0.3659 | 13 | 21 | 12499 | 0.4975 | 0.3932 |
| 23 | 1 | 0.1062 | 0.9854 | 1 | 0.4112 | 13 | 21 | 12498 | 0.4993 | 0.3580 |
| 24 | 1 | 0.1021 | 0.9991 | 1 | 0.4156 | 13 | 21 | 12499 | 0.4994 | 0.3581 |
| 25 | 1 | 0.1036 | 0.9973 | 1 | 0.4128 | 13 | 21 | 12499 | 0.4994 | 0.3581 |
| 26 | 1 | 0.1044 | 0.9979 | 1 | 0.4097 | 13 | 21 | 12500 | 0.4994 | 0.3582 |
| 27 | 1 | 0.1034 | 0.9978 | 1 | 0.4122 | 13 | 21 | 12500 | 0.4994 | 0.3581 |
| 28 | 1 | 0.1040 | 0.9877 | 1 | 0.4062 | 13 | 21 | 12499 | 0.4994 | 0.3581 |
| 29 | 1 | 0.1018 | 0.9976 | 1 | 0.4079 | 13 | 21 | 12500 | 0.4994 | 0.3582 |
| 30 | 1 | 0.1014 | 0.9968 | 1 | 0.4056 | 13 | 21 | 12500 | 0.4994 | 0.3582 |
| 35 | 1 | 0.1004 | 0.9937 | 1 | 0.4103 | 13 | 21 | 12500 | 0.4994 | 0.3581 |
| 40 | 1 | 0.1003 | 0.9938 | 1 | 0.4098 | 13 | 21 | 12500 | 0.4994 | 0.3581 |
| 45 | 1 | 0.1002 | 0.9898 | 1 | 0.4013 | 13 | 21 | 12500 | 0.4995 | 0.3581 |
| 50 | 1 | 0.1000 | 0.9887 | 1 | 0.4014 | 13 | 21 | 12500 | 0.4995 | 0.3581 |

Table 6.3: Mean value of uncertain input parameters and objective functions (oil recovery factor, *RF* and gas utilisation factor, *GUF*) for each generation during optimisation with genetic algorithm. Optimum solution is obtained after 50 generations.

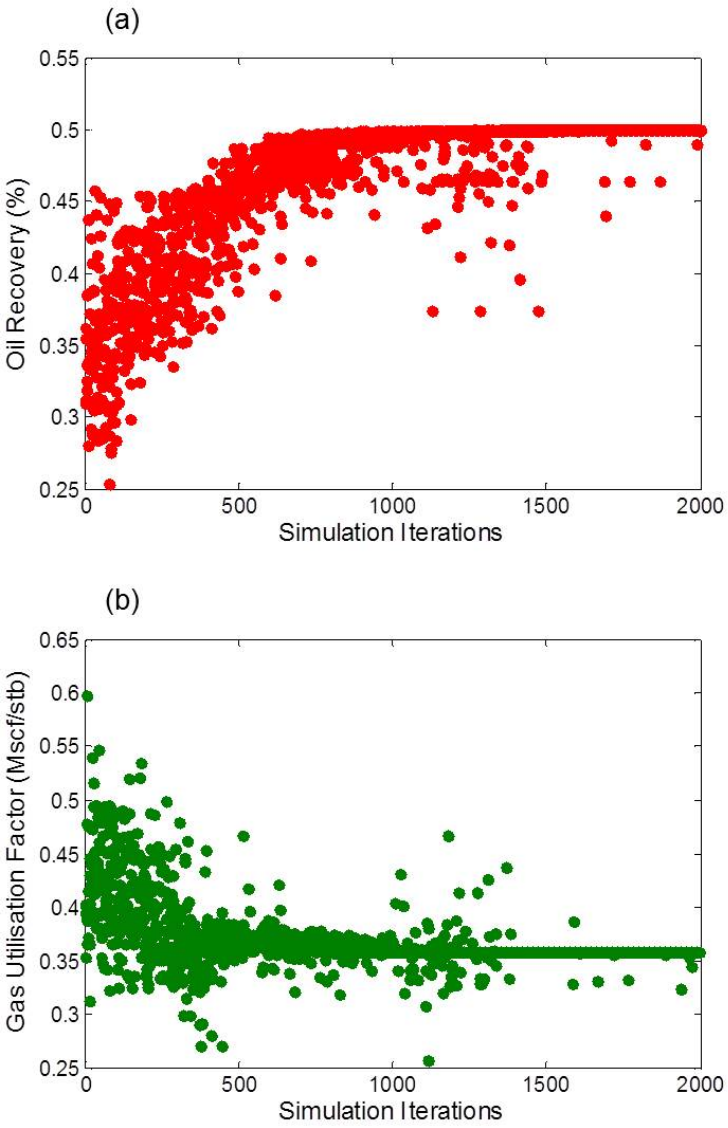


Figure 6.16: Multiple simulation iterations using aPCE surrogate model coupled with genetic algorithm for the optimisation of oil recovery (a) and net gas utilisation factor (b).

## 6.5 SUMMARY

Reservoir simulation and optimisation of $CO_2$ WAG injection in fractured carbonate reservoirs is a complex and time-consuming process. By applying surrogate models to approximate full-physics numerical simulations using a limited number of training and testing simulations that cover the parameter space and account for key uncertainties, significant reduction in the overall modelling time can be achieved. The surrogates can then help to understand the respective dependencies and correlations of uncertain input parameters and contribute to rapid simulation, optimisation and decision making under uncertainty. Surro-

gate models are not expected to replace full-physics black oil or compositional models but can save significant amounts of time during reservoir evaluation by eliminating unnecessary model runs that use up often limited computing resources. Once the most influential, sensitive or optimum simulations have been identified using the proxy model, the full physics simulation is evaluated at the corresponding sample points to confirm the results. If the proxy models have been extensively trained and tested using appropriate experimental design and goodness of fit measures, it is expected that the results should be identical.

In this chapter, data-driven surrogates have been used for the rapid simulation and optimisation of $CO_2$ WAG injection in a fractured carbonate reservoir model. The results show that data-driven surrogate modelling techniques from PCE (arbitrary polynomial chaos expansion, aPCE, and sparse polynomial chaos expansion, sPCE show a higher degree of accuracy in predicting oil recovery and GUF, when compared to data-driven surrogates from polynomial regression. PCE techniques capture the synergistic effects between low- and high-order polynomial terms and thereby provide higher accuracy. In particular, aPCE most closely approximates the actual simulations when trained and tested. aPCE techniques minimise the subjectivity of input data distributions by directly using the available information in a data-driven formulation of PCE and employing a global polynomial basis for arbitrary distributions of data. Furthermore, the objective function(s) was successfully optimised when the aPCE model was coupled with the genetic algorithm to carry out over 2000 rapid evaluations of the surrogate model.

A source of uncertainty in the surrogate modelling workflow which may propagate to the surrogate model prediction is the chosen experimental design. Deterministic designs may be biased towards the boundaries of the design while random designs may need more training and testing to constrain. This work combined deterministic (training) and random (testing) experimental design to account for the uncertainty from sampling bias and improve the reliability of proxy predictions. Another source of uncertainty in the workflow relates to the fracture permeability multipliers that were used to account for the variability of the fracture network connectivity. It is expected that comparing more geo-

logically constrained fracture network scenarios may offer more robust results. Although it is considerably faster to evaluate a data-driven surrogate than to run a full simulation case, it is self-evident that such a simple model must be constructed and used with care. The accuracy of the model should be thoroughly validated in order to estimate its prediction capability and the application of appropriate goodness of fit measures is essential to ensure that the surrogate reliably replaces the full simulation model inside and outside of the design space.

# 7

# SUMMARY, CONCLUSIONS AND FUTURE WORK

## 7.1 SUMMARY AND CONCLUSIONS

High-resolution outcrop analogue studies for complex subsurface reservoirs have become increasingly common, because they enable us to integrate reservoir characterisation with reservoir simulation. Distinct geological features that are observed in the outcrop can then be compared to complex flow phenomena present in real reservoirs. Hence, outcrop analogue studies contribute to the construction of static models that are better calibrated because they allow us to analyse the key geological structures that control the flow behaviour in the reservoir. Such static models can then be translated more reliably into dynamic models. Subsequently, the dynamic models enable us to compare, contrast and rank the performance of recovery mechanisms for specific carbonate reservoir types, thereby guiding reservoir modelling and simulation workflows.

The key outcomes of this thesis are as follows:

- In chapter 3, systematic numerical simulations of well testing and subsequent well-test analysis on synthetically generated pressure transients reveal that faults dominate the large-scale flow behaviour in the model despite the presence of significant small-scale heterogeneity. High-permeability oyster bioherms are also distinguishable in the pressure transients. Conversely, diagenetic hard grounds and mud mounds were not observed in the pressure transients. Secondary recovery simulations demonstrate that channelling of flow into high-permeability layers is a primary control on oil recovery in the heterogeneous carbonate reservoir. Hence, outcrop-

analogue based high-resolution simulations can provide important guidelines as to which geological heterogeneities need to be captured in real reservoir models such as faults, oyster bioherms and high permeability channels.

- Chapter 4 shows that by implementing miscible gas injection and WAG, a higher fraction of oil is recovered from the reservoir, due to reduction in the interfacial tension and improved microscopic sweep efficiency, compared to immiscible gas injection and WAG. In addition, chapter 4 shows how foam EOR improves mobility control and reservoir conformance by generating viscous pressure drop that diverts injected fluid from high permeability fractures and channels to the low permeability matrix. Consequently, a higher oil recovery was observed when foam EOR was employed compared to WAG injection.

- Chapter 5 reveals that the fracture network properties have the greatest impact on the simulation results, especially when the fracture intensity is low. The presence of connected fractures leads to rapid $CO_2$/water transport, increased bypassing of oil and poor $CO_2$ storage. Chapter 5 also shows that the effect of the wetting preference is non-trivial as increased water-wetness reduces the gas saturation in the matrix due to high capillary entry pressures. Increased imbibition in the water-wet medium also leads to higher oil recovery during water injection cycles. Conversely, the imbibition potential is very poor in the oil-wet medium leading to much lower recovery from water injection cycles.

- Chapter 6 shows that by applying data-driven surrogate models to approximate full-physics numerical simulations using a limited number of training and testing simulations that cover the parameter space and account for key uncertainties, we can significantly reduce the overall modelling time. On average, the computational cost for each surrogate model evaluation is 13.2 seconds compared to 8.2 hrs CPU time for a single full-physics simulation. In chapter 6, the benefit of coupling surrogate models with stochastic optimisation algorithms for rapid optimisation under uncertainty was demon-

strated using over 2000 progressive model evaluations to obtain an optimal oil recovery of 50 percent after 1500 days.

## 7.2 FUTURE WORK

This thesis integrates reservoir characterisation with reservoir simulation to explore fundamental aspects of EOR simulation and optimisation for fractured carbonate reservoirs using a high-resolution fractured carbonate reservoir model. There are other reservoir simulation aspects, however, that can be considered to improve upon the research presented here. Some recommendations are as follows:

- The ideas presented in this thesis would greatly benefit from application to a real subsurface reservoir model such that the findings can be calibrated to static and dynamic field data. In such a study, static subsurface data from well logs, and dynamic data from well testing, tracer testing and production logging can be used to robustly calibrate the matrix and fracture models.

- In this thesis, the fracture network was represented using DFN modelling approaches which generate a stochastic fracture network that is then upscaled to the geocellular grid. However, employing discrete fracture and matrix (DFM) models where fractures are explicitly represented may provide additional insights into recovery processes, especially in reservoirs where flow in the matrix is not negligible. Similarly, classical single rate transfer functions in the dual-medium models that account for fracture-matrix exchange were used in this work, but multi-rate transfer functions that account for variability in the rate of fracture-matrix exchange due to sub-grid heterogeneities are gaining increasing attention and should be tested going forward.

- In chapter 4, a semi-empirical foam model was used to account for foam mobility control due to the interaction of gas and surfactant. It is recommended that a fully mechanistic model which introduces additional com-

plexity to foam modelling and accounts for the rate of change of foam texture be tested.

- During the modelling of fracture-matrix interaction such as in chapter 5, it is recommended that geomechanical impacts on fracture evolution be considered. Specifically, the impact of geomechanics on fracture apertures due to overburden. It must be noted, however, that accounting for geomechanical impacts in fractured reservoir simulation is very challenging.

- In chapter 6, data-driven surrogates from polynomial regression and polynomial chaos expansion were used to generate good approximations of time-consuming numerical simulations. It would be interesting to see how other data-driven surrogate modelling techniques compare to the methods tested in this thesis. In particular, surrogates generated using artificial neural networks and kriging techniques could be very valuable for rapid simulation and optimisation of EOR processes.

# BIBLIOGRAPHY


A. Abdollahzadeh, A. Reynolds, M. Christie, D. Corne, G. Williams, and B. Davies. Estimation of Distribution Algorithms Applied to History Matching. *SPE Journal*, 2013.

A. S. Abushaikha and O. R. Gosselin. Matrix-Fracture Transfer Function in Dual-Media Flow Simulation: Review, Comparison and Validation. In *SPE Europec/EAGE Conference*, SPE 113890, 2008.

S. Agada and S. Geiger. Optimising Gas Injection in Carbonate Reservoirs Using High-Resolution Outcrop Analogue Models. In *SPE Reservoir Characterization and Simulation Conference and Exhibition*, SPE 166061, 2013.

S. Agada and S. Geiger. Wettability, Trapping and Fracture-Matrix Interaction during WAG Injection in Fractured Carbonate Reservoirs. In *SPE Improved Oil Recovery Symposium*, SPE 169054, 2014.

S. Agada, F. Chen, S. Geiger, G. Toigulova, S. Agar, R. Shekhar, G. Benson, O. Hehmeyer, F. Amour, M. Mutti, N. Christ, and A. Immenhauser. Numerical simulation of fluid-flow processes in a 3D high-resolution carbonate reservoir analogue. *Petroleum Geoscience*, 20(1):125–142, 2014.

S. Agada, S. Geiger, A.H. Elsheikh, E. Mackay, and S. Oladyshkin. Reduced Order Models for Rapid EOR Simulation in Fractured Carbonate Reservoirs. In *SPE Reservoir Simulation Symposium*, SPE 173205, 2015a.

S. Agada, K. Soni, and S. Geiger. Numerical Simulation of Foam EOR in Fractured Carbonate Reservoirs. In *EAGE IOR Conference*, A203, 2015b.

S. Agar and S. Geiger. Fundamental controls on fluid flow in carbonates: current workflows to emerging technologies. *Geological Society, London, Special Publications*, 406(1):1–59, 2015.

S. Agar, S. Geiger, S. Matthäi, R. Alway, S. Tomás, A. Immenhauser, R. Shekhar, J. Paul, G. Benson, Z. Karcz, and L. Kabiri. The Impact of Hierarchical Fracture Networks on Flow Partitioning in Carbonate Reservoirs: Examples Based on a Jurassic Carbonate Ramp Analog from the High Atlas , Morocco. In *SPE Annual Technical Conference and Exhibition*, SPE 135135, 2010.

B. Agarwal, H. Hermansen, J. E. Sylte, and L. K. Thomas. Reservoir characterization of ekofisk field: a giant, fractured chalk reservoir in the norwegian north sea. *SPE Reservoir Evaluation & Engineering*, 3(06):534–543, 2000.

M. Ahmed-Elfeel and S. Geiger. Static and Dynamic Assessment of DFN Permeability Upscaling. In *SPE Europec/EAGE Conference*, SPE 154369, 2012.

M. Ahmed-Elfeel, A. Al-dhahli, S. Geiger, and M. I. J. van Dijke. Multi-Scale Simulation of WAG Flooding in Naturally Fractured Reservoirs. In *SPE Europec/EAGE Conference*, SPE 164837, 2013.

M. Ahmed-Elfeel, S. Agada, C. Maier, and S. Geiger. Integrating Discrete Fracture Models for Static and Dynamic Calibration of Fractured Reservoirs. In *EAGE Conference Conference and Exhibition*, EAGE E103 05, 2014.

A. Al-Dhahli. *Pore to field scale modelling of three phase flow processes in heterogeneous reservoirs with arbitrary wettability*. PhD Thesis. Heriot-Watt University, 2013.

A. Al-Dhahli, M. I. van Dijke, and S. Geiger. Accurate modelling of pore-scale films and layers for three-phase flow processes in clastic and carbonate rocks with arbitrary wettability. *Transport in Porous Media*, 98(2):259–286, 2013.

A. Al-Dhahli, S. Geiger, and M. I. van Dijke. Impact of pore-scale three-phase flow for arbitrary wettability on reservoir-scale oil recovery. *Journal of Petroleum Science and Engineering*, 121:110–121, 2014.

A. Al-Futaisi and T. W. Patzek. Impact of wettability alteration on two-phase flow characteristics of sandstones: A quasi-static description. *Water Resources Research*, 39(2):1–13, 2003.

M. Al-Kobaisi, H. Kazemi, B. Ramirez, E. Ozkan, and S. Atan. A Critical Review for Proper Use of Water / Oil / Gas Transfer Functions in Dual-Porosity Natu-

rally Fractured Reservoirs : Part II. *SPE Reservoir Evaluation & Engineering*, 12 (2):211–217, 2009.

M. Al-Saad and I. Ibrahim. Facies and palynofacies characteristics of the Upper Jurassic Arab D reservoir in Qatar. *Revue de Paléobiologie, Genève*, 24(1):225–241, 2005.

W. AlHanai, A. AiMahdi, and M. Deeb. Use of stochastic characterization to select horizontal well trajectories in a heterogeneous carbonate reservoir. In *SPE Middle East Oil Show, Bahrain*, SPE 29811, 1995.

V. Alvarado, A. Ranson, K. Hernandez, E. Manrique, J. Matheus, T. Liscano, and N. Prosperi. Selection of EOR/IOR opportunities based on machine learning. In *13th European Petroleum Conference*, SPE 78332, 2002.

F. Amour, M. Mutti, N. Christ, A. Immenhauser, S. Agar, G. Benson, S. Tomás, R. Alway, and L. Kabiri. Capturing and modelling metre-scale spatial facies heterogeneity in a Jurassic ramp setting (Central High Atlas, Morocco). *Sedimentology*, 59(4):1158–1189, 2012.

F. Amour, M. Mutti, N. Christ, G. S. Immenhauser, A., Benson, S. M. Agar, and L. Kabiri. Outcrop analog for an oolitic carbonate ramp reservoir: A scale-dependent geologic modeling approach based on stratigraphic hierarchy. *AAPG Bulletin*, 97(5):845–871, 2013.

O. G. Apaydin and A. R. Kovscek. Surfactant Concentration and End Effects on Foam Flow in Porous Media. *Transport in Porous Media*, 43(3):511–536, 2001.

M. Ashraf, S. Oladyshkin, and W. Nowak. Geological storage of CO2: Application, feasibility and efficiency of global sensitivity analysis and risk assessment using the arbitrary polynomial chaos. *International Journal of Greenhouse Gas Control*, 19:704–719, 2013.

R. Askey and J. A. Wilson. *Some basic hypergeometric orthogonal polynomials that generalize Jacobi polynomials*. American Mathematical Society, 1985.

E. Aspenes, G. Ersland, A. Graue, J. Stevens, and B. A. Baldwin. Wetting phase bridges establish capillary continuity across open fractures and increase oil

recovery in mixed-wet fractured chalk. *Transport in Porous Media*, 74(1):35–47, 2008.

H. Ates, A. Bahar, S. Salem, M. Charfeddine, and M. G. Kelkar. Ranking and upscaling of geostatistical reservoir models using streamline simulation: A field case study. *SPE Reservoir Evaluation & Engineering*, 8(01):22–32, 2005.

M. Aurell, B. Badenas, D. Bosence, and D. Waltham. Carbonate production and offshore transport on a Late Carbonate production and offshore transport on a Late Jurassic carbonate ramp (Kimmeridgian, Iberian basin, NE Spain): evidence from outcrops and computer modelling. In: Wright, V. P. and Burchette, T. *Geological Society, London, Special Publications*, 149:137–161, 1998.

A. R. Awan, R. Teigland, and J. Kleppe. A survey of North Sea enhanced-oil-recovery projects initiated during the years 1975 to 2005. *SPE Reservoir Evaluation & Engineering*, 11(3):497–512, 2008.

M. Azeemuddin, S. G. Ghori, S. Saner, and M. N. Khan. Injection-Induced Hydraulic Fracturing in a Naturally Fractured Carbonate Reservoir : A Case Study from Saudi Arabia. In *SPE International Symposium on Formation Damage Control*, SPE 73784, 2002.

N. A. Azzolina, D. V. Nakles, C. D. Gorecki, W. D. Peck, S. C. Ayash, L. S. Melzer, and S. Chatterjee. Co2 storage associated with co2 enhanced oil recovery: A statistical analysis of historical operations. *International Journal of Greenhouse Gas Control*, 37:384–397, 2015.

S. Bachu, W. D. Gunter, and E. H. Perkins. Aquifer disposal of CO2: Hydrodynamic and mineral trapping. *Energy Conversion and Management*, 35(4):269–279, 1994.

T. Bäck and H. P. Schwefel. An overview of evolutionary algorithms for parameter optimization. *Evolutionary computation*, 1(1):1–23, 1993.

T. Bäck, D. B. Fogel, and Z. Michalewicz. *Evolutionary computation 1: Basic algorithms and operators*. CRC Press, 2000.

L. E. Baker. Three-phase relative permeability correlations. In *SPE Improved Oil Recovery Symposium*, SPE 17369, 1988.

W. Bangerth, H. Klie, M. F. Wheeler, P. L. Stoffa, and M. K. Sen. An optimization algorithm for the reservoir oil well placement problem. *Computational Geosciences*, 10:303–319, 2006.

N. Bech, B. Bourgine, C. Castaing, J. P. Chilés, N. P. Christensen, and P. Frykman. Fracture interpretation and flow modelling in fractured reservoirs. *European Commission, Directorate-General XII, EUR*, 18946, 2001.

M. Belayneh and J. W. Cosgrove. Hybrid veins from the southern margin of the Bristol Channel Basin. *Journal of Structural Geology*, 32:192–201, 2010.

M. Belayneh, S. Geiger, and S. K. Matthäi. Numerical simulation of water injection into layered fractured carbonate reservoir analogs. *AAPG Bulletin*, 90(10): 1473–1493, 2006.

K. Benisch and S. Bauer. Short- and long-term regional pressure build-up during CO2 injection and its applicability for site monitoring. *International Journal of Greenhouse Gas Control*, 19:220–233, 2013.

B. Berkowitz. Characterizing flow and transport in fractured geological media: A review. *Advances in water resources*, 25(8):861–884, 2002.

Z. R. Beydoun. Articles Arabian plate oil and gas : Why so rich and so prolific ? *Episode*, 21:74–81, 1998.

T. Blaker, H. K. Celius, T. Lie, H. A. Martinsen, L. Rasmussen, and F. Vassenden. Foam for Gas Mobility Control in the Snorre Field : The FAWAG Project. *SPE Reservoir Evaluation & Engineering*, 5(4):317–323, 1999.

G. Blatman and B. Sudret. An adaptive algorithm to build up sparse polynomial chaos expansions for stochastic finite element analysis. *Probabilistic Engineering Mechanics*, 25(2):183–197, 2010.

M. J. Blunt. Effects of heterogeneity and wetting on relative permeability using pore level modeling. *SPE Journal*, 2(1):70–87, 1997.

M. J. Blunt. An Empirical Model for Three-Phase Relative Permeability. *SPE Journal*, 5(4):435–445, 2000.

M. J. Blunt. Flow in porous media: pore-network models and multiphase flow. *Current Opinion in Colloid & Interface Science*, 6:197–207, 2001.

M. J. Blunt, M. D. Jackson, M. Piri, and P. H. Valvatne. Detailed physics, predictive capabilities and macroscopic consequences for pore-network models of multiphase flow. *Advances in Water Resources*, 25(8-12):1069–1089, 2002.

M. J. Blunt, B. Bijeljic, H. Dong, O. Gharbi, S. Iglauer, P. Mostaghimi, A. Paluszny, and C. Pentland. Pore-scale imaging and modelling. *Advances in Water Resources*, 51:197–216, 2013.

J. Bon, H. K. Sarma, and A. M. Theophilos. An investigation of minimum miscibility pressure for CO2-rich injection gases with pentanes-plus fraction. In *SPE International Improved Oil Recovery Conference, Kuala Lumpur, Malaysia*, SPE 97536, 2005.

V. Bortolotti, P. Macini, and F. Srisuriyachai. Laboratory evaluation of alkali and alkali-surfactant-polymer flooding combined with intermittent flow in carbonate rocks. In *SPE Asia Pacific Oil and Gas Conference and Exhibition*, SPE 122499, 2009.

O. Bour and P. Davy. On the connectivity of three-dimensional fault networks. *Water Resources Research*, 34(10):2611–2622, 1998.

B. Bourbiaux. Fractured reservoir simulation: a challenging and rewarding issue. *Oil & Gas Science and Technology*, 65(2):227–238, 2010.

B. Bourbiaux, R. Basquet, M. Cacas, J. Daniel, and S. Sarda. An Integrated Workflow to Account for Multi-Scale Fractures in Reservoir Simulation Models: Implementation and Benefits. In *Abu Dhabi International Petroleum Conference and Exhibition*, SPE 78489, 2002.

G. Bourdarot and S. G. Ghedan. Modified EOR Screening Criteria as Applied to a Group of Offshore Carbonate Oil Reservoirs. In *SPE Reservoir Characterisation and Simulation Conference and Exhibition*, SPE 148323, 2011.

D. Bourdet. *Well test analysis: The use of advanced interpretation models*. Elsevier Science, 2002.

G. E. Box, W. G. Hunter, and J. S. Hunter. *Statistics for experimenters*. Wiley, New York, 1978.

I. Bryant, D. Carr, P. Cirilli, N. Drinkwater, D. Mccormick, P. Tilke, J. Thurmond, and D. Lane. Use of 3D digital analogues as templates in reservoir modelling. *Petroleum Geoscience*, 6:195–201, 2000.

T. P. Burchette. Carbonate rocks and petroleum reservoirs: a geological perspective from the industry. *Geological Society, London, Special Publications*, 370(1): 17–37, 2012.

N. M. Burnside and M. Naylor. Review and implications of relative permeability of CO2/brine systems and residual trapping of CO2. *International Journal of Greenhouse Gas Control*, 23:1–11, 2014.

I. Bush. An Integrated Approach to Fracture Characterisation. *Oil Review Middle East*, 2:88–91, 2010.

G. T. Buzzard. Global sensitivity analysis using sparse grid interpolation and polynomial chaos. *Reliability Engineering & System Safety*, 107:82–89, 2012.

D. Cantrell and R. Hagerty. Microporosity in Arab Formation Carbonates, Saudi Arabia. *GeoArabia*, 4:129–153, 1999.

F. M. Carlson. Simulation of relative permeability hysteresis to the nonwetting phase. In *SPE Annual Technical Conference and Exhibition*, SPE 10157, 1981.

D. Casabianca, R. J. H. Jolly, and R. Pollard. The Machar Oil Field: waterflooding a fractured chalk reservoir. *Geological Society, London, Special Publications*, 270 (1):171–191, 2007.

J. M. Castel, C. Betzler, J. Rossler, H. Hussner, and M. Peinl. Integrating outcrop data and forward computer modelling to unravel the development of a Messinian carbonate platform in SE Spain (Sorbas Basin). *Sedimentology*, 54: 423 – 441, 2007.

V. Chandra, H. Hamdi, P. W. M. Corbett, and S. Geiger. Improving Reservoir Characterization and Simulation With Near-Wellbore Modeling. *SPE Reservoir Evaluation & Engineering*, 16:183–193, 2013.

V. Chandra, P. Wright, A. Barnett, R. Steele, P. Milroy, P. Corbett, and A. Mangione. Evaluating the impact of a late-burial corrosion model on reservoir permeability and performance in a mature carbonate field using near-wellbore upscaling. *Geological Society, London, Special Publications*, 406(1):427–445, 2015.

J. S. Chen, L. Wang, H. Y. Hu, and S. W. Chi. Subdomain radial basis collocation method for heterogeneous media. *International Journal for Numerical Methods in Engineering*, 80(2):163–190, 2009.

Q. Chen, M. G. Gerritsen, and A. R. Kovscek. Modeling Foam Displacement With the Local-Equilibrium Approximation : Theory and Experimental Verification. *SPE Journal*, 15(1):171–183, 2010.

V. C. Chen, K. L. Tsui, R. R. Barton, and M. Meckesheimer. A review on design, modeling and applications of computer experiments. *IIE transactions*, 38(4): 273–291, 2006a.

Z. Chen, G. Huan, and Y. Ma. *Computational methods for multiphase flows in porous media*. Siam, 2006b.

R. Chesnaux, D. M. Allen, and S. Jenni. Regional fracture network permeability using outcrop scale measurements. *Engineering Geology*, 108(3):259–271, 2009.

A. Chima and S. Geiger. An analytical equation to predict gas/water relative permeability curves in fractures. In *SPE Latin America and Caribbean Petroleum Engineering Conference*, SPE 152252, 2012.

K. Choi, M. D. Jackson, G. J. Hampson, A. D. Jones, and A. D. Reynolds. Predicting the impact of sedimentological heterogeneity on gas-oil and water-oil displacements: fluvio-deltaic Pereriv Suite Reservoir, Azeri-Chirag-Gunashli Oilfield, South Caspian Basin. *Petroleum Geoscience*, 17:143 – 163, 2011.

N. Christ, A. Immenhauser, F. Amour, M. Mutti, S. Tomás, S. M. Agar, R. Alway, and L. Kabiri. Characterization and interpretation of discontinuity surfaces in a Jurassic ramp setting (High Atlas, Morocco). *Sedimentology*, 59(1):249–290, 2012.

J. R. Christensen, E. H. Stenby, and A. Skauge. Review of WAG Field Experience. *SPE Reservoir Evaluation & Engineering*, 4:97–106, 2001.

M. A. Christie. Flow in porous media scale up of multiphase flow. *Current Opinion in Colloid & Interface Science*, 6:236–241, 2001.

M. A. Christie and M. J. Blunt. Tenth SPE comparative solution project: A comparison of upscaling techniques. *SPE Reservoir Evaluation & Engineering*, 4(04): 308–317, 2001.

H. Cinco-Ley. Well-test analysis for naturally fractured reservoirs. *Journal of Petroleum Technology*, 48(1):51–54, 1996.

E. A. Clerke. Permeability , Relative Permeability , Microscopic Displacement Efficiency , and Pore Geometry of M _ 1 Bimodal Pore Systems in Arab D Limestone. *SPE Journal*, 14:524–531, 2009.

CMG. *STARS User Guide.* Computer Modelling Group, 2014.

P. W. M. Corbett. Petroleum Geoengineering: Integration of Static and Dynamic Models. *SEG/EAGE Distinguished Lecturer Series*, 12, 2009.

P. W. M. Corbett and J. L. Jenson. Lithological and zonal porosity-permeability distributions in the Arab-D reservoir, Uthmaniyah field Saudi Arabia: Discussion. *AAPG Bulletin*, 84:1365–1367, 2000.

P. W. M. Corbett, H. Hamdi, and H. Gurav. Layered fluvial reservoirs with internal fluid cross flow: a well-connected family of well test pressure transient responses. *Petroleum Geoscience*, 18:219–229, 2012.

A. T. Corey. The interrelation between gas and oil relative permeabilities. *Producers monthly*, 19(1):38–41, 1954.

L. Cosentino, Y. Coury, J. M. Daniel, E. Manceau, P. Van Lingen, J. Cole, and M. Sengul. Integrated Study of a Fractured Middle East Reservoir with Stratiform Super K Intervals. Part II : Upscaling and Dual Media Simulation. In *Middle East Oil Show*, page SPE 68184, 2001.

L. A. N. Costa, C. Maschio, and D. José Schiozer. Application of artificial neural networks in a history matching process. *Journal of Petroleum Science and Engineering*, 123:30–45, 2014.

L. P. Dake. *Fundamentals of Reservoir Engineering*. Elsevier, 1998.

L. P. Dake. *The practice of reservoir engineering*. Elsevier, 2001.

A. Datta-Gupta and M. J. King. *Streamline simulation: theory and practice*. Richardson, TX: Society of Petroleum Engineers, 2007.

M. R. Dernaika, I. Incorporated, M. A. Basioni, A. Dawoud, and M. Z. Kalam. Variations in Bounding and Scanning Relative Permeability Curves With Different Carbonate Rock Types. *SPE Reservoir Evaluation & Engineering*, 16(3): 265–280, 2013.

B. Dershowitz, P. Lapointe, T. Eiben, and L. Wei. Integration of Discrete Feature Network Methods With Conventional Simulator Approaches. *SPE Reservoir Evaluation & Engineering*, 3(2):165–170, 2000.

P. E. Deveugle, M. D. Jackson, G. J. Hampson, M. E. Farrell, A. R. Sprague, J. Stewart, and C. S. Calvert. Characterization of stratigraphic architecture and its impact on fluid flow in a fluvial dominated deltaic reservoir analog: upper Cretaceous Ferron Sandstone Member, Utah. *AAPG Bulletin*, 95:693–727, 2011.

G. Di Donato, H. Lu, Z. Tavassoli, and M. J. Blunt. Multirate-Transfer Dual-Porosity Modeling of Gravity Drainage and Imbibition. *SPE Journal*, 12(1): 77–88, 2007.

F. Doster, J. M. Nordbotten, and M. A. Celia. Impact of capillary hysteresis and trapping on vertically integrated models for CO2 storage. *Advances in Water Resources*, 62:465–474, 2013.

K. A. Dowsland and J. M. Thompson. *Simulated annealing. In Handbook of Natural Computing*. Springer Berlin Heidelberg, 2012.

R. J. Dunham. Classification of carbonate rocks according to depositional texture. In Ham, W. E. Classification of carbonate rocks. *American Association of Petroleum Geologists Memoir*, 1:108–121, 1962.

P. Egermann, O. Vizika, L. Kallet, C. Requin, and F. Sonier. Hysteresis in three-phase flow: Experiments, modelling and reservoir simulations. In *IEA Workshop on Enhanced Oil Recovery, Edinburgh*, 2000.

A. M. Egwuenu, R. T. Johns, and Y. Li. Improved Fluid Characterization for Miscible Gas Floods. *SPE Reservoir Evaluation & Engineering*, 11(4):655–665, 2008.

A. E. Eiben and J. E. Smith. *Introduction to evolutionary computing*. Springer Science & Business Media, 2003.

M. S. Eldred and J. Burkardt. Comparison of non-intrusive polynomial chaos and stochastic collocation methods for uncertainty quantification. *AIAA paper*, 976:1–20, 2009.

A. H. Elsheikh, I. Hoteit, and M. F. Wheeler. Efficient Bayesian inference of subsurface flow models using nested sampling and sparse polynomial chaos surrogates. *Computer Methods in Applied Mechanics and Engineering*, 269:515–537, 2014.

H. D. Enge, S. J. Buckley, A. Rotevatn, and J. A. Howell. From outcrop to reservoir simulation model: workflow and procedures. *Geosphere*, 3:469–490, 2007.

R. M. Enick, D. K. Olsen, J. R. Ammer, and W. Schuller. Mobility and Conformance Control for CO2 EOR via Thickeners, Foams, and Gels-A Literature Review of 40 Years of Research and Pilot Tests. In *SPE Improved Oil Recovery Symposium*, 2012.

J. B. Ericsson, H. C. McKean, and R. J. Hooper. Facies and curvature controlled 3D fracture models in a cretaceous carbonate reservoir, Arabian Gulf. *Geological Society, London, Special Publications*, 147:299–312, 1998.

A. Ettehadtavakkol, L. W. Lake, and S. L. B. CO2-EOR and storage design optimization. *International Journal of Greenhouse Gas Control*, 25:79–92, 2014.

A. Falls, G. Hirasaki, T. Patzek, D. Gauglitz, D. Miller, and T. Ratulowski. Development of a mechanistic foam simulator: the population balance and generation by snap-off. *SPE Reservoir Engineering*, 3:884–892, 1988.

H. Farran, J. Harris, S. A. Jabri, R. R. Jackson, S. A. Khayari, and T. Thomas. An integrated approach for evaluating and characterising horizontal well inflow and productivity in heterogeneous carbonate reservoirs. In *International Petroleum Technology Conference, Doha, Qatar*, IPTC 10492, 2005.

M. A. Ferno, A. Haugen, and A. Graue. Wettability effects on the matrix fracture fluid transfer in fractured carbonate rocks. *Journal of Petroleum Science and Engineering*, 77(1):146–153, 2011.

P. Fitch, M. Jackson, and G. Hampson. A hierarchical approach to classifying stratigraphic and sedimentological heterogeneities in carbonate ramp reservoirs with application to integrated flow simulation studies. *Petroleum Geoscience*, 20, 2014.

A. I. Forrester and A. J Keane. Recent advances in surrogate-based optimization. *Progress in Aerospace Sciences*, 45(1):50–79, 2009.

F. Friedmann, A. Chawathe, and D. K. Larue. Assessing uncertainty in channelized reservoirs using experimental designs. *SPE Reservoir Evaluation & Engineering*, 6(4):264–274, 2003.

J. F. Gale, S. E. Laubach, R. A. Marrett, J. E. Olson, J. Holder, and R. M. Reed. Predicting and characterizing fractures in dolostone reservoirs: Using the link between diagenesis and fracturing. *Geological Society, London, Special Publications*, 35(1):177–192, 2004.

B. Garcia-Fresca, J. L. Lucia, J. M. Sharp, and S. Kerans. Outcrop-constrained hydrogeological simulations of brine reflux and early dolomitization of the Permian San Andres Formation. *AAPG Bulletin*, 96(9), 2012.

J. Garland, J. Neilson, S. E. Laubach, and K. J. Whidden. Advances in carbonate exploration and reservoir analysis. *Geological Society, London, Special Publications*, 370(1):1–15, 2012.

S. Geiger and S. Matthai. What can we learn from high-resolution numerical simulations of single- and multi-phase fluid flow in fractured outcrop analogues? *Geological Society, London, Special Publications*, 374(1):125–144, 2012.

S. Geiger, S. K. Matthäi, J. Niessner, and R. Helmig. Black Oil Simulations for Three Component Three Phase Flow in Fractured Porous Media. *SPE Journal*, 14:338–354, 2009.

S. Geiger, M. Dentz, and I. Neuweiler. A Novel Multi-Rate Dual-Porosity Model for Improved Simulation of Fractured and Multiporosity Reservoirs. *SPE Journal*, 18(4):670–684, 2013.

M. Gen and R. Cheng. *Genetic algorithms and engineering optimization*. John Wiley & Sons, 2000.

M. G. Gerritsen and L. J. Durlofsky. Modeling fluid flow in oil reservoirs. *Annual Review of Fluid Mechanics*, 37:211–238, 2005.

R. Ghanem and P. D. Spanos. A stochastic Galerkin expansion for nonlinear random vibration analysis. *Probabilistic Engineering Mechanics*, 8(3):255–264, 1993.

J. R. Gilman and H. Kazemi. Improvements in simulation of naturally fractured reservoirs. *SPE Journal*, 23(4):695–707, 1983.

A. A. Giunta, S. F. Wojtkiewicz, and M. S. Eldred. Overview of modern design of experiments for computational simulations. In *41st AIAA Aerospace Sciences Meeting and Exhibition*, pages AIAA–2003–0649, 2003.

C. Gogu and J. Passieux. Efficient surrogate construction by combining response surface methodology and reduced order modeling. *Structural and Multidisciplinary Optimization*, 47(6):821–837, 2013.

C. Gogu, R. T. Haftka, S. K. Bapanapalli, and B. V. Sankar. Dimensionality reduction approach for response surface approximations: application to thermal design. *AIAA journal*, 47(7):1700–1708, 2009.

Golder-Associates. *FracMan Version 7.4 User Manual*. Golder Associates Incorporated, Redmond, WA, 2010.

J. S. Gomes, M. T. Ribeiro, C. J. Strohmenger, S. Negahban, and M. Z. Kalam. Carbonate Reservoir Rock Typing the Link between Geology and SCAL. In *Abu Dhabi International Petroleum Conference and Exhibition*, SPE 118284, 2008.

L. Guerreiro, A. C. Silva, V. Alcobia, and A. Soares. Integrated Reservoir Characterisation of a Fractured Carbonate Reservoir. In *SPE International Petroleum Conference and Exhibition in Mexico*, SPE 58955, 2000.

R. Gupta and K. K. Mohanty. Wettability alteration mechanism for oil recovery from fractured carbonate rocks. *Transport in Porous Media*, 87(2):635–652, 2011.

H. Haegland, A. Assteerawatt, H. K. Dahle, G. T. Eigestad, and R. Helmig. Comparison of celland vertex centered discretization methods for flow in a two dimensional discrete fracture matrix system. *Advances in Water Resources*, 32: 1740– 1755, 2009.

Y. Hajizadeh, V. Demyanov, L. Mohamed, and M. Christie. Comparison of evolutionary and swarm intelligence methods for history matching and uncertainty quantification in petroleum reservoir models. *Intelligent Computational Optimization in Engineering*, 366:209–240, 2011.

A. Haugen, M. A. Fernø, A. Graue, and H. J. Bertin. Experimental study of foam flow in fractured oil-wet limestone for enhanced oil recovery. *SPE Reservoir Evaluation and Engineering*, 15(2):218, 2012.

R. N. Healy, E. D. Holstein, and J. P. Batycky. Status of Miscible Flooding Technology. In *14th World Petroleum Congress*, volume 7(3), pages 407–416, 1994.

J. C. Helton and F. J. Davis. Latin hypercube sampling and the propagation of uncertainty in analyses of complex systems. *Reliability Engineering & System Safety*, 81(1):23–69, 2003.

H. Hermansen, L. K. Thomas, J. E. Sylte, and B. T. Aasboe. Twenty five years of ekofisk reservoir management. In *SPE Annual Technical Conference and Exhibition*, 1997.

H. Hermansen, G. H. Landa, J. E. Sylte, and L. K. Thomas. Experiences after 10 years of waterflooding the ekofisk field, norway. *Journal of Petroleum Science and Engineering*, 26(1):11–18, 2000.

G. Hirasaki, C. A. Miller, and M. Puerto. Recent advances in surfactant EOR. *SPE Journal*, 16(04):889–907, 2011.

G. J. Hirasaki. A Review of Steam-Foam Process Mechanisms. *SPE Journal*, page SPE 19518, 1989.

B. T. Hoffman and W. Narr. Using production logs (PLT) to estimate the size of fracture networks. *Journal of Petroleum Science and Engineering*, 98-99:11–18, 2012.

C. Hollis, V. Vahrenkamp, S. Tull, A. Mookerjee, C. Taberner, and Y. Huang. Pore system characterisation in heterogeneous carbonates: An alternative approach to widely-used rock-typing methodologies. *Marine and Petroleum Geology*, 27 (4):772–793, 2010.

C. Hollis, S. Price, H. Dijkm, L. Wei, D. Frese, M. van Rijen, and M. Al Salhi. Uncertainty in a Giant Fractured Carbonate Field, Oman, Using Experimental Design, in Y. Z. Ma, and P. R. La Pointe, eds., Uncertainty analysis and reservoir modeling. *AAPG Memoir*, 96:137–157, 2011.

L. W. Holm. Miscibility and Miscible Displacement. *SPE Journal*, 3:817–818, 1986.

R. Holm, M. van Dijke, and S. Geiger. Three-phase flow modelling using pore-scale capillary pressures and relative permeabilities for mixed-wet media at the continuum-scale. *Transport in porous media*, 81(3):423–442, 2010.

S. Hosder. Stochastic response surfaces based on non intrusive polynomial chaos for uncertainty quantification. *International Journal of Mathematical Modelling and Numerical Optimisation*, 3(1):117–139, 2012.

M. Hui and M. J. Blunt. Effects of Wettability on Three Phase Flow in Porous Media. *The Journal of Physical Chemistry B*, 104(16):3833–3845, 2000.

M. Iding and P. Ringrose. Evaluating the impact of fractures on the performance of the In Salah CO2 storage site. *International Journal of Greenhouse Gas Control*, 4(2):242–248, 2010.

S. S. Isukapalli, A. Roy, and P. G. Georgopoulos. Stochastic response surface methods (SRSMs) for uncertainty propagation: application to environmental and biological systems. *Risk analysis*, 18(3):351–363, 1998.

M. D. Jackson, P. H. Valvatne, and M. J. Blunt. Prediction of wettability variation and its impact on flow using pore- to reservoir-scale simulations. *Journal of Petroleum Science and Engineering*, 39(3-4):231–246, 2003.

M. D Jackson, P. H Valvatne, and M. J. Blunt. Prediction of Wettability Variation Within an Oil / Water Transition Zone and Its Impact on Production. *SPE Journal*, 10:184–195, 2005.

M. D. Jackson, G. J. Hampson, and R. P. Sech. Three-dimensional modeling of a shoreface-shelf parasequence reservoir analog: Part 2. geologic controls on fluid flow and hydrocarbon recovery. *AAPG Bulletin*, 93(1):183–1208, 2009.

P. P. Jadhunandan and N. R. Morrow. Effect of Wettability on Waterflood Recovery for Crude-Oil/Brine/Rock Systems. *SPE Reservoir Engineering*, 10(01): 40–46, 1995.

S. Jenni, L. Hu, R. Basquet, G. Marsily, and B. Bourbiaux. History matching of a stochastic model of field-scale fractures: methodology and case study. *Oil & Gas Science and Technology*, 62(2):265–276, 2007.

J. W. Jennings, S. C. Ruppel, and W. B. Ward. Geostatistical Analysis of Permeability Data and Modeling of Fluid-Flow Effects in Carbonate Outcrops. *SPE Reservoir Evaluation & Engineering*, 3:293–303, 2000.

J. Jensen, L. Lake, P. Corbett, and D. Goggin. *Statistics for petroleum engineers and geoscientists*. Prentice-Hall, 1997.

G. R. Jerauld. General Three-Phase Relative Permeability Model for Prudhoe Bay. *SPE Reservoir Engineering*, 12(4):225–263, 1997.

K. Jessen, A. R. Kovscek, and F. M. Orr. Increasing CO2 storage in oil recovery. *Energy Conversion and Management*, 46(2):293–311, 2005.

Z. Jiang, A. Al-Dhahli, M. I. J. van Dijke, S. Geiger, G. D. Couples, J. Ma, and C. Maier. Multi-scale pore-network modelling of WAG in carbonates. In *17th EAGE Symposium on Improved Oil Recovery, St. Petersburg, Russia*, 2013.

V. Joekar-Niasar, S. M. Hassanizadeh, and A. Leijnse. Insights into the relationships among capillary pressure, saturation, interfacial area and relative permeability using pore-network modeling. *Transport in Porous Media*, 74(2):201–219, 2008.

V. Joekar-Niasar, F. Doster, R. T. Armstrong, D. Wildenschild, and M. a. Celia. Trapping and hysteresis in two-phase flow in porous media: A pore-network study. *Water Resources Research*, 49(7):4244–4256, 2013.

R. T. Johns, H. Yuan, and B. Dindoruk. Quantification of displacement mechanisms in multicomponent gasfloods. In *SPE Annual Technical Conference and Exhibition*, SPE 77696, 2002.

R. Juanes, E. J. Spiteri, F. M. Orr, and M. J. Blunt. Impact of relative permeability hysteresis on geological CO2 storage. *Water Resources Research*, 42(12):1–13, 2006.

Z. Kalam, A. S. Al-Rawahi, I. A. Al-Hosani, S. Negahban, and A. A Rehman. Miscible gas injection tests in Carbonates and its impact on field development. In *SPE Reservoir Characterisation and Simulation Conference and Exhibition*, SPE 148374, 2011.

A. M. Kallehbasti, R. J. Paroodbari, N. Alizadeh, R. R. Ravari, and M. Amani. Feasibility Study of Miscible Gas Injection in a Carbonate Oil Reservoir; A Systematic Experimental and Simulation Approach. In *Abu Dhabi International Petroleum Conference and Exhibition*, SPE 161816, 2012.

M. Karimi-Fard, L. J. Durlofsky, and K. Aziz. An efficient discrete-fracture model applicable for general-purpose reservoir simulators. *SPE Journal*, 9:227–236, 2004.

H. Kazemi, J. R. Gilman, and A. M. Elsharkawy. Analytical and Numerical Solution of Oil Recovery From Fractured Reservoirs With Empirical Transfer Functions. *SPE Reservoir Engineering*, 7(2):219–227, 1992.

J. A. M. Kenter. Carbonate platform flanks: slope angle and sediment fabric. *Sedimentology*, 37(5):777–794, 1990.

C. Kerans, J. L. Lucia, and R. K. Senger. Integrated characterization of carbonate ramp reservoirs using Permian San Andres formation outcrop analogs. *AAPG Bulletin*, 78(2):181–216, 1994.

J. E. Killough. Reservoir Simulation With History-Dependent Saturation Functions. *SPE Journal*, 16(01):37–48, 1976.

M. J. King, K. S. Burn, P. Wang, W. Muralidharan, F. Alvarado, and M. Xianlin. Optimal coarsening of 3D reservoir models for flow simulation. In *SPE Annual Technical Conference and Exhibition*, SPE 95759, 2006.

P. R. King, S. V. Buldyrev, N. V. Dokholyan, S. Havlin, Y. Lee, G. Paul, H. E. Stanley, and N. Vandesteeg. Predicting oil recovery using percolation theory. *Petroleum Geoscience*, 7:105–107, 2001.

O. Kirstetter, P. W. M. Corbett, J. Somerville, and C. MacBeth. Elasticity/saturation relationships using flow simulation from an outcrop analogue for 4D seismic modelling. *Petroleum Geoscience*, 12:205–219, 2006.

B. Koehrer, T. Aigner, and M. Poppelrelter. Field-scale geometries of Upper Khuff reservoir geobodies in an outcrop analogue (Oman Mountains, Sultanate of Oman). *Petroleum Geoscience*, 17:3–16, 2011.

A. Kovscek and C. Radke. Fundamentals of foam transport in porous media. In: Schramm, L. (Ed.), Foams: Fundamentals and Applications in the Petroleum Industry. In *American Chemical Society, Washington, DC, ACS Symposium No. 242*, 1994.

A. R. Kovscek. Screening criteria for CO2 storage in oil reservoirs. *Petroleum Science and Technology*, 20(7):841–866, 2002.

A. R. Kovscek and M. D. Cakici. Geologic storage of carbon dioxide and enhanced oil recovery. II. Cooptimization of storage and recovery. *Energy Conversion and Management*, 46(11):1941–1956, 2005.

A. R. Kovscek, H. Wong, and C. J. Radke. A pore-level scenario for the development of mixed wettability in oil reservoirs. *AIChE Journal*, 39(6):1072–1085, 1993.

A. R. Kovscek, T. W. Patzek, and C. J. Radke. A mechanistic population balance model for transient and steady-state foam flow in Boise sandstone. *Chemical Engineering Science*, 50(23):3783–3799, 1995.

S. Koziel and X. Yang. *Computational Optimization, Methods and Algorithms*, volume 356 of *Studies in Computational Intelligence*. Springer Berlin Heidelberg, Berlin, Heidelberg, 2011.

F. Kuchuk and D. Biryukov. Transient Pressure Test Interpretation for Continuously and Discretely Fractured Reservoirs. In *SPE Annual Technical Conference and Exhibition*, SPE 158096, 2012.

L. W. Lake. *Enhanced oil recovery*. Prentice Hall Inc., 1989.

L. W. Lake, R. L. Schmidt, and P. B. Venuto. A Niche for Enhanced Oil Recovery in the 1990s. *Schlumberger Oilfield Review*, 4(1):55–61, 1992.

C. S. Land. Calculation of Imbibition Relative Permeability for Two- and Three-Phase Flow From Rock Properties. *SPE Journal*, 8(02):149–156, 1968.

E. A. Lange. Correlation and prediction of residual oil saturation for gas-injection-enhanced-oil-recovery processes. *SPE Reservoir Evaluation & Engineering*, 1:127–133, 1998.

F. Lapponi, G. Casini, I. Sharp, W. Blendinger, N. Fernandez, I. Romaire, and D. Hunt. From outcrop to 3D modelling: a case study of a dolomitized carbonate reservoir, Zagros Mountains, Iran. *Petroleum Geoscience*, 17(3):283–307, 2011.

J. A. Larsen and A. Skauge. Methodology for Numerical Simulation With Cycle-Dependent Relative Permeabilities. *SPE Journal*, 3:163–173, 1998.

A. Leach, C. F. Mason, and K. V. T. Veld. Co-optimization of enhanced oil recovery and carbon sequestration. *Resource and energy Economics*, 33(4):893–912, 2011.

R. J. Lenhard and M. Oostroom. A parametric model for predicting relative permeability-saturation-capillary pressure relationships of oil-water systems in porous media with mixed wettability. *Transport in Porous Media*, 31:109–131, 1998.

R. J. Lenhard and J. C. Parker. A model for hysteretic constitutive relations governing multiphase flow: 2. Permeability-saturation relations. *Water Resources Research*, 23(12):2197–2206, 1987.

E. Leung, M. Nukhaev, V. Gottumukkala, H. Samosir, and A. El-Fattah, M. Ogunsanwo, O. Gonzalez. Horizontal well placement and completion optimisation

in carbonate reservoirs. In *SPE Caspian Carbonates Technology Conference*, SPE 140048, 2010.

D. Levitt, S. Dufour, G. Pope, D. Morel, and P. Gauer. Design of an ASP flood in a high-temperature, high-salinity, low-permeability carbonate. In *International Petroleum Technology Conference, Bangkok, Thailand*, IPTC 14915, 2012.

D. Li and B. Beckner. Optimal uplayering for scaleup of multimillion-cell geologic models. In *SPE Annual Technical Conference and Exhibition*, SPE 62927, 2000.

H. Li and D. Zhang. Probabilistic collocation method for flow in porous media: Comparisons with other stochastic methods. *Water Resources Research*, 43(9), 2007.

S. Li and Y. Zhang. Model complexity in carbon sequestration: A design of experiment and response surface uncertainty analysis. *International Journal of Greenhouse Gas Control*, 22:123–138, 2014.

Y. Li, X. Li, S. Teng, and D. Xu. Improved models to predict gas–water relative permeability in fractures and porous media. *Journal of Natural Gas Science and Engineering*, 19:190–201, 2014.

P. M. Lichaa, H. Alpustun, J. H. Abdul, W. A. Nofal, and A. B. Fuseni. Wettability evaluation of a carbonate reservoir rock. *Advances in Core Evaluation III, Reservoir Management*, 327, 1993.

H. Liu, B. G. Tellez, T. Atallah, and M. Barghouty. The role of CO2 capture and storage in Saudi Arabia's energy future. *International Journal of Greenhouse Gas Control*, 11:163–171, 2012.

H. Y. Lu, G. Di Donato, and M. J. Blunt. General transfer functions for multiphase flow in fractured reservoirs. *SPE Journal*, 13(3):289–297, 2008.

F. J. Lucia, C. Kerans, and J. W. Jennings. Carbonate Reservoir Characterization. *Journal of Petroleum Technology*, 55(6):70–72, 2003.

K. Ma, R. Farajzadeh, J. L. Lopez-Salinas, C. Miller, S. L. Biswal, and G. J. Hirasaki. Non-uniqueness, Numerical Artifacts, and Parameter Sensitivity in

Simulating Steady-State and Transient Foam Flow Through Porous Media. *Transport in Porous Media*, 102(3):325–348, 2014.

H. G. Machel, M. Borrero, E. Dembicki, H. Huebscher, P. Luo, and Y. Zhao. The Grosmont: the world's largest unconventional oil reservoir hosted in carbonate rocks. In: Advances in Carbonate Exploration and Reservoir Analysis. *Geological Society, London, Special Publications*, 370:49–81, 2012.

C. W. MacMinn, M. L. Szulczewski, and R. Juanes. CO2 migration in saline aquifers. Part 2. Capillary and solubility trapping. *Journal of Fluid Mechanics*, 688:321–351, 2011.

C. Maier, K. Schmid, M. Ahmed, and S. Geiger. Multi-Rate Mass-Transfer Dual-Porosity Modelling Using the Exact Analytical Solution for Spontaneous Imbibition. In *SPE/EAGE Europec Conference*, SPE 164926, 2013.

G. H. Makel. The modelling of fractured reservoirs: constraints and potential for fracture network geometry and hydraulics analysis. *Geological Society, London, Special Publications*, 292(1):375–403, 2007.

E. Manrique, C. Thomas, R. Ravikiran, M. Izadi, M. Lantz, J. Romero, and V. Alvarado. EOR: current status and opportunities. In *SPE Improved Oil Recovery Symposium*, SPE 130113, 2010.

E. J. Manrique, V. E. Muci, and M. E. Gurfinkel. EOR Field Experiences in Carbonate Reservoirs in the United States. *SPE Reservoir Evaluation & Engineering*, 10(6):667–686, 2007.

T. Manzocchi. The connectivity of two-dimensional networks of spatially correlated fractures. *Water resources research*, 38(9):1–19, 2002.

C. Martavaltzi, A. Dakik, S. Agrawal, and A. Gupta. Wettability alteration of carbonates by optimizing brine and surfactant composition. In *Kuwait international petroleum conference and exhibition*, SPE 163348, 2012.

G. J. Massonat and D. Bandizol. Interdependence between geology and well test interpretation. In *SPE Annual Technical Conference and Exhibition*, SPE 22740, 1991.

S. K. Matthäi, S. Geiger, S. G. Roberts, A. Paluszny, M. Belayneh, A. Burri, and A. Mezentsev. Numerical simulations of multiphase fluid flow in structurally complex reservoirs. *Geological Society, London, Special Publications*, 292:405–429, 2007.

H. G. Matthies and A. Keese. Galerkin methods for linear and nonlinear elliptic stochastic partial differential equations. *Computer Methods in Applied Mechanics and Engineering*, 194(12):1295–1331, 2005.

J. McCall. Genetic algorithms for modelling and optimisation. *Journal of Computational and Applied Mathematics*, 184(1):205–222, 2005.

Z. Michalewicz. *Genetic algorithms+ data structures= evolution programs*. Springer Science & Business Media, 1996.

M. Mitchell. *An Introduction to Genetic Algorithms*. MIT Press, Cambridge, Massachusetts, 1999.

L. Mohamed, M. Christie, and V. Demyanov. Comparison of Stochastic Sampling Algorithms for Uncertainty Quantification. *SPE Journal*, 15:31–38, 2010.

K. Mohan, R. Gupta, and K. K. Mohanty. Wettability Altering Secondary Oil Recovery in Carbonate Rocks. *Energy & Fuels*, 25(9):3966–3973, 2011.

B. Montaron. Carbonate evolution. *Oil and Gas Middle East*, 4:26–31, 2008.

D. C. Montgomery. *Design and analysis of experiments*. John Wiley & Sons, 2008.

H. Moritz. Least-squares collocation. *Reviews of Geophysics and Space Physics*, 16 (3):421–430, 1978.

N. R. Morrow. Wettability and its effect on oil recovery. *Journal of Petroleum Technology*, 42(12):1476–1484, 1990.

N. R. Morrow and G. Mason. Recovery of oil by spontaneous imbibition. Current Opinion in Colloid & Interface Scienc. *Current Opinion in Colloid & Interface Science*, 6(4):321–337, 2001.

J. R. Murphy and N. R. Thomson. Two phase flow in a variable aperture fracture. *Water Resources Research*, 29(10):3453–3476, 1993.

M. Mutti, D. Bernoulli, G. P. Eberli, and A. Vecsei. Depositional geometries and facies associations in an Upper Cretaceous prograding carbonate platform margin. Orfento Supersequence, Maiella, Italy. *Journal of Sedimentary Research*, 66:749 – 765, 1996.

R. H. Myers, D. C. Montgomery, and C. M. Anderson-Cook. *Response surface methodology: process and product optimization using designed experiments*. John Wiley & Sons, 2009.

M. Namdar Zanganeh. *Simulation and Optimization of Foam EOR Processes*. Delft University of Technology, 2011.

M. Namdar Zanganeh and W. R. Rossen. Optimization of Foam Enhanced Oil Recovery : Balancing Sweep and Injectivity. *SPE Reservoir Evaluation & Engineering*, 16(1):51–59, 2013.

M. Namdar Zanganeh, J. F. Kraaijevanger, H. W. Buurman, J. D. Jansen, and W. R. Rossen. Challenges in adjoint-based optimization of a foam EOR process. *Computational Geosciences*, 18(3-4):563–577, 2014.

R. Nelson. *Geologic analysis of naturally fractured reservoirs*. Gulf Professional Publishing, 2001.

M. Oda. Permeability tensor for discontinuous rock masses. *Geotechnique*, 35(4): 483–495, 1985.

N. E. Odling, P. Gillespie, B. Bourgine, C. Castaing, and J. P. Chiles. Variations in fracture system geometry and their implications for fluid flow in fractured hydrocarbon reservoirs. *Petroleum Geoscience*, 5(4):373–384, 1999.

T. M. Okasha, J. J. Funk, and H. N. Al-Rashidi. Fifty Years of Wettability Measurements in the Arab-D Carbonate Reservoir. In *15th SPE Middle East Oil & Gas Conference*, SPE 105114, 2007.

S. Oladyshkin, H. Class, R. Helmig, and W. Nowak. A concept for data-driven uncertainty quantification and its application to carbon dioxide storage in geological formations. *Advances in Water Resources*, 34(11):1508–1518, 2011.

S. Oladyshkin, F. P. J. de Barros, and W. Nowak. Global sensitivity analysis: A flexible and efficient framework with an example from stochastic hydrogeology. *Advances in Water Resources*, 37:10–22, 2012.

J. E. Onwunalu and L. J. Durlofsky. A New Well-Pattern-Optimization Procedure for Large-Scale Field Development. *SPE Journal*, 16:594–607, 2011.

D. Palermo, T. Aigner, S. Nardon, and W. Blendinger. Three-dimensional facies modeling of carbonate sand bodies: Outcrop analog study in an epicontinental basin (Triassic, southwest Germany). *AAPG Bulletin*, 94:475 – 512, 2010.

M. Pancharoen, M. A. Fernø, and A. R. Kovscek. Modeling foam displacement in fractures. *Journal of Petroleum Science and Engineering*, 100:50–58, 2012.

H. Panjalizadeh, N. Alizadeh, and H. Mashhadi. A workflow for risk analysis and optimization of steam flooding scenario using static and dynamic proxy models. *Journal of Petroleum Science and Engineering*, 121:78–86, 2014.

T. W. Patzek. Field applications of steam foam for mobility improvement and profile control. *SPE Reservoir Engineering*, 11(2):79–86, 1996.

J. E. Pavlas. MPP simulation of complex water encroachment in a large carbonate reservoir in Saudi Arabia. In *SPE Annual Technical Conference and Exhibition*, SPE 71628, 2001.

D. Y. Peng and D. B. Robinson. A new two-constant equation of state. *Industrial & Engineering Chemistry Fundamentals*, 15:59–64, 1976.

K. R. Petvipusit, A. H. Elsheikh, T. C. Laforce, P. R. King, and M. J. Blunt. Robust optimisation of CO2 sequestration strategies under geological uncertainty using adaptive sparse grid surrogates. *Computational Geosciences*, 18(5):763–778, 2014.

A. Pierre, C. Durlet, P. Razin, and E. H. Chellai. Spatial and temporal distribution of ooids along a Jurassic carbonate ramp: Amellago outcrop transect, High-Atlas, Morocco. *Geological Society, London, Special Publications*, 329(1):65–88, 2010.

M. Piri and M. J. Blunt. Three-dimensional mixed-wet random pore-scale network modeling of two-and three-phase flow in porous media. I. Model description. *Physical Review E*, 71(2):026301, 2005.

J. O. Pizarro and C. C. Branco. Challenges in implementing an EOR project in the pre-salt province deep offshore Brasil. In *SPE EOR Conference at Oil and Gas West Asia*, SPE 155665, 2012.

A. Poisson, M. Hadri, A. Milhi, M. Julien, and J. Andrieux. The central High-Atlas (Morocco). Litho- and chronostratigraphic correlations during Jurassic times between Tinjdad and Tounfite. Origin of subsidence. *Memoirs of the Natural History Museum*, 179:237–256, 1998.

L. W. Pomar, A. Obrador, and H. Westphal. Sub-wavebase cross-bedded grainstones on a distally steepened carbonate ramp, Upper Miocene, Menorca, Spain. *Sedimentology*, 49:139 – 169, 2002.

J. K. Pringle, A. R. Westerman, J. D. Clark, N. J. Drinkwater, and A. R. Gardiner. 3D high-resolution digital models of outcrop analogue study sites to constrain reservoir model uncertainty: an example from Alport Castles, Derbyshire, UK. *Petroleum Geoscience*, 10:343–352, 2004.

K. Pruess, T. Xu, J. Apps, and J. Garcia. Numerical modeling of aquifer disposal of CO2. *SPE Journal*, 8(1):49–60, 2003.

R. Qi, T. C. LaForce, and M. J. Blunt. Design of carbon dioxide storage in oil fields. In *SPE Annual Technical Conference and Exhibition*, SPE 115663, 2008.

R. Qi, T. Laforce, and M. Blunt. Design of carbon dioxide storage in aquifers. *International Journal of Greenhouse Gas Control*, 3(2):195–205, 2009.

P. Quandalle and J. C. Sabathier. Typical features of a multipurpose reservoir simulator. *SPE Reservoir Engineering*, 4(4):475–480, 1989.

N. V. Queipo, R. T. Haftka, W. Shyy, T. Goel, R. Vaidyanathan, and P. Kevin Tucker. Surrogate-based analysis and optimization. *Progress in aerospace sciences*, 41(1):1–28, 2005.

B. Ramirez, H. Kazemi, and E. Ozkan. A Critical Review for Proper Use of Water / Oil / Gas Transfer Functions in Dual-Porosity Naturally Fractured Reservoirs : Part I. *SPE Reservoir Evaluation & Engineering*, 12(2):200–210, 2009.

A. Rawahi, H. Hafez, A. Al-yafei, S. Ghori, K. Putney, and T. Matthews. Maximize the Ultimate Recovery by Designing & Optimizing a CO2 Miscible Gas Injection Pilot in Giant Carbonate Oil Reservoir, Abu Dhabi. In *Abu Dhabi International Petroleum Conference and Exhibition*, SPE 162277, 2012.

K. Rawnsley and L. Wei. Evaluation of a new method to build geological models of fractured reservoirs calibrated to production data. *Petroleum Geoscience*, 7 (1):23–33, 2001.

G. Reijnders, N. Al-mohannadi, M. Pöppelreiter, S. Finlay, G. Bodewitz, and L. Al-oreibi. Simulating the Outcrop: Surface To Subsurface Integration of a Carbonate Reservoir , Khuff Formation , Oman. In *Abu Dhabi International Petroleum Conference and Exhibition*, SPE 118332, 2008.

W. J. Renkema and W. R. Rossen. Success of SAG Foam Processes in Heterogeneous Reservoirs. In *SPE Annual Technical Conference and Exhibition*, SPE 110408, 2007.

P. Ringrose, G. Pickup, J. Jensen, and M. Forrester. The Ardross reservoir gridblock analog: sedimentology, statistical representivity, and flow upscaling. *AAPG Memoir*, 71:265–275, 1999.

E. Romm. *Fluid flow in fractured rocks*. Nedra Publishing House, 1966.

A. Rotevatn, S. J. Buckley, J.A. Howell, and H. Fossen. Overlapping faults and their effect on fluid flow in different reservoir types: a LIDAR-based outcrop modeling and flow simulation study. *AAPG Bulletin*, 93:407–427, 2009.

A. V. Ryazanov, M. I. J. Van Dijke, and K. S. Sorbie. Two-phase pore-network modelling: existence of oil layers during water invasion. *Transport in Porous Media*, 80(1):79–99, 2009.

A. V. Ryazanov, K. S. Sorbie, and M. I. J. van Dijke. Structure of residual oil as a function of wettability using pore-network modelling. *Advances in Water Resources*, 63:11–21, 2014.

V. A. Sajjadian, A. M. Emadi, and E. Khaghani. Simulation study of secondary water and gas injection in a typical Iranian naturally fractured carbonate oil reservoir. In *18th World Petroleum Congress*, pages Paper 18–0870, 2005.

P. Samier, L. Quettier, and M. Thiele. Applications of streamline simulations to reservoir studies. *SPE Reservoir Evaluation & Engineering*, 5(04):324–332, 2002.

N. I. SayedAkram and D. Mamora. Simulation Study on Surfactant-Polymer Flood Performance in Fractured Carbonate Reservoir. In *SPE Saudi Arabia Section Technical Symposium and Exhibition*, SPE 149106, 2011.

K. S. Schmid and S. Geiger. Universal scaling of spontaneous imbibition for water-wet systems. *Water Resources Research*, 48(3), 2012.

K. S. Schmid and S. Geiger. Universal scaling of spontaneous imbibition for arbitrary petrophysical properties: Water-wet and mixed-wet states and Handy's conjecture. *Journal of Petroleum Science and Engineering*, 101:44–61, 2013.

R. P. Sech, M. D. Jackson, and G. J. Hampson. Three-dimensional modeling of a shoreface-shelf parasequence reservoir analog: Part 1. Surface-based modeling to capture high-resolution facies architecture. *AAPG Bulletin*, 93:1155–1181, 2009.

M. K. Sen, A. Datta-gupta, P. L. Stoffa, L. W. Lake, and G. A. Pope. Using Simulated Annealing and Genetic Algorithms. *SPE Formation Evaluation*, 4: 49–55, 1995.

D. Shan and W. R. Rossen. Optimal Injection Strategies for Foam IOR. *SPE Journal*, 9(2):132–150, 2004.

R. Shekhar, I. Sahni, G. Benson, S. M. Agar, F. Amour, S. Tomas, N. Christ, R. Alway, M. Mutti, A. Immenhauser, Z. Karcz, and L. Kabiri. Sensitivities to Flow-modeling Assumptions for a Heterogeneous Carbonate Ramp - An Example from a Jurassic Carbonate Ramp. In *EAGE Conference & Exhibition*, K032, 2010.

R. Shekhar, I. Sahni, G. Benson, S. Agar, F. Amour, S. Tomás, and L. Kabiri. Modelling and simulation of a Jurassic carbonate ramp outcrop, Amellago, High Atlas Mountains, Morocco. *Petroleum Geoscience*, 20(1):109–123, 2014.

T. W. Simpson, V. Toropov, V. Balabanov, and F. A. Viana. Design and analysis of computer experiments in multidisciplinary design optimization: a review of how far we have come or not. In *12th AIAA/ISSMO multidisciplinary analysis and optimization conference*, 2008.

A. Skauge, M. G. Aarra, L. Surguchev, H. A. Martinsen, and L. Rasmussen. Foam-Assisted WAG : Experience from the Snorre Field. In *SPE Improved Oil Recovery Symposium*, SPE 75157, 2002.

K. S. Sorbie. *Polymer improved oil recovery*. Blackie and Son, Glasgow, 1991.

G. H. Spence, G. D. Couples, T. I. Bevan, R. Aguilera, J. W. Cosgrove, J. Daniel, and J. Redfern. Advances in the study of naturally fractured hydrocarbon reservoirs: a broad integrated interdisciplinary applied topic. *Geological Society, London, Special Publications*, 374:1–22, 2014.

N. Speyer, K. Li, and R. Horne. Experimental measurement of two-phase relative permeability in vertical fractures. In *Workshop on Geothermal Reservoir Engineering, Stanford, California*, 2007.

E. J. Spiteri and R. Juanes. Impact of relative permeability hysteresis on the numerical simulation of WAG injection. *Journal of Petroleum Science and Engineering*, 50(2):115–139, 2006.

E. J. Spiteri, R. Juanes, M. J. Blunt, and F. M. Orr. A New Model of Trapping and Relative Permeability Hysteresis for All Wettability Characteristics. *SPE Journal*, 13(3):277–288, 2008.

F. I. Stalkup. Displacement behaviour of the condensing/vaporizing gas drive process. In *SPE Annual Technical Conference and Exhibition*, SPE 16715, 1987.

D. Stauffer and A. Aharony. *Introduction to percolation theory*. CRC press, 1994.

M. Stein. Large sample properties of simulations using Latin hypercube sampling. *Technometrics*, 29(2):143–151, 1987.

K. D. Stephen and M. Dalrymple. Reservoir simulations developed from an outcrop of incised valley fill strata. *AAPG Bulletin*, 86:797–822, 2002.

D. Stern. Mechanisms of Miscible Oil Recovery: Effects of Pore-Level Fluid Distribution. In *SPE Annual Technical Conference and Exhibition*, SPE 22652, 1991.

G. Stewart. *Well Test Analysis*. Heriot Watt University Press, 2005.

H. L. Stone. Probability model for estimating three-phase relative permeability. *Journal of Canadian Petroleum Technology*, 22:214–218, 1970.

H. L. Stone. Estimation of three-phase relative permeability and residual oil data. *Journal of Canadian Petroleum Technology*, 12:53, 1973.

S. Subbey, C. Mike, and M. Sambridge. A strategy for rapid quantification of uncertainty in reservoir performance prediction. In *SPE Reservoir Simulation Symposium*, page SPE 79678, 2003.

L. M. Surguchev, J. E. Hanssen, D. A. Coombe, and I. Svorstoel. Simulation of WAG and gas Injection with potential sweep improvement by application of foam. In *8th European Symposium on Improved Oil Recovery*, 1995.

M. L. Szulczewski, C. W. MacMinn, H. J. Herzog, and R. Juanes. Lifetime of carbon capture and storage as a climate-change mitigation technology. *Proceedings of the National Academy of Sciences*, 109(14):5185–5189, 2012.

J. J. Taber, F. D. Martin, and R. S. Seright. EOR Screening Criteria Revisited Part 1 : Introduction to Screening Criteria and Enhanced Recovery Field Projects. *SPE Reservoir Engineering*, 12(3):189–198, 1997.

S. H. Talebian, R. Masoudi, I. Tan, and P. Zitha. Foam assisted CO2-EOR: A review of concept, challenges, and future prospects. *Journal of Petroleum Science and Engineering*, 120:202–215, 2014.

Z. Tavassoli, R. W. Zimmerman, and M. J. Blunt. Analytic analysis for oil recovery during counter-current imbibition in strongly water-wet systems. *Transport in Porous Media*, 58(2):173–189, 2005.

G. F. Teletzke, R. C. Wattenbarger, and J. R. Wilkinson. Enhanced Oil Recovery Pilot Testing Best Practices. *SPE Reservoir Evaluation & Engineering*, 13(1):143–154, 2010.

M. R. Thiele, M. G. Gerritsen, and M. J. Blunt. *Streamline simulation*. Society of Petroleum Engineers, 2011.

L. K. Thomas, T. N. Dixon, C. E. Evans, and M. E. Vienot. Ekofisk waterflood pilot. *Journal of petroleum technology*, 39(02):221–232, 1987.

G. Toigulova. *Upscaling of a Carbonate Reservoir Outcrop Analogue*. Heriot Watt University, 2012.

S. Tomás, M. Homann, M. Mutti, F. Amour, N. Christ, A. Immenhauser, S. M. Agar, and L. Kabiri. Alternation of microbial mounds and ooid shoals (Middle Jurasssic, Morocco): Response to paleoenvironmental changes. *Sedimentary Geology*, 294:68–82, 2013.

A. Toublanc, S. Renaud, J. E. Sylte, C. K. Clausen, T. Eiben, and G. Nadland. Ekofisk Field: fracture permeability evaluation and implementation in the flow model. *Petroleum Geoscience*, 11(4):321–330, 2005.

P. H. Valvatne and M. J. Blunt. Predictive pore scale modeling of two phase flow in mixed wet media. *Water Resources Research*, 40(7), 2004.

C. van der Land, R. Wood, K. Wu, M. van Dijke, Z. Jiang, P. Corbett, and G. Couples. Modelling the permeability evolution of carbonate rocks. *Marine and Petroleum Geology*, 48:1–7, 2013.

M. I. J. Van Dijke, K. S. Sorbie, and S. R. McDougall. Saturation-dependencies of three-phase relative permeabilities in mixed-wet and fractionally wet systems. *Advances in Water Resources*, 24(3):365–384, 2001.

H. Vatanparast, A. H. Alizadeh, A. Bahramian, and H. Bazdar. Wettability alteration of low-permeable carbonate reservoir rocks in presence of mixed ionic surfactants. *Petroleum Science and Technology*, 29(18):1873–1884, 2011.

R. L. Vaughan, S. A. Khan, L. J. Weber, O. Suwaina, A. Al-Mansoori, A. Ghani, C. J. Strohmenger, M. A. Herrmann, and D. Hulstrand. Integrated characterization of UAE outcrops: from rocks to fluid flow simulation. In *Abu Dhabi International Petroleum Conference and Exhibition*, SPE 88730, 2004.

E. Vennin, F. S. P. van Buchem, P. Joseph, F. Gaumet, M. Sonnenfeld, M. Rebelle, H. Fakhfakh-Ben Jemia, and H. Zijlstra. A 3D outcrop analogue model for

Ypresian nummulitic carbonate reservoirs: Jebel Ousselat, northern Tunisia. *Petroleum Geoscience*, 9:145 – 161, 2003.

J. Villadsen and M. L. Michelson. *Solution of differential equation models by polynomial approximation*. Prentice-Hall, 1978.

J. E. Warren and P. J. Root. The Behavior of Naturally Fractured Reservoirs. *SPE Journal*, 3(03):245–255, 1963.

L. Wei. Well Test Pressure Derivatives and the Nature of Fracture Networks. In *SPE International Petroleum Conference and Exhibition*, SPE 59014, 2000.

L. Wei, J. Hadwin, E. Chaput, K. Rawnsley, and P. Swaby. Discriminating Fracture Patterns in Fractured Reservoirs by Pressure Transient Tests. In *SPE Annual Technical Conference and Exhibition*, SPE 49233, 1998.

C. D. White and M. D. Barton. Translating outcrop data to flow models, with applications to the Ferron sandstone. *SPE Reservoir Evaluation & Engineering*, 2:341–350, 1999.

D. Wildenschild, R. T. Armstrong, A. L. Herring, I. M. Young, and C. J. William. Exploring capillary trapping efficiency as a function of interfacial tension, viscosity, and flow rate. *Energy Procedia*, 4:4945–4952, 2011.

M. Wilkinson, R. S. Haszeldine, A. E. Fallick, N. Odling, S. J. Stoker, and R. W. Gatliff. CO2 mineral reaction in a natural analogue for CO2 storage implications for modeling. *Journal of Sedimentary Research*, 79(7):486–494, 2009.

J. A. Witteveen, S. Sarkar, and H. Bijl. Modeling physical uncertainties in dynamic stall induced fluid structure interaction of turbine blades using arbitrary polynomial chaos. *Computers and structures*, 85(11):866–878, 2007.

J. Wriedt, M. Deo, W. S. Han, and J. Lepinski. A methodology for quantifying risk and likelihood of failure for carbon dioxide injection into deep saline reservoirs. *International Journal of Greenhouse Gas Control*, 20:196–211, 2014.

D. Xiu and G. Karniadakis. Modeling uncertainty in steady state diffusion problems via generalized polynomial chaos. *Computer Methods in Applied Mechanics and Engineering*, 191(43):4927–4948, 2002.

D. Xiu and G. Karniadakis. Modeling uncertainty in flow simulations via generalized polynomial chaos. *Journal of Computational Physics*, 187(1):137–167, 2003.

W. Yan, C. A. Miller, and G. J. Hirasaki. Foam sweep in fractures for enhanced oil recovery. *Colloids and Surfaces A: Physicochemical and Engineering Aspects*, 282(October 2005):348–359, 2006.

P. Zhang, G. E. Pickup, and M. A. Christie. A new practical method for upscaling in highly heterogeneous reservoir models. *SPE Journal*, 13(01):68–76, 2008.

Y. Zhang and N. V. Sahinidis. Uncertainty Quantification in CO2 Sequestration Using Surrogate Models from Polynomial Chaos Expansion. *Industrial & Engineering Chemistry Research*, 52(9):3121–3132, 2012.

A. A. Zick. A combined condensing/vaporizing mechanism in the displacement of oil by enriched gas. In *SPE Annual Technical Conference and Exhibition*, SPE 15493, 1986.